Processing of sky compass signals at different stages of the polarization-vision pathway in the brain of the desert locust *(Schistocerca gregaria)*

Prozessierung von Himmelskompasssignalen auf verschiedenen Ebenen der Polarisationssehbahn im Gehirn der Wüstenheuschrecke *(Schistocerca gregaria)*

Dissertation
zur
Erlangung des Doktorgrades
der Naturwissenschaften
(Dr. rer. nat.)

dem Fachbereich Biologie
der Philipps-Universität Marburg
vorgelegt von
Basil el Jundi
aus Stuttgart
Marburg/Lahn, 2011

Vom Fachbereich Biologie der Philipps-Universität Marburg als
Dissertation am _____ angenommen.

Erstgutachter: Prof. Dr. Uwe Homberg
Zweitgutachter: Prof. Dr. Joachim Schachtner

Tag der mündlichen Prüfung am: _____

Contents

Erklärung: Eigene Beiträge und veröffentlichte Teile der Arbeit

Laut §8, Absatz 3 der Promotionsordnung der Philipps-Universität Marburg (Fassung vom 12.4.2000) müssen bei den Teilen der Dissertation, die aus gemeinsamer Forschungsarbeit entstanden sind, „die individuellen Leistungen des Doktoranden deutlich abgrenzbar und bewertbar sein.“ Dies betrifft die Kapitel 1 – 4, die Beiträge werden im Folgenden detailliert erläutert.

Kapitel 1: A Distinct Layer of the Medulla Integrates Sky Compass Signals in the Brain of an Insect

- Durchführung von 98% der Experimente (56 von 57 Ableitungen).
- Auswertung und statistische Analyse aller Daten.
- Modellrechnungen wurden von Dr. Keram Pfeiffer innerhalb einer Kooperation erstellt.
- Dextran-Injektionspräparate wurden in Kooperation mit Dr. Keram Pfeiffer erstellt (Injektion durch Dr. Keram Pfeiffer, Präparation und immunhistochemische Aufbereitung durch den Autor der Doktorarbeit).
- Immunhistochemische Aufbereitung aller fluoreszenzmarkierter Präparate und Auswertung mittels konfokaler Mikroskopie.
- Anfertigung von 60% (3 von 5) der dreidimensionalen Rekonstruktionen injizierter Neuronen, Anfertigung aller dreidimensional rekonstruierter Gehirnareale.
- Anfertigung aller Abbildungen.
- Anfertigung des Manuskriptes in Zusammenarbeit (Korrektur) mit Prof. Dr. Uwe Homberg.
- Dieses Kapitel wurde in dieser Form am 08.09.2011 beim Journal PLoS One (PONE-D-11-17679) eingereicht und am 07.10.2011 zur Revision zugelassen.

Kapitel 2: Receptive Field Properties and Intensity-Response Functions of Polarization-Sensitive Neurons of the Anterior Optic Tubercle in Gregarious and Solitarious Locusts

- Durchführung aller 113 präsentierten Ableitungen.
- Auswertung und statistische Analyse aller Daten.
- Immunhistochemische Aufbereitung aller fluoreszenzmarkierter Präparate.
- Anfertigung aller Abbildungen.
- Anfertigung des Manuskriptes in Zusammenarbeit (Korrektur) mit Prof. Dr. Uwe Homberg.
- Dieses Kapitel ist für eine Einreichung beim Journal of Neurophysiology vorgesehen.

Kapitel 3: Evidence for the Possible Existence of a Second Polarization-Vision Pathway in the Locust Brain

- Durchführung aller 5 präsentierten Ableitungen.
- Auswertung und statistische Analyse aller Daten.
- Anatomische Auswertung eines Dauerpräparates von Prof. Dr. Uwe Homberg und Dr. Stefan Würden.
- Immunhistochemische Aufbereitung aller fluoreszenzmarkierter Präparate.
- Anfertigung aller dreidimensional rekonstruierten Neuronen, Anfertigung aller dreidimensional rekonstruierten Gehirnareale.
- Anfertigung aller Abbildungen.
- Anfertigung des Manuskriptes in Zusammenarbeit (Korrektur) mit Prof. Dr. Uwe Homberg.
- Dieses Kapitel wurde in der vorliegenden Form beim Journal of Insect Physiology veröffentlicht (el Jundi B., Homberg U. (2010) Evidence for the possible existence of a second polarization-vision pathway in the locust brain. *J. Insect Physiol.* 56: 971-979).

Kapitel 4: The Locust Standard Brain: A 3D Standard of the Central Complex as a Platform for Neural Network Analysis

- Anfertigung der immunhistochemischen Präparate durch Constanze Lenschow.
- Teilweise Anfertigung der dreidimensional rekonstruierten Zentralkomplexe durch den Autor der vorliegenden Doktorarbeit. Überwiegend wurden die dreidimensionalen Rekonstruktionen der Zentralkomplexe durch Constanze Lenschow unter Anleitung von Dr. Stanley Heinze und dem Autor der Doktorarbeit erstellt.
- Etablierung der ‚Iterative Shape Averaging' Standardisierungsmethode für dreidimensionale Modelle (geschrieben von Dr. Torsten Rohlfing) im Labor von Prof. Dr. Uwe Homberg.
- Errechung des standardisieren Zentralkomplexes mit Hilfe des Linux-Rechenclusters der Philipps-Universität Marburg.
- Rehydrieren und Auswertung der von Dr. Stanley Heinze injizierten zwei Zentralkomplex-Neurone.
- Dreidimensionale Rekonstruktion aller Neurone und den entsprechenden Gehirnarealen.
- Registrierung der Neurone in den standardisierten Zentralkomplex-Atlas.
- Erstellung aller Abbildungen.
- Anfertigung des Manuskriptes in Zusammenarbeit (Korrektur) mit Prof. Dr. Uwe Homberg.
- Dieses Kapitel wurde in der vorliegenden Form beim Journal Frontiers in Systems Neuroscience veröffentlicht (el Jundi B., Heinze S., Lenschow C., Kurylas A., Rohlfing T., Homberg U. (2010) The locust standard brain: A 3D standard of the central complex as a platform for neural network analysis. *Front. Syst. Neurosci.* 3: 21).

Die Abfassung der Dissertation in englischer Sprache wurde vom Dekan des Fachbereiches Biologie am _____ genehmigt.

Zusammenfassung

Obwohl Insekten ein relativ kleines Gehirn aufweisen, zeigen sie außergewöhnliche Leistungen in räumlicher Orientierung und Navigation. Während langer Wanderflüge oder der Rückkehr zu einem Nestplatz können sie die ideale Route bestimmen und verfolgen, die sie auf kürzestem und schnellstem Weg zu ihrem Ziel führt. Hierbei können vor allem Kompasssignale des Himmels eine erhebliche Rolle spielen. Neben der Sonne, dem hellsten Punkt am Himmel, liefern weitere Himmelssignale wie der Farbgradient oder das Polarisationsmuster des Himmels Möglichkeiten zur Orientierung. Beide Himmelserscheinungen entstehen als Resultat der Streuung von Sonnenlicht an atmosphärischen Partikeln und bilden präzise Referenzen am Himmel. Der Himmelsfarbgradient zwischen der solaren und der antisolaren Hemisphäre beruht auf Unterschieden im Verhältnis von lang- und kurzwelligem Licht. Das natürliche polarisierte Licht am Himmel formt ein Muster, in dem die Schwingungsrichtung (*E*-Vektoren) des polarisierten Lichtes in konzentrischen Kreisen um die Sonne angeordnet sind (Abbildung 1A). Der Grad der Polarisation des Lichtes nimmt dabei bis zu einer Winkelentfernung von 90° zur Sonne zu und ist wie alle Himmelskompasssignale abhängig von der Position der Sonne.

Verhaltensversuche haben gezeigt, dass Bienen *(Apis mellifera)* und Ameisen *(*Gattung *Cataglyphis)* linear polarisiertes Licht des Himmels zur Navigation nutzen (von Frisch, 1949; Wehner, 2003). Auch in verschiedenen anderen Insektenspezies, wie der Feldgrille *(Gryllus campestris)* oder der Wüstenheuschrecke *(Schistocerca gregaria)*, konnte eine Polarotaxis nachgewiesen werden (Brunner und Labhart, 1987; Mappes und Homberg, 2004). Alle bisher untersuchten polarisations-empfindlichen Insekten verfügen über eine spezialisierte Augenregion zur Detektion von polarisiertem Licht, die sich dorsal am Komplexauge morphologisch vom restlichen Komplexauge hervorhebt und als dorsale Randregion bezeichnet wird (Labhart und Meyer, 1999; Homberg und Paech, 2002, Abbildung 1C).

Angesichts ihres relativ großen Gehirnes und der damit einhergehenden guten physiologischen Zugänglichkeit hat sich die Wüstenheuschrecke *Schistocerca gregaria* als hervorragendes Modellobjekt erwiesen, um die neuronalen Prinzipien der Verarbeitung von polarisiertem Licht im Insektengehirn zu erforschen. Mittels Farbstoffinjektionen sowie intrazellulärer Ableitungen konnte das grundlegende Verschaltungsnetzwerk charakterisiert werden, das der Prozessierung von polarisiertem Licht zu Grunde liegt. Polarisationssensitive Neurone im Gehirn sind durch typische physiologische Eigenschaften charakterisiert: Zum einen weisen sie bei Stimulation mit einem rotierenden Polarisationsfilter eine sinusförmige Modulation der Aktionspotentialfrequenz auf, wobei sie bei einer bestimmten *E*-Vektor Orientierung (Φ_{max}) maximal aktiviert werden. Weiterhin werden beinahe alle polarisationssensitiven Zellen bei einer Stimulusorientierung orthogonal zu Φ_{max} maximal inhibiert (Φ_{min}), was als Gegenpol-Eigenschaft der Zellen bezeichnet wird (Labhart, 1988).

Die Verarbeitung von Polarisationssignalen findet in sukzessiv angeordneten Gehirnarealen der Heuschrecke statt, die die sogenannte Polarisationssehbahn bilden (Homberg, 2004; siehe Introduction, Seite 16, Figure 1). Die Axone der Fotorezeptoren in der dorsalen Randregion ziehen aus dem Auge in zwei distinkte, ebenfalls dorsal lokalisierte Randregionen der optischen Neuropile Lamina und Medulla. Durch Farbstoffinjektionen konnte gezeigt werden, dass Transmedulla-Neurone – auch als „Line Tangential“-Neurone bezeichnet – die dorsale Randregion der Medulla mit einem Bereich im Zentralhirn verbinden, der als anteriorer optischer Tuberkel bezeichnet wird. Neurone dieses Areals wurden durch intrazelluläre Ableitungen detailliert charakterisiert: Während die Tuberkelneurone LoTu1 und TuTu1 eine Verbindung der anterioren optischen Tuberkel beider Gehirnhälften bilden, senden TuLAL1-Zellen die Polarisationsinformation zu den nächsten Stationen der Polarisationssehbahn, der medianen Olive und dem lateralen Dreieck (Pfeiffer et al., 2005). Hier transferieren TuLAL1 Neurone die Polarisationssignale auf Eingangsneurone des Zentralkomplexes (Träger et al., 2008). Der Zentralkomplex besteht aus vier Untereinheiten: Der unteren Einheit und der oberen Einheit des Zentralkörpers, den dazu posterior gelegenen Noduli, sowie der dorsal lokalisierten

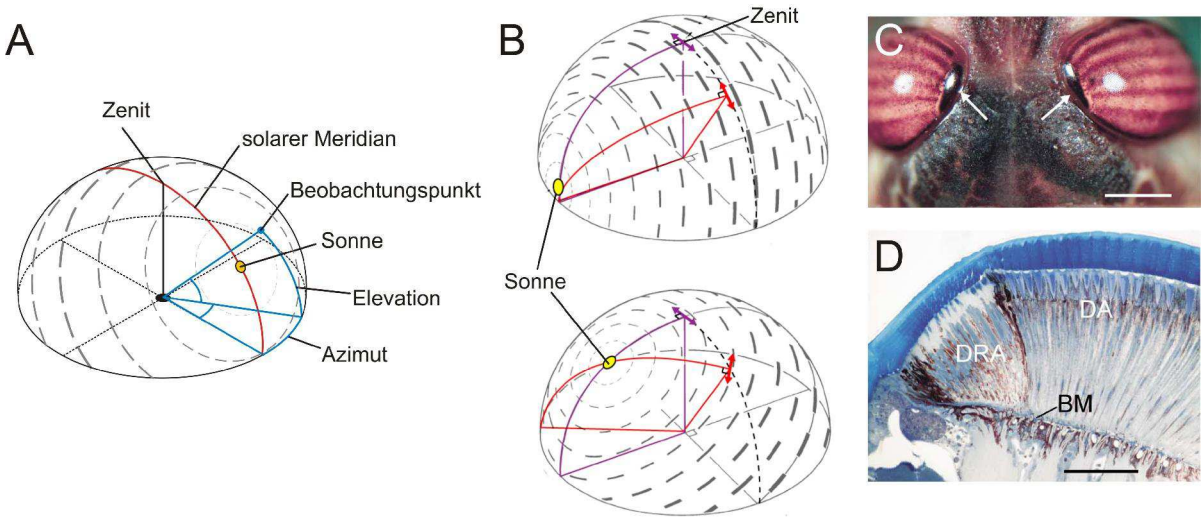

Abbildung 1: Himmelspolarisationsmuster und die dorsale Randregion der Wüstenheuschrecke. (A) Polarisationsmuster des Himmels bei einer solaren Elevation von 40°. Graue Balken zeigen die *E*-Vektoren, der Polarisationsgrad ist durch die Dicke der Striche dargestellt. Die Zenitrichtung ist durch die schwarze durchgezogene Linie dargestellt. Der solare Meridian ist als rote Linie gezeigt. Der blaue Punkt stellt einen Beobachtungspunkt am Himmel bei einer Elevation von 45° und einem Azimut von 30° dar. (B) Das Himmelspolarisationsmuster bei bestimmten solaren Elevationen. Violette Pfeile: *E*-Vektor Orientierung im Zenit. Rote Pfeile: *E*-Vektor Orientierung in einem bestimmten Beobachtungspunkt. Bei niedrigen solaren Elevationen ist die Winkelbeziehung zwischen dem solaren Azimut und der *E*-Vektor Orientierung für alle Beobachtungspunkte am Himmel etwa 90° (obere Abbildung). Bei höheren Sonnenständen ist außerhalb des solaren Meridians für alle Beobachtungspunkte die Winkeldifferenz ungleich 90° (untere Abbildung). (C) Dorsalansicht auf einen Heuschreckenkopf. Die dorsale Randregion (weiße Pfeile) hebt sich klar durch die dunkle Pigmentierung vom restlichen Auge ab. (D) Frontalschnitt durch die dorsale Randregion (DRA) und durch das dorsale Auge (DA). Die dorsale Randregion ist deutlich stärker pigmentiert und die optische Achse der Fotorezeptoren der dorsalen Randregion ist nach kontralateral gerichtet. BM: Basismembran. Maßstabsbalken: 1000 µm (C), 200 µm (D). B verändert nach Heinze und Reppert (2011); C, D aus Homberg und Paech (2002).

Protozerebralbrücke. Das Neuropilgefüge des Zentralkomplexes (mit Ausnahme der Noduli) ist durch eine hochkonservierte Neuroarchitektur charakterisiert, in der die Neuronen 16 regelmäßige Kolumnen ausbilden. Durch intrazelluläre Ableitungen kombiniert mit anatomischen Untersuchungen konnte gezeigt werden, dass Neurone benachbarter Kolumnen in der Protozerebralbrücke einen um 28° versetzten Vorzugsvektor (Φ_{max}, siehe oben) aufweisen, und so eine topographische kompassartige Repräsentation von Raumrichtungen relativ zur horizontalen Sonnenrichtung bilden (Heinze und Homberg, 2007). Der Zentralkomplex erfüllt somit möglicherweise eine Rolle als interner Kompass im Heuschreckengehirn, in dem die räumliche Orientierung des Tieres relativ zum solaren Meridian kodiert wird. Ausgangsneurone des Zentralkomplexes könnten die Polarisationssignale auf absteigende Neurone übertragen, deren Axone wiederum zu den Kontrollzentren in den Thorakalganglien projizieren (Träger und Homberg, 2011).

Während die Verarbeitung des polarisierten Lichtes im Heuschreckengehirn sehr gut untersucht ist, ist die Modulation der Polarisationsinformation und deren Kombination mit weiteren Navigationssignalen kaum untersucht. Die Kombination verschiedener Navigationssignale stellt eine erhebliche Herausforderung für ein neuronales Netzwerk dar, ist jedoch erforderlich, um die Relevanz des Signalinhaltes zu modulieren und mit dem Verhalten des Tieres zu verknüpfen. Weiterhin wären Heuschreckenschwärme auch nur dann fähig, das Himmelpolarisationsmuster während ihrer langen Wanderungen adäquat zu nutzen und eine konstante Wanderroute zu halten, wenn zusätzlich Zeitinformation in das neuronale Netzwerk integriert werden würde.

Nach aktuellem Kenntnisstand ist der anteriore optische Tuberkel ein Gehirnareal, in dem eine solche Integration verschiedener Signale stattfinden könnte. So wurde für Intertuberkelneurone gezeigt, dass sie neben Polarisationssignalen auch auf unpolarisierte Lichtreize reagieren. Jedoch ist die Reaktion der Zellen abhängig von der Wellenlänge und der Position des Lichtstimulus im visuellen Feld des Tieres. Eine Reizung der Zellen mit Grünlicht im ipsilateralen Sehfeld führte zur Erregung, während sie auf unpolarisiertes UV Licht mit einer Hemmung reagierten (Kinoshita et al., 2007). Diese Eigenschaft der Neurone, die auch als Gegenfarbreaktion bezeichnet wird, könnte die

Tuberkelzellen dazu befähigen, das Himmelspolarisationsmuster mit dem spektralen Farbgradienten des Himmels zu kombinieren.

Um die Kombination der Polarisationsinformation mit weiteren visuellen Reizen zu untersuchen, und um einen tieferen Einblick in Vorgänge der Zeitkompensation und Modulation des Polarisationsnetzwerks zu gewinnen, wurden in dieser Arbeit elektrophysiologische und anatomische Untersuchungen polarisationssensitiver Neurone durchgeführt. Hierbei wurden auf beinahe allen Ebenen der Polarisationssehbahn im Heuschreckegehirn Studien durchgeführt. Die vorliegende Arbeit ist in vier Kapitel gegliedert, deren Inhalt im Folgenden zusammengefasst ist.

Kapitel 1: A Distinct Layer of the Medulla Integrates Sky Compass Signals in the Brain of an Insect

Wie bereits erwähnt, kombinieren Neurone des anterioren optischen Tuberkels Polarisationssignale mit spektralen unpolarisierten Lichtreizen, die entsprechend des Farbgradienten des Himmels auf UV und Grünlicht gegensätzlich reagieren. Im Zenit ist der Winkelabstand zwischen *E*-Vektor und dem solaren Azimut 90° und unabhängig von der solaren Elevation (Abbildung 1B, violette Pfeile). In allen weiteren Punkten am Himmel ändert sich die Winkelbeziehung zwischen polarisiertem Licht und Azimutinformation abhängig von der Sonnenerhebung substantiell über den Tagesverlauf (Abbildung 1B, rote Pfeile). Da die optische Achse der Fotorezeptoren der dorsalen Randregion zur kontralateralen Himmelshemisphäre gerichtet ist (Abbildung 1D, Homberg und Paech, 2002), und die Intertuberkelzellen des anterioren optischen Tuberkels nur über die ipsilaterale dorsale Randregion Signale erhalten (Pfeiffer et al., 2005), sollte demnach die Winkelbeziehung zwischen polarisiertem Licht und Azimutrichtung abhängig von der Erhebung der Sonne sein. Weiterhin muss sich kontinuierlich über den Tagesverlauf der Winkelabstand der Vorzugsrichtungen beider Informationen zueinander ändern. Um diese Zweideutigkeit der dadurch entstehenden Signale herauszurechnen, kompensieren Interneurone des anterioren optischen Tuberkels beide Signale in einer zeitabhängigen Weise (Pfeiffer und Homberg, 2007). Somit müssen Neurone des anterioren optischen Tuberkels neben den Himmelskompassinformationen auch Zeitsignale erhalten, um so eine Zeitkompensation zwischen beiden Signalen zu gewährleisten.

Die Integration von Himmelskompassinformationen im optischen Lobus ist bisher kaum verstanden. Der optische Lobus gliedert sich von lateral nach median in die Lamina, die Medulla und den Lobulakomplex. Anterior zur Medulla ist weiterhin noch die akzessorische Medulla lokalisiert und auf der Lamina und Medulla sitzen jeweils dorsal die bereits beschriebenen dorsalen Randregionen auf. Sowohl Lamina, als auch Medulla sind retinotop organisiert, wobei letztere insgesamt aus zehn Schichten besteht.

Um die Integration und Kombination polarisierter und unpolarisierter Lichtsignale in das Gehirn zu untersuchen, wurde von Neuronen der Medulla des optischen Lobus abgeleitet und gleichzeitig mit polarisiertem Licht aus dorsaler Richtung stimuliert. Zusätzlich wurde getestet, ob die Neurone auch auf unpolarisierte Lichtreize reagieren und so befähigt wären, den chromatischen Gradienten am Himmel wahrzunehmen. Hierfür wurde ein grüner und ultravioletter Lichtpunkt mit gleicher Photonenflussrate auf einer Kreisbahn mit einer Elevation von 45° um den Kopf bewegt. Um die Winkeldifferenz zwischen der Vorzugsrichtung des polarisierten Lichtes und der Azimutorientierung adäquat interpretieren zu können, wurde auf eine weitere Stimulusapparatur zurückgegriffen. Mit Hilfe dieser Apparatur konnte das polarisierte Licht entlang des links-rechts Meridians aus verschiedenen Elevationen präsentiert und somit die Ausbreitung und Orientierung des rezeptiven Feldes bestimmt werden. Zusätzlich wurden Untersuchungen durchgeführt, bei denen die okulare Dominanz der Zellen durch Abdecken jeweils eines Auges getestet wurde. Alle Neurone wurden, im Anschluss nach einer Farbstoffinjektion, histologisch und immunhistochemisch aufbereitet und ausgewählte Präparate hochaufgelöst dreidimensional rekonstruiert.

Insgesamt konnten fünf polarisationsempfindliche Neurontypen der Medulla in 57 Ableitungen analysiert und beschrieben werden. Von drei dieser Neurontypen wurde mehrmals in verschiedenen Experimenten abgeleitet, wodurch eine detaillierte physiologische Charakterisierung möglich wurde. Während das tangentiale intrinsische Medullaneuron 2 (TIM2) ausschließlich in der Medulla und der

dorsalen Randregion der Medulla Verzweigungen aufwies, innervierte der Neurontyp TIM1 zusätzlich noch die akzessorische Medulla. Ein ähnlicher Typ, jedoch mit zusätzlichen Verzweigungen in der Lamina, wurde als tangentiales Medulla Lamina 1 (TML1) Neuron definiert. Schließlich wurden Neurontypen charakterisiert, die eine interhemisphärische Verbindung der Medullae (MeMe) bildeten. Während der Typ MeMe1 zusätzlich im kontralateralen optischen Lobus in die akzessorische Medulla verzweigte, zeigte MeMe2 Verästelungen posterior im Zentralgehirn. Alle Neurontypen, die in mehreren Ableitungen dokumentiert wurden, zeigten jeweils eine klare Präferenz für eine bestimme *E*-Vektor Orientierung, was darauf schließen ließ, dass diese Neuronentypen als einzelne, identifizierbare Neurone in jeder Gehirnhemisphäre vorkommen.

Um zu verstehen, wie einige der Zelltypen Polarisationssignale erhalten, ohne in der dorsalen Randregion der Medulla zu verzweigen, wurden Gehirnpräparate einzelmarkierter Neurone zusätzlich geschnitten und die Gehirnschnitte mit Hilfe eines Antikörpers gegen das präsynaptische Vesikelprotein Synapsin behandelt. Dadurch war eine genaue Definition der durch die Neurone innervierten Schichten der Medulla möglich. Interessanterweise ergab die detailliert Analyse, dass alle Neurontypen entweder ausschließlich in Medullaschicht 4 (TIM1, TIM2, MeMe1) oder aber in Schicht 3 und 4 der Medulla verzweigten. Um zu untersuchen, durch welche Schicht die Transmedulla-Zellen projizieren, wurden zusätzlich Dextran-Injektionen in den anterioren optischen Tuberkel durchgeführt. Alle Transmedulla-Neurone verzweigen, ähnlich wie die abgeleiteten polarisationssensitiven Neurone in Schicht 4 der Medulla. Demnach konnte hier zum ersten Mal eine Rolle für eine bestimmte Medullaschicht im Insektengehirn nachgewiesen werden. Schicht 4 der Medulla bildet demnach eine frühe Station zur Verarbeitung von polarisiertem Licht.

Neben polarisiertem Licht reagierten alle untersuchten Neurontypen auch auf einen unpolarisierten grünen oder ultravioletten Lichtreiz, der sich um die Kopfkapsel auf einer Kreisbahn bewegte. Im Gegensatz zu den Gegenfarbzellen im anterioren optischen Tuberkel, zeigten jedoch die Neurone in dieser frühen Verarbeitungsstation auf Grün- und UV-Licht jeweils die gleiche Vorzugsrichtung.

Als nächstes wurden die rezeptiven Felder entlang des links-rechts Meridians und die okulare Dominanz der Neurone untersucht, um so Rückschlüsse auf die Winkeldifferenz der Vorzugsrichtungen zwischen *E*-Vektor Orientierung und Azimutrichtung ($\Delta\Phi_{max}$) zu ziehen. Dabei wurde untersucht, wie stark die Zellen an bestimmten Positionen des visuellen Sehfeldes sinusförmig moduliert werden. Die Experimente zeigten, dass alle Zelltypen (TIM1, MeMe1, TML1) ausschließlich vom ipsilateralen Auge Eingang erhalten und dass die Zentren der rezeptiven Felder in der kontralateralen (TIM1, MeMe1) oder ipsilateralen (TML1) Himmelshemisphäre positioniert sind. Da demnach alle Neurontypen rezeptive Felder aufwiesen, die nicht zenitzentriert sind, sollten die Neurone das Verhältnis zwischen *E*-Vektor Orientierung und Azimuttuning über den Tagesverlauf entsprechend der Sonnenelevation ausrichten (siehe Abbildung 1B). Erstaunlicherweise waren die $\Delta\Phi_{max}$-Werte der Neurone über den gesamten Tagesverlauf invariant und waren zellspezifisch unterschiedlich. Dies könnte dafür sprechen, dass die Himmelskompasssignale zeitlich unkompensiert in den optischen Lobus integriert werden, und erst in der nächsten Station der Polarisationssehbahn (anteriorer optischer Tuberkel) durch Zeitsignale justiert werden. Zusammenfassend lässt sich in diesem Kapitel schlussfolgern, dass eine bestimmte Schicht der Medulla (Schicht 4) Himmelskompassinformationen (polarisiertes Licht und chromatischer Gradient des Himmels) tageszeitunabhängig miteinander kombiniert.

Kapitel 2: Receptive Field Properties and Intensity–Response Functions of Polarization-Sensitive Interneurons of the Anterior Optic Tubercle in Gregarious and Solitarious Locusts

In diesem Kapitel wurden die Neurone einer Zwischenstation der Polarisationssehbahn, dem anterioren optischen Tuberkel, detailliert physiologisch untersucht. Die Reaktion der Intertuberkelneurone LoTu1 und TuTu1 auf unpolarisierte Lichtreize, sowie deren Reaktion auf dorsal präsentiertes Licht, wurden bereits in früheren Studien charakterisiert, wobei Kenntnisse über die rezeptiven Felder der Neurone bisher fehlten. Weiterhin konnte in Studien gezeigt werden, dass es

höchstwahrscheinlich pro Gehirnhemisphäre eine LoTu1 Zelle gibt, während die TuTu1 Neurone als Paar in jeder Hemisphäre des Gehirnes vorkommen (Homberg et al., 2003). Beide Intertuberkelzellen erhalten hauptsächlich über die ipsilaterale dorsale Randregion Polarisationssignale und werden bei niedrigen Polarisationsgraden inhibiert (Pfeiffer et al., 2005; 2011). Die geringe Anzahl an Intertuberkelneuronen pro Gehirnhemisphäre deutet darauf hin, dass diese Zelltypen im anterioren optischen Tuberkel modulatorische Funktionen einnehmen. Im Gegensatz dazu kommen TuLAL1 Neurone in einer deutlich höheren Neuronenanzahl vor (Homberg et al. 2003) und spielen höchstwahrscheinlich bei der eigentlichen Prozessierung von polarisiertem Licht zu Orientierungszwecken eine Rolle. Während jedoch die Intertuberkelzellen relativ gut untersucht wurden, ist auf physiologischer Ebene über die TuLAL1-Neurone nur wenig bekannt. Aufgrund ihrer sehr dünnen Neurite sind Ableitungen dieser Zellen nur sehr schwer zu erhalten und wurden in früheren Arbeiten nur spärlich präsentiert.

Interessanterweise kommen Wüstenheuschrecken in zwei Phasen vor, die sich durch die äußere Erscheinung sowie durch ihr Verhalten stark voneinander unterscheiden. Während die gregäre Heuschreckenform tagaktiv ist und riesige Heuschreckenschwärme während ihrer Wanderperioden bildet, meidet die solitäre Heuschreckenform Kontakte zu anderen Artengenossen (außer zur Reproduktion) und migriert als einzeln lebendes Tier während der Nacht (Roffey, 1963; Waloff, 1963). Da die Untersuchungen in dieser Arbeit sowohl an gregären, als auch an solitären Heuschrecken durchgeführt wurden, konnten so zusätzlich mögliche Anpassungen des Polarisationssystems auf die verschiedenen Lebensgewohnheiten der unterschiedlichen Phasen analysiert werden.

Der anteriore optische Tuberkel bildet eine leichte Erhebung an der anterioren Oberfläche des Gehirnes, wodurch ein gezieltes Ableiten der polarisationssensitiven Neurone möglich war und insgesamt in diesem Abschnitt 113 Exprimente durchgeführt wurden. Als visueller Stimulus diente wie im vorherigen Kapitel ein rotierender Polarisationsfilter, der mittels eines Schienensystems auf einem Perimeter entlang des links-rechts Meridians verschoben werden konnte. Zusätzlich erlaubten Graufilter, die rechnergesteuert in den Strahlengang des Lichtstimulus geschoben werden konnten, ein Reduzieren der Lichtintensität in logarithmischen Stufen. In diesen Untersuchungen wurden die Zellen mit polarisiertem Blaulicht, bzw. wahlweise auch mit „weißem“ Licht stimuliert.

Entsprechend der optischen Achse der dorsalen Randregion hatten beide Intertuberkelzellen rezeptive Felder, die im Mittel ihr Zentrum bei einer Elevation von 60° in der kontralateralen Hemisphäre des Sehfelds hatten. Die Intertuberkelzellen zeigten weiterhin im Mittel ein sehr breites rezeptives Feld, was darauf schließen lässt, dass sie von einer erheblichen Anzahl an Fotorezeptorzellen Eingang erhalten. Im Gegensatz dazu waren die rezeptiven Felder der TuLAL1-Neurone deutlich enger und hatten Zentren an unterschiedlichen Positionen des Sehfeldes. Unterschiede zwischen den rezeptiven Feldern der gregären und solitären Heuschrecken konnten nicht beobachtet werden.

Als nächstes wurden die Antworten der Intertuberkelneurone auf verschiedene Lichtintensitäten im Zentrum des rezeptiven Feldes getestet und zwischen solitären und gregären Tieren verglichen. Hierbei wurde die Stärke der Modulation, sowie die Gerichtetheit der Zellantworten (wie die Aktionspotentiale um Φ_{max} konzentriert sind) bei unterschiedlichen Lichtintensitäten getestet. Die Intensitäts/Antwort-Kurven zeigten, dass es weder bei LoTu1, noch bei TuTu1-Zellen einen Unterschied im Antwortverhalten zwischen beiden Heuschreckenformen gibt.

Interessanterweise zeigte sich jedoch, dass sich die Modulationsstärke der LoTu1-Zelle bei jeder Lichtintensitätsstufe des polarisierten Lichtes graduell änderte, während TuTu1- und TuLAL1-Zellen bis zu einer bestimmten Intensitätsschwelle intensitätsunabhängig reagierten. Weitere Analysen zeigten, dass die LoTu1-Zelle im Gegensatz zu den anderen Tuberkelneuronen nachts mit einer deutlich höheren Reaktionsstärke und einer erhöhten Gerichtetheit auf polarisiertes Licht reagierte. Überdies wurde die LoTu1-Zelle bei Stimulation mit sehr hellem „weißen“ polarisierten Licht inhibiert, während die TuTu1-Zelle intensitätsunabhängig die gleiche Modulationsstärke zeigte wie bei niedrigeren Intensitäten.

Zusammenfassend konnte demnach in diesem Kapitel gezeigt werden, dass es keinen Unterschied zwischen solitären und gregären Heuschrecken bezüglich der Detektion von polarisiertem Licht in Neuronen des anterioren optischen Tuberkels gibt. Dies könnte darauf schließen lassen, dass solitäre Tiere andere Navigationshinweise bei Nacht zur Orientierung nutzen müssten. Weiterhin deuten die

Daten darauf hin, dass die LoTu1-Zelle eine spezielle Funktion im neuronalen Netzwerk des anterioren optischen Tuberkels hat, die abhängig von der Lichtintensität ist. Da am blauen Himmel sowohl der Polarisationsgrad, als auch die Lichtintensität abhängig von der Sonnenelevation sind, und sich demnach über den Tagesverlauf ändern, wäre die LoTu1 Zelle ein idealer Kandidat, um eine zeitabhängige, modulatorische Funktion im Tuberkel einzunehmen. So könnte LoTu1 die Neurone des Tuberkels mit Zeitsignalen beliefern oder zeitlich die Sensitivität der TuLAL1-Neurone modulieren.

Kapitel 3: Evidence for the Possible Existence of a Second Polarization-Vision Pathway in the Locust Brain

Die Wüstenheuschrecke ist vor allem für ihre Wanderungen über lange Distanzen bekannt. Um dabei über den Tag eine konstante Flugrichtung zu gewährleisten, ist es essentiell, dass die Tiere Kenntnis über die Tageszeit besitzen, um die tagesperiodische Wanderung der Sonne und damit des Himmelspolmusters bei der Richtungsbestimmung berücksichtigen zu können. Neueste Experimente zeigen, dass absteigende polarisationssensitive Neurone aus dem Gehirn der Heuschrecke über den Tagesverlauf Änderungen im *E*-Vektor-Tuning zeigen, die darauf schließen lassen, dass die Neurone zeitkompensierte Signale zu den Thorakalganglien senden (Träger und Homberg, 2011). Somit scheint die Heuschrecke einen zeitkompensierten inneren Kompass zu nutzen, um eine stabile Wanderungsrichtung zu gewährleisten. Wie jedoch Zeitinformation in das System integriert wird, ist bis jetzt noch vollkommen unerforscht. Eine entscheidende Rolle könnte hierbei die akzessorische Medulla spielen, die in Fliegen und Schaben als zirkadianes Schrittmacherzentrum die Flug- und Laufaktivität kontrolliert (Helfrich-Förster, 1998).

In diesem Kapitel wurden intrazelluläre Ableitungen an Neuronen der akzessorischen Medulla durchgeführt, sowie im posterioren optischen Tuberkel, einem kleinen Neuropil im posterioren Zentralhirn. Polarisationssensitive Neurone des Zentralkomplexes, die maßgeblich an der Etablierung der kartenähnlichen Repräsentation von *E*-Vektoren beteiligt sind (TB-Neurone), verzweigen im posterioren optischen Tuberkel extensiv und verbinden diesen mit der Protozerebralbrücke (Heinze und Homberg, 2007).

Dieses Kapitel postuliert eine zweite Polarisationssehbahn, die zum Zentralkomplex über einen posterioren Trakt Polarisationssignale transferiert. Ein bereits beschriebenes Neuron aus Kapitel 1, das tangentiale intrinsische Medulla Neuron 1 (TIM1) zeigt, dass die dorsale Randregion der Medulla mit der akzessorischen Medulla in Verbindung steht, und demnach die akzessorsiche Medulla Polarisationssignale aus der dorsalen Randregion der Medulla erhalten könnte. Weiterhin wurde ein Neuron, das aus einer früheren Arbeit bekannt ist und das die akzessorische Medulla mit dem posterioren optischen Tuberkel verbindet, dreidimensional rekonstruiert und als Kandidat vorgestellt, um Polarisationsinformation in das posteriore Zentralgehirn zu transferieren. Im posterioren optischen Tuberkel wurde zusätzlich zu den TB-Zellen ein weiterer neuartiger polarisationssensitiver Zelltyp beschrieben, der die posterioren optischen Tuberkel beider Hemisphären miteinander verbindet. Da sowohl in der akzessorischen Medulla, als auch im posterioren optischen Tuberkel polarisationssensitive Zellen vorkommen, liegt es nahe, dass auch Neurone, die beide Neuropile miteinander verbinden polarisationssensitiv sind. Demnach zieht der vorgeschlagene zweite Polarisationssignalweg durch die akzessorische Medulla, die möglicherweise, ähnlich wie bei Fliegen und Schaben eine Rolle als zirkadianes Hauptschrittmacherzentrum einnimmt. Während die anteriore Polarisationssehbahn die Orientierung relativ zur Sonne kodiert, könnte so über den zweiten Polarisationssignalweg zeitkompensierte Polarisationsinformation zum Zentralkomplex gesendet werden. Die Signale beider Polarisationssehbahnen würden in der Protozerebralbrücke konvergieren und einen zeitlich kompensierten inneren Kompass in der Protozerebralbrücke ausbilden.

Ein Problem des polarisierten Lichts als Richtungshinweis ist die Zweideutigkeit des Signals, die ein Resultat seiner 180°-Periodizität ist. Interessanterweise zeigten die Neurone, die die posterioren optischen Tuberkel interhemisphärisch miteinander verbinden, Präferenzen bezüglicher ihrer Verzweigungen im posterioren optischen Tuberkel. Während ein Neurontyp ipsilateral im dorsalen Bereich des posterioren optischen Tuberkels und im kontralateralen Tuberkel ventral verzweigte, innervierte der zweite Intertuberkel Typ den posterioren optischen Tuberkel ipsilateral im ventralen

Bereich und dorsal im kontralateralen Tuberkel. Durch eine mögliche inhibierende Funktion könnten diese Zellen durch eine Interaktion mit den TB1-Zellen eine entscheidende Rolle bei einer Etablierung einer 360° *E*-Vektorkarte in der Protozerebralbrücke spielen und so die Zweideutigkeit der Richtungsinformation des polarisierten Lichtes herausrechnen.

Kapitel 4: The Locust Standard Brain: a 3D Standard of the Central Complex as a Platform for Neural Network Analysis

Während in den Kapiteln 1-3 unter anderem physiologische Untersuchungen durchgeführt wurden, ist dieses Kapitel eine rein anatomische Studie. Fokus war die letzte Station der Polarisationssehbahn im Gehirn der Heuschrecke, der Zentralkomplex. Neben der Verarbeitung von polarisiertem Licht ist der Zentralkomplex entscheidend in eine Vielzahl von Prozessierungsvorgängen im Insektengehirn involviert. So wird ihm eine zentrale Rolle unter anderem in der Bein- und Flugkoordination des Tieres (Strauss und Heisenberg, 1993; Ilius et al., 1994), der räumlichen Orientierung (Strauss et al., 2002), sowie der Ausbildung eines Gedächtnisses für Landmarkenorientierung (Liu et al., 2006) zugesprochen. Entsprechend seiner Vielzahl an Funktionen besteht der Zentralkomplex aus einer großen Zahl an Neurontypen. Mindestens 13 Zelltypen sind beispielsweise allein in die Verarbeitung von polarisiertem Licht involviert.

Um einen tieferen Einblick in die Verarbeitungsprozesse des Zentralkomplexes zu erhalten, ist ein fundiertes Wissen über die synaptische Verknüpfung der einzelnen Zellen erforderlich. Ziel der Arbeit war es, einzelne Neurone aus verschiedenen Gehirnpräparaten gleichzeitig in einem standardisierten Zentralkomplex darzustellen, um so mögliche Verschaltungen zwischen diesen Neuronen auf anatomischer Ebene zu untersuchen.

Bezüglich der Verarbeitung des polarisierten Lichtes ist vor allem ein Neurontyp, die CPU-Zellen, von besonderer Bedeutung: Sie bilden den Ausgang aus dem Zentralkomplex, und zeigen eine sehr hohe Hintergrundvariabilität, was sich als eine mögliche Multimodalität dieses Zelltyps deuten lässt. Weiterhin besitzen CPU-Neurone in zwei Untereinheiten des Zentralkomplexes Verzweigungsbäume, in welchen sie höchstwahrscheinlich synaptischen Eingang erhalten. Während sie in der Protozerebralbrücke sehr wahrscheinlich Polarisationssignale erhalten, könnte über den weiteren Informationseingang in der oberen Einheit des Zentralkörpers unpolarisierte Information integriert werden. Interessanterweise hat eine weitere Zelle, das „Giant fan-shaped“ (GFS)- Neuron synaptische Ausgangsregionen in der oberen Einheit des Zentralkörpers. In einer Studie konnte gezeigt werden, dass das GFS-Neuron im Flug eine höhere Aktivität aufweist und auf Bewegungsreize im ipsilateralen Sehfeld reagiert (Homberg, 1994). Demnach könnte das GFS-Neuron die CPU-Zelle kontextabhängig modulieren und so den Polarisationsinformationsgehalt der CPU-Zelle je nach Kontext erhöhen oder verringern.

Um die mögliche Verbindung beider Zellen zu untersuchen, und um generell die Verarbeitung von Information im Zentralkomplex studieren zu können, wurde im ersten Teil der Arbeit ein standardisierter Atlas des Zentralkomplexes erzeugt. 20 individuelle Zentralkomplexe wurden aus Schnittpräparaten nach immunhistochemischer Aufbereitung aus Graubilddatenstapeln jeweils hochaufgelöst dreidimensional rekonstruiert. Mittels eines Linuxclusters wurde basierend auf den individuellen Graubilddatenstapeln ein Standardgraubilddatenstapel des Zentralkomplexes erzeugt. Durch die Übertragung der Transformations- und Deformationsparameter auf die entsprechenden dreidimensional rekonstruierten 20 Zentralkomplexe konnte ein virtueller dreidimensionaler Standardatlas des Zentralkomplexes generiert werden.

Als nächstes wurden in unterschiedlichen Gehirnpräparaten ein CPU-Neuron, sowie die GFS-Zelle hochaufgelöst dreidimensional rekonstruiert und in den standardisierten dreidimensionalen Zentralkomplexatlas registriert. Die gleichzeitige Visualisierung beider Neurone im Zentralkomplex-Standardatlas zeigte eine Überlappung der Verzweigungen beider Neurone in einer Schicht der oberen Einheit des Zentralkörpers. Somit konnte gezeigt werden, dass das GFS-Neuron ein guter Kandidat ist, um die Polarisationsinformation der CPU-Zelle kontextabhängig zu modulieren.

Referenzen

Brunner D, Labhart T (1987) Behavioural evidence for polarization vision in crickets. *Physiol Entomol* 12: 1-10.

Helfrich-Förster C, Stengl M, Homberg U (1998) Organization of the circadian system in insects. *Chronobiol Int* 15: 567-594.

Heinze S, Homberg U (2007) Maplike representation of celestial *E*-vector orientations in the brain of an insect. *Science* 315: 995-997.

Heinze S, Reppert SM (2011) Sun compass integration of skylight cues in migratory monarch butterflies. *Neuron* 69: 345-358.

Homberg U (1994) Flight-correlated activity changes in neurons of the lateral accessory lobes in the brain of the locust *Schistocerca gregaria*. *J Comp Physiol A* 175: 597-610.

Homberg U (2004) In search of the sky compass in the insect brain. *Naturwissenschaften* 91: 199-208.

Homberg U, Hofer S, Pfeiffer K, Gebhardt S (2003) Organization and neural connections of the anterior optic tubercle in the brain of the locust, *Schistocerca gregaria*. *J Comp Neurol* 462: 415-430.

Homberg U, Paech A (2002) Ultrastructure and orientation of ommatidia in the dorsal rim area of the locust compound eye. *Arthropod Struct Dev* 30: 271-280.

Ilius M, Wolf R, Heisenberg M (1994) The central complex of *Drosophila melanogaster* is involved in flight control: studies on mutants and mosaics of the gene ellipsoid body open. *J Neurogenet* 9: 189-206.

Kinoshita M, Pfeiffer K, Homberg U (2007) Spectral properties of identified polarized-light sensitive interneurons in the brain of the desert locust *Schistocerca gregaria*. *J Exp Biol* 210: 1350-1361.

Labhart T (1988) Polarization-opponent interneurons in the insect visual system. *Nature* 331: 435-437.

Labhart T, Meyer EP (1999) Detectors for polarized skylight in insects: a survey of ommatidial specializations in the dorsal rim area of the compound eye. *Microsc Res Tech* 47: 368-379.

Liu G, Seiler H, Wen A, Zars T, Ito K, Wolf R, Heisenberg M, Liu L (2006) Distinct memory traces for two visual features in the *Drosophila* brain. *Nature* 439: 551-556.

Mappes M, Homberg U (2004) Behavioral analysis of polarization vision in tethered flying locusts. *J Comp Physiol A* 190: 61-68.

Pfeiffer K, Homberg U (2007) Coding of azimuthal directions via time-compensated combination of celestial compass cues. *Curr Biol* 17: 960-965.

Pfeiffer K, Kinoshita M, Homberg U (2005) Polarization-sensitive and light-sensitive neurons in two parallel pathways passing through the anterior optic tubercle in the locust brain. *J Neurophysiol* 94: 3903-3915.

Pfeiffer K, Negrello M, Homberg U (2011) Conditional perception under stimulus ambiguity: Polarization-and azimuth-sensitive neurons in the locust brain are inhibited by low degrees of polarization. *J Neurophysiol* 105: 28-35.

Roffey J (1963) Observations on night flight in the desert locust (*Schistocerca gregaria* Forskål). *Anti-Locust Bulletin* 39: 1-32.

Strauss R (2002) The central complex and the genetic dissection of locomotor behaviour. *Curr Opin Neurobiol* 12: 633-638.

Strauss R, Heisenberg M (1993) A higher control center of locomotor behavior in the *Drosophila* brain. *J Neurosci* 13: 1852-1861.

Träger U, Homberg U (2011) Polarization-sensitive descending neurons in the locust: connecting the brain to thoracic ganglia. *J Neurosci* 31: 2238-2247.

Träger U, Wagner R, Bausenwein B, Homberg U (2008) A novel type of microglomerular synaptic complex in the polarization vision pathway of the locust brain. *J Comp Neurol* 506: 288-300.

von Frisch K (1949) Die Polarisation des Himmelslichtes als orientierender Faktor bei den Tänzen der Bienen. *Experientia* 5: 142 - 148.

Waloff Z (1963) Field studies on solitary and transiens desert locusts in the Red Sea area. *Anti-Locust Bulletin* 40: 1-91.

Wehner R (2003) Desert ant navigation: how miniature brains solve complex tasks. *J Comp Physiol A* 189: 579-588.

Introduction

Animal Navigation

An indispensable necessity for the survival of animals is their ability to evade or approach distinct stimuli. Crayfish respond to a frightening external stimulus with a knee-jerk like tail flip as escape reaction to veer away from a danger zone (Wine and Hagiwara, 1977). Many moths are attracted to potential mating partners or suitable host plants via odor gradients (Jacobson, 1966; Hansson, 1995). In contrast to this relative simple taxis, the ability of navigation is a common phenomenon of many animals that requires more complex neural processing procedures. Birds that migrate from breeding places to overwintering habitats are a prime example of such navigational feats. Other examples include sea turtles that are able to return through long distances to the hatching beach were they were born or fruit bats that are able to home in on their preferred individual feeding tree in a straight line (Tsoar et al., 2011).

Navigation means the calculation of the own geographical position, evaluation of the ideal route and distance to a distinct target and based on these, the active determination of a travel route. Furthermore, it implies the active movement towards the place of destination with a constant update of the moving direction and the orientation of the animal relative to the target site (Collett and Collett, 2000). Beside these, navigation requires also a pronounced spatial memory or in some seasonal migrating animals like birds a genetical determination of the direction and distance of the migration route.

Although insect brains are small in comparison to those of vertebrates, some species show astonishing navigational abilities. Homing ants or honeybees are able to determine optimal routes back to their nest (Wehner, 1992). Monarch butterflies seasonally migrate from the USA to their winter habitats in central Mexico, covering thousands of kilometers (Brower, 1995). To execute these navigational and orientational behaviors, insects use two basic mechanisms: In familiar terrains, landmarks are used as references to evaluate the target direction, while in unfamiliar regions compass signals of the sky have an increased relevance as navigational clue.

Sky Compass Signals

Directional information provided by the sky offers a precise reference for insects to ideally navigate in terrains where landmarks are rarely available or during long distance migrations. At daytime, solar compass signals can be used as accurate directional cues to determine the moving route. The position of the sun is defined by the sun azimuth and the solar elevation. However, due to the earth's rotation and tilt, the position of the sun in the sky is strongly dependent on the season, the time of day and the geographical location on earth. Therefore, for a role of the sun as adequate navigational clue, knowledge about these three aspects is crucial.

In addition to the direct view of the sun, the natural daylight sky offers several major compass signals by which animals are able to define the position of the sun. Sunlight scattering through atmospheric constituents (gas molecules, aerosol particles) produces characteristic patterns of intensity and chromatic gradients as well as a pattern of skylight polarization in the sky, which can be described by the Rayleigh scattering model (Strutt, 1871; Coulson, 1988).

The celestial intensity gradient results from a higher amount of scattered solar light in the direction of the sun. This gives rise to an anisotropic radiance distribution with higher intensity of light in the vicinity of the sun compared to the antisolar hemisphere (Coemans et al., 1994).

Furthermore, while light of short wavelengths (300-460 nm) exhibits a relatively homogeneous distribution in the blue sky, the intensity of longer wavelength light (460-700 nm) is higher in the solar hemisphere. This aspect induces a spectral gradient in the blue sky in which the ratio between light of longer wavelengths and light of shorter wavelengths is higher in the solar hemisphere than in the opposite sky hemisphere (Coemans et al., 1994).

Finally, a pattern of partly polarized light occurs at the sky. Sunlight can be described as a transversal wave, which means that electric fields (*E*-vectors) oscillate perpendicular to the direction of the beam of sun light. Solar radiation that enters the atmosphere oscillates in all possible directions, thus showing a random orientation of electric fields and no polarization. While sunlight that scatters at atmospheric molecules in an orientation unequal 90° remains unpolarized, light that is scattered in perpendicular directions becomes polarized and, in contrast to unpolarized light, *E*-vectors then oscillate only in one orientation. Thereby, a characteristic polarization pattern arises at the clear sky in which the *E*-vectors are arranged tangentially in circles around the sun (Strutt, 1871; Wehner, 2001). The degree of polarization increases from 0% (unpolarized sunlight) in the vicinity of the sun to a maximum of 75% under optimal conditions at an angular distance of 90° from the sun (Coulson, 1988; Brines and Gould, 1982). Thus both, the *E*-vector orientation and the degree of polarization at a distinct celestial point are strongly dependent on the solar elevation and, thus, on the time of day.

At night, the moon is the brightest spot in the sky and serves as celestial reference object for spatial orientation and navigation for nocturnal insects (Jander, 1957; Warrant and Dacke, 2010). Similar to sun-related compass signals at daytime, a lunar intensity and color gradient are generated in the sky and a polarization pattern can be observed around the moon (Horváth and Varjú, 2004). However, these night sky compass signals are considerably dimmer than the corresponding cues at daylight and accordingly require specializations of the visual system of the insects (Warrant and Dacke, 2011; Dacke et al., 2011).

Insect Navigation via Sky Compass Signals

Behavioral evidences for the utilization of the intensity and/or color gradient of the sky as cues to calculate the solar position in insect are rare. Experiments on ants which were not able to see the sun or to orientate by means of celestial polarization patterns showed that the animals were still able to navigate homeward by using the chromatic contrast and/or the intensity gradient of the sky (Wehner, 1997). Experiments in bees, likewise, suggest that they use the color gradient of the sky as compass signal. Bees interpreted long wavelength light as the direction towards the sun, while UV light was construed as the antisolar hemisphere (Edrich et al., 1979; Brines and Gould, 1979; Rossel and Wehner, 1984). Apart from insects, recent studies on sandhoppers (Crustacea, Arthropoda) clearly revealed the use of the skylight intensity gradient as sky compass cue (Ugolini et al., 2009).

In contrast to the analysis of the orientation of insects to celestial intensity and color signals, the detection and utilization of polarized light signals has been studied extensively. First, von Frisch (1949) observed that the dancing direction of honey bees at the nest entrance changed when the *E*-vector orientation of the sky was manipulated with a polarization filter. Following experiments showed that ants, dung beetles and monarch butterflies also use polarization signals of the sky as orientational cues during migration or homing (Wehner, 2003: Dacke et al., 2003a; Reppert et al., 2004).

Perception of Celestial Polarized Light

Common to all insects that use polarized light within the context of navigation is a specialized dorsal area of the compound eye, termed the dorsal rim area (DRA) (Labhart and Meyer, 1999; Stalleicken et al., 2005; Dacke et al., 2003b). The DRAs optical axis is oriented toward the sky and their ommatidia house photoreceptors which are highly adapted to detect polarized light signals: they are well-aligned, non-twisted and homochromatic to avoid bleeding with the color vision of the main retina. To further reduce self-screening effects, the rhabdomers of the photoreceptors are shorter than those in the main compound eye. In addition, in each ommatidium, photoreceptor microvilli are arranged orthogonally, representing two perpendicularly oriented polarization analyzers. Finally, screening pigments between the ommatidia are reduced, which leads to decreased optics of the DRA while simultaneously the visual fields are advantageously increased (Labhart and Meyer, 1999: Homberg, 2004; Homberg et al., 2011).

In addition to the above mentioned insects, in other insect species, including flies (von

Philipsborn and Labhart, 1990) and crickets (Brunner and Labhart, 1987), a polarotactic behavior was observed when presenting polarized light from above. Thus, a broad taxonomic range of insects is able to use polarized light of the sky as reference for spatial orientation.

The Desert Locust *Schistocerca gregaria*

Desert locusts are well-known for forming huge swarms consisting of millions of animals and their long-range migrations throughout North Africa and the Middle East. Experiments on tethered flying locusts showed that the animals respond with a 180°-periodicity of yaw-torque to a dorsally rotating polarizer. This suggests that locusts are able to use celestial polarized light as navigational cue (Mappes and Homberg, 2004).

Like other locust species, the desert locust *S. gregaria* occurs in two phases, a gregarious and a solitarious form. At high population densities, locusts aggregate in flying swarms of gregarious locusts while at lower abundances, animals avoid each other and migrate as individuals (solitarious locusts). Recent experiments showed that the transformation from the solitarious to the gregarious form is dependent on the population density and is mediated by the level of serotonin in the thoracic ganglia (Anstey et al., 2009). Both locust phases show considerable differences in their appearance and their behavior (Uvarov, 1966, Simpson et al., 1999). Furthermore, while locusts of the gregarious phase are diurnal, solitary specimen prefer to migrate during the night (Waloff, 1963; Roffey, 1963). This corresponds to the fact that solitarious locusts possess substantially larger eyes than gregarious animals (Rogers et al., 2010). Differences of both phases are also reflected in the size of the brain and in the proportion of brain areas involved in the processing of visual information (Ott and Rogers, 2010).

Polarization-Sensitive Interneurons & the Polarization Vision Pathway in the Locust Brain

Due to the relatively large brain size, desert locusts have been used as model organisms to analyze physiological and anatomical properties of the neural network underlying the processing of polarized light signals. In the brain, polarization-sensitive (POL) neurons innervate specific brain areas (referred to as neuropils) that specialize in the processing of polarized light information. These neuropils are connected by distinct fiber bundles and are elements of a so-called ‘polarization vision pathway’ in the locust brain (Figure 1; Homberg, 2004).

The first POL-neuron in an insect brain was described in the optic lobe of the field cricket *Gryllus campestris* (Labhart, 1988). This neuron, termed POL1 neuron, showed several characteristics during stimulation with polarized light which are typical for POL-cells. POL-neurons exhibit a sinusoidal modulation of the firing activity during stimulation with a rotating polarizer (Labhart, 1996; Labhart and Meyer, 2002). Furthermore, most POL-neurons are maximally activated at a particular preferred *E*-vector orientation (Φ_{max}) and are maximally inhibited at a perpendicular stimulus position (Φ_{min}), thus showing polarization opponent responses to polarized light (Labhart, 1988).

As in other insects, desert locusts detect polarization signals of the sky with photoreceptors located in the DRA of the compound eye (Mappes and Homberg, 2004). These photoreceptors show typical adaptations facilitating the detection of polarized light (as already mentioned above) and their axons project to distinct areas of the optic neuropils, namely the dorsal rim areas of the lamina and the medulla (Homberg and Paech, 2002). In contrast to the main lamina and medulla, both of which are retinotopically organized, for the dorsal rim areas of the lamina and medulla no evidences for a retinotopic neuroarchitecture were proven. Tracer-injections into the dorsal rim area of the medulla revealed that a fiber bundle of so-called line tangential neurons passes the medulla through one layer and projects into the central brain. The neurons arborize in the ventralmost layer of the anterior lobe of the lobula complex and finally enter a small neuropil of the central brain, the anterior optic tubercle (Homberg et al., 2003a). As a result of the small axon diameter displayed by the line tangential neurons, physiological data about these neurons could not be obtained to date.

While the anterior optic tubercle in the locust brain consists of an upper and a lower unit, ramifications of POL-neurons are restricted to the lower unit of the anterior optic tubercle

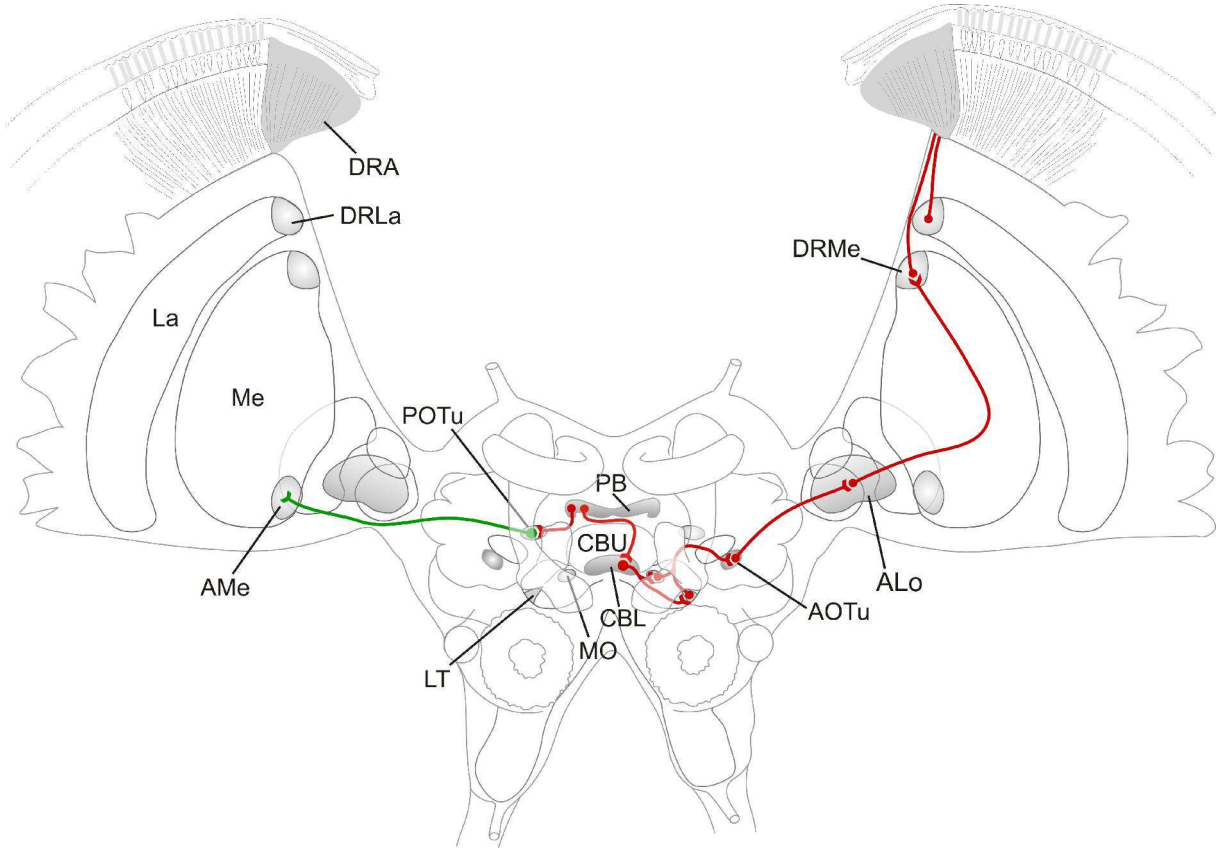

Figure 1: Frontal view of a drawing of the brain of the desert locust *Schistocerca gregaria* showing the polarization vision pathway (red). In addition, a connection between the accessory medulla *(AMe)* and the posterior optic tubercle *(POTu)* is illustrated (green). Areas that are involved in the processing of polarized light signals are highlighted in grey. *ALo* anterior lobe of the lobula complex*; AOTu* anterior optic tubercle*; CBL* lower division of the central body; CBU upper division of the central body; *DRA* dorsal rim area of the compound eye; *DRLa* dorsal rim area of the lamina; *DRMe* dorsal rim area of the medulla; *La* lamina; *LT* lateral triangle*; Me* medulla; *MO* median olive; *PB* protocerebral bridge. Adapted from Heinze (2009).

(Pfeiffer et al., 2005). Four types of POL-neurons of the anterior optic tubercle are have been characterized physiologically (Pfeiffer et al., 2005; Kinoshita et al., 2007). Two of these neurons are intertubercle neurons that establish a bilateral connection between the anterior optic tubercles of both hemispheres. The LoTu1 cell most likely occurs as a single neuron per brain hemisphere, arborizing in both anterior optic tubercles and forming additional ramifications in the anterior lobes of the lobula complexes of both hemispheres (Vitzthum et al., 2002). It is an exceptional POL-neuron because it is excited at Φ_{max} but lacked an orthogonal inhibitory input during stimulation with polarized light and thus does not show polarization opponency. In the second type of intertubercle neuron, termed TuTu1, branches are restricted to the anterior optic tubercles of both hemispheres. Most likely two TuTu1 exist per hemisphere. Both cell types, LoTu1 and TuTu1 receive polarization input only from the ipsilateral eye (Pfeiffer et al., 2005) and are inhibited at low degrees of polarized light (Pfeiffer et al., 2011). The other two neuron types, termed TuLAL1a and 1b, were analyzed only rarely. They connect the anterior optic tubercle with the next processing stage of the polarization vision pathway, the lateral accessory lobe (Homberg et al., 2003a; Pfeiffer et al., 2005).

The next stage of the polarization vision pathway is the lateral accessory lobe which consists of four subunits: The large areas of the dorsal and ventral shell as well as two distinct areas called the lateral triangle and the median olive (Homberg, 1994). The TuLAL1 neurons of the anterior optic tubercle ramify exclusively in the lateral triangle and the median olive. While arborizations of the TuLAL1a neurons are restricted to the lateral triangle, TuLAL1b cells have synaptic output in the median olive and/or the lateral triangle of the lateral accessory lobe (Homberg et al., 2003a; Pfeiffer et al., 2005).

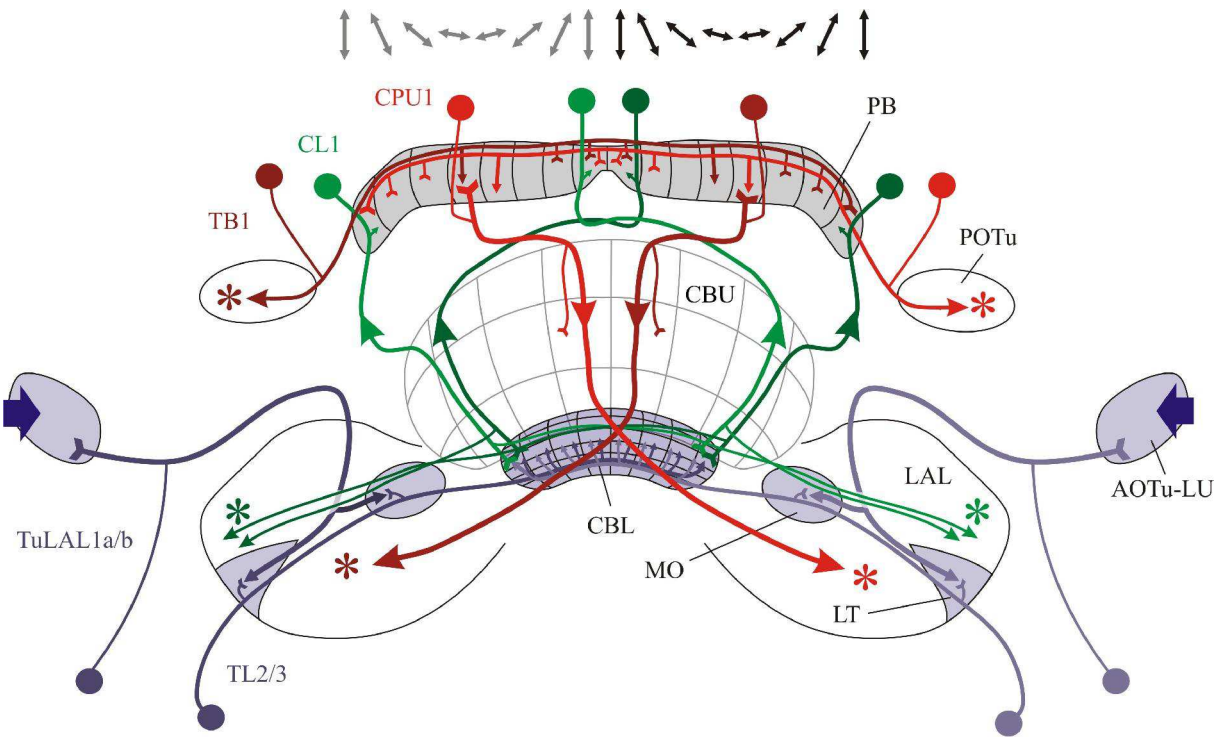

Figure 2: Proposed hypothetical model of the neural network of the central complex underlying the processing of polarized light signals. Neurons of the anterior optic tubercle and input cells of the central complex are illustrated in shades of blue, while neurons of an intermediate stage are shown in shades of green. Shades of red indicate output cells of the central complex. Polarized light signals are transferred from the lower unit of the anterior optic tubercle (AOTu-LU) to the median olive (MO) and the lateral triangle (LT) of the lateral accessory lobe (LAL) via TuLAL1a/b neurons. TL2/3 neurons transmit signals to the lower division of the central body (CBL). At the following intermediate stage, CL1 cells could send polarization information from the CBL to the protocerebral bridge (PB). For better visualization only four of the 16 CL1 cells are shown. Small axons of the CL1 cells project to small areas near the LT of LAL (green asterisks). TB1 cells and CPU1 neurons contribute to a topographic representation of *E*-vectors in the columns of the PB (shown for CPU1 neurons as double arrows above the PB). While TB1 cells provide an output from the PB to the posterior optic tubercle (POTu) (red asterisks in the POTu), CPU1 cells (only two of 16 CPU1 cells are shown) transfer signals to post-synaptic neurons in the LAL (red asterisks in the LAL). CPU1 neurons have additional synaptic input in the upper division of the central body (CBU). Taken from Homberg et al. (2011).

In the lateral triangle and median olive, the TuLAL1 neurons are connected to the input neurons TL2 and TL3 of the central complex. Again, while one type of neuron, TL2, arborizes in the lateral triangle, the TL3 cell type has synaptic input in the median olive and/or in the lateral triangle (Müller et al., 1997). Together with the TuLAL1 cells, the TL neurons of the central complex form characteristic microglomerular structures in the lateral triangle and the median olive (Träger et al., 2008).

The central complex is a group of neuropils spanning the midline of the brain. It consists of four subunits, the upper division of the central body, the lower division of the central body, the protocerebral bridge, and the paired noduli (Heinze and Homberg, 2008). Except for the noduli, all subunits of the central complex exhibit a regular neuroarchitecture of 16 linear arrays of vertical columns (Williams et al., 1975). The vertical columns of the upper and lower divisions of the central body are intersected by horizontal layers. While the upper division of the central body consists of three horizontal layers, the lower division of the central body can be divided into six layers (Homberg, 1991; Müller et al., 1997). The nodulus of each hemisphere consists of a lower and upper division, latter can further subdivided into three horizontal layers (Heinze and Homberg, 2008).

The central complex is the final stage of the polarization vision pathway and houses a large set of POL-neurons; at least 13 types of POL-cells have been identified in recent experiments (Vitzthum et al., 2002; Heinze and Homberg, 2007; 2009). Heinze et al. (2009) have analyzed the physiological properties of central-complex neurons in detail (general tuning characteristics, receptive field structures, ocular dominance), and

the authors proposed a hypothetical model, in which the transformation flow of polarized light information through the central complex is described (Figure 2). TL2 and TL3 neurons transmit polarization signals from the lateral triangle and the median olive of the lateral accessory lobe to the lower division of the central body. While TL2 neurons transfer polarized light signals only from the ipsilateral eye, TL3 cells send information from both eyes to the lower division of the central body. Thus, two parallel input pathways exist at the level of the input stage of the central complex (Heinze et al., 2009). Next, TL2 cells project signals to the CL1 cells of the contralateral hemisphere, which then project to the protocerebral bridge. In the protocererbal bridge, TB neurons that connect the central complex with a small neuropil located posteriorly in the brain (posterior optic tubercle) receive the polarization signals from CL1 neurons. Together with CP1 and CPU1 cells they contribute to a topographic representation of *E*-vectors in the columns of the protocerebral bridge (Heinze and Homberg, 2007). CPU1 cells again transfer polarized light information to the ventral shell of the lateral accessory lobe, and finally, polarized light information is sent via two types of descending neurons to thoracic motor control centers (Träger et al., 2011).

Combination & Modulation of Sky Compass Signals

In addition to the integration and processing of a single sensory signal, a major challenge for a neural network is the combination of a multiplicity of signals. As already mentioned, bees are able to detect celestial polarized light signals as well as spectral cues of the sky, but how are both sky compass signals processed and combined in the insect brain?

Kinoshita et al. (2007) analyzed the POL-interneurons of the locust anterior optic tubercle in detail and presented unpolarized light stimuli of different wavelengths and from different positions of the visual field. Surprisingly, while the interneurons were excited by light of a particular wavelength from ipsilateral direction, the cells were inhibited during stimulation with light of a different wavelength. These color opponent responses led to the idea that neurons of the anterior optic tubercle are able to respond to both, to sky polarized light signals and to celestial spectral cues. Pfeiffer and Homberg (2007) stimulated LoTu1 and TuTu1 cells with unpolarized green or UV light spots that moved around the locust head. Both cells showed color opponency and TuTu1 also an additional spatial opponency to green light: While TuTu1 neurons were excited by a green light spot in the ipsilateral field of view, they were strongly inhibited when the green light spot passed the contralateral visual field. In contrast, a circling UV light spot revealed higher activation contralaterally while in the ipsilateral field of view the neurons showed an inhibition or no effects. Intertubercle neurons of the anterior optic tubercle therefore appear to be likely candidates for calculating the azimuthal direction of the sun from the chromatic contrast, the intensity gradient and the polarization pattern of the blue sky. Combined with the sensitivity of the cells to different degrees of polarization (Pfeiffer et al., 2011), these cells are able to determine the solar azimuth as well as the solar elevation, and thus, the exact position of the sun based on sky compass signals.

Similar experiments showed that POL-cells of monarch butterflies also responded to unpolarized light stimuli (Heinze and Reppert, 2011). However, the azimuthal direction of the neurons to all analyzed wavelength was similar. Therefore, the authors suggest that for the internal navigation compass of the monarch butterfly the intensity gradient of the sky has more relevance than the spectral contrast.

In addition to the combination of sky compass signals, the modulation of navigational information in a context-dependent manner is indispensable. While neurons of earlier stages of the polarization vision pathway are most likely specialized to process solely sky compass signals, central- complex neurons have a variety of functional roles. In general, the insect central complex plays a crucial role in walking and leg coordination (Strauss and Heisenberg, 1993), flight control (Ilius et al., 1994), spatial orientation (Strauss et al., 2002), memory for visual landmarks (Liu et al., 2006) and visual place learning (Ofstad et al., 2011). Interestingly, output neurons of the central complex (CPU2 and CPU4) are conditionally polarization-sensitive and are sometimes polarization blind. Therefore, these neurons could be recruited dependent on the internal state of the insect (Heinze and Homberg, 2009). Furthermore neurons of the locust central complex show substantial changes in their firing activity during

flight (Homberg, 1994). Taken together, as a brain area that is involved in a variety of functional roles, output POL-neurons of the central complex have to modulate sky compass signals dependent on the actual behavior (walking, flying) and dependent on motivational input.

Long-term extracellular recordings from interneurons in the optic lobe of bees further showed that the sensitivity of the response strength of visual neurons is modulated over a 24 hour period (Kaiser and Steiner-Kaiser, 1983). Interneurons responded at day with an increased sensitivity than during the night. Thus, the sensitivity of the neurons might be adapted to the sleep-wakefulness rhythm of the bees and most likely is controlled by a circadian master clock.

Time-Compensation

During long distance migrations of insects celestial compass signals are useless for navigation without information about the time of day. Time signals are crucial for two mechanisms. First they are essential to combine sky compass signals precisely. As a result of the changes of the sun, the angular difference at a particular point in the sky between *E*-vector orientation of polarized light and solar azimuthal direction is different from 90° (except for points along the solar meridian) and, moreover, changes permanently throughout the day (Pfeiffer and Homberg, 2007). Accordingly, the intertubercle neurons of the anterior optic tubercle show a daytime-dependent adjustment in *E*-vector tuning suited to compensate changes in solar elevation during the day (Pfeiffer and Homberg, 2007; Homberg et al., 2011). In a similar way, interneurons in the brain of the monarch butterfly adjust the angular difference between sky compass information over the course of the day (Heinze and Reppert, 2011). Second, by using a sun compass, a constant migratory direction is only possible when diurnal changes of azimuthal directions are compensated. Experiments on bees, ants and monarch butterflies show that these animals employ a time-compensated internal sun compass during migration or homing (Lindauer, 1960; Wehner, 1992; Mouritsen and Frost, 2002). Furthermore, recent studies in the monarch butterfly suggest that circadian clocks in the antennae play a crucial role in time compensation for compass navigation (Merlin et al., 2009). In the locust brain, descending neurons show a shift of Φ_{max} of 21.5°/h throughout the day. This fits to the diurnal changes of the solar azimuth (15°/h) and suggests that descending neurons signal time-compensated spatial directions to thoracic motor circuits in the desert locust (Träger and Homberg, 2011).

The master clock of insects is most likely located in the accessory medulla. The accessory medulla is a small neuropil at the anterior edge of the medulla. Studies on flies and cockroaches suggest that the accessory medulla is an internal circadian clock of the insect brain, controlling motor activity (Helfrich-Förster et al., 1998; Homberg et al., 2003b). Although in locusts the functional role of the accessory medulla as circadian clock has not yet been shown, the striking anatomical similarities to the accessory medullae of other insects suggest that it is most likely the internal clock in the locust brain (Homberg et al., 1991). Homberg and Würden (1997) further showed a connection between the accessory medulla and the posterior optic tubercle, and thus, a possible connection to POL-neurons of the central complex. Therefore the accessory medulla could play a role in time-compensation of polarized light signals by providing time of day signals to neurons of the central complex.

Scope of this Work

A number of recent studies have explored the neural basis of sky compass orientation in locusts by focusing on the processing of polarized light signals in the brain. In contrast, (1) the mechanisms of compensation for changes of solar position over the course of the day and (2) the integration of different signals from the sky (polarization pattern, solar position, chromatic gradient) are poorly understood, particularly at the level of the optic lobe. Finally, (3) no data exist comparing the sky compass system in diurnal gregarious locusts with that of nocturnal solitarious locusts. Towards these goals, polarization-sensitive neurons at different levels of the polarization vision pathway were analyzed physiologically through intracellular recordings and anatomically by means of detailed three-dimensional reconstructions of neuronal arborizations. First, neurons of the medulla in the optic lobe were analyzed and characterized to

understand the combination and integration of sky compass information in the locust brain. These experiments showed that neurons of a distinct layer of the medulla (layer 4) integrate polarized light information from the dorsal rim area of the compound eye in the locust brain. In addition, all polarization-sensitive neurons responded also to an unpolarized green/UV light spots that moved around the locust head. Taken together, this chapter shows that neurons of medulla layer 4 combine polarized light information of the sky with azimuth-dependent unpolarized light input that might represent celestial chromatic contrast information. In the next chapter, receptive field properties and responses of neurons to different light intensity conditions were studied. These investigations focused on neurons of the anterior optic tubercle – the next processing stage of the polarization pathway – and compared the physiology of these neurons in gregarious and solitarious locusts. The data showed that both locust phases rely on the same sky navigation system, although they have strikingly different life styles. The experiments revealed novel aspects of the response characteristics of intertubercle neurons and a possible modulatory role of the LoTu1 neuron in the anterior optic tubercle in both locust phases. In the third chapter, evidence for a second polarization vision pathway in the brain is presented. This pathway connects the dorsal rim area of the medullae via the accessory medullae to the central complex and might provide time-compensated polarized light signals to the central complex. Finally, chapter four presents a standardized three-dimensional atlas of the central complex and reveals a possible connection between a particular type of polarization-sensitive columnar neuron and a neuron that is modulated during flight. This chapter illustrates how the polarization-vision network of the central complex might be modulated in a context-dependent manner.

References

Anstey ML, Rogers SM, Ott SR, Burrows M, Simpson SJ (2009) Serotonin mediates behavioral gregarization underlying swarm formation in desert locusts. *Science* 323: 627-630.

Brines ML, Gould JL (1979) Bees have rules. *Science* 206: 571-573.

Brines ML, Gould JL (1982) Skylight polarization patterns and animal orientation. *J Exp Biol* 96: 69-91.

Brower LP (1995) Understanding and misunderstanding the migration of the monarch butterfly (Nymphalidae) in North America: 1857-1995. *J Lepidopt Soc* 49: 304-385.

Brunner D, Labhart T (1987) Behavioural evidence for polarization vision in crickets. *Physiol Entomol* 12: 1-10.

Coemans M, Vos Hzn JJ, Nuboer JFW (1994) The relation between celestial colour gradients and the position of the sun, with regard to the sun compass. *Vision Res* 34: 1461-1470.

Collett TS, Collett M (2000) Path integration in insects. *Curr Opin Neurobiol* 10: 757-762.

Coulson (1988) Polarization and intensity of light in the atmosphere. Deepak, Hampton, VA.

Dacke M, Byrne MJ, Baird E, Scholtz CH, Warrant EJ (2011) How dim is dim? Precision of the celestial compass in moonlight and sunlight. *Phil Trans Royal Soc B* 366: 697-702.

Dacke M, Nilsson DE, Scholtz CH, Byrne M, Warrant EJ (2003a) Animal behaviour: insect orientation to polarized moonlight. *Nature* 424: 33.

Dacke M, Nordström P, Scholtz CH (2003b) Twilight orientation to polarised light in the crepuscular dung beetle *Scarabaeus zambesianus*. *J Exp Biol* 206: 1535-1543.

Edrich W, Neumeyer C, von Helversen O (1979) “Anti-sun orientation” of bees with regard to a field of ultraviolet light. *J Comp Physiol A* 134: 151-157.

Hansson BS (1995) Olfaction in Lepidoptera. *Experientia* 51: 1003-1027.

Heinze S (2009) Characterization of polarization sensitive neurons of the central complex in the brain of the desert locust (*Schistocerca gregaria*). PhD-thesis, University of Marburg.

Heinze S, Gotthardt S, Homberg U (2009) Transformation of polarized light information in the central complex of the locust. *J Neurosci* 29: 11783-11793.

Heinze S, Homberg U (2007) Maplike representation of celestial *E*-vector orientations in the brain of an insect. *Science* 315: 995-997.

Heinze S, Homberg U (2008) Neuroarchitecture of the central complex of the desert locust: intrinsic and columnar neurons. *J Comp Neurol* 511: 454-478.

Heinze S, Homberg U (2009) Linking the input to the output: new sets of neurons complement the polarization vision network in the locust central complex. *J Neurosci* 29: 4911-4921.

Heinze S, Reppert SM (2011) Sun compass integration of skylight cues in migratory monarch butterflies. *Neuron* 69: 345-358.

Helfrich-Förster C, Stengl M, Homberg U (1998) Organization of the circadian system in insects. *Chronobiol Int* 15: 567-594.

Homberg U (1991) Neuroarchitecture of the central complex in the brain of the locust *Schistocerca gregaria* and *S. americana* as revealed by serotonin immunocytochemistry. *J Comp Neurol* 303: 245-254.

Homberg U (1994) Flight-correlated activity changes in neurons of the lateral accessory lobes in the brain of the locust *Schistocerca gregaria*. *J Comp Physiol A* 175: 597-610.

Homberg U (2004) In search of the sky compass in the insect brain. *Naturwissenschaften* 91: 199-208.

Homberg U, Heinze S, Pfeiffer K, Kinoshita M, el Jundi B (2011) Central neural coding of sky polarization in insects. *Phil Trans Royal Soc B* 366: 680-687.

Homberg U, Hofer S, Pfeiffer K, Gebhardt S (2003a) Organization and neural connections of the anterior optic tubercle in the brain of the locust, *Schistocerca gregaria*. *J Comp Neurol* 462: 415-430.

Homberg U, Paech A (2002) Ultrastructure and orientation of ommatidia in the dorsal rim area of the locust compound eye. *Arthropod Struct Dev* 30: 271-280.

Homberg U, Reischig T, Stengl M (2003b) Neural organization of the circadian system of the cockroach *Leucophaea maderae*. *Chronobiol Int* 20: 577-591.

Homberg U, Würden S (1997) Movement-sensitive, polarization-sensitive, and light-sensitive neurons of the medulla and accessory medulla of the locust, *Schistocerca gregaria*. *J Comp Neurol* 386: 329-346.

Homberg U, Würden S, Dircksen H, Rao KR (1991) Comparative anatomy of pigment-dispersing hormone-immunoreactive neurons in the brain of orthopteroid insects. *Cell Tissue Res* 266: 343-357.

Horváth G, Varjú D (2004) Polarized light in animal vision: polarization patterns in nature. Springer, Berlin.

Ilius M, Wolf R, Heisenberg M (1994) The central complex of *Drosophila melanogaster* is involved in flight control: studies on mutants and mosaics of the gene ellipsoid body open. *J Neurogenet* 9: 189-206.

Jacobson M (1966) Chemical insects attractants and repellents. *Annu Rev Entomol* 11: 403-422.

Jander R (1957) Die optische Richtungsorientierung der Roten Waldameise (*Formica rufa*). *Z Vergl Physiol* 40: 162-238.

Kaiser W, Steiner-Kaiser J (1983) Neuronal correlates of sleep, wakefulness and arousal in a diurnal insect. *Nature* 301: 707-709.

Kinoshita M, Pfeiffer K, Homberg U (2007) Spectral properties of identified polarized-light sensitive interneurons in the brain of the desert locust *Schistocerca gregaria*. *J Exp Biol* 210: 1350-1361.

Labhart T (1988) Polarization-opponent interneurons in the insect visual system. *Nature* 331: 435-437.

Labhart T (1996) How polarization-sensitive interneurones of crickets perform at low degrees of polarization. *J Exp Biol* 199: 1467-1475.

Labhart T, Meyer EP (1999) Detectors for polarized skylight in insects: a survey of ommatidial specializations in the dorsal rim area of the compound eye. *Microsc Res Tech* 47: 368-379.

Labhart T, Meyer EP (2002) Neural mechanisms in insect navigation: polarization compass and odometer. *Curr Opin Neurobiol* 12: 707-714.

Lindauer M (1960) Time-compensated sun orientation in bees. *Cold Spring Harbor Symp Quant Biol* 25: 371-377.

Liu G, Seiler H, Wen A, Zars T, Ito K, Wolf R, Heisenberg M, Liu L (2006) Distinct memory traces for two visual features in the *Drosophila* brain. *Nature* 439: 551-556.

Mappes M, Homberg U (2004) Behavioral analysis of

polarization vision in tethered flying locusts. *J Comp Physiol A* 190: 61-68.

Merlin C, Gegear RJ, Reppert SM (2009) Antennal circadian clocks coordinate sun compass orientation in migratory monarch butterflies. *Science* 325: 1700-1704.

Mouritsen H, Frost BJ (2002) Virtual migration in tethered flying monarch butterflies reveals their orientation mechanisms. *Proc Natl Acad Sci U S A* 99: 10162-10166.

Müller M, Homberg U, Kühn A (1997) Neuroarchitecture of the lower division of the central body in the brain of the locust (*Schistocerca gregaria*). *Cell Tissue Res* 288: 159-176.

Ofstad TA, Zuker CS, Reiser MB (2011) Visual place learning in *Drosophila melanogaster*. *Nature* 474: 204-207.

Ott SR, Rogers SM (2010) Gregarious desert locusts have substantially larger brains with altered proportions compared with the solitarious phase. *Proc R Soc Lond B* 277: 3087-3096.

Pfeiffer K, Homberg U (2007) Coding of azimuthal directions via time-compensated combination of celestial compass cues. *Curr Biol* 17: 960-965.

Pfeiffer K, Kinoshita M, Homberg U (2005) Polarization-sensitive and light-sensitive neurons in two parallel pathways passing through the anterior optic tubercle in the locust brain. *J Neurophysiol* 94: 3903-3915.

Pfeiffer K, Negrello M, Homberg U (2011) Conditional perception under stimulus ambiguity: Polarization-and azimuth-sensitive neurons in the locust brain are inhibited by low degrees of polarization. *J Neurophysiol* 105: 28-35.

Reppert SM, Zhu H, White RH (2004) Polarized light helps monarch butterflies navigate. *Curr Biol* 14: 155-158.

Roffey J (1963) Observations on night flight in the desert locust (*Schistocerca gregaria* Forskål). *Anti-Locust Bulletin* 39: 1-32.

Rogers SM, Harston GWJ, Kilburn-Toppin F, Matheson T, Burrows M, Gabbiani F, Krapp HG (2010) Spatiotemporal receptive field properties of a looming-sensitive neuron in solitarious and gregarious phases of the desert locust. *J Neurophysiol* 103: 779-792.

Rossel S, Wehner R (1984) Celestial orientation in bees: the use of spectral cues. *J Comp Physiol A* 155: 605-613.

Simpson S, McCaffery A, Hägele BF (1999) A behavioural analysis of phase change in the desert locust. *Biol Rev* 74: 461-480.

Stalleicken J, Mukhida M, Labhart T, Wehner R, Frost B, Mouritsen H (2005) Do monarch butterflies use polarized skylight for migratory orientation? *J Exp Biol* 208: 2399-2408.

Strauss R (2002) The central complex and the genetic dissection of locomotor behaviour. *Curr Opin Neurobiol* 12: 633-638.

Strauss R, Heisenberg M (1993) A higher control center of locomotor behavior in the *Drosophila* brain. *J Neurosci* 13: 1852-1861.

Strutt JW (1871) On the light from the sky, its polarization and color. *Phil Mag* 41: 274-279.

Träger U, Homberg U (2011) Polarization-sensitive descending neurons in the locust: connecting the brain to thoracic ganglia. *J Neurosci* 31: 2238-2247.

Träger U, Wagner R, Bausenwein B, Homberg U (2008) A novel type of microglomerular synaptic complex in the polarization vision pathway of the locust brain. *J Comp Neurol* 506: 288-300.

Tsoar A, Nathan R, Bartan Y, Vyssotski A, Dell'Omo G, Ulanovsky N (2011) Large-scale navigational map in a mammal. *Proc Natl Acad Sci U S A* 108: E718-E724.

Ugolini A, Galanti G, Mercatelli L (2009) Difference in skylight intensity is a new celestial cue for sandhopper orientation (Amphipoda, Talitridae). *Animal Behav* 77: 171-175.

Uvarov B (1966) Grasshoppers and locusts. A handbook of general acridology. Cambridge, Cambridge UP.

Vitzthum H, Müller M, Homberg U (2002) Neurons of the central complex of the locust *Schistocerca gregaria* are sensitive to polarized light. *J Neurosci* 22: 1114-1125.

von Frisch K (1949) Die Polarisation des Himmelslichtes als orientierender Faktor bei den Tänzen der Bienen. *Experientia* 5: 142 - 148.

von Philipsborn A, Labhart T (1990) A behavioural study of polarization vision in the fly, *Musca domestica*. *J Comp Physiol A* 167: 737 - 743.

Waloff Z (1963) Field studies on solitary and transiens desert locusts in the Red Sea area. *Anti-Locust Bulletin* 40: 1-91.

Warrant E, Dacke M (2010) Visual orientation and navigation in nocturnal arthropods. *Brain Behav Evol* 75: 156-173.

Warrant E, Dacke M (2011) Vision and visual navigation in nocturnal insects. *Annu Rev Entomol* 56: 239-254.

Wehner R (1992) Arthropods. In: Papi, F. (Ed.), Animal homing. Chapman and Hall, London, pp. 45-144.

Wehner R (1997) The ant's celestial compass system: spectral and polarization channels. Basel, Birkhäuser.

Wehner R (2001) Polarization vision – a uniform sensory capacity? *J Exp Biol* 204: 2589-2596.

Wehner R (2003) Desert ant navigation: how miniature brains solve complex tasks. *J Comp Physiol A* 189: 579-588.

Williams JLD (1975) Anatomical studies of the insect central nervous system: a ground-plan of the midbrain and an introduction to the central complex in the locust, *Schistocerca gregaria* (Orthoptera). *J Zool* 176: 67-86.

Wine JJ, Hagiwara G (1977) Crayfish escape behavior. *J Comp Physiol A* 121: 145-172.

A Distinct Layer of the Medulla Integrates Sky Compass Signals in the Brain of an Insect

A Distinct Layer of the Medulla Integrates Sky Compass Signals in the Brain of an Insect

Basil el Jundi[1], Keram Pfeiffer[2] and Uwe Homberg[1*]

[1]Department of Biology, Animal Physiology, University of Marburg, 35032 Marburg, Germany

[2]Department of Physiology and Biophysics, Dalhousie University, Halifax, NS, B3H4R2, Canada

Abstract

Mass migration of desert locusts is a common phenomenon in North Africa and the Middle East but how these insects navigate is still poorly understood. Laboratory studies suggest that locusts are able to exploit the sky polarization pattern as a navigational cue. Like other insects, locusts detect polarized light through a specialized dorsal rim area (DRA) of the eye. Polarization signals are transmitted through the optic lobe to the anterior optic tubercle (AOTu) and, finally, to the central complex in the brain. Whereas neurons of the AOTu integrate sky polarization and chromatic cues in a daytime dependent manner, the central complex holds a topographic representation of azimuthal directions suggesting a role as an internal sky compass. To understand further the integration of sky compass cues we studied polarization-sensitive (POL) neurons in the medulla that may be intercalated between DRA photoreceptors and AOTu neurons. Five types of POL-neuron were characterized and four of these in multiple recordings. All neurons had wide arborizations in medulla layer 4 and most, additionally, in the dorsal rim area of the medulla and in the accessory medulla, the presumed circadian clock. The neurons showed type-specific orientational tuning to zenithal polarized light and azimuth tuning to unpolarized green and UV light spots. In contrast to neurons of the AOTu, we found no evidence for color opponency and daytime dependent adjustment of sky compass signals. Therefore, medulla layer 4 is a distinct stage in the integration of sky compass signals that precedes the time-compensated integration of celestial cues in the AOTu.

Funding: This work was supported by grants from the Deutsche Forschungsgemeinschaft (HO 950/16-2 and HO 950/20-1).

***Email:** homberg@biologie.uni-maburg.de

Introduction

Many insects show impressive navigational skills during homing and seasonal migrations [1,2]. The sun is often the most important directional cue. It is the brightest spot in the sky and gives rise to a characteristic pattern of polarization (Fig. 1A) and chromatic contrast across the sky. All of these features may serve as references to determine azimuthal directions [3].

Desert locusts *(Schistocerca gregaria)* migrate in huge swarms throughout North Africa and the Middle East. Behavioral experiments on tethered flying locusts suggest that they are able to perceive the plane of sky polarization [4]. Like other insects, desert locusts detect polarized light with photoreceptors located in a specialized dorsal rim area (DRA) of the compound eye [5,6]. DRA photoreceptors are specifically adapted for high polarization sensitivity and transmit polarization information to dorsal rim areas of the lamina and medulla in the optic lobe. In the brain, polarization-sensitive (POL) interneurons respond with sinusoidal modulation of firing rate during zenithal stimulation with light passing through a rotating polarizer [7,8]. Most POL-neurons are maximally excited at a particular *E*-vector orientation (Φ_{max}) and are maximally inhibited at an orthogonal orientation, termed Φ_{min} (polarization opponency).

In the locust brain, polarized light signals are processed in distinct neuropils [9]. Small field transmedulla neurons, previously termed "line tangential neurons" [9,10], ramify in the dorsal rim area of the medulla (DRMe) and transfer polarization signals via the lobula to the anterior optic tubercle (AOTu). Second-order interneurons continue from the AOTu to the lateral accessory lobe [10,11]. Signals are, finally, processed in the central complex [12], which holds a topographic representation of zenithal *E*-vectors and may, thus, act as an internal sky compass [13]. Output neurons from the central complex project again to the lateral accessory lobe [12,14] and, finally, polarization information is sent via descending neurons to thoracic motor control centers [15].

In addition to polarization signals, POL-neurons of the AOTu respond to other celestial cues such as the color and azimuth of a light spot, which might allow them to distinguish between the solar and antisolar sky hemispheres [8,16]. Moreover, these neurons show a daytime-dependent adjustment in *E*-vector tuning suited to compensate for daytime changes in solar elevation.

Whereas the neural mechanisms underlying sky compass navigation in the locust central brain have been studied in detail [8,11-13,16], neural circuits in the optic lobe that mediate integration of different orientation signals are virtually unexplored. In particular, the origin of polarization-opponency, the site of convergence of celestial compass signals, and the site and mechanism of daytime compensation for changes in solar elevation are unknown. To address these issues, we analyzed POL-neurons in the medulla of the locust optic lobe. All POL-neurons ramified in the same medulla layer, and most of them had sidebranches in the accessory medulla. Beside polarized light, neurons responded to unpolarized green or UV light spots that moved around the locust head. In contrast to neurons of the AOTu, no evidence was found for a daytime-dependent compensation of solar elevation in the responses of the neurons, suggesting that time compensation occurs at a stage between the medulla and the AOTu of the brain.

Materials and Methods

Animals and preparation

Experiments were performed on sexually mature desert locusts (*Schistocerca gregaria)*. Animals from our laboratory colony were reared under crowded conditions at 28°C in a 12 h light/dark cycle. Some locusts from this colony were raised in a greenhouse and had direct view of the sky. Experiments on the greenhouse reared animals were performed between August 26 and September 30. Animals were cold anesthetized (at least 30 min), their legs and wings were removed, and their mouthparts were closed with wax. The locusts were fixed anterior uppermost to a metal holder, and a ridge of wax was attached frontally from the mouthparts to the anterior edge of the compound eyes. After opening the head capsule, fat, trachea and muscles above the brain were removed. To reduce hemolymph pumping, the abdomen was opened posteriorly, the intestine was removed, and the abdomen was constricted with a tightly knotted thread. The brain was stabilized further by a wire platform inserted between the esophageal connectives. To facilitate electrode penetration, the neural sheath above the optic lobe was removed. During animal preparation and recording of neural activity the brain was immersed in locust saline [17]. A silver wire inserted into the hemolymph/saline in the opened head capsule was used as the reference electrode.

Electrophysiology

For intracellular recordings, sharp glass electrodes (resistance: 60-200 MΩ) were drawn from borosilicate capillaries (inner diameter: 0.75 mm; outer diameter: 1.5 mm; Hilgenberg, Malsfeld, Germany) with a Flaming/Brown horizontal puller (P-97, Sutter, Novata, CA, USA). The tips of the electrodes were filled with 4% Neurobiotin (Vector Laboratories, Burlingame, UK) in 1 M KCl and their shanks, with 1 M KCl. Neural signals were amplified (10×) with a custom-built amplifier and monitored by a custom-built audiomonitor and a digital oscilloscope (Hameg HM 205–3, Frankfurt/Main, Germany). A CED 1401 plus interface (Cambridge Electronic Design, UK) was used to sample the signals at a rate of 5 kHz. The sampled signals were stored on a computer using the software Spike2 (version 6.02; Cambridge Electronic Design). To identify the recorded neuron Neurobiotin was injected iontophoretically with constant depolarizing current (2-3 nA).

Visual stimulation

Two visual stimulus devices were used (Fig. 1B,C). The first device allowed us to test the neural responses to polarized blue light and to unpolarized chromatic light spots (Fig. 1B). Linearly polarized light from the zenith was produced by passing the light of a blue LED (Luxeon LED emitter, LXHL-BB01, 1 W, 470 nm, Philips Lumileds Lighting Company, San Jose, CA, USA) through a rotating polarizer (HNP'B, Polaroid, Cambridge, MA, USA). The angular extent of the stimulus at the locust eye was ~5.4°. The polarizer was rotated in clockwise (0°-360°) and counter clockwise (360°-0°) directions with an angular velocity of 30°/s. In addition, an unpolarized green (530 nm) or UV (350 nm) light spot produced by a xenon arc (XBO 150W, LOT-Oriel Group, Darmstadt, Germany) and passed through a light guide, interference filters, and a circular neutral density wedge moved at an elevation of about 45° around the center of the locust's head. Unpolarized light was presented through a quartz light guide (Schott Fiber Optics, Mainz, Germany). Photon flux for both stimuli was adjusted to 2.3×10^{13} photons/cm^{2}s. The angular size of the unpolarized light spot was ~3.8°, movement velocity around the head was 30°/s.

With the second stimulation device polarized blue light was presented at different elevations of the visual field to analyze the receptive field structure across the left-right meridian (Fig. 1C). Polarized blue light (450 nm, photon flux 8.1×10^{12} photons/cm^{2}s) was obtained from a xenon arc and passed through a light guide (Schölly Fiberoptic, Denzingen, Germany) and a linear polarizer (HNP'B, Polaroid, Waltham, MA, USA). The light guide and the polarization filter were attached to a perimeter that allowed us to present polarized light through the rotating polarizer from different elevations (rotational speed 30°/s, 360° clockwise and counter clockwise rotations). The angular size of the stimulus at the locust eye was ~4.7°. Ocular dominance was tested by shielding one eye from the light source with a handheld piece of cardboard during dorsal polarized light stimulation. The terms ipsilateral and contralateral stimulation are defined with respect to the position of the soma of the recorded neuron in the brain. An *E*-vector orientation of 0° was defined as being parallel to the body axis of the animal.

Immunocytochemistry

After injection of Neurobiotin into the recorded neurons, brains were dissected from the head and were fixed in a solution of 4% paraformaldehyde, 0.25%

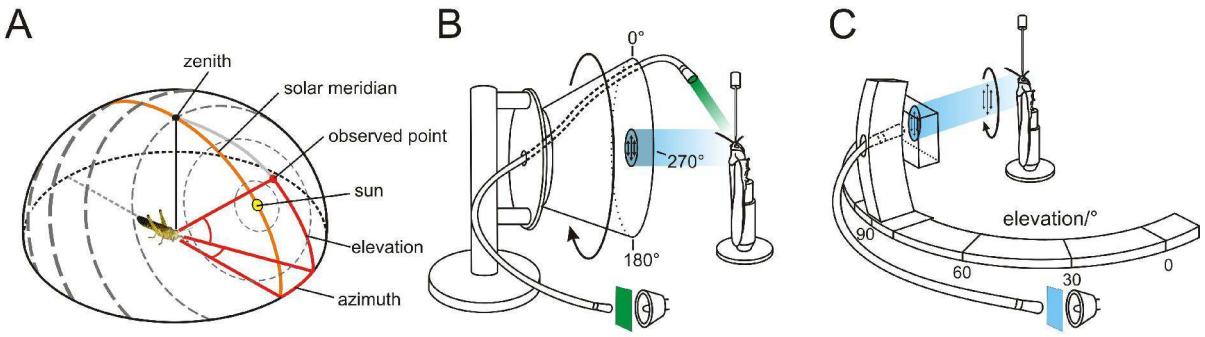

Figure 1. Experimental setups. (A) Polarization pattern of the blue sky at a solar elevation of 40°. Grey bars show *E*-vector orientation and degree of polarization (thicknesses of bars). The zenithal direction is shown as a black solid line, the solar meridian is illustrated in orange. The red spot indicates an observed point in the sky at an elevation of 45° and an azimuth of 20°. (B) Stimulus device used to analyze polarization sensitivity and azimuthal response to monochromatic unpolarized stimuli. The animal was stimulated with zenithal polarized light produced by a blue LED (470 nm) that passed a rotating polarization filter. In addition, an unpolarized green (530 nm) or UV (350 nm) light spot provided by light from a xenon lamp was moved in clockwise and counter clockwise directions around the head at an elevation of about 45°. The stimuli were presented successively during recordings from the neurons. (B) Experimental device used for measuring the bilateral extent of the receptive field across the left-right meridian. Monochromatic blue light (450 nm) provided through a light guide and a rotating polarizer was delivered from a perimeter that allowed the presentation of polarized light from different elevations along the left-right meridian.

glutaraldehyde, and 2% saturated picric acid in 0.1 M phosphate buffer (Neurobiotin fixative) overnight at 4°C. Afterwards, brains were rinsed 1 h with 0.1 M phosphate buffered saline (PBS, pH 7.4) and were then incubated for at least 3 days with streptavidin conjugated to Cy3 (1:1000; Cy3-streptavidin; Dianova, Hamburg, Germany) in 0.1 M phosphate buffered saline containing 0.3% Triton X-100 (PBT). The brains were then rinsed two times in 0.1 M PBT, followed by rinses in 0.1 M PBS and were dehydrated in an ascending ethanol series (25%-100%, 15 min each). After treatment in an ethanol/methyl salicylate (1:1, 15 min) solution, brains were cleared in methyl salicylate for 35 min and, finally, mounted in Permount (Fisher Scientific, Pittsburgh, PA, USA) between two glass coverslips. To prevent compression of the brains, ten reinforcement rings (Zweckform, Oberlaindern, Germany) were used as spacers.

For detailed anatomical analysis of selected neurons, brains were rehydrated and sectioned as described in detail by [18]. Briefly, the embedding medium was removed by incubation in xylene (2-4 h). Brains were rehydrated in a descending ethanol series and were embedded in gelatine/albumin overnight at 4°C. The brains were then sectioned in frontal plane at 130 or 250 µm with a vibrating-blade microtome (Leica VT1200 S, Leica Microsystems, Wetzlar, Germany). They were preincubated with 5% normal goat serum (NGS; Jackson ImmunoResearch ,Westgrove, PA, USA) in 0.1 M PBT overnight at 4°C and were then incubated for 6 days with a monoclonal mouse antibody against synapsin I (SYNORF1, dilution 1:50; [19]; kindly provided by Dr. E. Buchner, Würzburg) and with Cy3-streptavidin (1:1000) in 0.1 M PBT containing 1% NGS. After incubation with the secondary antibody, goat anti-mouse conjugated to Cy5 (Cy5-GAM, 1:300; Jackson ImmunoResearch, Westgrove, PA, USA) and with Cy3-streptavidin (1:1000) in 1% NGS and 0.1 M PBT for 4 d at 4°C, sections were dehydrated, cleared and embedded in Permount between two coverslips.

Tracer application

For tracing of neuronal pathways, a piece of cuticle was removed from the frontal part of the head capsule. Air sacs and trachea were removed to expose the brain. A small piece of the neural sheath above the target area was removed with forceps. Glass micropipettes were drawn from borosilicate glass and broken to a tip diameter of 10-50 µm. The tip of the pipette was dipped into petroleum jelly and then into biotinylated dextran (3000 MW, lysine fixable, Invitrogen, Eugene, OR, USA) under visual control to confirm that a few tracer crystals were attached to the petroleum jelly. The pipette was attached to a block of plasticine and was manually inserted into the target area. Residual, superficial tracer was removed by extensive rinses with locust saline. The head capsule was then closed by replacing the previously removed piece of cuticle.

For tracing of photoreceptor axons from the dorsal rim area, the cornea and crystalline cones of dorsal rim ommatidia were removed and a drop of dextran conjugated to Alexa fluor 488 (10,000 MW, anionic; fixable; Invitrogen) was applied. The eye was sealed with petroleum jelly. Animals were kept overnight at 4°C in a moist chamber to allow tracer uptake and distribution. The next day, brains were dissected out of the head capsule and were fixed in Neurobiotin fixative at 4°C overnight. Subsequently, brains were rinsed for 1 h with 0.1 M PBS at room temperature and were treated with 1mg/ml collagenase-dispase (in 0.05 Tris-HCl, pH 7.6) for 1 h. After additional rinsing with 0.1 M PBT for 2 h (6 × 20 min) the brains were preincubated (4°C, overnight) with 5% NGS in 0.1 M PBT containing 0.02 % sodium azide. Subsequently, the wholemount preparations were incubated (4-6 days at 4°C) with anti-synapsin I (1:50) and with Cy3-

streptavidin (1:1000) in 0.1 M PBT containing 1%NGS and 0.02 % sodium azide. After extensive rinsing, the brains were incubated with Cy5-GAM (1:300) and Cy3-streptavidin (1:1000) in 0.1 M PBT, 1% NGS and 0.02 % sodium azide for up to three days at 4°C. After rinsing, preparations were dehydrated, cleared and mounted in Permount.

Image acquisition, processing and 3D reconstruction

Brain sections were scanned with a confocal laser scanning microscope (CLSM, Leica TCS SP5) using a 20× (HCX PL APO 20×/0.70 Imm UV, working distance: 260 µm; Leica) or a 40× (HCX PL APO 40×/1.25 Oil UV, working distance: 100µm; Leica) oil objective. The Cy3 signal was scanned by using a DPSS (561 nm) laser and Cy5-fluorescence was detected with a HeNe (633 nm) laser. All neurons were scanned in several image stacks with a resolution of 1024 × 1024 (voxel size: 0.1-0.5 × 0.1-0.5 × 0.5-1.5 µm).

The AOTu-injected wholemount preparations were scanned at 1024 × 1024 pixel resolution with a 10× (HC PL APO 10×/0.40 Imm CS, working distance: 360, Leica) oil objective and with a voxel size of 1 × 1 × 3 µm. In addition to Cy3- and Cy5-fluorescence, the Alexa-488 signal was detected with an Ar (488nm) laser. As a result of the thickness of the wholemount preparations the brains were scanned from anterior and posterior.

The obtained image stacks were processed on a personal computer using Amira 4.1.2 or 5.2.1 software (Visage Imaging, Fürth, Germany). The procedure for aligning corresponding image stacks and the three dimensional (3D) reconstructions of brain areas based on anti-synapsin staining were described in detail in [20]. 3D reconstructions of the neurons were performed using the Amira add-on tool *SkeletonTree* generated by [21]. For the reconstruction of a neuron, corresponding image stacks were not merged but were oriented with respect to each other. The neuron was reconstructed by opening the image stacks consecutively and labeling the particular part of the neuron. Volume rendering visualization of the AOTu injected brains were displayed in Amira 4.1.2. To reduce background staining and to visualize only the region of interest in the central brain, the image stack was masked using the module 'Arithmetic'.

Data analysis

Spike trains were evaluated by a script in Spike2, written by one of the authors (KP). To study the neural response to polarized and unpolarized light, events during the 360° rotations were detected through threshold-based event detection and were assigned to the particular *E*-vector orientation during rotation of the polarizer or to the corresponding angle during circling of the unpolarized light spot. These angles were then analyzed statistically for significant difference from randomness using Oriana 2.02 software (Kovach Computing Services, Anglesey, UK). Responses of neurons to polarized light were analyzed through the Rayleigh test for axial data whereas the neural activities during stimulation with the moving unpolarized light spots were examined using the Rayleigh test for circular data. If the distribution of angles was significantly different from randomness (α=0.05) the corresponding mean angle of the distribution was defined as the preferred *E*-vector orientation (Φ_{max}) or as the preferred azimuthal direction of the neuron. The distribution of the preferred orientations of different recordings from the same neuron type was analyzed statistically using Rao's spacing test [22]. The clustering of the distribution of the preferred orientations around the averaged Φ_{max} of the neurons was analyzed through the length of the mean vector *r* (Oriana). The *r* value ranges from 0 to 1; a value closer to 1 indicates that the observations are clustered more closely around the mean Φ_{max} than with a lower value. To determine whether the mean angles of two samples differed significantly from each other, we used the Watson-Williams F-test for circular data. Mean background activities of the neurons were measured by spike counts during time periods of the recordings without stimulation and current injection. The mean frequency during stimulation was visualized using a moving average algorithm (bin size: 1s).

To quantify and compare the neural response strength at different elevations across the left-right meridian or during stimulation of only one eye, the response amplitude value R was calculated [23]. To that end the stimulation period was divided into 18 bins (each 20° wide), and for each bin the difference between the specific spike frequency and the mean frequency during the whole stimulation period was calculated. The sum from all bins was defined as the response value R. The widths of the receptive fields were defined by the half-maximal response amplitude compared to the background activity. Circular plots of the mean activity of the neurons, receptive field plots, and ocular dominance diagrams were created in Origin 6.0 (Microcal, Northhampton, CA).

Model calculations

Receptive fields were modeled by creating a circular raster of sample points with a diameter of 110° for MeMe1 neurons and 90° for TML1 neurons. This corresponds to the lateral extent of their visual fields with at least 50% response strength. Calculation of the raster was carried out in two steps, similar to the method described by [24]. In the first step, we created a zenith-centered raster. Sample points were distributed on circles of equal latitude with the difference in latitude between two circles being 2°. The circumference *c* of each circle was given by

$$c = 2\pi \cos\beta \qquad (1)$$

where β = latitude of the respective circle. The number of points on each circle *n* was calculated as

$$n = \frac{c * 180°}{2° * \pi} \quad (2)$$

The distance d between two points on each circle of latitude was

$$d = 2\pi / n . \quad (3)$$

In the second step, this zenith-centered raster was moved to the appropriate location in space by vector transformation.

For each sample point we then calculated the *E*-vector and the degree of polarization according to the single scattering Rayleigh model [25] as described by [16] and [26]. While the natural polarization pattern of the sky follows the Rayleigh model rather well in terms of *E*-vector orientation [27], the degree of polarization *(d)* is usually much lower and even under optimal conditions does not exceed 0.75 [28]. We therefore multiplied the d value by 0.75. The longitudinal axis of the animal was defined as being parallel to the 0°-180° meridian. Calculations were done for a solar azimuth set to the preferred direction of green light (Φ_{max}green) of the respective neuron. Solar elevation was varied between 0° and 90° in steps of 1°. For each step, the average *E*-vector orientation within the visual field was calculated from the individual *E*-vectors at each raster point, weighted by the respective degree of polarization. This is equivalent to calculating the second order mean angle as described by [22]. The mean degree of polarization was calculated as the arithmetic mean of the individual degrees of polarization at each point within the visual field. Mean *E*-vector and mean degree of polarization were plotted against the elevation of the sun.

Results

Polarization-sensitive neurons in the optic lobe

To analyze the processing of polarized light signals in the optic lobe, neurons of the medulla were studied through intracellular recordings combined with dye injections. For detailed anatomical analysis all recorded neurons were imaged and were reconstructed in three dimensions. In addition to transmedulla neurons that send polarization vision information from the optic lobe into the central brain [10], we identified three major classes of polarization-sensitive (POL) neurons in 57 recordings.

Tangential intrinsic medulla neurons

The first class of POL-neurons, termed tangential intrinsic medulla neurons (TIM), had ramifications in the medulla and in the dorsal rim area of the medulla (DRMe, Fig. 2, Movie S1). The tangential intrinsic medulla neuron 1 (TIM1) was studied in 9 experiments and was already introduced by [29]. The morphologies of the 9 neurons were indistinguishable suggesting that all recordings were from the same neuron. It ramified through an entire layer of the medulla and arborized additionally in the DRMe (Fig. 2A-D) and in the accessory medulla (AMe, Fig. 2B) a small neuropil at the anterior-median edge of the medulla that in cockroaches and flies serves as the master circadian clock in the brain [30-32]. Its soma was located anteromedially from the medulla, and its primary neurite entered the medulla at its median proximal edge (Fig. 2C,D). After entering the medulla, the primary neurite split into two main neurites. One collateral (arrow in Fig. 2D) projected dorsally, ramified in the DRMe and gave off several large sidebranches that arborized throughout a single layer of the medulla (white processes in Fig. 2C). The second collateral (double arrow in Fig. 2D) projected ventrally within the same medulla layer and arborized, in addition, extensively in the AMe. Sidebranches originating from the ventral collateral extended widely through the entire medulla layer (red arborizations in Fig. 2C), similar to the ramifications from the dorsal collateral. Owing to the complex and uniform branching pattern, identification of possible input and output regions of TIM1 was difficult. Sensitivity to zenithal polarized light (see below) suggested that the neuron received input via its dorsal collateral. The dense arborizations in the AMe were the least varicose parts of the neuron (Fig. 2B) and might be a second input region. Arborizations of the ventral collateral were varicose, and therefore, possibly output regions.

TIM1 neurons responded with polarization opponency to polarized light from dorsal direction, i.e. they were maximally activated at a particular *E*-vector orientation (Φ_{max}) and were maximally inhibited at an orthogonal *E*-vector (Φ_{min}) (Fig. 2H). The neurons had a mean background spiking activity of 14.2 ± 7.9 (SD) impulses/s and an average maximum activity at Φ_{max} of 32.3 ± 15.5 (SD) impulses/s during stimulation with dorsally presented polarized light. The distribution of Φ_{max} orientations of the 9 recorded neurons was significantly different from randomness (Rao's spacing test, $p < 0.01$) and ranged from 80° to 140° with an average Φ_{max} of 113° ± 18° (SD) (Fig. 2J). Stationary polarized light at an *E*-vector-orientation of 0° (i.e. near Φ_{min}) led to phasic on-inhibition.

A second tangential intrinsic medulla neuron, termed TIM2 was studied in one experiment only. In contrast to TIM1, the branches of TIM2 were concentrated in the DRMe, dorsal regions of the medulla, and in a ventral area of the medulla (Fig. 2E, Movie S2). The cell body of TIM2 was located anteriorly in the optic lobe, dorsomedially from the AMe. Its primary neurite entered the medulla and bifurcated into two main neurites. One neurite projected extensively into dorsal parts of the medulla, and a few branches entered the DRMe. The second main neurite ramified in the ventralmost region of the medulla. No arborizations were observed in the AMe. In contrast to the TIM1 neuron, the polarity of the TIM2 neuron was well defined. Arborizations in the dorsal region of the medulla and in the DRMe were fine (Fig. 2F), suggesting input synapses whereas endings in the ventral region of the medulla were highly varicose (Fig. 2G).

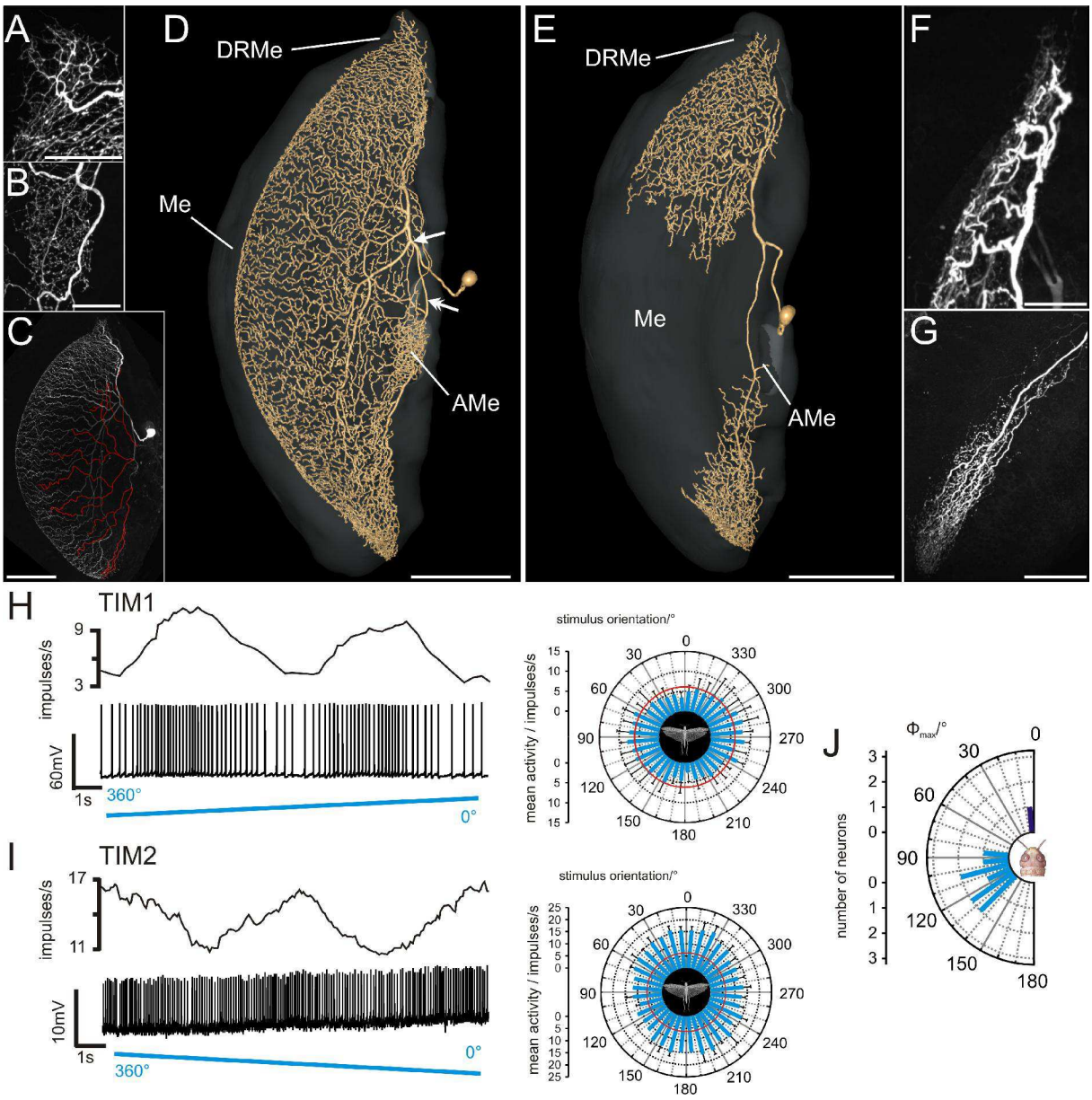

Figure 2. Morphology and physiology of tangential intrinsic medulla neurons (TIM1, TIM2). (A) Ramifications of a TIM1 neuron in the dorsal rim area of the medulla, maximum intensity view of confocal images. (B) Maximum intensity projection of the arborizations of a different TIM1 neuron in the accessory medulla. (C) Maximum intensity visualization of a TIM1 neuron (same neuron as shown in A) illustrates varicose and, thus, potential output regions (labeled in red) that originate from a ventrally projecting neurite. (D) Three-dimensional reconstruction of a TIM1 neuron within the medulla (Me, transparent), anterolateral view. After entering the medulla, the primary neurite splits into two main fibers. One collateral (arrow) projects dorsally, the other one (double arrow) projects to the accessory medulla (AMe) and the ventral medulla. DRMe, dorsal rim area of the medulla; AMe, accessory medulla. (E) Ramifications of a TIM2 neuron in the medulla (Me) reconstructed in three dimensions. Neuropils are shown in transparent grey, anterolateral view. (F) Arborizations of the TIM2 neuron in dorsal regions of the medulla and in the DRMe, maximum intensity projection of confocal image stack. (G) Maximum intensity projection of ramifications of TIM2 in the ventral medulla. The arborizations were more varicose. (H) Firing rate of TIM1 neuron, shown in A and G, during stimulation with polarized blue light. The polarizer was rotated 360° in clockwise direction. Upper trace: mean spike frequency during stimulation (moving average of spike rate in window size 1s); lower trace: spike train; right plot: circular diagram of mean spiking frequency plotted against *E*-vector orientation (bin size: 10°; n=6; error bars = standard deviation, Φ_{max}= 99°, Rayleigh test, p = 2.45×10^{-5}). Red circle indicates background activity of the neuron. (I) Mean spiking frequency (upper trace, moving average of spike rate in 1s time windows) and spike train (lower trace) of the TIM2 neuron shown in D stimulated with polarized light. The polarizer rotated 360° in counter clockwise direction. Right panel: mean spike activity and background activity (red circle) of the TIM2 neuron from ten 360° rotations of the polarization filter (bin width: 10°, error bars = SD, Φ_{max}= 4°, Rayleigh test, p = 0.003). (J) Distribution of the mean preferred orientations of TIM1 neurons (n=9, bright blue) and the TIM2 neuron (n=1, dark blue) (bin size: 10°). The Φ_{max} values were calculated from equal numbers of clockwise and counter clockwise rotations of the polarizer. All TIM1 neurons were analyzed in the medulla of the left brain hemisphere. The distribution of Φ_{max} orientations of the recorded TIM1 neurons was significantly different from randomness (mean Φ_{max} angle: 113° ± 18° (SD), Rao's spacing test, p < 0.01; length of mean vector *r* = 0.819). Scale bars: (A,B,E) 50µm; (G) 100µm; (C,D,E) 200µm.

The neuron had a background spike rate of 6.3 impulses/s, and the spike frequency increased to a maximum of 22.6 impulses/s at Φ_{max}. Like in TIM1 neurons, spiking activity in TIM2 was sinusoidally

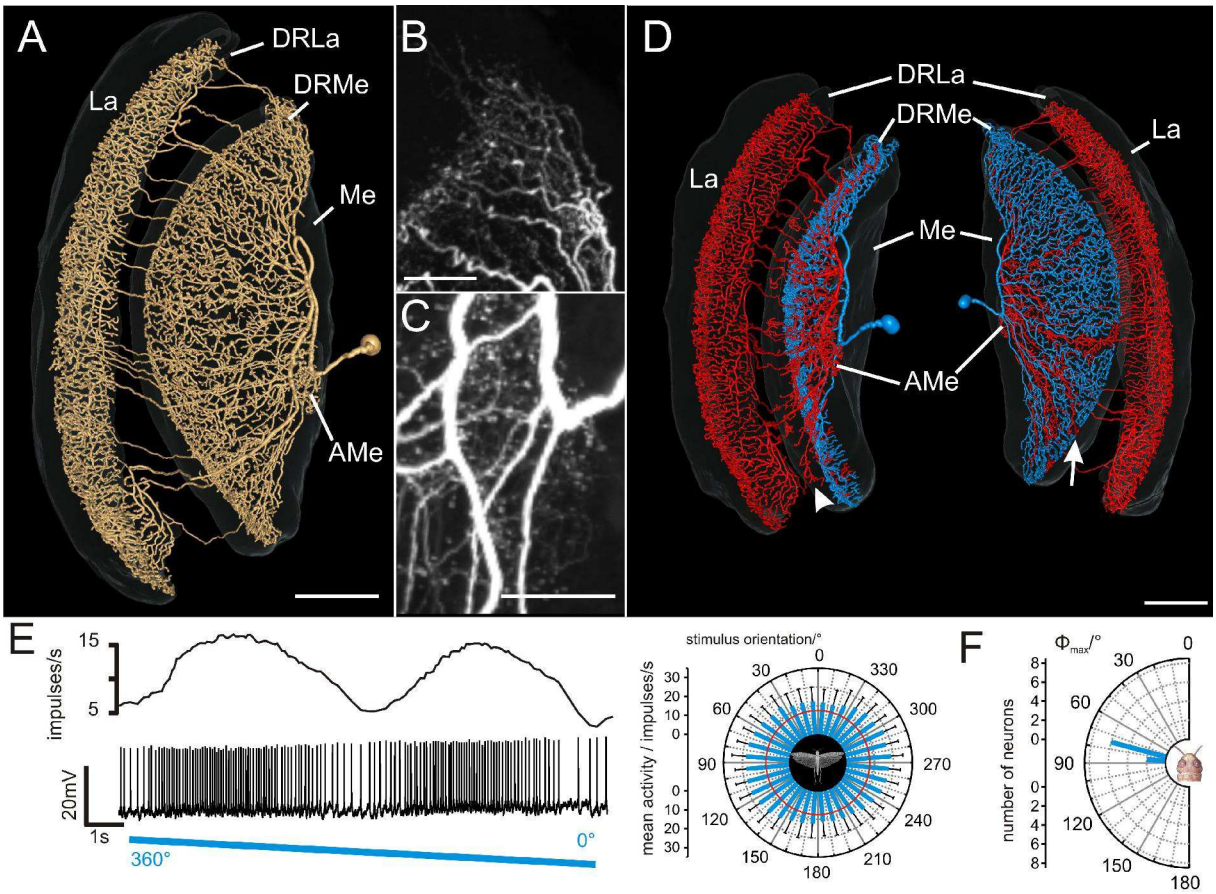

Figure 3. Anatomy and response properties of the tangential medulla-lamina neuron type 1 (TML1). (A) Three-dimensional reconstruction of the TML1 neuron and innerved brain areas (grey, transparent), anterolateral view; AMe, accessory medulla; DRMe, dorsal rim area of the medulla; DRLa, dorsal rim area of the lamina; La, lamina; Me, medulla. (B) Maximum intensity projection of the arborizations of the TML1 neuron in the DRMe. (C) Ramification of the neuron in the AMe, maximum intensity projection of an image stack. (D) Three-dimensional reconstruction of the TML1 neuron shown in A-C; left side: anteromedian view; right side: posteromedian view. Ramifications labeled in blue have smooth fiber terminals. The reconstructed red part of the neuron has a varicose appearance and may, therefore, be the output region of the neuron. Presumed output sites are in medulla layer 1 (white arrowhead) and in the same layer as the presumed inputs (white arrow). (E) Spike train (lower trace) and mean spiking frequency (upper trace) of the TML1 neuron shown in A-D during stimulation with a rotating polarizer (moving average, bin size: 1s). Right panel: Circular diagram of the mean frequency plotted against the stimulus orientation (bin size 10°, n=12, error bars= SD, Φ_{max}= 84°, Rayleigh test, $p = 3.11 \times 10^{-9}$). The background activity of the neuron is indicated by the red circle. (F) Mean preferred Φ_{max} orientations of the recorded TML1 neurons (n=8). The values are means from equal numbers of clockwise and counter clockwise rotations of the polarizer. All neurons were recorded in the left medulla. The distribution of Φ_{max} angles differs significantly from randomness (mean Φ_{max} angle: 77° ± 5.5° (SD); Rao's spacing test, $p < 0.01$; length of mean vector $r = 0.982$). Scale bars: (A,D) 200µm; (B,C) 50µm.

modulated during stimulation with a rotating *E*-vector, but did not show polarization opponency, i.e. no *E*-vector orientation inhibited the TIM2 neuron (Fig. 2I). The Φ_{max} angle of the recorded neuron was 4° (Fig. 2J).

Tangential medulla-lamina neurons

Eight recordings were obtained from a tangential medulla neuron with projections to the lamina, termed TML1. The strikingly similar morphology and physiology strongly suggest that all recordings were from the same neuron. TML1 had wide arborizations in the medulla, the DRMe, the AMe, and the lamina (Fig. 3A, Movie S3). The giant soma of TML1 was located anteromedially from the medulla. The primary neurite entered the medulla at the level of the AMe and projected toward dorsal regions of the medulla. Several fibers branched off from the main neurite and gave rise to an extensive meshwork throughout a narrow layer of the medulla and dense ramifications in the DRMe (Fig. 3B). The main neurite made a loop and projected back toward the AMe (Fig. 3C) and the ventral face of the medulla (Fig. 3D, red part of the neuron). Several sidebranches from this looping neurite again entered the narrow medulla layer (Fig 3D, white arrow). Other processes gave rise to beaded terminals in the AMe. Another set of side branches from the looping fiber entered the most anterior layer of the medulla with varicose terminals (layer 1, Fig. 3D, white arrowhead). Many of these fibers continued through the first optic chiasm to the lamina. They entered the lamina posteriorly and gave rise to extensive varicose arborizations through the innermost layer of the lamina, but did not invade the dorsal rim area of the lamina (DRLa) (Movie S3). The distinctly different arborizations in different parts of the optic lobe suggest that TML1 neurons receive synaptic input in the medulla and DRMe (Fig. 3D, blue part of the

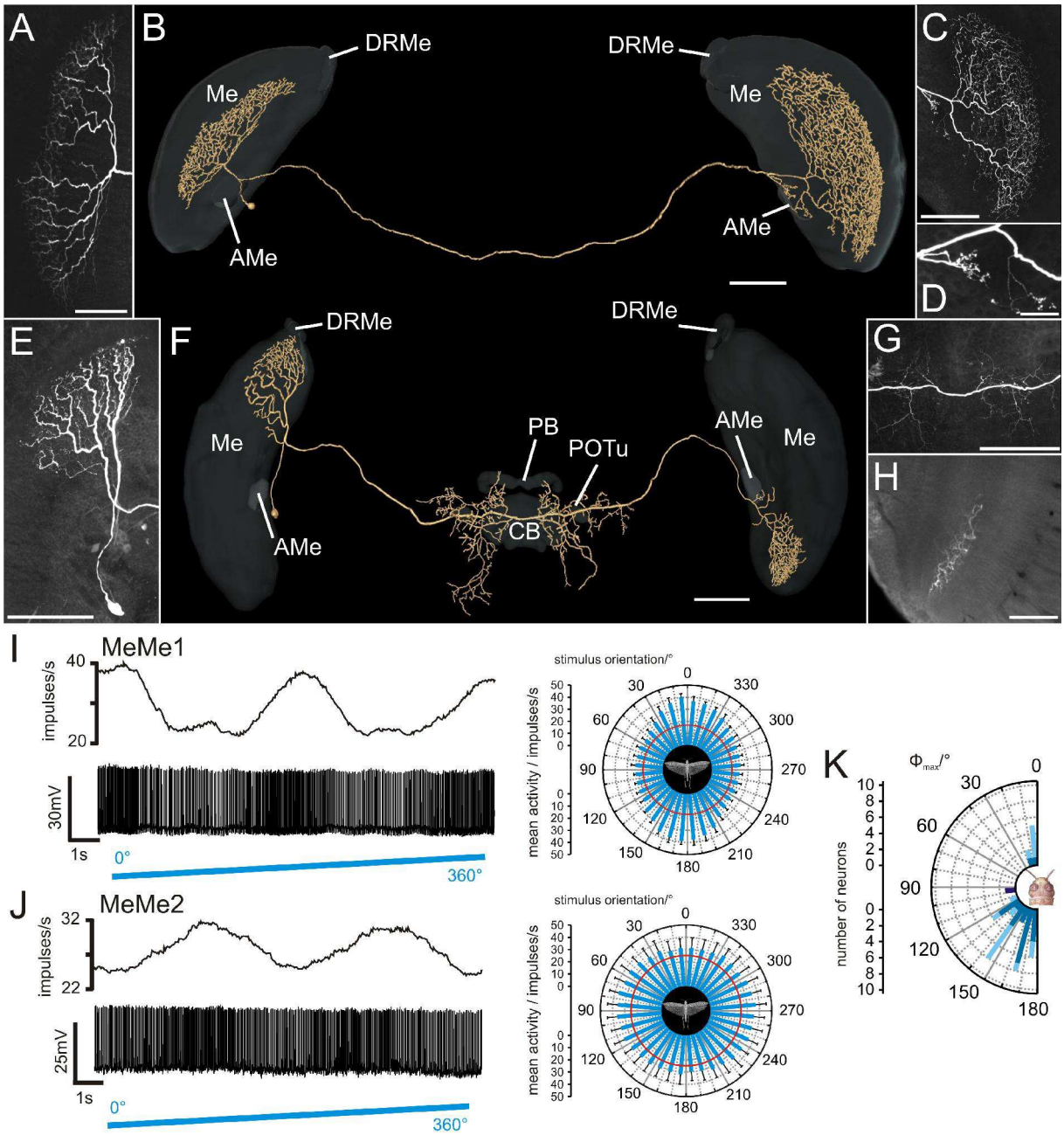

Figure 4. Morphology and physiology of intermedulla neurons (MeMe1, MeMe2). (A) Maximum intensity view of the arborizations of a MeMe1 neuron in the ipsilateral medulla. (B) Three-dimensional visualization of the MeMe1 neuron together with the medulla (Me), accessory medulla (AMe), and dorsal rim area of the medulla (DRMe) (grey, transparent). Anterior view. (C) Ramification of the MeMe1 neuron in the contralateral medulla. (D) A few sidebranches of the MeMe1 neuron arborize in the contralateral AMe. (E) Maximum intensity visualization of a MeMe2 neuron in the ipsilateral medulla. (F) Anterior view of a three-dimensionally reconstructed MeMe2 neuron. Neuropils of the optic lobes and brain areas in the central brain (CB: central body; PB: protocerebral bridge; POTu: posterior optic tubercle) are shown in transparent grey. The neuron did not enter the CB, PB or the POTu. (G) Varicose ramifications of the MeMe2 neuron in the posterior protocerebrum. (H) Axial slice at a depth of about 185 µm shows arborizations of the MeMe2 neuron in the contralateral medulla. (I) Physiology of the MeMe1 neuron, shown in A-D, during stimulation with polarized blue light, rotated in clockwise direction. The neuron showed sinusoidal modulation of spike activity (lower trace) during stimulation with a rotating polarizer. Upper trace: Mean spike frequency (moving average, bin width: 1s). Right panel: mean spike activity of the MeMe1 neuron plotted in a circular diagram (bin size: 10°; n=10; error bars= SD; red circle= background activity; Φ_{max}= 163°; Rayleigh test, $p < 10^{-12}$). (J) Response of MeMe2 neuron, shown in E and G to polarized light. Lower lane: spike train of the neuron. Upper lane: mean spike frequency during stimulation (moving average of spike rate in 1s time windows). The right panel shows a circular plot of the mean spike frequency plotted against *E*-vector orientation (bin size 10°, n=6, error bars= SD, Φ_{max}= 99°, Rayleigh test, p = 0.037). Red circle represents background activity of the neuron. (K) Distribution of Φ_{max} orientations from 37 MeMe1 neurons and one MeMe2 neuron. Values are plotted for neurons with cell bodies in the left brain hemisphere (n = 24, blue). Values from 13 MeMe1 neurons with cell bodies in the right brain hemisphere were mirrored against the longitudinal axis of the animal (light blue). The orientation of Φ_{max} of all MeMe1 neurons differed significantly from a uniform distribution (mean Φ_{max}: 159° ± 20° (SD); Rao's spacing test, $p < 0.01$; length of mean vector r =0.784). The recorded MeMe2 neuron had a preferred *E*-vector angle of 99° (dark blue). Scale bars: (A,H) 100µm; (B,C,E,F,G) 200µm; (D) 50µm.

3D-reconstructed neuron). Possible outputs may be the AMe, layer 1 of the medulla, and the lamina (Fig. 3D, red regions of the neuron).

TML1 neurons had a mean background activity of 7.4 ± 6.2 (SD) impulses/s. Zenithal stimulation with polarized light led to strong tonic excitation, which was modulated sinusoidally during rotation of the polarizer (Fig. 3E). The neurons were maximally activated up to peak frequencies of 26.2 ± 12.4 impulses/s. The preferred *E*-vector orientation of TML1 neurons was significantly different from a uniform distribution (Rao's spacing test, $p < 0.01$). Φ_{max} orientations were tightly clustered between 70° and 90° with a mean of 77° ± 5.5° (SD) (Fig. 3F).

Intermedulla neurons

Intermedulla neurons, termed medulla-medulla neurons (MeMe) were recorded in 39 experiments (Fig. 4). MeMe neurons connected the medullae of the right and left hemispheres of the brain. The medulla-medulla neuron 1 (MeMe1) was studied in 37 experiments. All stained neurons had indistinguishable morphology and similar physiological properties again suggesting that all recordings were from the same neuron in different animals. MeMe1 neurons had their soma anteromedially from the medulla in the vicinity of the AMe. Their primary neurite projected posteriorly from the AMe into the ipsilateral medulla (Fig. 4A,B, Movie S4) and bifurcated into two main neurites. One fiber projected into the ipsilateral medulla and gave rise to smooth arborizations in a single layer of the medulla (Fig. 4A). The ramifications did not extend completely throughout the medulla layer but were restricted to an anteromedian region of the layer. The second main neurite left the medulla and ran toward the posterior surface of the optic lobe. It entered the posterior optic tract and commissure to the contralateral optic lobe. There, the fiber turned anteriorly again, entered the medulla and gave rise to a varicose meshwork of processes in a single medulla layer (Fig. 4C). Some varicose sidebranches entered the contralateral AMe (Fig. 4D).

MeMe1 neurons had a mean background spiking rate of 14.1 ± 9.2 (SD) impulses/s in darkness and showed no or only weak polarization opponency (Fig. 4I). Presentation of polarized light at an *E*-vector orientation of 0° from dorsal direction led to phasic on-inhibition that was followed by weak tonic excitation. During rotation of the polarizer the neurons were maximally activated at Φ_{max} up to a mean spike frequency of 33.1 ± 14.3 (SD) impulses/s. The Φ_{max} values of the MeMe1 neurons were significantly different from a random distribution (Rao's spacing test, $p < 0.01$) and had a mean *E*-vector of 159° ± 20° (SD) (Fig. 4K).

The second type of intermedulla neuron, called medulla-medulla neuron 2 (MeMe2) was encountered in two experiments (Fig. 4E-H, Movie S5). The soma of MeMe2 was located anteriorly close to the AMe. The primary neurite entered the medulla, ran dorsally and ramified in a single layer (Fig. 4E). The arborizations of the neuron were restricted to the dorsalmost region of the medulla and parts of the DRMe. An axonal fiber left the optic lobe posteriorly and projected into the posterior central brain. It gave rise to varicose side branches in the median protocerebrum posteriorly from the central complex (Fig. 4F,G). Some processes entered the lateral ocellar tracts. The main neurite continued to the contralateral optic lobe, entered the optic lobe anteriorly, passed the lobula and ran ventrally toward the medulla. It entered the medulla, projected to the ventralmost part of the medulla and arborized in a single medulla layer (Fig. 4H).

The background spiking rate of the MeMe2 neurons ranged from 10.5 to 25.5 impulses/s. Both neurons responded with strong tonic excitation to stimulation with polarized light (*E*-vector at 0°) from the zenith. Sinusoidal modulation of spiking activity during rotation of the polarizer was significant in only one of the two recordings and showed maximum activity of 49.3 impulses/s at Φ_{max} (99°, Fig. 4J,K).

POL-neurons share innervation of medulla layer 4

To reveal possible sites of synaptic contact between the medulla POL-neurons, we compared the medulla layers that were innervated by the different cell types. Furthermore, we wanted to find out how POL-neurons without synaptic input in the DRMe, like the MeMe1 neurons, receive polarized light information.

Toward this goal, we rehydrated and sectioned the brain preparations with the dye-injected neurons and labeled the brain sections, in addition, with antibodies against the presynaptic vesicle protein synapsin. This allowed us to identify individual layers of the medulla and to define the medulla layers innervated by the different POL-neurons (Fig. 5). An anatomical landmark of the medulla that simplified the definition of layers was a large dark spot that resulted from a fiber bundle running horizontally along the equator through the medulla (Fig. 5, asterisks). This fiber bundle was located medially from layer 4 of the medulla (as defined by [33]) and facilitated distinction of layers 4 and 5. Another relevant feature was a thin salient dark sheet that separated layers 3 and 4 (arrowheads in Fig. 5).

TIM1 and TIM2 neurons (Fig. 5A,B) and MeMe1 neurons (Fig. 5D) passed the medulla exclusively through layer 4. TML1 and MeMe2 neurons mainly extended via layer 3 but in both cell types numerous sidebranches projected into medulla layer 4 (Fig 5 C,E).

In addition to the neurons characterized physiologically, we studied the morphology of transmedulla neurons that link the DRMe to the anterior optic tubercle (AOTu) [10]. Owing to the small neurites of these neurons, recordings from transmedulla neurons were not obtained. Injections of biotinylated dextran into the lower unit of the AOTu labeled the polarization vision pathway from the DRMe to the lateral accessory lobe (Fig. 6A). The somata of the transmedulla neurons were clustered

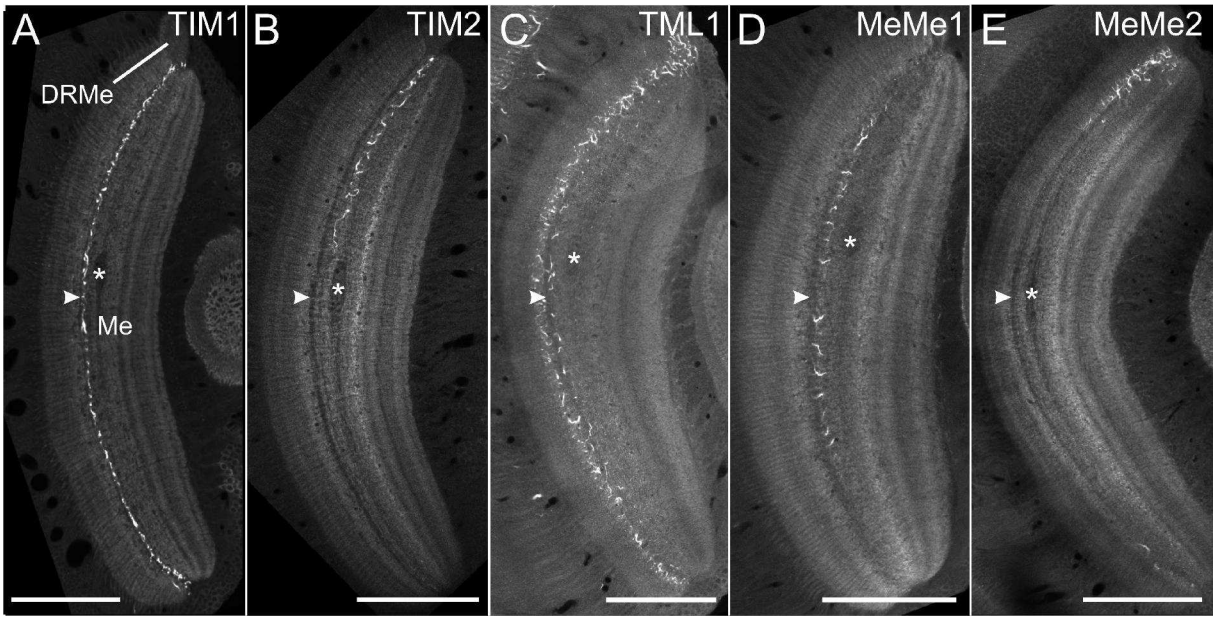

Figure 5. All polarization-sensitive neurons arborize in the same layer of the medulla. (A) Ramifications of the TIM1 neuron (of Fig. 2C) in the medulla. Frontal slices through the medulla at a depth of about 304µm. (B) Anterior view of the arborizations of the TIM2 neuron at a depth of about 472.5µm. (C) Axial slice through the medulla and the TML1 neuron at a depth of about 298µm. (D) Ramifications of the MeMe1 neuron in the ipsilateral medulla at a depth of about 200µm from the anterior surface. (E) Frontal view of the arborizations of the recorded MeMe2 neuron in the ipsilateral medulla at a level of about 245µm. Asterisks show a horizontally projecting fiber bundle that traversed the medulla medially from layer 4 and served as an anatomical landmark for the definition of layers. White arrowheads point to a narrow dark sheet that separated layers 3 and 4. All recorded POL-neurons arborized in medulla layer 4 as defined by [33]. Scale bars: 200µm.

near the anterior surface of the optic lobe distally from the medulla. The neurons arborized densely in the DRMe, projected through a distinct layer of the medulla and ran via the anterior optic tract to the anterior lobula and into the AOTu. As in TIM1, TIM2 and MeMe1 neurons, the ramifications of transmedulla neurons within the medulla were restricted to layer 4 (Fig. 6B). Taken together, our data suggest that polarized light information is integrated in the brain via medulla layer 4.

Azimuth-dependent responses to unpolarized light

In the daylight sky, the ratio between light of long wavelengths (460-700 nm) and light of short wavelengths (300-460 nm) is higher in the solar hemisphere than in the antisolar hemisphere [34]. POL-neurons of the AOTu respond, in addition to polarized light, to unpolarized green and ultraviolet light. Their responses to those stimuli suggest that they could aid in distinguishing the solar and antisolar hemispheres of the sky based on the respective content of wavelengths [16]. Owing to the wide ramifications in the medulla of the POL-neurons studied here, it seemed likely that they, likewise, receive information about the spectral gradient of the sky.

To explore this, we stimulated the POL-neurons of the medulla with an unpolarized green (530nm) and UV (350nm) light spot that moved around the locust's head on a circular path at an elevation of 45°. To study whether the tuning to chromatic properties of the sky is hard-wired or requires learning, we performed these experiments on two groups of animals. The first group was raised indoors under artificial illumination, whereas the second group was raised in a greenhouse with open view to the sky.

33 of a total of 36 analyzed neurons (91%) (5 TML1; 4 TIM1; 1 TIM2; 26 MeMe1) responded with a significant azimuth-dependent modulation of spike rate ($p > 0.05$). 12 of these neurons were recorded in animals, reared with direct view of the blue sky (4 TML1; 1 TIM1, 7 MeMe1). During stimulation with a green or UV light spot, all 12 neurons showed an increase in spike rate, when the stimulus was presented ipsilaterally, whereas in the contralateral field of view no response or an inhibition of firing activity was observed (Fig. 7). Two of the four analyzed TML1 neurons responded to both green and UV light in an azimuth dependent way, whereas two other neurons only responded to the green light spot. Stimulation of the TML1 neurons with a circling green light spot led to activation when presented ipsilaterally and to inhibition when presented contralaterally, or it had no effect on the contralateral side (Fig. 7A,C). When stimulating TML1 neurons with UV light, the neurons showed a similar but weaker response (Fig. 7B,C). The TIM1 neuron was tonically activated during the whole stimulus period, but excitation in the ipsilateral visual field was substantially stronger (Fig 7D). The response to the UV light spot was weaker, but again with a higher firing rate when the stimulus was in the ipsilateral visual field. Like the TIM1 neuron, MeMe1 neurons were activated by green light from all azimuthal directions but most strongly in the ipsilateral field of view (Fig. 7E). Stimulation with UV light led to strong inhibition in four MeMe1

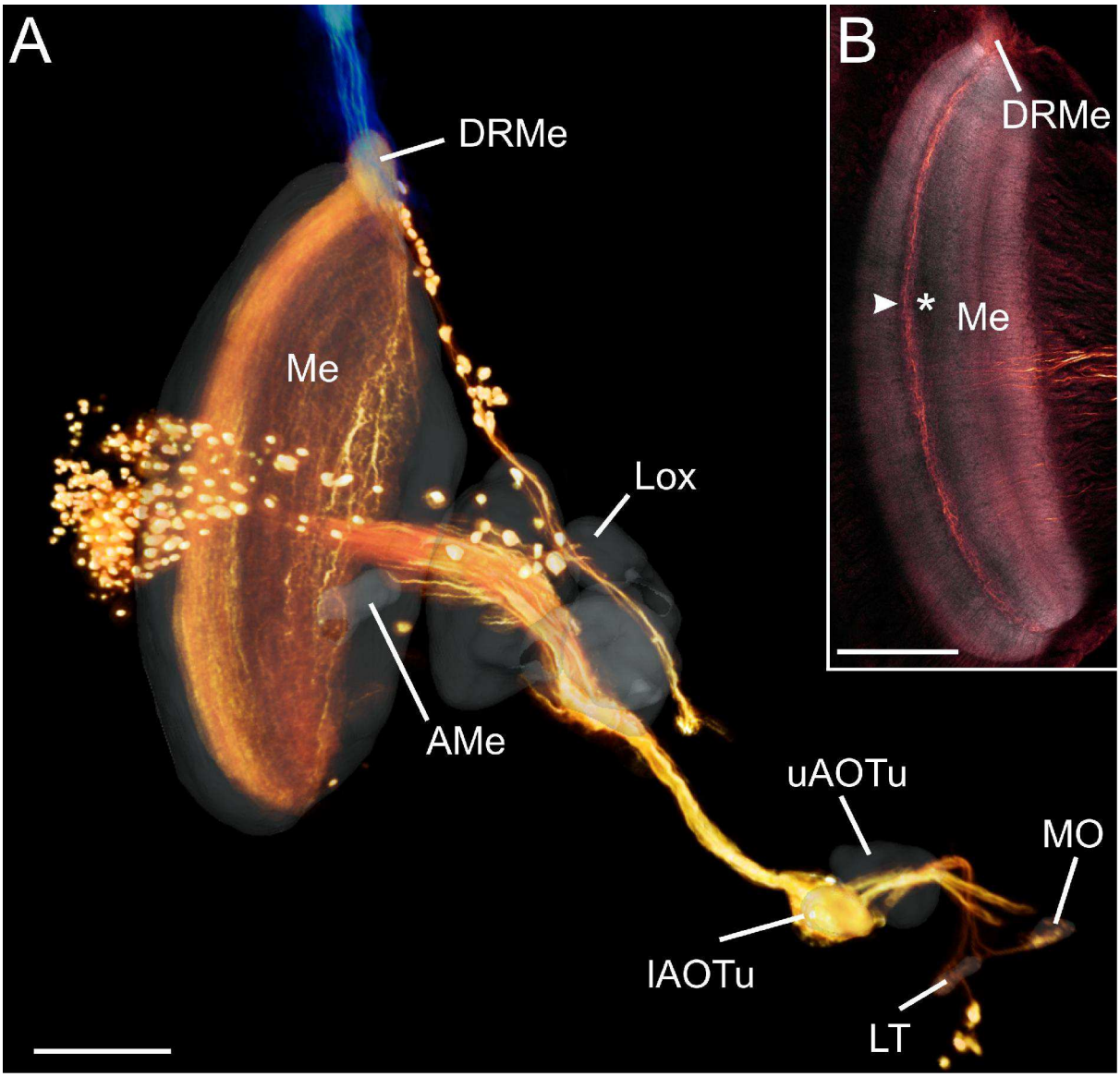

Figure 6. Transmedulla neurons connected to the anterior optic tubercle in the locust brain. (A) Volume rendering visualization of dextran injected into the lower unit of the anterior optic tubercle (lAOTu) revealed the polarization vision pathway from the dorsal rim area of the medulla (DRMe) via the anterior lobula of the lobula complex (Lox) and the AOTu to the lateral triangle (LT) and the median olive (MO) of the lateral accessory lobe. In addition, photoreceptors of the dorsal rim area were stained through injection with dextran conjugated to Alexa488 (blue). Cell bodies of the transmedulla neurons are clustered anteromedially and distally from the medulla. Whether the additional somata and associated fiber bundle dorso-medially from the medulla had ramifications in the DRMe or were stained by leakage of dye into adjacent dorsal areas of the medulla, could not be determined. The innerved brain areas are shown in transparent grey. AMe, accessory medulla; uAOTu, upper unit of the anterior optic tubercle. (B) Axial view of the ramifications of the transmedulla neurons at a depth of 390µm. Asterisk points to landmark fiber bundle through the medulla; white arrowhead points to dark sheet separating layers 3 and 4. The transmedulla neurons arborize in medulla layer 4, like the recorded POL-neurons. Scale bars: 200µm.

neurons when the stimulus was in the contralateral field of view (Fig 7E).

The distribution of the azimuthal tunings to the unpolarized green light spot of all recorded medulla neurons from animals raised in the greenhouse differed significantly from randomness (Fig. 8A, left panel; Rao's spacing test, $p < 0.01$) and had a mean preferred azimuth of 97° ± 41.3° (SD). The preferred azimuthal tunings to the UV light spot of these neurons also differed significantly from a random distribution (Fig 8A, right panel; Rao's spacing test, $p < 0.01$) with a mean preferred direction at 103° ± 45° (SD). Thus, the azimuthal tuning of medulla POL-neurons to unpolarized light spots was, unlike that of POL-neurons of the AOTu [16], independent of the wavelength tested. Interestingly, when analyzing the preferred azimuthal direction to unpolarized green light in laboratory-reared animals, the distribution was not significantly different from randomness (Fig 8B). Therefore the azimuthal tuning differed between animals raised with direct view to the blue sky and laboratory-reared animals. In contrast, when comparing the *E*-vector tuning of the medulla neurons between these animals we found no difference between the preferred *E*-vector orientations (Watson-Williams F-test, for MeMe1: $F_{1,36} = 0.001$; $p = 0.972$;

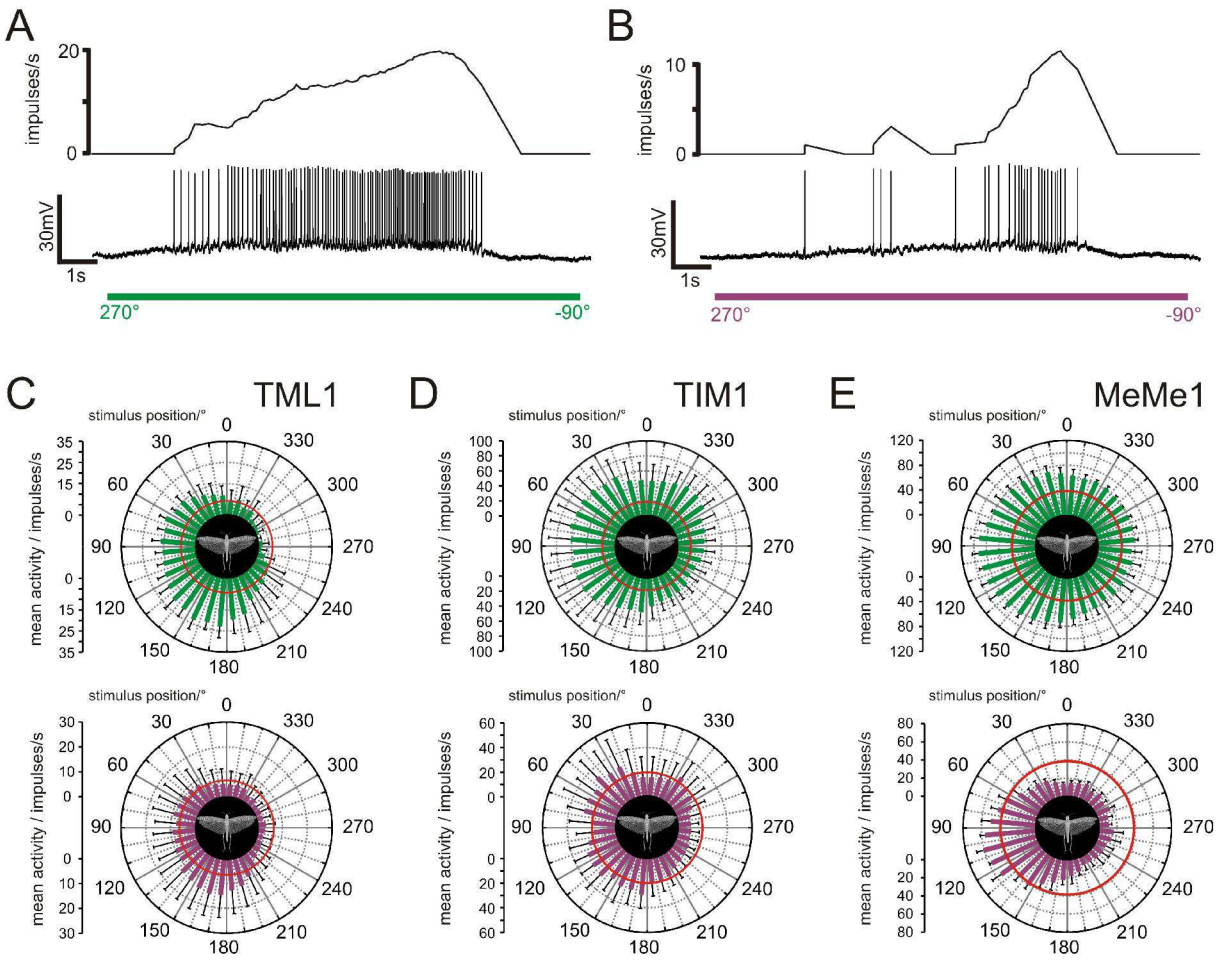

Figure 7. Azimuth-dependent responses of medulla POL-neurons to unpolarized light. All data are from animals raised in a greenhouse. (A,B) Responses of a TML1 neuron to a green and an UV light spot that moved at an elevation of 45° around the head. Upper traces: Mean spike frequency visualized with a moving average bin size of 1s. Lower trace: Spike train. (A) Response of the TML1 neuron to clockwise movement of a green light spot. (B) Response of the same neuron to clockwise movement of a UV light spot. (C-E) Circular diagrams of mean firing rates of medulla POL-neurons plotted against stimulus position. Upper circular plots show responses to a circling green light spot, lower plots, to a circling UV light spot. Bin size of all plots is 10°; error bars= SD; red circles indicate background activity of the neurons. (C) Responses of a TML1 neuron to a green light spot (n=6; Φ_{max}green = 124°, $p < 10^{-12}$) and to a UV light spot (n=8; Φ_{max}UV = 136°, $p < 10^{-12}$). (D) Responses of a TIM1 neuron to a green light spot (n=10; Φ_{max}green = 67°, $p < 10^{-12}$) and to a UV light spot (n=8; Φ_{max}UV = 91°, $p < 10^{-12}$). (E) Responses of a MeMe1 neuron to a green light spot (n=4) revealed a mean azimuthal direction to green of 97° ($p < 10^{-12}$) and during presentation of a UV light spot (n=4) a mean azimuthal direction to UV of 101° ($p < 10^{-12}$).

for TML1: $F_{1,6} = 0.442$; $p = 0.531$). Because both groups of animals originated from the same laboratory colony, it is likely that visual experience of the sky had an effect on the azimuthal tuning of medulla POL-neurons in the greenhouse-reared locusts.

Receptive field structure and ocular dominance

For an appreciation of the relation between polarized light information and azimuthal information, it is important to know the receptive field of the neurons for polarized light. For neurons with a receptive field centered to a point along the solar meridian, the angle between their *E*-vector tuning and their azimuthal tuning to an unpolarized light stimulus - if interpreted as sun - should be 90°. For all other points of the sky the absolute angular difference between those two directions is smaller than 90°. Moreover, owing to diurnal changes of solar elevation, the angular difference between the solar azimuth and the celestial *E*-vector orientation has to be continuously compensated during the course of day [16,35].

To examine these relations we shifted the *E*-vector stimulus along the left-right meridian to determine the center and bilateral extension of the receptive fields for polarized light in the recorded medulla neurons. In addition, we tested, whether the neurons received monocular or binocular polarized-light input. To define the strength of modulation to polarized light at different positions in the visual field and between ipsi- and contralateral eye stimulation from dorsal direction, we calculated the response amplitude value R. For a comparison of different recordings, R values were normalized to the largest response value or, in case of ocular dominance, to the response to dorsal stimulation of both eyes.

The receptive field for polarized light of TIM1 neurons was investigated in five animals. It was centered at an elevation of 60° contralaterally and had a width of about 85° along the left-right meridian (Fig.

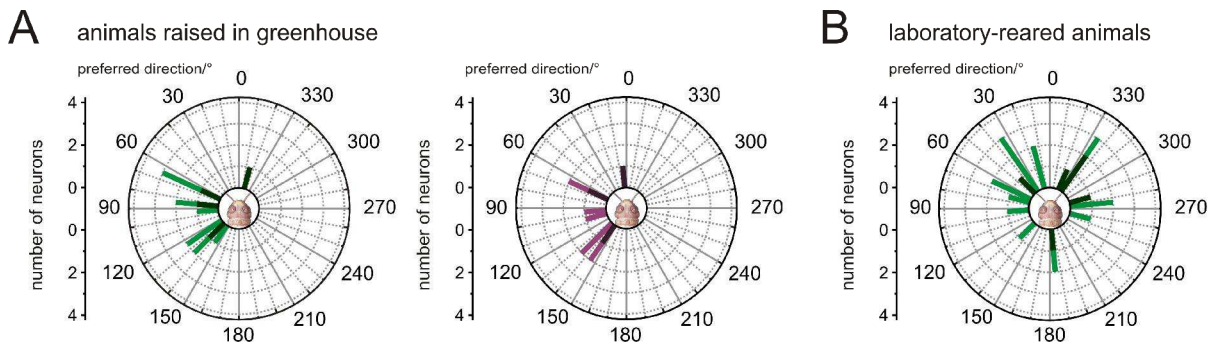

Figure 8. Directional sensitivity to unpolarized light spots in laboratory- and greenhouse-raised animals. (A) Left panel: Distribution of Φ_{max}green values of medulla neurons tested in greenhouse-reared animals. Preferred directions are plotted for neurons with cell body in the left brain hemisphere (bright green). Values from neurons with somata in the right brain hemisphere were mirrored (dark green). The distribution of Φ_{max}green values differed significantly from randomness (n=12; Rao's spacing test, $p < 0.01$, length of mean vector $r = 0.771$; mean preferred direction: 97° ± 41.3° (SD)). Right panel: Distribution of Φ_{max}UV values from the same neurons as in the left panel. Values are plotted for cells with somata in the left brain hemisphere (light violet), values from neurons with somata in the right optic lobe were mirrored (dark violet). The distribution differed significantly from randomness (n=9; Rao's spacing test, $p < 0.01$, length of mean vector r = 0.735; mean preferred direction: 103° ± 45° (SD)). (B) Distribution of Φ_{max}green values of medulla POL-neurons analyzed in laboratory-raised animals. Values are plotted for neurons with somata in the left brain hemisphere (light green). Values from neurons with somata in the right brain hemisphere were mirrored against the dorsoventral axis of the animal (dark green). The preferred azimuthal directions of the neurons are distributed randomly (n=21; Rao's spacing test, $p > 0.05$, length of mean vector $r = 0.348$).

9A). In contrast to TIM1 neurons, the receptive field of TML1 neurons was centered to the ipsilateral side at an elevation between 30° and 60° (Fig. 9B). The width of the receptive field of the TML1 neurons was about 90°. The receptive field along the left-right meridian of MeMe1 neurons was studied in ten experiments. They had a large receptive field of about 110° along the left-right meridian which was, like that of TIM1 neurons, centered at an elevation of 60° contralaterally (Fig. 9C). In all three cell types, *E*-vector tuning (Φ_{max}) did not differ systematically at different positions along the left-right meridian (not shown).

The ocular dominance of three TIM1, one TML1 and three MeMe1 neurons was analyzed by monocular stimulation of the ipsi- and contralateral eye (Fig. 9D). TIM1 and MeMe1 neurons showed a substantial difference in the response strength between stimulation of the ipsilateral and contralateral eye (Fig 9D). In addition, the response to stimulation of both eyes did not differ from the response to stimulation of only the ipsilateral eye. Ocular dominance of the TML1 neuron was investigated in one animal. Whereas stimulation of the ipsilateral eye resulted in a strong sinusoidal modulation, no spiking activity occurred during stimulation of the contralateral eye with zenithal polarized light.

No evidence for solar elevation compensation in the medulla

Because the receptive fields of the medulla neurons for polarized light are not centered to the zenith, the angle between the solar azimuth and the neurons' preferred *E*-vector orientation ($\Delta\Phi_{max}$) becomes increasingly different from 90° with increasing solar elevation. Assuming that the green light spot is interpreted as the sun, we, therefore calculated the angular relation and its daytime dependence between *E*-vector tuning to polarized blue light and azimuthal tuning to green light of neurons recorded from animals raised in the greenhouse ($\Delta\Phi_{max}$, Fig. 10A-C). In these animals, $\Delta\Phi_{max}$ values ranged from about 48° in the TIM1 neuron to about 140° in TML1 neurons. The distribution of $\Delta\Phi_{max}$ values in MeMe1 neurons and TML1 neurons was significantly different from randomness (Fig. 10D, Rao's spacing test, $p < 0.01$). The $\Delta\Phi_{max}$ values of MeMe1 neurons were clustered between 70° and 120° whereas the $\Delta\Phi_{max}$ distribution of TML1 neurons ranged from 100 to 140°. Furthermore, the $\Delta\Phi_{max}$ values differed significantly between the TML1 neurons and the MeMe1 neurons (Fig. 10E, Watson-Williams F-test, $F_{1,9} = 6.095$; $p = 0.036$). Whereas the TML1 neurons had a mean $\Delta\Phi_{max}$ value of 122.6° ± 12.5° (SD) (Fig. 10B,E), the mean $\Delta\Phi_{max}$ in MeMe1 neurons was 96.6°± 18.7° (SD) (Fig. 10C,E). To examine, whether $\Delta\Phi_{max}$ changed during the day, we plotted the $\Delta\Phi_{max}$ values against the time of day when the recordings were performed (Fig. 10F). If the neurons compensated the changing *E*-vector-orientation during the day in a way similar to neurons of the AOTu, $\Delta\Phi_{max}$ values should be low at noon and rise towards the evening [16]. Surprisingly, the medulla neurons did not show daytime-dependent changes in their $\Delta\Phi_{max}$ (Fig. 10F). The values were similar at noon and in the evening although the neurons were recorded during the same time of year as those of the AOTu. Furthermore, the response strength (R values) of the neurons did not differ significantly over the course of the day (not shown). The experiments suggest that circadian signals that are essential to compensate celestial compass cues for daytime changes in solar elevation are integrated into the polarization vision system at a processing stage between TML1/MeMe1 neurons and neurons of the AOTu.

To estimate changes in spiking activity with changing solar elevation, we calculated the mean *E*-vector and the mean degree of polarization within the

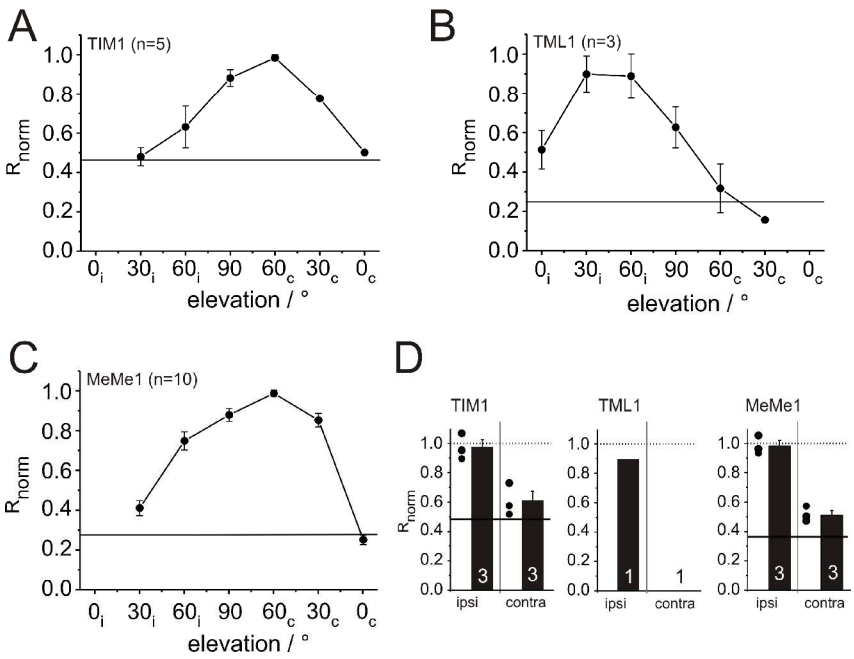

Figure 9. Receptive field size and position along the left-right meridian and ocular dominance of medulla POL-neurons. (A-C) Receptive fields of the neurons. Response amplitudes R were measured at particular elevations along the left-right meridian and were normalized to the largest R value (R_{norm}). For better visualization, the averaged R_{norm} values were connected by lines. Error bars indicate standard error. The terms ipsilateral (i) and contralateral (c) were defined with respect to the position of the soma of the analyzed cell. Horizontal lines indicate normalized background variability of the neurons, measured in a section of the spike train without stimulation. (A) Averaged receptive field of TIM1 neurons (n=5). The receptive field is centered to an elevation of 60° contralaterally. (B) Receptive field of TML1 neurons (n=3). The center of the receptive field is positioned in the ipsilateral field of view. (C) The receptive field center of MeMe1 neurons (n=10) is located at an elevation of 60° contralaterally. (D) Ocular dominance of the medulla neurons. The R values were calculated for zenithal monocular stimulation of the ipsilateral (ipsi) and contralateral eye (contra) and were normalized to the R value during stimulation of both eyes. The averaged R_{norm} values for monocular stimulation are shown as bars (error bars=SE). In addition, in the TIM1- and MeMe1-diagram the normalized R values of the individual neurons are shown as black dots. Stimulation of both eyes (R_{norm} =1.0) is indicated as dashed lines. Mean background variability of the analyzed TIM1- and MeMe1-neurons is shown as solid black line.

receptive field of MeMe1 and TML1 neurons at different solar elevations (Fig. 11). Both calculations were performed for a solar azimuth identical to the Φ_{max}green value (MeMe1: 77.5° ± 39.6° (SD); TML1: 133.27° ± 7.6° (SD)). The receptive field centers for polarized light were assumed as 60° contralateral for MeMe1 and 45° ipsilateral for TML1 (Fig. 9B,C).

In MeMe1 neurons, the mean *E*-vector within the receptive field was relatively constant (between 165° and 180°) at all solar elevations (Fig. 11A) and close to the mean Φ_{max} for polarized light of MeMe1 (159°). The mean degree of polarization ranged from 0.28 to 0.54 with a maximum at 30°. Therefore, MeMe1 should respond most strongly when the sun is ipsilaterally at an elevation of 30°. This coincides with the strongest *E*-vector at an elevation of 60° contralaterally. In TML1 neurons the elevation of the sun had a substantial effect on the mean *E*-vector orientation, owing to the ipsilateral position of the receptive field for polarized light (Fig. 11B). At low solar elevations (0°-30°) the degree of polarization was highest, and the mean *E*-vector within the receptive field was close to Φ_{max} of TML1 (77°). With higher solar elevations, the degree of polarization became lower and the mean *E*-vector differed increasingly from the *E*-vector tuning of TML1 (Fig. 11B). This should result in an increasingly smaller contribution of the polarization channel to spiking activity in TML1 at higher solar elevations.

Discussion

Intracellular recordings revealed five types of POL-neuron with ramifications in the medulla of the desert locust. Some of these neurons had additional processes in the AMe and/or the DRMe. In addition to responses to polarized light, the neurons showed azimuth-dependent responses to green and UV light spots. Outdoors, the most likely sources of these stimuli will be the sky polarization pattern and the intensity gradient and chromatic contrast in the sky. Ramifications of all neurons in medulla layer 4 suggest that this layer integrates signals from the polarization pattern of the sky with unpolarized celestial cues for sky compass signaling.

POL-neurons in the locust medulla

Four neurons, TIM1, TML1 and MeMe1 and MeMe2, were studied through multiple recordings. In the TIM1, TML1, and MeMe1 neurons the distributions of Φ_{max} were different from randomness. The preferred *E*-vector orientations of the neurons were clustered narrowly around their average Φ_{max}. Combined with the striking similarities in morphologies, this suggests that TIM1, TML1 and MeMe1 and MeMe2 neurons occur as single neurons per brain hemisphere. TML1- and MeMe1 neurons were reported previously by [36] as “medulla tangential with lamina projections” (TML1) and “medulla tangential with contralateral optic-lobe projections” (MeMe1). Furthermore, the TIM1 cell was described by [29] as “intrinsic medulla neuron”. Those studies, however, presented data from single recordings only with highly incomplete characterization. In another species, the cricket *Gryllus campestris*, medulla POL-neurons were studied extensively [37-39]. One type, termed POL1, resembles MeMe1 cells but has additional ramifications in the ipsilateral AMe and DRMe [38]. In contrast to MeMe1, POL1-neurons showed strong polarization opponency and occurred as three subtypes with Φ_{max} around 0°, 60° and 120° [38,40]. A second

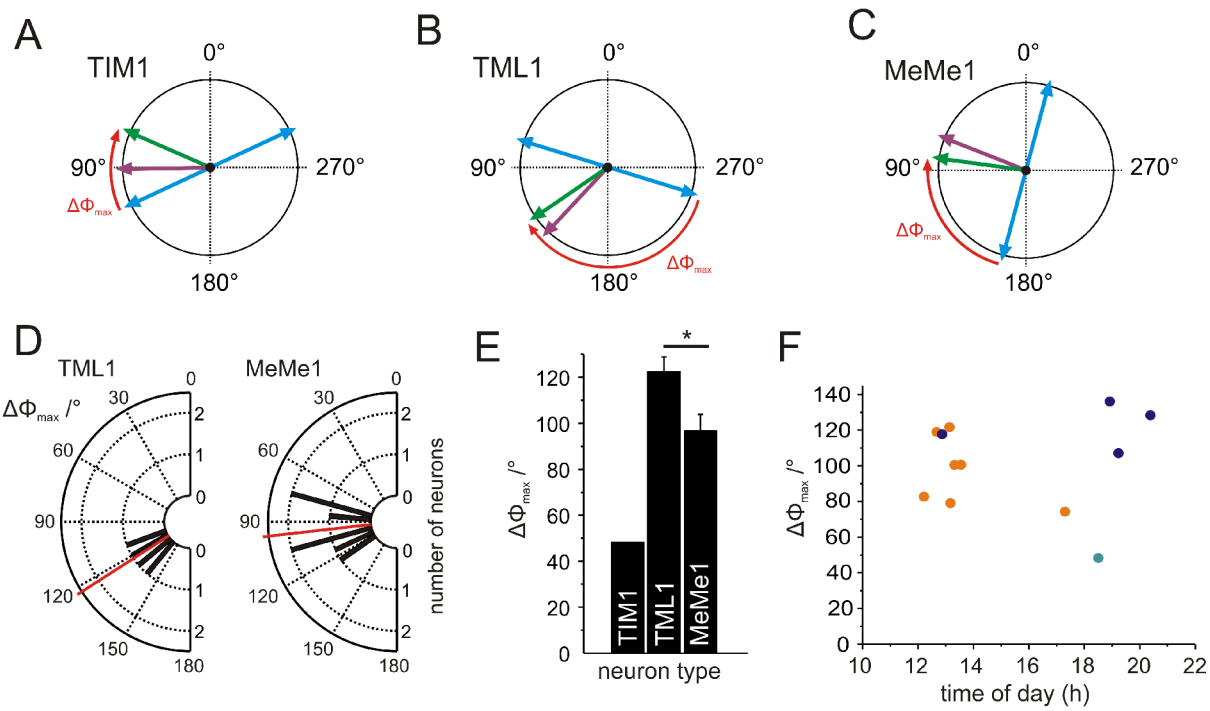

Figure 10. Relationship between tuning to zenithal polarized blue light and azimuthal tuning to unpolarized light in medulla POL-neurons of greenhouse-raised animals. (A-C) Tuning of individual neurons to polarized light (blue bidirectional arrows) and to unpolarized light (green light: green arrows; UV light: violet arrows). Red arrows indicate the calculated angles between the preferred *E*-vector orientation and preferred azimuthal direction ($\Delta\Phi_{max}$) shown in D-F. (A) TIM1 neuron. (B) TML1 neuron. (C) MeMe1 neuron. (D) Distribution of the angular differences between *E*-vector tuning and azimuthal green-light tuning ($\Delta\Phi_{max}$) of the TML1 (n=4) and the MeMe1 neurons (n=7). Red lines show the averaged $\Delta\Phi_{max}$ values. In both neurons the distribution of $\Delta\Phi_{max}$ values differs significantly from randomness (bin size: 10°; Rao's spacing test, $p < 0.01$). (E) The averaged $\Delta\Phi_{max}$ values of the TIM1 neuron, the TML1 neurons (n=4) and the MeMe1 neurons (n=7). $\Delta\Phi_{max}$ differs significantly between TML1 neurons and MeMe1 neurons (Watson-Williams F-test, $F_{1,9} = 6.095$; $p = 0.036$). (F) The $\Delta\Phi_{max}$ values of the medulla neurons plotted against time of day of the recording. Orange dots indicate $\Delta\Phi_{max}$ values of MeMe1 neurons, blue dots the $\Delta\Phi_{max}$ values of TML1 neurons, and the green dot, the $\Delta\Phi_{max}$ value of the TIM1 neuron.

type of POL-neuron in the cricket brain, termed POL3, had arborizations restricted to the medulla and AMe [24] similar to the locust TIM1 neuron but, unlike TIM1, POL3 again showed polarization opponency. It therefore appears that a similar inventory of POL-neurons is present in crickets and locusts, however with species-specific differences in morphologies and physiological properties.

Although not studied physiologically, transmedulla neurons are likely to transmit polarized-light information from the medulla to the AOTu [10]. Arborizations of the TIM1, TIM2 and MeMe1 neurons were, like those of the transmedulla neurons, confined to layer 4 of the medulla. TML1 and MeMe2 neurons mainly arborized in layer 3 but entered layer 4 with numerous sidebranches. Layer 4 of the medulla may, therefore, be specialized to integrate sky compass information in the brain.

Sensitivity to polarized light

Behavioral studies in tethered flying locusts showed that polarotaxis is mediated by photoreceptors in the DRA [4]. The DRA consists of ommatidia with optical axes directed upwards and up to 30° to the contralateral side [6]. To avoid interference with the color vision system, DRA photoreceptors are homochromatic with highest sensitivity in the blue range [41]. In each DRA ommatidium, photoreceptor microvilli are arranged in two blocks of orthogonal orientation [6]. This has been suggested to be the basis for polarization opponency found in POL-neurons of crickets [42] and in central-brain neurons of locusts [8]. In contrast, most medulla neurons studied here were excited at Φ_{max} but lacked an orthogonal inhibitory input. This could mean that these neurons, perhaps unlike transmedulla neurons, are not a direct link in the polarization vision pathway, but rather modulate polarization vision in the medulla.

TIM1, TML1 and MeMe1 neurons received polarized light information from the ipsilateral eye. Therefore, the commissural MeMe neurons do not provide input to the contralateral TIM1, TML1 and MeMe1 neurons. Corresponding to the contralaterally directed optical axes of DRA photoreceptors [6], the receptive fields of the TIM1 and MeMe1 neurons were centered at an elevation of 60° contralaterally. Unexpectedly, the TML1 neuron had a receptive field centered in the ipsilateral hemisphere. Similar to some central-complex neurons and descending neurons [12,15], TML1 was still strongly polarization sensitive when the stimulus was at the ipsilateral equator (0° elevation), a position that can hardly be detected by DRA photoreceptors. It is, therefore, likely that those responses were mediated by photoreceptors in the lateral eye. Behavioral experiments reported that locusts detect polarized reflections of water surfaces

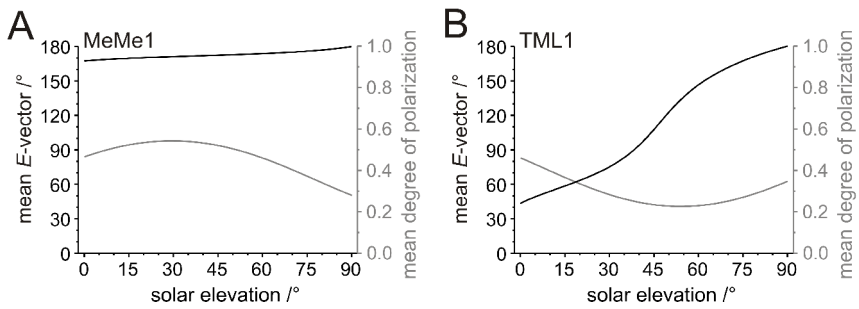

Figure 11. Models of mean *E*-vector and mean degree of polarization within the receptive field of MeMe1- and TML1 neurons at different elevations of the sun. The model was calculated according to the single scattering Rayleigh model [25]. The models are based on circular receptive fields with a diameter of 110° for MeMe1 neurons and 90° for TML1 neurons, corresponding to their width along the left-right meridian. Receptive field centers were defined according to response amplitudes along the left-right meridian shown in Fig. 9 (MeMe1: 60° contralateral; TML1: 45° ipsilateral). The Φ_{max}green values (MeMe1: 77.5° ± 39.6° (SD); TML1: 133.27° ± 7.6° (SD)) were taken as the respective solar azimuths. (A) Mean *E*-vector orientation (black line) and mean polarization degree (grey line) in the receptive field of MeMe1. (B) Mean *E*-vector orientation (black line) and mean degree of polarization (grey line) in the receptive field of TML1 plotted against solar elevation.

with ventral eye regions [43], which is known particularly for insects living near water surfaces such as backswimmers [44]. Taken together, the data suggest the existence of eye regions in locusts that extend the field of view for polarized light toward ventral directions.

Sensitivity to chromatic stimuli

All neurons had extensive arborizations in the medulla, and these sites probably mediated their responses to the unpolarized lights. Neurons of the AOTu, likewise, responded to unpolarized light and showed color-opponent responses to UV and green light [45] which was argued to aid in the discrimination between the solar and antisolar hemispheres [16]. POL-neurons of the medulla did not show color opponency. Instead their azimuthal tuning to UV and green light was strikingly similar in the ipsilateral field of view. Wavelength independence was also observed in the spectral responses of POL-neurons of the monarch butterfly [35], suggesting that monarch butterflies use the solar azimuth itself as a celestial cue. Color opponency in AOTu neurons, therefore, most likely results from convergence of specific color-coding and polarization-coding transmedulla neurons in the AOTu.

Green light induced strong tonic excitation when stimulating the ipsilateral eye. In contrast, ultraviolet light elicited inhibition at the contralateral eye. Because polarization input in medulla neurons is mediated through the ipsilateral eye, contralateral UV inhibition must be provided through commissural neurons that are not sensitive to polarized light. Based on these data it will be interesting to analyze spatial tuning to spectral cues in the central complex. Central-complex neurons receive bilateral polarization input and have zenith-centered receptive fields for polarized light [12]. We, therefore, predict that these neurons receive a combination of spatially opponent and color opponent chromatic input for a solar elevation-independent compass signal.

Rearing conditions had a strong effect on the azimuthal chromatic tuning of the medulla POL-neurons. Likewise, rearing of locusts with or without direct view to the blue sky had considerable effect on the *E*-vector tuning of AOTu neurons [16]. Both observations suggest that meaningful integration of sky chromatic and polarization signals strongly depends on visual experience of the sky during development.

Integration of sky compass cues and circadian clock

The medulla POL-neurons showed cell-type specific tuning to dorsal polarized light and to a particular azimuth of unpolarized light. In contrast to POL-neurons of the AOTu, the next central stage in the polarization vision pathway, we found no evidence for daytime dependent changes in tuning characteristics in medulla TML1 and MeMe1 neurons. Therefore, the signaling strength in medulla POL-neurons does not only depend on solar azimuth, but also on solar elevation. Modeling sky polarization in the receptive fields of MeMe1 and TML1 at solar azimuths corresponding to Φ_{max}green shows that the *E*-vector response of TML1 will change much more dramatically with changing solar elevation than that of MeMe1 (Fig. 11). In contrast, the spike rate of TML1 should be less sensitive to changes in solar azimuth, because the high degree of polarization in the ipsilateral sky will provide substantial input when the sun is in the contralateral (non-preferred) hemisphere. An important function of the medulla neurons studied here probably lies in the communication between the sky compass and the circadian systems. Both TML1 and MeMe1 neurons had varicose and, therefore, presumably output processes in the AMe, the presumptive circadian clock of the brain [30,46]. The different dependencies of medulla neurons on solar elevation and solar azimuth might, therefore, provide a highly differentiated zeitgeber signal to the circadian clock and could also contribute to photoperiodic timing, which is probably associated with the circadian clock [47]. If communication of the medulla with the AMe is bidirectional, as suggested by the ramifications of TIM1 in the AMe, the circadian clock could, on the other hand, directly influence the integration of sky polarization and chromatic information at the entrance to the AOTu.

Acknowledgements

We are grateful to Tim-Henning Humberg for 3D reconstructions of the MeMe-neurons. We thank Dr. Ronny Rosner and Corinna Pracht for contributing physiological data of one MeMe2 neuron. We thank Dr. Erich Buchner for providing the anti-synapsin antibody, Miklós Bech for helpful suggestions on the manuscript, and Martina Kern and Karl Heinz Herklotz for maintaining the locust cultures.

Supporting Information

Movie S1 Movie presenting a 360° vertical rotation of the three-dimensional reconstruction of the TIM1 neuron shown in Figure 2D. The innerved brain areas are shown in transparent grey.

Movie S2 Movie of the 3D reconstructed TIM2 neuron illustrated in Figure 2E. The medulla is shown in transparent grey.

Movie S3 Short movie of the ramification of the TML1 neuron in the medulla (transparent grey) reconstructed in three-dimensions (same neuron as in Figure 3A and D).

Movie S4 Movie illustrating the three-dimensionally reconstructed MeMe1 neuron of Figure 4B and the medullae of both hemispheres (transparent grey) rotating around the vertical axis.

Movie S5 Movie showing a 3D model of the MeMe2 cell (same as in Figure 4F). Optic lobe neuropils and brain areas of the central brain are shown in transparent grey. Vertical rotation.

References

1. Wehner R (1984) Astronavigation in insects. Annu Rev Entomol 29: 277-298.
2. Frost BJ, Mouritsen H (2006) The neural mechanisms of long distance animal navigation. Curr Opin Neurobiol 16: 481-488.
3. Rossel S, Wehner R (1984) Celestial orientation in bees: the use of spectral cues. J Comp Physiol [A] 155: 605-613.
4. Mappes M, Homberg U (2004) Behavioral analysis of polarization vision in tethered flying locusts. J Comp Physiol [A] 190: 61-68.
5. Labhart T, Meyer EP (1999) Detectors for polarized skylight in insects: a survey of ommatidial specializations in the dorsal rim area of the compound eye. Microsc Res Tech 47: 368-379.
6. Homberg U, Paech A (2002) Ultrastructure and orientation of ommatidia in the dorsal rim area of the locust compound eye. Arthropod Struct Dev 30: 271-280.
7. Vitzthum H, Müller M, Homberg U (2002) Neurons of the central complex of the locust *Schistocerca gregaria* are sensitive to polarized light. J Neurosci 22: 1114-1125.
8. Homberg U, Heinze S, Pfeiffer K, Kinoshita M, el Jundi B (2011) Central neural coding of sky polarization in insects. Phil Trans R Soc B 366: 680-687.
9. Homberg U (2004) In search of the sky compass in the insect brain. Naturwissenschaften 91: 199-208.
10. Homberg U, Hofer S, Pfeiffer K, Gebhardt S (2003) Organization and neural connections of the anterior optic tubercle in the brain of the locust, *Schistocerca gregaria*. J Comp Neurol 462: 415-430.
11. Pfeiffer K, Kinoshita M, Homberg U (2005) Polarization-sensitive and light-sensitive neurons in two parallel pathways passing through the anterior optic tubercle in the locust brain. J Neurophysiol 94: 3903-3915.
12. Heinze S, Gotthardt S, Homberg U (2009) Transformation of polarized light information in the central complex of the locust. J Neurosci 29: 11783-11793.
13. Heinze S, Homberg U (2007) Maplike representation of celestial *E*-vector orientations in the brain of an insect. Science 315: 995-997.
14. el Jundi B, Heinze S, Lenschow C, Kurylas A, Rohlfing T, Homberg U (2010) The locust standard brain: a 3D standard of the central complex as a platform for neural network analysis. Front Syst Neurosci 3: 21.
15. Träger U, Homberg U (2011) Polarization-sensitive descending neurons in the locust: connecting the brain to thoracic ganglia. J Neurosci 31: 2238-2247.
16. Pfeiffer K, Homberg U (2007) Coding of azimuthal directions via time-compensated combination of celestial compass cues. Curr Biol 17: 960-965.
17. Clements AN, May TE (1974) Studies on locust neuromuscular physiology in relation to glutamic acid. J Exp Biol 60: 673-705.
18. Heinze S, Homberg U (2008) Neuroarchitecture of the central complex of the desert locust: intrinsic and columnar neurons. J Comp Neurol 511: 454-478.
19. Klagges BRE, Heimbeck G, Godenschwege TA, Hofbauer A, Pflugfelder GO, Reifegerste R, Reisch D, Schaupp M, Buchner S, Buchner E (1996) Invertebrate synapsins: a single gene codes for several isoforms in *Drosophila*. J Neurosci 16: 3154-3165.
20. el Jundi B, Huetteroth W, Kurylas AE, Schachtner J (2009) Anisometric brain dimorphism revisited: Implementation of a volumetric 3D standard brain in *Manduca sexta*. J Comp Neurol 517: 210-225.
21. Schmitt S, Evers JF, Duch C, Scholz M, Obermayer K (2004) New methods for the computer-assisted 3-D reconstruction of neurons from confocal image stacks. Neuroimage 23: 1283-1298.
22. Batschelet E (1981) Circular statistics in biology. London: Academic. 371 p.
23. Labhart T (1996) How polarization-sensitive interneurones of crickets perform at low degrees of polarization. J Exp Biol 199: 1467-1475.
24. Petzold J (2001) Polarisationsempfindliche Neuronen im Sehsystem der Feldgrille *Gryllus campestris:* Elektrophysiologie, Anatomie und Modellrechnungen. PhD thesis, University of Zurich.
25. Strutt JW (1871) On the light from the sky, its polarization and color. Phil Mag 41: 274-279.
26. Pfeiffer K, Negrello M, Homberg U (2011) Conditional perception under stimulus ambiguity: polarization- and azimuth-sensitive neurons in the locust brain are inhibited by low degrees of polarization. J Neurophysiol 105: 28-35.
27. Suhai B, Horváth G (2004) How well does the Rayleigh model describe the E-vector distribution of skylight in clear and cloudy conditions? A full-sky polarimetric study. J Opt Soc Am A Opt Image Sci Vis 21: 1669-1676.
28. Brines ML, Gould JL (1982) Skylight polarization patterns and animal orientation. J Exp Biol 96: 69-91.
29. el Jundi B, Homberg U (2010) Evidence for the possible existence of a second polarization-vision pathway in the locust brain. J Insect Physiol 56: 971-979.
30. Helfrich-Förster C, Stengl M, Homberg U (1998) Organization of the circadian system in insects. Chronobiol Int 15: 567-594.
31. Helfrich-Förster, C (2004) The circadian clock in the brain: a structural and functional comparison between mammals and insects. J Comp Physiol [A] 190: 601-613.
32. Homberg U, Würden S, Dircksen H, Rao KR (1991) Comparative anatomy of pigment-dispersing hormone-immunoreactive neurons in the brain of orthopteroid insects. Cell Tissue Res 266: 343-357.
33. Wendt B, Homberg U (1992) Immunocytochemistry of dopamine in the brain of the locust *Schistocerca gregaria*. J Comp Neurol 321: 387-403.
34. Coemans M, Vos Hzn JJ, Nuboer JFW (1994) The relation between celestial colour gradients and the position of the sun, with regard to the sun compass. Vision Res 34: 1461-1470.
35. Heinze S, Reppert SM (2011) Sun compass integration of skylight cues in migratory monarch butterflies. Neuron 69:

345-358.
36. Homberg U, Würden S (1997) Movement-sensitive, polarization-sensitive, and light-sensitive neurons of the medulla and accessory medulla of the locust, *Schistocerca gregaria*. J Comp Neurol 386: 329-346.
37. Labhart T (1988) Polarization-opponent interneurons in the insect visual system. Nature 331: 435-437.
38. Labhart T, Petzold J (1993) Processing of polarized light information in the visual system of crickets. In: Wiese K, Gribakin FG, Popov AV, Renninger G, editors. Sensory systems of arthropods. Basel: Birkhäuser. pp. 158-169.
39. Labhart T, Petzold J, Helbling H (2001) Spatial integration in polarization-sensitive interneurones of crickets: a survey of evidence, mechanisms and benefits. J Exp Biol 204: 2423-2430.
40. Labhart T, Meyer EP (2002) Neural mechanisms in insect navigation: polarization compass and odometer. Curr Opin Neurobiol 12: 707-714.
41. Eggers A, Gewecke M (1993) The dorsal rim area of the compound eye and polarization vision in the desert locust *(Schistocerca gregaria)*. In: Wiese K, Gribakin FG, Popov AV, Renninger G, editors. Sensory systems of arthropods. Basel: Birkhäuser. pp 101-109.
42. Wehner R, Labhart T (2006) Polarization vision. In: Warrant E, Nilsson DE, editors. Invertebrate vision. Cambridge: Cambridge UP. pp 291-348.
43. Shashar N, Sabbah S, Aharoni N (2005) Migrating locusts can detect polarized reflections to avoid flying over the sea. Biol Lett 1: 472-475.
44. Horváth G (1995) Reflection-polarization patterns at flat water surfaces and their relevance for insect polarization vision. J Theor Biol 175: 27-37.
45. Kinoshita M, Pfeiffer K, Homberg U (2007) Spectral properties of identified polarized-light sensitive interneurons in the brain of the desert locust *Schistocerca gregaria*. J Exp Biol 210: 1350-1361.
46. Homberg U, Reischig T, Stengl M (2003) Neural organization of the circadian system of the cockroach *Leucophaea maderae*. Chronobiol Int 20: 577-591.
47. Shiga S, Numata H (2007) Neuroanatomical approaches to the study of insect photoperiodism. Photochem Photobiol 83: 76-86.

Receptive Field Properties and Intensity-Response Functions of Polarization-Sensitive Neurons of the Anterior Optic Tubercle in Gregarious and Solitarious Locusts

Receptive field properties and intensity-response functions of polarization-sensitive neurons of the anterior optic tubercle in gregarious and solitarious locusts

Basil el Jundi[1] and Uwe Homberg[1]
[1] *Department of Biology, Animal Physiology, University of Marburg, 35032 Marburg, Germany*

el Jundi B, Homberg U. Many migrating insects rely on the plane of sky polarization as a cue to detect spatial directions. In desert locusts (*Schistocerca gregaria*), as in other insects, polarized light is perceived by photoreceptors in a specialized dorsal eye region. Desert locusts occur in two phases, a gregarious swarming phase that migrates during the day and a solitarious, nocturnal phase. Neurons in a small brain area, the anterior optic tubercle (AOTu), are critically involved in processing polarized light in the locust brain. While polarization-sensitive (POL) intertubercle cells, LoTu1 and TuTu1, interconnect the AOTu of both hemispheres, TuLAL1 neurons transmit sky compass signals to a polarization compass in the central brain. To better understand possible adaptations of the polarization vision system to a diurnal vs. nocturnal life style we analyzed receptive field properties, intensity/response relationships and daytime dependence of responses of the AOTu neurons in gregarious and solitarious locusts. Surprisingly, no differences in the physiology of these neurons were found between the two locust phases suggesting that both phases rely on the same sky navigation system. Instead, clear differences were observed between different types of AOTu neurons. While TuTu1 and TuLAL1 neurons encoded *E*-vector orientation independent of light intensity and would thus be operational in bright daylight, LoTu1 was inhibited by high light intensity and provided strong polarization signaling only at dim light conditions. The presence of a high and low intensity polarization channel might, therefore, allow both phases to use the same polarization coding system despite their different activity cycles.

INTRODUCTION

Many navigating animals rely on external visual signals for spatial orientation. Insects use mainly two mechanisms to calculate moving directions during flight or walking. In familiar areas they are able to use visual landmarks as directional cues while in unknown terrains and during long-distance migrations, compass signals from the sky are more relevant (Giurfa and Capaldi 1999; Collett and Collett 2000). Besides the direct position of the sun, the plane of sky polarization serves as a crucial reference for spatial directions during seasonal migration or homing (Wehner and Labhart 2006). Celestial polarized light signals are detected by photoreceptors in a specialized region of the compound eye, the dorsal rim area (DRA) (Labhart and Meyer 1999). While diurnal insects including ants, bees and monarch butterflies refer to polarized light generated by the sun (Frost and Mouritson 2006; Wehner 1984), nocturnal dung beetles rely on the dim polarization pattern produced around the moon (Dacke et al. 2003; 2004).

Desert locusts *(Schistocerca gregaria)* perform long-distance migrations in huge swarms throughout North Africa and the Middle East and have been used as model organisms to analyze neural networks underlying the processing of sky compass signals in the brain. Behavioral experiments on tethered flying locusts suggest that they are able to use polarized light signals from the blue sky to define their course during migration (Mappes and Homberg 2004). Like other locust species, desert locusts occur in two phases, a gregarious and a solitarious phase, that show substantial differences in appearance and behavior (Uvarov 1966, Simpson et al. 1999). While gregarious locusts migrate in swarms during the day, solitarious locusts are nocturnal and preferentially migrate as individuals during the night (Waloff 1963; Roffey 1963). Considerable differences in the size and proportion of brain areas underlying the processing of visual signals were found between both phases (Ott and Rogers 2010), and, at the neural level, differences were demonstrated in the physiology of a looming-sensitive interneuron (Rogers et al. 2010).

Polarized light information is processed in distinct areas in the locust brain (Homberg 2004; Homberg et al. 2011). The anterior optic tubercle (AOTu) is a major relay station for processing polarized light information and transfers polarized light signals from the optic lobe to the central complex (Homberg et al. 2003). The tubercle receives signals from the dorsal rim area of the medulla and layer 4 of the distal medulla via transmedulla neurons (el Jundi et al. submitted). Two classes of polarization-sensitive (POL)-neurons, intertubercle cells and neurons of the tubercle-lateral accessory lobe tract, were identified in the AOTu (Pfeiffer et al. 2005). Three intertubercle neurons, a single LoTu1 and a pair of TuTu1 cells interconnect the AOTu of both hemispheres (Pfeiffer et al. 2005). The second class of neuron, TuLAL1-cells, transfers polarization signals to input neurons of the central complex (Träger et al. 2008). POL-neurons typically are modulated sinusoidally during zenithal stimulation

Correspondence to: Uwe Homberg, Fachbereich Biologie, Tierphysiologie, Universität Marburg, D-35032 Marburg, Germany (E-mail: homberg@biologie.uni-marburg.de).

with a rotating polarizer (Labhart 1988). Except for the LoTu1 cell, all POL-neurons of the AOTu show polarization opponency, i.e. they are maximally activated at a distinct *E*-vector orientation (Φ_{max}) and are maximally inhibited at an orthogonal orientation (Φ_{min}) (Pfeiffer et al. 2005). The LoTu1 neuron lacks an inhibitory part at Φ_{min}, suggesting a particular role in the neural network of the AOTu.

In addition to polarized light, all POL-neurons of the AOTu also respond to unpolarized chromatic stimuli which might allow them to distinguish between the solar and antisolar hemispheres of the sky (Kinoshita et al. 2007; Pfeiffer and Homberg 2007). Orientational tuning of these neurons to polarized light signals varies in a daytime dependent manner suggesting that the neurons compensate for daytime changes in solar elevation (Pfeiffer and Homberg 2007; Homberg et al. 2011).

To further characterize the signaling properties of the AOTu neurons, we have studied their receptive field properties, intensity/response functions, and daytime dependent differences in sensitivity to polarized light. To reveal possible adaptations to different lifestyles, data were obtained from gregarious and solitarious locusts. Surprisingly, we found no differences between solitarious and gregarious locusts in the physiological parameters of these neurons. In contrast, the properties of the different types of AOTu neurons differed markedly. TuTu1 and TuLAL1 neurons appeared to be adapted to signal *E*-vector orientation during the day independent of light intensity, while LoTu1 showed an increased sensitivity and response amplitude during the night suggesting optimal signaling of *E*-vector contrast under twilight conditions. Therefore, gregarious and solitarious locusts might possess similar adaptations for high and low light intensity detection of the sky polarization pattern.

METHODS

Locust rearing

Gregarious desert locusts (*Schistocerca gregaria)* were raised under crowded conditions at a constant temperature of 28°C on a 12h:12h light/dark cycle. Rearing conditions for solitarious animals followed the procedures of Roessingh et al. (1993). Animals were kept individually in small boxes at 26.5°C, 60% humidity and 12 h light/dark photoperiod and had neither visual nor olfactory contact. In general, full transition to the solitarious phase required three generations of animals kept in isolated conditions. A number of morphological markers were used as indicators for successful generation of solitarious animals. Solitarious nymphs had a bright green coloration in contrast to a yellow-dark brown patterning of gregarious nymphs (Simpson et al. 1999). Freshly hatched adults were light green in the solitarious state but had a pinkish coloration when they were gregarious. Sexually mature males were of yellow color with black patches in the gregarious state and were more uniformly brown-grey colored as solitarious animals. Another marker for solitarious adults was a light midline stripe along the dorsal thorax, which was less prominent in gregarious animals.

Preparation and electrophysiology

Only sexually mature locusts (1-3 weeks after imaginal molt) were used for the experiments.
Recordings were performed from AOTu neurons during the subjective night and subjective day of the animals. In both cases preparation of the animals was performed under identical conditions using a cold light source (Leica, KL 1500, Leica Microsystems, Wetzlar, Germany) for illumination.

Animals were cold anesthetized for at least 30 min. Legs and wings were cropped and stumps were closed with glue or wax. Mouthparts were sealed with wax, and animals were mounted with tape to a metal holder in a vertical orientation. A ridge of wax was brought up frontally between the mouthparts and the anterior edge of the compound eyes. The head capsule was opened anteriorly, and fat and trachea surrounding the brain were removed. To obtain stable recordings, the esophagus was cut, the abdomen was opened posteriorly, and the gut was removed from the opened abdomen. The abdomen was sealed with a tightly knotted thread. A wire platform was inserted between the esophageal connectives and was fixed at the ridge of wax to increase stabilization. Electrode penetration was facilitated by removing the neural sheath at the right anterior optic tubercle. During the whole preparation procedure, lasting for about 45 minutes and during recording of neurons, the brain was immersed in locust saline (Clements and May 1974).

Neurons of the AOTu were recorded intracellularly using sharp microelectrodes (resistance: 60-190 MΩ). The electrodes were drawn from borosilicate capillaries (inner diameter: 0.75 mm; outer diameter: 1.5 mm; Hilgenberg, Malsfeld, Germany) using a Flaming/Brown horizontal puller (P-97, Sutter, Novata, CA). Tips of the glass micropipettes were filled with 4% Neurobiotin (Vector Laboratories, Burlingame, UK) in 1 M KCl and shanks, with 1 M KCl. A silver wire inserted into the hemolymph solution served as reference electrode. Neural activity of neurons of the AOTu was amplified (10×) with a custom-made amplifier and monitored with an oscilloscope (Hameg HM 205–3, Frankfurt/Main, Germany). After digitizing at a sampling rate of 5 kHz (CED 1401 plus, Cambridge Electronic Design, UK), signals were stored on a personal computer using Spike2 software (version 6.02; Cambridge Electronic Design, UK). After recording, a constant depolarizing current was used to inject Neurobiotin iontophoretically into the neurons (2-3 nA, 1-5 min).

Stimulation

Locusts of both phases were stimulated with polarized monochromatic blue light obtained from a xenon lamp (XBO 150W, LOT-Oriel Group; Darmstadt, Germany, photon flux 1.8 $\times 10^{13}$ photons/cm^{2}s, 30.82 µW/cm^2), after passing a monochromatic filter (450 nm), a light guide (Schölly Fiberoptic, Denzingen, Germany) and a motor-driven linear polarizer (HNP'B, Polaroid, Cambridge, MA). The polarization filter was rotated through 360° in clockwise (0-360°) and counter clockwise (360-0°) directions with a constant speed of 30°/s. A set of neutral density filters between the light guide and the xenon lamp allowed changing the light intensity in logarithmic steps.

The polarization filter and the end of the light guide were attached to a perimeter device that enabled to test the neuronal responses to stimulation from various points along the left-right meridian. In one experiment, ocular dominance was tested by shielding one eye from the light source with a handheld piece of cardboard during stimulation with zenithal polarized light. Recordings were performed under dim ambient light conditions. During intensity/response measurements background light was reduced further by covering the front of the Faraday cage with a light-tight curtain.

Zenithal stimulation of the animal was defined as 90° elevation, lateral stimulations at an angular distance of 90° from the zenith were defined as 0° ipsilateral or contralateral stimulation. The terms ipsi- and contralateral refer to the position of the soma of the recorded neuron. The angular size of the stimulus at the locust eye was about 4.7°. For stimulation with zenithal polarized bright white light (39.17 mW/cm^2) the 450nm-monochromatic filter was moved out of the light beam.

Histology

To determine the morphology of the recorded neuron, Neurobiotin was injected into the recorded neuron. Brains were dissected out of the head and were fixed over night in 4% paraformaldehyde at 4 °C. Then, brains were washed 4 × 15 min with 0.1 M phosphate buffered saline (PBS, pH 7.4) and were incubated with streptavidin conjugated to Cy3 (1:1000; Dianova, Hamburg, Germany) in 0.1 M PBS containing 0.3% Triton X-100 (PBT). After an incubation period of three days, brains were again rinsed two times in 0.1 M PBT and then in 0.1 M PBS and were dehydrated in an ascending ethanol series (25%-100%, 15 min each). After treatment with a solution of ethanol/methyl salicylate (1:1, 15 min), brains were cleared in methyl salicylate for at least 35 min. The wholemount preparations were finally embedded in Permount (Fisher Scientific, Pittsburgh, PA, USA) between two glass coverslips using ten reinforcement rings as spacers (Zweckform, Oberlaindern, Germany).

Data analysis

The sampled spike trains were evaluated by using the Spike2-software with a custom designed script (kindly provided by Dr. K. Pfeiffer, Halifax, Canada). Action potentials were detected through threshold-based event detection. Events were visualized as mean spiking frequency using a gliding average algorithm (moving average of firing rate in window size: 1s). Background activities of the recorded cells were measured by counting of spikes divided by the respective time in a part of the spike train without stimulation. To define the *E*-vector tuning of the neurons, events during clockwise and counter clockwise rotations of the polarizer were assigned to the corresponding *E*-vectors and lists of these angles were analyzed using Oriana 2.02 software (Kovach Computing Services, Anglesey, UK). The angle of the mean vector *r* averaged from equal numbers of clockwise and counter clockwise rotations of the polarizer was defined as the *E*-vector tuning (Φ_{max}) of that neuron. In addition, the length of *r* describes the concentration of action potentials around Φ_{max} and is, thus, a measure for the directedness of the response during rotation of the polarizer (Batschelet 1981; Pfeiffer et al. 2011).

To quantify the modulation strength of the neurons during polarized-light stimulation, we calculated the response strength R (Labhart 1996). The stimulation period of the rotating polarizer was divided into 18 consecutive bins of 20°. In each bin we calculated the difference between the actual spike frequency and the mean spike frequency during the total stimulation period. The sum of the absolute value of all 18 bins was defined as the response strength R. Background variabilities of the cells were calculated in the same way in a section of the spike train without stimulation. Relative R values were obtained by normalizing the modulation strength at a given position of the visual field to the maximum value (R_{norm}). The widths of the receptive fields were determined by analyzing the elevations of half-maximal response strength in relation to the background variability. For visualization, data points of the receptive fields were connected by lines. Φ_{max}-distributions within the receptive field were obtained by subtracting the absolute deviation of the Φ_{max} value at each elevation from the preferred zenithal orientation.

In intensity/response diagrams, the response strengths were normalized against the modulation strength at log 0 (R_{norm}). Intensity/response curves were fitted by applying a modified Naka-Rushton function to the data (Naka and Rushton 1966)

$$R_{norm} = R_{norm(\max)} \cdot \frac{I^{\nu}}{(I^{\nu} + K^{\nu})} \qquad (1)$$

where I is the intensity of the stimulus, K is the intensity of the stimulus at 50% $R_{norm(max)}$, and υ is an exponent.

Box plots were created with the software Origin 6.0 (Microcal, Northhamton, CA, USA). The median value was indicated through a horizontal line and boxes denoted the 25% and 75% quartiles of the data. The 5% and 95% range of the data were visualized through whiskers.

Statistics

Circular statistics were performed in Oriana 2.02. Responses of neurons to polarized light were analyzed statistically through the Rayleigh test for axial data (Batschelet 1981). Neurons were defined as polarization sensitive if the distribution of angles was significantly different from randomness (α=0.05). The distribution of the preferred orientations of different recordings from the same neuron type was analyzed through Rao's spacing test (significance level, 0.05). To test whether the Φ_{max}-distribution of corresponding neurons differed between solitarious and gregarious animals, the Watson-Williams *F* test (significance level, 0.05) was used.

Further quantitative comparisons of the data were made by using the SPSS software (Version 11.5). The Shapiro-Wilk test (significance level, 0.05) was used to test for normality of data and the Levene test (significance level, 0.05) to test for homogeneity of variance. For data that were not distributed normally or if the variance was inhomogeneous the Mann-Whitney *U* test (significance level, 0.05) was applied. In the case of a normal distribution of the data and homogeneity of variance, the two samples were analyzed through a student's *t* test (significance level, 0.05). If data were compared from the same recorded neuron, quantitative analysis was performed through a paired student *t* test (significance level, 0.05). For statistical evaluation of multiple groups a one-way ANOVA combined with Tukey-honestly significant difference (HSD) *post hoc* test was applied (significance level, 0.05). If the Shapiro-Wilk test or the Levene test were significant, ANOVA with

Games-Howell *post hoc* test was used (significance level, 0.05). Linear regressions were calculated using Origin 6.0. The correlation coefficient (R_{corr}) was measured and the significance of regression was tested through a *t* test against a slope of 0 (significance level, 0.05).

RESULTS

This study presents electrophysiological data from 113 intracellular recordings from polarization-sensitive (POL) neurons of the anterior optic tubercle (AOTu) in the locust brain. Four types of neuron were analyzed, two types of intertubercle neuron that transfer polarization information from the ipsilateral to the contralateral AOTu and two types of neuron that connect the AOTu to the lateral accessory lobe. The lobula-tubercle neuron 1 (LoTu1) exists as a single neuron per hemisphere. It arborizes in the lower units of both AOTus and has further ramifications in the ipsi- and contralateral anterior lobulae (Vitzthum et al. 2002). In contrast, the arborizations of the tubercle-tubercle neuron 1 (TuTu1, 2 neurons per hemisphere) are restricted to the lower units of the AOTus of both hemispheres. The other two types of neuron, termed tubercle-lateral accessory lobe neurons (TuLAL) consist of about 100 neurons per brain hemisphere (Homberg et al. 2003). TuLAL1a neurons connect the AOTu with the ipsilateral lateral accessory lobe via the tubercle-accessory lobe tract (Pfeiffer et al. 2005). TuLAL1b neurons ramify in the anterior lobula, the AOTu and the lateral accessory lobe (Pfeiffer et al. 2005).

Receptive field structure and general tuning of AOTu neurons in gregarious and solitarious locusts

TuTu1 intertubercle neurons were analyzed in 20 recordings from gregarious animals and 13 recordings from solitarious locusts (Fig. 1). TuTu1 neurons responded with polarization opponency to a dorsally rotating polarizer with excitation at Φ_{max} and inhibition at Φ_{min} (Figs. 1*A*,*B*). TuTu1 neurons from gregarious locusts had a background activity of 25.5 ± 11.4 (SD) imp/s and a background variability of 38.9 ± 15.0 (SD). They showed an average absolute response strength R of 176.2 ± 98.9 (SD) to polarized light stimulation. The Φ_{max} values of the gregarious TuTu1 neurons had three preferred orientations, one at approximately 36°, another around 120° and a third at around 175°. Receptive field properties of TuTu1 neurons of gregarious animals were analyzed in 19 recordings. In 16 recordings the bilateral expansion of the receptive fields was analyzed during the subjective day (*Zeitgeber* time 0h-12h), while in three gregarious locusts receptive field properties were analyzed between *Zeitgeber* time 12 to 24h (subjective night). No differences between the receptive fields of TuTu1 cells recorded at night or during the day were noted. The averaged receptive field of all 19 TuTu1 neurons had a width of about 110° and was centered eccentrically at an elevation of 60° in the contralateral hemisphere (Fig. 1*C*).

TuTu1 neurons of solitarious animals had a mean background activity of 29.1 ± 10.87 (SD) imp/s and a mean background variability of 44.9 ± 23.52. Both values did not differ significantly between solitarious and gregarious animals (student's *t* test, p = 0.38, p = 0.33, respectively). TuTu1 neurons from solitarious locusts had an averaged response strength R of 144.20 ± 61 (SD), which was not significantly different from that of TuTu1 cells from gregarious animals (Mann-Whitney *U* test, p = 0.55). Φ_{max} orientations of TuTu1 neurons were distributed more randomly in solitarious locusts (Fig. 1*E*), but this distribution did not differ significantly from the distribution of Φ_{max} orientations of TuTu1 cells in gregarious locusts (Watson-Williams *F* test, p = 0.8). Receptive field properties were analyzed in 11 neurons at night and 2 neurons during the day, but as in gregarious animals no differences were observed between the two groups. The averaged receptive field of all TuTu1 cells of solitarious animals had a width of about 120°. Similar to the receptive field in gregarious locusts, it was centered eccentrically between 60° and 30° in the contralateral hemisphere (Fig. 1*C*). No significant differences were observed between solitarious and gregarious locusts at any tested position in the visual field.

The LoTu1 neuron was analyzed in 69 experiments (Fig. 2). In contrast to TuTu1 neurons, LoTu1 was most strongly activated at Φ_{max} but lacked an inhibition at Φ_{min} (Figs. 2*A*,*B*). In 40 recordings, LoTu1 properties were tested in gregarious animals. The neurons had a background activity of 13.3 ± 10.1 (SD) imp/s, a mean background variability of 21.3 ± 7.3 (SD), and a response strength R of 72.4 ± 27.8 (SD) in the center of the receptive field. The Φ_{max} orientations of the recorded neurons in gregarious animals showed a non-random distribution (Rao's spacing *U* test, p < 0.01) and ranged – with three exceptions – from about 76° to 176°, with a mean Φ_{max} orientation at 128.4° ± 31.6 (SD) (Fig. 2*D*). The receptive field structure of LoTu1 was analyzed in 33 gregarious animals. 26 recordings were obtained during the subjective day and in seven animals recordings were performed during the night. No significant differences were found between receptive fields of both groups at any of the tested elevations (ANOVA analysis with Games-Howell *post hoc* test). Similar to TuTu1 cells, the gregarious LoTu1 neuron had an eccentric receptive field with the strongest response at an elevation of 60° contralaterally (Fig. 2*C*). The width of the receptive field was about 130° along the left-right meridian.

Physiological properties of the LoTu1 cell in solitarious locusts were analyzed in 26 animals. The averaged background activity of 14.9 ± 8.1 (SD) imp/s and the mean background variability of 19.4 ± 6.1 (SD) was not different from the corresponding firing properties in gregarious animals (Mann-Whitney *U* test, p=0.34, p = 0.25, respectively). The neurons showed an absolute response strength of 85.9

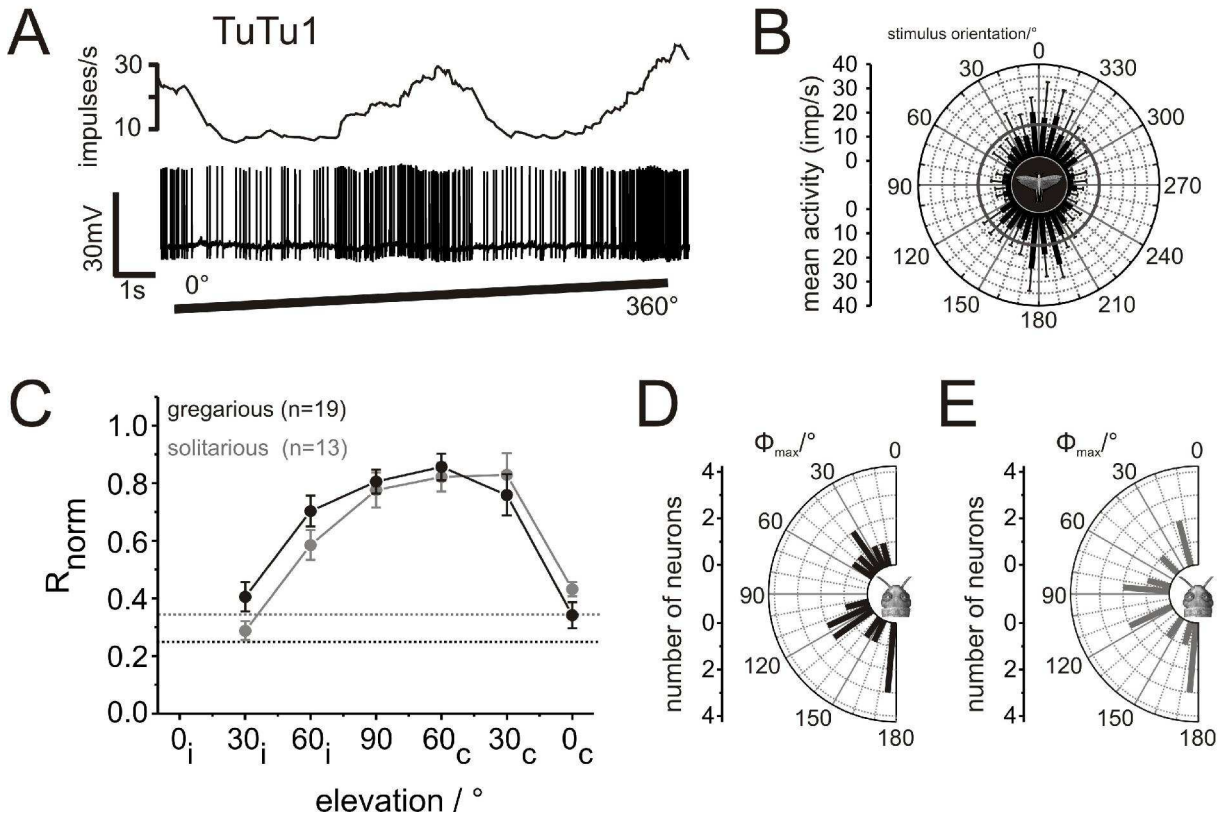

FIG. 1. Physiology of TuTu1 neurons from gregarious and solitarious locusts. *A*: Spike train of a TuTu1 neuron from a gregarious animal during dorsal stimulation with polarized blue light. The polarizer was rotated in clockwise direction; lower trace: spike train; upper trace: mean spiking frequency (moving average of spike rate in 1s time window). *B*: Circular plot of the mean spiking rate of the neuron shown in *A* plotted against the *E*-vector orientation of the polarizer (bin size: 10°; n=4; error bars = standard deviation, Φ_{max} = 174°, Rayleigh test, $p < 10^{-12}$). Grey circle indicates the background activity of the neuron in darkness. *C*: Mean response amplitudes of TuTu1 neurons from gregarious (*n* = 19, black) and solitarious (*n* = 13, grey) locusts along the left-right meridian. Normalized response strength (R_{norm}) was measured at different elevations in the ipsilateral (i) and contralateral (c) field of view. For better visualization, data points are connected by solid lines. Response amplitudes and mean background variabilites (dotted lines) were normalized to the maximum R value in the visual field of each neuron. In gregarious animals, eight neurons showed the strongest response at an elevation of 30° contralaterally (30c), seven cells at an elevation of 60° contralaterally (60c), one neuron at zenithal stimulation (90), and three neurons in the ipsilateral visual field (60i). Of a total of 13 receptive fields analyzed in solitarious animals, five neurons showed the strongest modulation at an elevation of 30° contralaterally (30c), four neurons at 60° contralaterally (60c), and three neurons at zenithal stimulation (90). Error bars denote standard errors. *D*: Distribution of Φ_{max} orientations of TuTu1 neurons of gregarious locusts obtained during zenithal stimulation (*n* = 16; bin width: 10°). *E:* Distribution of zenithal *E*-vector orientations of TuTu1 neurons from solitarious animals plotted against the number of recorded neurons (*n* = 13; bin size: 10°). All values are plotted for cells with perikarya in the left brain hemisphere. Φ_{max} values of neurons with cell bodies in the right hemisphere were mirrored against the longitudinal axis of the animal.

± 33.16 (SD) in the center of the receptive field which did not differ significantly from the response strength in gregarious locusts (student *t* test, p = 0.1). Φ_{max} orientations of LoTu1 neurons in solitarious animals were distributed more randomly (Figure 2*E*), but statistically no differences were observed between the *E*-vector tuning in gregarious and solitarious animals (Watson-Williams *F* test, p=0.07). The receptive field properties of LoTu1 neurons from solitarious animals were studied in 25 recordings (nine cells at the subjective day and 16 neurons at *Zeitgeber* time 12-24h). Again, no significant differences were found in the receptive field properties between gregarious and solitarious locusts that were recorded during the subjective night or the subjective day (ANOVA analysis with Games-Howell *post hoc* test). In all groups, LoTu1 neurons had a receptive field of highly similar width (about 135°) and shape (Fig. 2*C*). As in gregarious locusts, the strongest response of LoTu1 in solitarious locusts was centered at an elevation between the zenith and 60° contralateral.

Owing to the small diameter of TuLAL1 neurites, recordings from these neurons were relatively difficult and, thus, in previous work these types of neuron were analyzed only rarely. We studied TuLAL1 neurons in eleven recordings (Figs. 3,4). The size of the receptive field along the left-right meridian of TuLAL1a cells was analyzed in seven recordings (two gregarious and five solitarious locusts). In all recordings, TuLAL1a neurons showed polarization opponency (Figs. 3*A*,*B*). The background activity of the two gregarious TuLAL1a neurons ranged from 36.2 to 45.5 imp/s and the background variability ranged from 16.5 to 34. Both receptive fields were zenith-centered and quite narrow (about 60°) (Fig. 3*C*). The response strength R of both cells ranged from 105.49 to 115.74. The Φ_{max} orientation of both neurons was around 30° whereas the Φ_{max} orientations

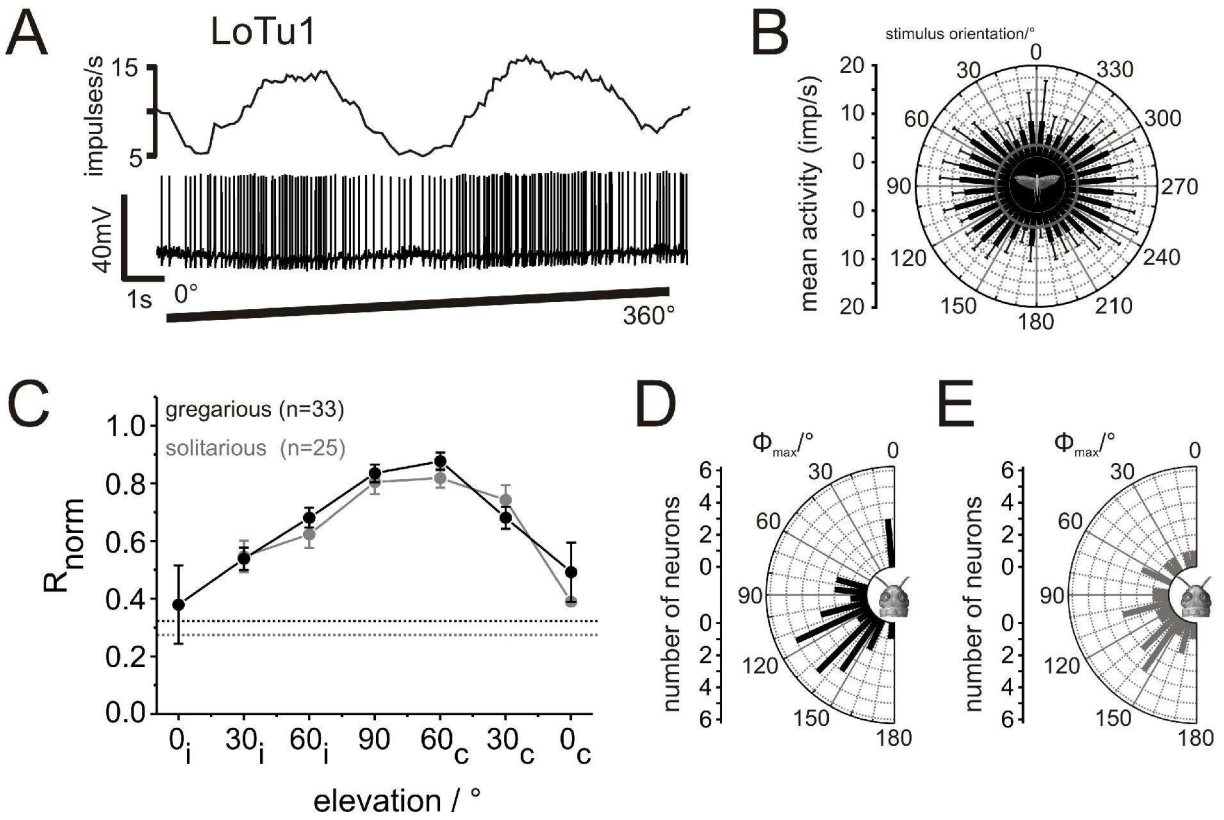

FIG. 2. Analysis of LoTu1 neurons in gregarious and solitarious locusts. *A*: Unfiltered spike train (lower trace) and mean firing frequency (upper trace) of a LoTu1 neuron during stimulation with polarized blue light (clockwise rotation) obtained from a gregarious animal (moving average, bin size: 1s). *B*: Circular diagram of the mean spike frequency of the neuron shown in *A* plotted against the orientation of the polarizer (bin size: 10°; $n = 6$; error bars = standard deviation, $\Phi_{max} = 94°$, Rayleigh test, $p = 5.74 \times 10^{-6}$). Grey circle shows the background activity of the LoTu1 neuron. *C*: Averaged receptive field width along the left-right meridian of LoTu1 analyzed in gregarious ($n = 33$, black) and solitarious ($n = 25$, grey) animals. Relative response strength (R_{norm}) is plotted at different elevations of the polarizer along the right left meridian of the visual field. In each neuron, R and the mean background variability (dotted lines) were normalized to the highest R value in the visual field. In gregarious locusts, one neuron responded maximally to polarized light from the contralateral horizon (0c), two neurons at an elevation of 30° contralaterally (30c), and 16 neurons at an elevation of 60° contralaterally (60c). Ten neurons showed the strongest sinusoidal modulation during presentation of polarized light from dorsal (90), two neurons at 60° ipsilaterally (60i), and two further cells at an elevation of 30° in the ipsilateral hemisphere (30i). In solitarious animals, eight neurons responded maximally to polarized light at an elevation of 30° in the contralateral field of view (30c), six neurons at a position of 60° in the contralateral hemisphere (60c), and eight cells during zenithal stimulation with polarized light (90). Three LoTu1 neurons from solitarious animals showed the strongest responses in the ipsilateral hemisphere (two neurons at 60i, one cell at 30i). Error bars show standard error. *D*: Φ_{max} distribution of LoTu1 neurons ($n = 29$) from gregarious animals. Only neurons that showed significant responses during zenithal stimulation were considered. The distribution of the preferred orientations to polarized light differed significantly from a uniform distribution (mean Φ_{max} angle: 131° ± 29.4° (SD); Rao's spacing test, $p < 0.01$, bin size: 10°). *E:* The distribution of Φ_{max} from solitarious animals ($n = 24$) did not differ from randomness (Rao's spacing test, $p > 0.05$; bin width: 10°). All values were treated as if originating from neurons with somata in the left brain hemisphere. For cells with cell bodies in the right hemisphere, values were mirrored against the longitudinal axis of the animal.

of the five TuLAL1a neurons from solitarious animals were distributed randomly (Fig. 3*F*). Without stimulation, neurons in solitarious animals had a mean background activity of 38.7 ± 19.66 (SD) imp/s and a mean background variability of 38.5 ± 9.2 (SD). No significant differences were observed in response strength, background activity, and background variability of TuLAL1a neurons between solitarious and gregarious locusts. The receptive fields of the solitarious TuLAL1a neurons varied considerably in bilateral size and position and had centers in the contralateral or ipsilateral hemisphere (Fig. 3*D*). In one TuLAL1a cell from a gregarious locust, ocular dominance was tested by monocular stimulation of the ipsi- and contralateral eye (Fig. 3*E*). In contrast to the intertubercle neurons (Pfeiffer et al. 2005), the neuron responded with similar response strength to ipsilateral, contralateral, and bilateral polarized-light stimulation (Fig. 3*E*).

Recordings from TuLAL1b neurons were obtained from four gregarious animals (Fig. 4). Three of the four neurons showed polarization opponency (Figs. 4*A*,*B*), while one TuLAL1b neuron was only activated during stimulation with polarized light. All four cells arborized in the lateral triangle as well as in the median olive of the lateral accessory lobe. The four neurons had a background activity of 18.5 ± 5.6 (SD) imp/s and a background variability of 34.24 ± 16.9 (SD) in darkness. TuLAL1b neurons had a mean response strength of about 155 ± 46.8 (SD) in the center of the receptive field. As in TuLAL1a neurons, receptive field structures of individual TuLAL1b cells varied substantially in bilateral extension and position of the receptive field along the left-right meridian.

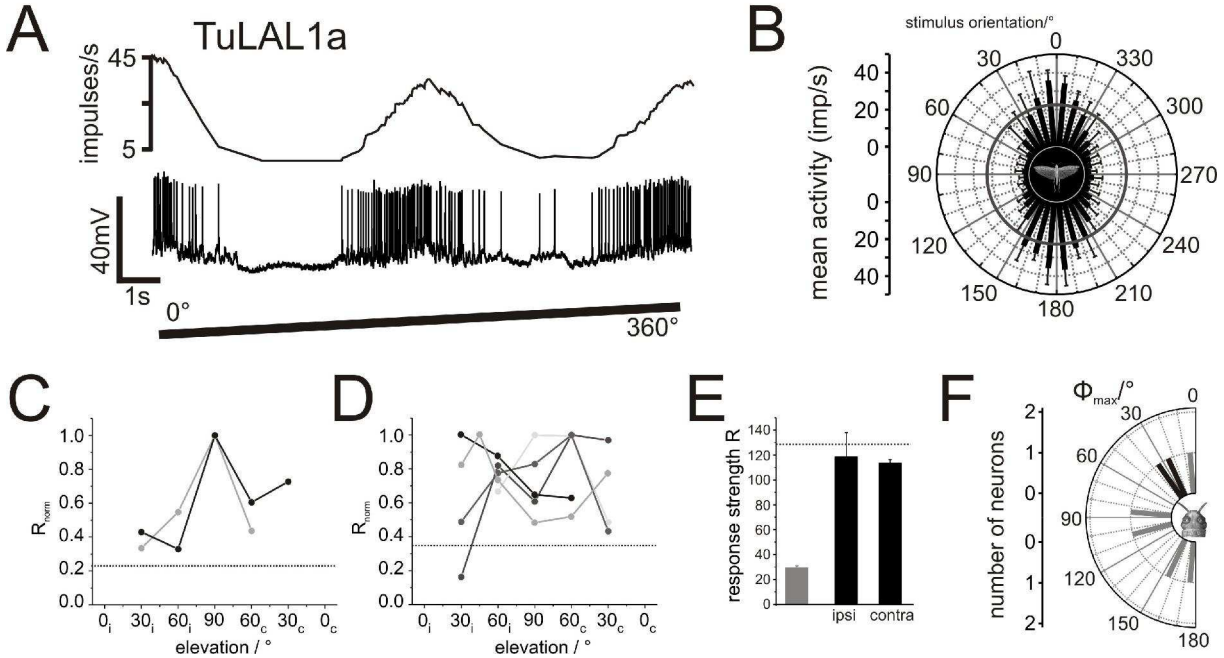

FIG. 3. Polarization-sensitive TuLAL1a neurons recorded in gregarious and solitarious locusts. *A:* Neural activity and mean firing rate of a TuLAL1a neuron during zenithal stimulation with a rotating polarizer (clockwise rotation, blue light, 450nm); lower trace shows the spike train, whereas the mean spiking activity is visualized in the upper trace with a moving average bin size of 1s. *B*: Circular diagram of mean frequencies of action potentials of the neuron in *A* plotted against *E*-vector orientation of the polarizer (n = 4, error bars = SD, bin size: 10°; Φ_{max} = 158°; Rayleigh test, $p < 10^{-12}$). Grey circle indicates background firing activity without stimulation. *C, D:* The normalized modulation strength (R_{norm}) of two gregarious (*C)* and five solitarious (*D)* animals plotted against the elevation of the stimulus along the left-right meridian. In each neuron, the R value was measured at different elevations and was normalized to the strongest response of the neuron in the visual field. Normalized variabilities of firing activity in darkness are shown as dotted lines. *E:* Ocular dominance test of a TuLAL1a neuron from a gregarious locust. Grey bar shows the background variability of the neuron. The response strength R for zenithal monocular stimulation of the ipsilateral eye (ipsi) and contralateral eye (contra) with a rotating polarizer was normalized to the response strength (dotted line) for binocular stimulation. Error bars = SD. *F*: The distribution of Φ_{max} orientation analyzed in the center of the receptive fields of seven TuLAL1a neurons recorded from gregarious (black bars, n = 2) and solitarious (grey bars, n = 5) animals plotted against the number of recorded neurons (bin size: 10°). All values are plotted as if originating from neurons with somata in the left brain hemisphere.

The cells had receptive field centers in the zenith, the ipsilateral or the contralateral hemisphere. Preferred *E*-vector orientations in the receptive field center were between 130° to 180° in three neurons and about 5° in one neuron.

Taken together, no differences in the general physiological properties and in receptive field structures of POL-neurons of the AOTu between gregarious and solitarious locusts were observed. Both intertubercle neurons had large receptive fields centered to the contralateral hemisphere. In contrast, the receptive fields of TuLAL1 neurons were considerably more narrow and varied substantially in shape and position.

Intensity-response functions of AOTu neurons in solitarious and gregarious locusts

While gregarious locusts migrate during the day, solitarious animals preferentially migrate during the night (Walloff 1963; Roffey 1963). We were therefore interested to see whether these different lifestyles are reflected in the polarization vision network in the locust AOTu. Intensity/response (I/R) functions were obtained by changing the intensity of the polarized blue light stimulus in the center of the receptive field over a range of 4 log units (Fig. 5). Neurons recorded during the subjective day (*Zeitgeber* time 0h-12h) were treated separately from neurons recorded during the subjective night (*Zeitgeber* time 12h-24h).

TuTu1 neurons were analyzed during the subjective day in 7 gregarious and 6 solitarious animals (Fig. 5*A*). The response strengths of the gregarious TuTu1 neurons were saturated between log I = 0 and log I = -2 and showed a sharp drop to background levels between log I = -3 and -4 (Fig. 5*A*). The I/R function of solitarious animals was intensity-independent between log I = 0 and -3, but at a logarithmic step of -4 the response broke down to background levels (Fig. 5*A*). Statistically, no differences were observed at each intensity step of the I/R function of TuTu1 neurons between gregarious and solitarious locusts.

I/R functions of LoTu1 neurons are based on 24 recordings in gregarious locusts and 18 recordings from solitarious animals. 18 LoTu1 neurons of gregarious locusts and five LoTu1 neurons of solitarious animals that were recorded during the day (Fig. 5*B*) showed similar I/R curves that gradually decreased to background levels between log I = 0 and log I = -4. In addition, recordings from seven LoTu1 neurons in gregarious animals and 13 LoTu1 neurons of solitarious animals during the night revealed

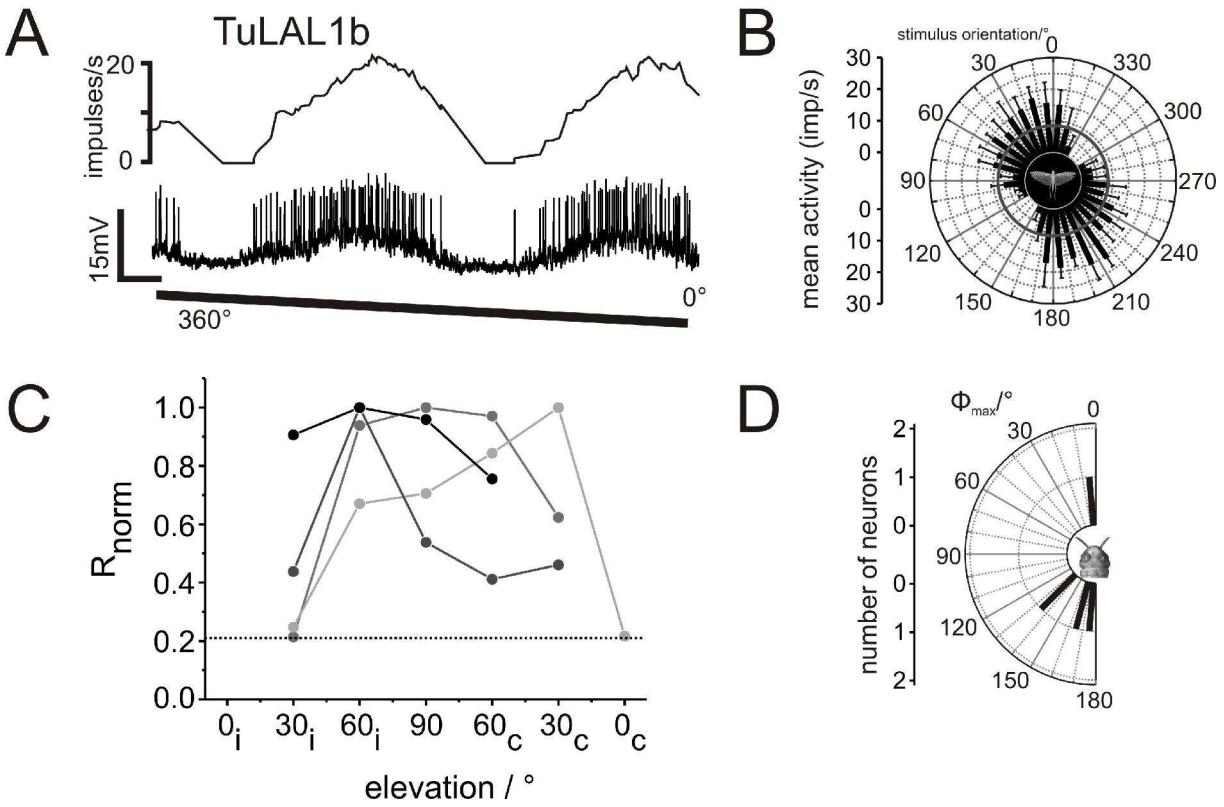

FIG. 4. Physiological analysis of TuLAL1b neurons from gregarious animals. *A:* Spike train (upper trace) and mean spiking frequency (lower trace) of a TuLAL1b neuron during zenithal stimulation with a polarizer that rotated in counter clockwise direction (moving average, bin width: 1s). *B*: Circular plot of the mean firing rate of the TuLAL1b neuron in *A* plotted against the orientation of the polarized light-stimulus (n = 4, error bars = SD, bin size: 10°; Φ_{max} = 7°; Rayleigh test, p = 1.22 × 10^{-5}). Grey solid circle shows the background activity of the neuron. *C:* Receptive field properties along the left-right meridian of four neurons from gregarious locusts. For each neuron, the modulation strength R was measured at different elevations of the ipsilateral (i) and contralateral (c) field of view and was normalized to the maximum R value in the receptive field (R_{norm}). Mean background variability is denoted as dotted line. *D*: The distribution of preferred *E*-vector orientations of the four TuLAL1b neurons in the center of the receptive fields. Data are plotted as if originating from neurons with perikarya in the left brain hemisphere of the animal.

similar sensitivity curves (Fig. 5*C*). As in TuTu1 neurons, I/R curves from LoTu1 did not differ significantly between solitarious and gregarious locusts.

As mentioned earlier, the response value R is a measure for the modulation strength of firing activity during stimulation but does not give information about the directedness of the response. Therefore we tested whether the length of the mean vector *r,* which serves as a measure for the directedness of the response to polarized light (Pfeiffer et al. 2011), differed between both locust phases (Fig. 5*C,D*). No significant differences in the directedness of TuTu1 (Fig. 5*C*) and LoTu1 neurons (Fig. 5*D*) between solitarious and gregarious locusts were found. Taken together the data suggest that there are no differences in the neural network of the AOTu underlying the processing of polarized light between both locust phases.

Differences in neural responses between AOTu neurons

The I/R curves between both types of intertubercle neurons differed substantially. Whereas the response strength to polarized light of the TuTu1 neurons remained relatively constant between log I = 0 and log I = -3 but declined to background levels within the final log unit (Fig. 6*A*), the modulation strength in the LoTu1 neuron decreased gradually from one logarithmic intensity step to the next (Fig. 6*B*). This is also reflected in the statistical analysis: In TuTu1 neurons the response at log I = 0 differed only from the response at the lowest light intensity step (log I = -4, Fig. 6*A*), whereas in the LoTu1 neuron the response to the highest analyzed light intensity differed significantly from all other light intensities (Fig. 6*B*). Furthermore several light intensity steps in LoTu1 differed significantly among each other. The I/R curves of the TuLAL1a and TuLAL1b neurons were similar to the I/R function of TuTu1 neurons, but showed a slightly more shallow decline between log I = -2 and log I = -4 to baseline levels (Figs. 6*C,D*). Thus, in contrast to TuTu1 and TuLAL1 neurons which may signal *E*-vector orientation above threshold levels independent from light intensity, the response in LoTu1 is strongly dependent on the intensity of the polarized light throughout all intensities tested.

We next compared the response properties of the neurons in greater detail to further characterize the distinct roles of the different cell types in the processing of polarized light. Because no differences

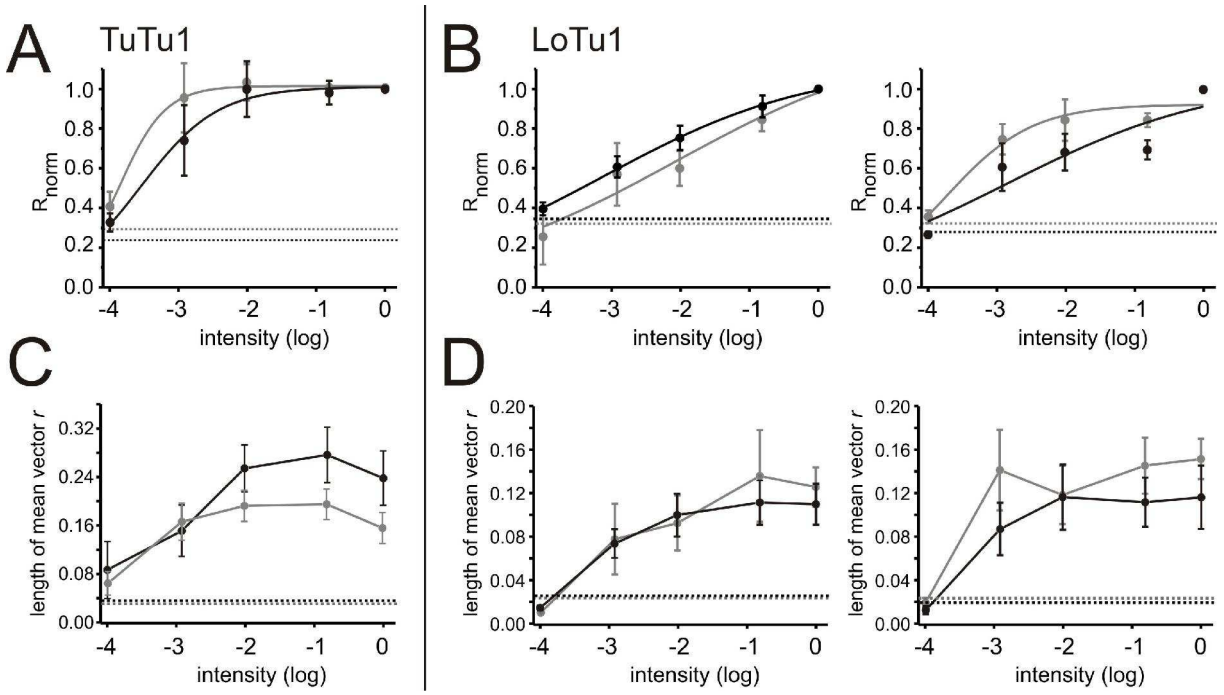

FIG. 5. Normalized intensity/response (I/R) functions of intertubercle neurons of gregarious and solitarious locusts to stimulation with polarized blue light in the center of their receptive fields. Maximum light intensity (log I = 0) was 1.8 $\times 10^{13}$ photons/cm^{2}s. The response strength R (*A,B)* and the length of mean vector *r* (*C,D)* were calculated at each light intensity. Solid curves in *A* and *B* are fitted through a modified Naka-Rushton function, and dotted lines denote the background variability. In *C,D* the data points are connected through solid lines for better visibility; broken lines show the directedness of the cells without stimulation. Error bars in all diagrams indicate standard errors. *A:* No differences are observed in the I/R function of TuTu1 neurons from gregarious locusts (*n* = 7, black fit, Naka-Rushton fitting parameters, $R_{norm(max)}$ = 1.02, K = -3.5 log units, υ = 0.74) analyzed during the day (*Zeitgeber* Time (ZT): 0-12h) and solitarious animals (n = 6, grey curve, $R_{norm(max)}$= 1.01, K = -4.34 log units, υ = 1.3) recorded during the night (ZT:12-24h) (log I = -1, -3 and -4 are tested through a student *t* test; log I = -2 tested through a Mann-Whitney *U* test, p > 0.05). *B:* I/R functions of LoTu1. Left figure shows the I/R functions from gregarious locusts (n = 18, black line, $R_{norm(max)}$ = 1.12, K = -2.6 log units, υ = 0.29) and solitarious animals (n = 5, grey line, $R_{norm(max)}$ = 1.27, K = -0.19 log units, υ = 0.26) analyzed during the day. The right diagram shows I/R functions of LoTu1 neurons from gregarious (n = 7, black plot, $R_{norm(max)}$ = 1.05, K = -1.95 log units, υ = 0.29) and solitarious animals (n = 13, grey fit, $R_{norm(max)}$ = 0.92, K = -3.99 log units, υ = 0.69) measured at ZT 12 -24. No differences were found between gregarious and solitarious LoTu1 neurons and between the I/R curves at ZT 0-12 and ZT 12-24 (log I = -1 and log I = -4 tested through an ANOVA analysis with Games-Howell *post hoc* test, log I = -2/-3 analyzed through an ANOVA combined with Tukey-HSD *post hoc* test, p > 0.05). *C,D*: Directedness of the response at different intensities of polarized light; same set of neurons as in *A,B*. No significant differences are present in TuTu1 neurons (*C,* log I = -1/-2 tested through a student *t* test; log I = -3/-4 tested by a Mann-Whitney *U* test) and in LoTu1 neurons (*D*, ANOVA analysis with Games-Howell *post hoc* test) between the two locust phases.

between solitarious and gregarious locusts were found in general tuning characteristics and light intensity dependence, data from both forms were pooled for the following analyses. LoTu1 neurons showed a significantly lower background firing rate than TuTu1 and TuLAL1a neurons (Fig. 7*A*). Furthermore the background spiking rate in darkness was significantly lower in TuLAL1b cells than in TuLAL1a neurons. While LoTu1 neurons showed low background variability and response strength to polarized light stimulation, TuTu1 neurons showed significantly higher background firing variability and a higher response strength R (Fig. 7*B,C*). No statistical differences were observed between TuLAL1a and TuLAL1b neurons in background variability and response strength R and between the intertubercle cells and the TuLAL1 neurons. Finally, the directedness of the response showed no differences between all AOTu neuron types (Fig. 7*D*).

In the next step we analyzed possible correlations between the tuning characteristics. Not surprisingly, the response strength of all cell types correlated significantly with the length of the mean vector *r* (data not shown). However, in all other tuning properties, no significant correlations were found except for a correlation between the background activity and the length of mean vector *r*. While in TuTu1 neurons no correlation between the background spiking activity and the length of the mean vector *r* was found (Fig. 7*E*), a linear correlation was present in LoTu1 (Fig. 7*F*; *t* test for slope = 0, R: -0.5, p=0.0001). A similar correlation was found, when all TuLAL1 cells were plotted together (Fig. 7*G*; *t* test for slope = 0, R: -0.65, p=0.03).

In the next analysis, the distributions of Φ_{max} within the receptive field were investigated (Fig. 8). In contrast to TuTu1 cells which did not show systematic changes in the preferred *E*-vector orientation within the receptive field (Fig. 8*A*), the preferred *E*-vector angle of LoTu1 increased within the receptive field from ipsi- to contralateral positions (Fig. 8*B*, *t* test for slope = 0, R: 0.23, p=0.005). Likewise, in TuLAL1a neurons deviations from zenithal Φ_{max}–values depended on the hemispheric side of the stimulus (Fig. 8*C, t* test for slope = 0, R:

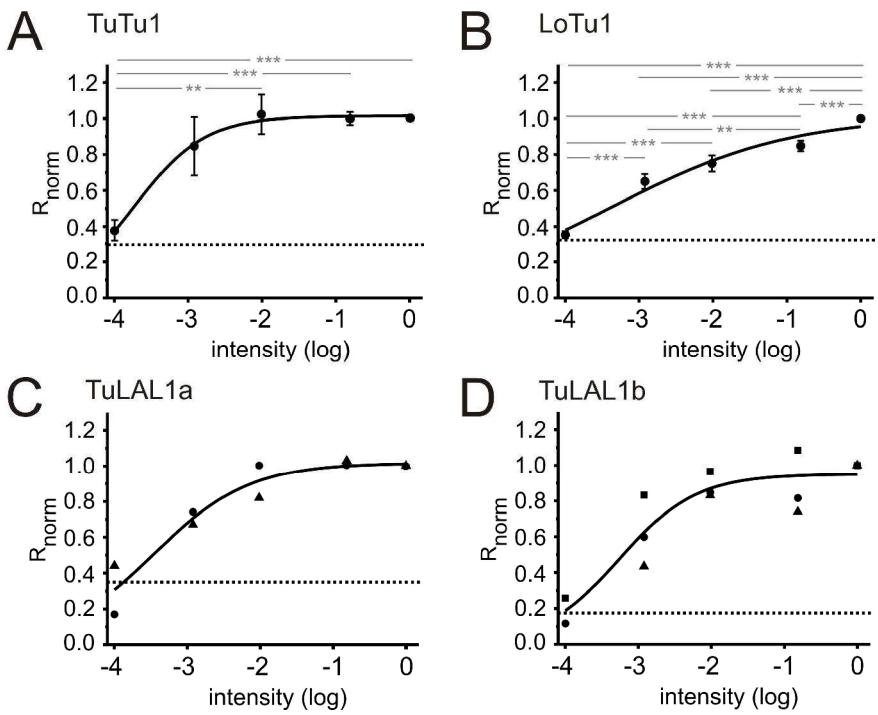

FIG. 6. Normalized intensity/response (I/R) functions of AOTu neuron types to stimulation in the center of the receptive fields. Maximum light intensity (log I = 0) was 1.8 $\times 10^{13}$ photons/cm^2 s. Solid curves are fitted through a modified Naka-Rushton function. Dotted lines indicate background variability. Error bars in all diagrams indicate standard errors. *A:* I/R function from all analyzed TuTu1 cells (*n* = 13, data are taken from Fig.5 *A,* $R_{norm(max)}$ = 1.01, K = -4 log units, υ = 0.9). *B:* I/R function from all measured LoTu1 neurons (*n* = 43, data are the same as in Fig. 5*B*, $R_{norm(max)}$ = 1.01, K = -3.16 log units, υ = 0.36). Whereas in LoTu1 the response amplitude increases steadily through all intensity steps (*B*), the maximum response strength in TuTu1 (*E*) is already reached at log I = -2 (ANOVA analysis combined with Games-Howell *post hoc* test; significance levels, *p < 0.05, **p < 0.01, ***p < 0.001). *C:* I/R function from twoTuLAL1a neurons ($R_{norm(max)}$ = 1.02, K = -3.34 log units, υ = 0.67). *D:* I/R plot from three TuLAL1b neurons ($R_{norm(max)}$ = 0.95, K = -2.9 log units, υ = 0.25).

0.43, p=0.03), while in TuLAL1b cells no changes of the Φ_{max} values within the field of view were found (Fig. 8*D*).

To elucidate further differences between the AOTu neurons, we next analyzed the correlation between tuning characteristics and the time of day of the recording (Fig. 9). TuTu1 neurons did not show any systematic changes in background activity (*t* test for slope = 0, correlation coefficient R: 0.16, p=0.39) or variability (*t* test for slope = 0, R: 0.31, p=0.09) depending on the time of day (data not shown). We also did not observe a correlation between the directedness of the response to polarized light in the center of the receptive field and the time of day (*t* test for slope = 0, R: 0.15, p=0.39, data not shown) nor between the response strength R in the center of the receptive field and the *Zeitgeber* time (Fig. 9*A*; *t* test against slope = 0, R: 0.16, p=0.37). The neurons responded to polarized blue light during the subjective day and subjective night with similar modulation strength (Fig. 9*D*, Mann-Whitney *U* test, p=0.63). Also, the response directedness did not differ between TuTu1 neurons recorded at night and during the day (Mann-Whitney *U* test, p=0.89). Similar to the conditions observed in TuTu1 neurons, no correlation between the general tuning characteristics (background activity, background variability), directionality, or response strength (Fig. 9*C*) and the time of day was observed in TuLAL1 cells. LoTu1 cells showed no correlation between background activity or background variability and the time of day (*t* test against slope = 0, correlation coefficients R: 0.05 and -0.03 respectively, p=0.64, p=0.83, data not shown). Although the length of the mean vector *r* in the center of the receptive field did not change systematically with daytime (*t* test against slope = 0, R: 0.24, p=0.07, data not shown), LoTu1 neuron showed an increased directedness in neurons that were recorded at night compared to neurons that were recorded during the day (Fig. 9*E*; Mann-Whitney *U* test, p=0.04). In addition, a correlation between the response strength R in the center of the receptive field and the time of day of the recordings was found (Fig. 9*B*; *t* test for slope = 0, R: 0.41, p=0.002). LoTu1 also showed a significantly higher response strength to polarized blue light at night than during the day (Fig. 9*E,* two tailed *t* test, p= 0.0004). To further substantiate the effect of daytime on the response strength and directionality in LoTu1, we recorded from a LoTu1 neuron over a period of two hours between the *Zeitgeber* times 10:50 h to 13:00 h and stimulated the neuron every 30 minutes with polarized blue light within the center of the receptive field (Fig. 9*F*,*G*). While no changes were noted in background activity, background variability, and the *E*-vector tuning during this time frame (Fig. 9*F*), an increase in response strength to polarized light and directionality of the response were observed at *Zeitgeber* times 11:50 and 12:20 (Fig. 9*G*). The response strength and directedness decreased again 1 hour after the beginning of the subjective night, but might already have been affected by deterioration of the condition of the animal.

Responses to high intensities of polarized light

After analyzing responses under low-light conditions, we were interested in how the interneurons of the AOTu responded to stimulation with polarized light at higher light intensities as occurring, e.g., at noon on a cloudless sky. Therefore

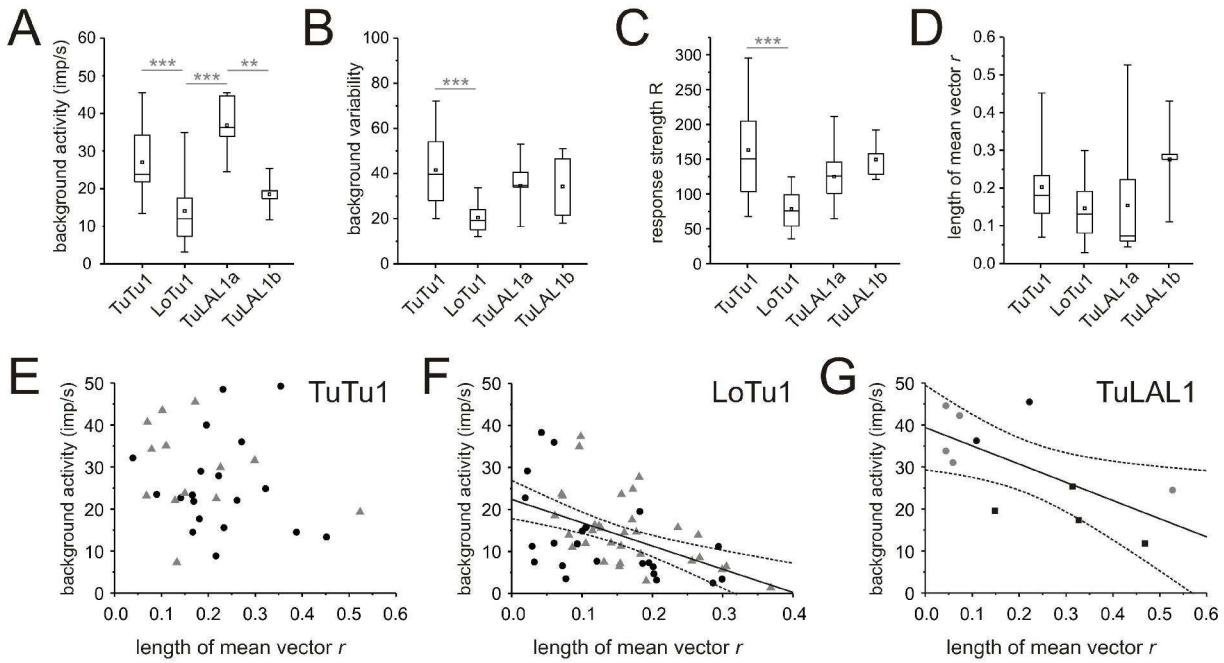

FIG. 7. General tuning characteristics, response strengths, and directedness of the response in the four AOTu neuron types. All box plots show the median (horizontal lines) and corresponding mean values (squares), and the 25% and 75% quartiles (boxes). The whiskers indicate the 5-95% range of the data. *A:* Background activities of TuTu1, LoTu1, TuLAL1a, and TuLAL1b neurons. *B:* Background varibilities of the neurons of the AOTu. *C:* Response strength of the AOTu neurons to polarized light presented in the center of the receptive fields. *D:* Directedness (length of mean vector *r*) of the polarization response in the AOTu neurons. In all cases (*A-D*), ANOVA analysis combined with Games-Howell *post hoc* test was applied for statistical analysis (significance levels, *p < 0.05, **p < 0.01, ***p < 0.001). *E:* Background spiking frequency of TuTu1 neurons plotted against the directedness of the response (length of mean vector *r*). Gregarious locusts are indicated as black circles, solitarious animals are shown as grey triangles. No correlation between background frequency and directedness of the neurons was noted (n = 31; R_{corr} = -0.17, *t* test against slope of 0, p = 0.32). *F:* Correlation of the background firing activity and the directedness in LoTu1 neurons (black circles: gregarious locusts; grey triangles: solitarious locusts; n = 55; R_{corr} = -0.49, *t* test against slope of 0, p = 0.0004). *G:* Correlation between background activity and directedness in TuLAL1 neurons. TuLAL1a neurons are shown as circles, TuLAL1b cells are indicated as squares. Data from gregarious animals are shown in black and from solitarious animals, in grey (n = 11; R_{corr} = -0.65, *t* test against slope of 0, p = 0.02). In *F* and *G* linear regressions are shown as solid lines, 95% confidence bands are shown as dotted lines.

we stimulated LoTu1 and TuTu1 neurons with high intensity polarized white light (about 26.8 × 10^4 lx) that ranged in a similar order of magnitude as illumination from the sun at noon (see Appendix, Fig. A3*A,D*). As shown by Kinoshita et al. (2007) both intertubercle neurons have broad spectral sensitivities and are excited at Φ_{max} during presentation with different wavelengths of polarized light. Whereas LoTu1 was activated during stimulation with polarized blue light, high-intensity polarized white light resulted in strong inhibition of spiking activity without any action potentials in three out of 19 recorded LoTu1 neurons. The other neurons responded with reduced modulation of spiking activity (Fig. 10*A-D*). An opposite light-on response - activation at low light intensities and inhibition at high light intensities - was typical for LoTu1 (Fig. 10*A,C*). Accordingly, the response strength of the LoTu1 neuron was significantly higher during stimulation with polarized blue light compared to stimulation with polarized bright white light (Fig. 10*E*).

TuTu1 cells were analyzed in 7 experiments. In contrast to LoTu1, TuTu1 cells showed no significant difference in the responses between blue light stimulation and bright white light stimulation (Fig. 10*G*). To further exclude the possibility that the effect of the reduced response strength in LoTu1 neurons is the result of the different spectral composition of the stimuli, we determined I/R relationships for different intensities of white light stimulation (Fig. 10*F,H*). Five LoTu1 neurons showed a bell-shaped sensitivity curve with a maximum response strength at log I = -2 and reduced response strength at lower and higher intensities (Fig. 10*F*). Statistically, the response strengths between log I = -1 and -3 were significantly stronger than the background variability, whereas the modulation strengths at log I = 0 and -4 were not different from background variability. In one investigated TuTu1 neuron the response strength at log I = 0 was similar to the modulation strength at intensities between log I = -1 to -3, again exhibiting an intensity-independent response (Fig. 10*H*). Taken together, these data confirm that the reduced modulation strength in LoTu1 at bright white light is an effect of light intensity.

DISCUSSION

We have analyzed general neural activities, *E*-vector-tuning, receptive field properties, and

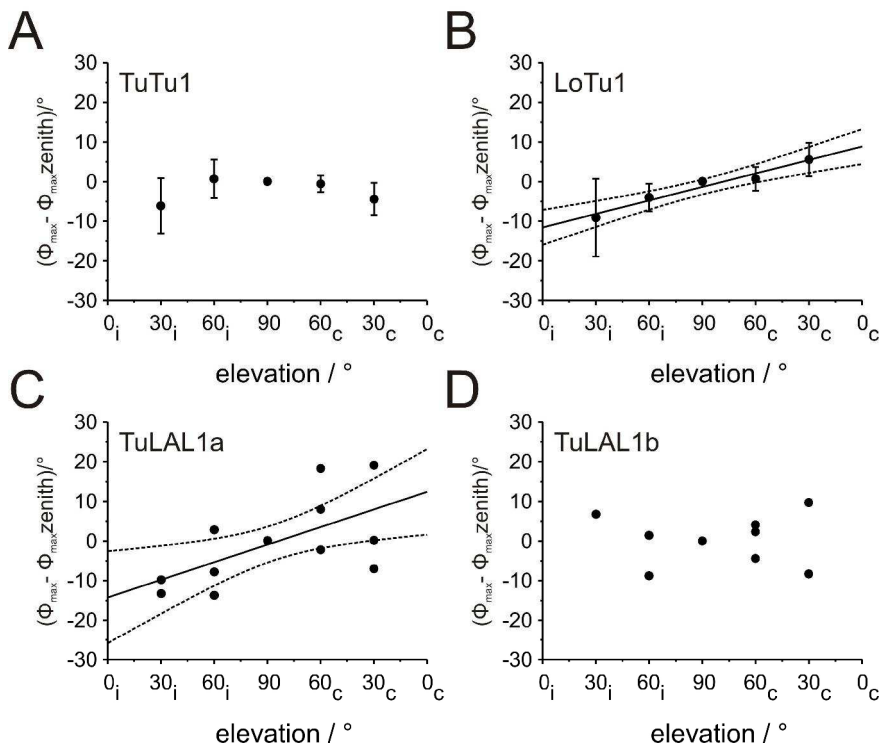

FIG. 8. Φ_{max}-distribution of AOTu neurons at different elevations along the left-right meridian. Data were obtained by subtracting the absolute deviation of the preferred orientation angle at each tested position from the Φ_{max} value in the zenith. Only neurons that showed a significant response to polarized light during zenithal stimulation (Rayleigh test, $p < 0.05$) were included. In these analyses we did not distinguish between solitarious and gregarious locusts because we did not find any differences in the receptive field structures and the zenithal Φ_{max} values. *A:* The Φ_{max} distribution of TuTu1 cells (n = 29) does not change systematically along the left-right meridian (R_{corr} = -0.03, t test against slope of 0, p = 0.76). *B:* LoTu1 neurons (n = 44) showed a significant correlation between *E*-vector tuning and corresponding position along the left-right meridian (R_{corr} = 0.23, p = 0.005). Linear regression is shown as solid line, confidence intervals (95%) are shown as dotted curves. For better visibility, only averaged preferred direction values are shown in *A* and *B* (error bars = SE). *C:* Distribution of Φ_{max} values along the left-right meridian of TuLAL1a cells (n = 5). A correlation between the position of the polarized light-stimuli along the left-right meridian and Φ_{max} orientation of the neurons was observed (R_{corr} = 0.61, p = 0.01). Linear regression is shown as solid line, 95% confidence bands are shown as dotted lines. *D:* No correlation between observed *E*-vector tuning and elevation of the polarized light-stimuli was found in TuLAL1b cells (R_{corr} = -0.03, p = 0.93).

intensity/response functions to polarized light in four classes of AOTu neurons in the locust brain. To our surprise, we found no difference in these physiological parameters between gregarious and solitarious locusts despite their different life styles and activity patterns. Consistent differences in physiological parameters were, however, found when comparing the different neuronal cell types. LoTu1 was exclusively activated by polarized light at moderate light intensities, while TuTu1 and TuLAL1 neurons showed polarization opponency. Above a certain threshold of light intensity, TuTu1 and TuLAL1 cells showed invariance to changing light intensities and daytime, while the *E*-vector response of LoTu1 was highly dependent on light levels as well as on time of day. In addition, stimulation with polarized light intensities mimicking illuminance levels of midday sunlight led to strong reduction of *E*-vector dependent responses in LoTu1 but not in TuTu1 neurons. Taken together, these observations suggest that TuTu1 and TuLAL1 neurons provide a robust compass signal throughout the day, while LoTu1 is tuned to signal polarization information at low light conditions during sunset or sunrise.

General tuning properties

While the response strength between TuTu1 and LoTu1 neurons differed significantly, no differences were found in the averaged directedness of the response between any of the AOTu cell types. This indicates that the tuning width is similar in all AOTu neurons. In addition, the higher background variability of the TuTu1 neurons compared to the LoTu1 cell could mean that TuTu1 neurons receive synaptic input from a larger number of neurons than the LoTu1 cell. Furthermore, in LoTu1 and TuLAL1 neurons, a correlation between background activity and directedness was found. This implies that in these cell types the background activity has an effect on the tuning width around Φ_{max}. For LoTu1 this is not surprising because its activity at Φ_{min} is similar to background levels. Experiments in flies showed that neural activities of visual neurons in the brain are modified during flight or walking (Rosner et al. 2010; Maimon et al. 2010; Chiappe et al. 2010). In visual neurons of locusts a change of firing activity dependent on the behavioral state was also observed (Homberg 1994). If the spiking rate of LoTu1 and TuLAL1 neurons were, likewise, modified during walking or flight, the directedness of the response to polarized light should also be modified in a behavior dependent context.

The *E*-vector tuning of LoTu1 in gregarious animals was significantly different from a random distribution. It had a mean value of about 128°, which is similar to the mean Φ_{max} of 134° reported for LoTu1 by Pfeiffer et al. (2005). The TuTu1 neurons from gregarious animals, likewise, showed two tuning peaks around 120° and 180° as reported by Pfeiffer et al. (2005), but, in addition, we found a third Φ_{max} peak near 35°. While the uniform tuning of LoTu1 supports anatomical evidence for the presence of only a single neuron per hemisphere, the third *E*-vector tuning type for TuTu1 neurons is not supported by anatomical data which did not reveal more than two neurons per

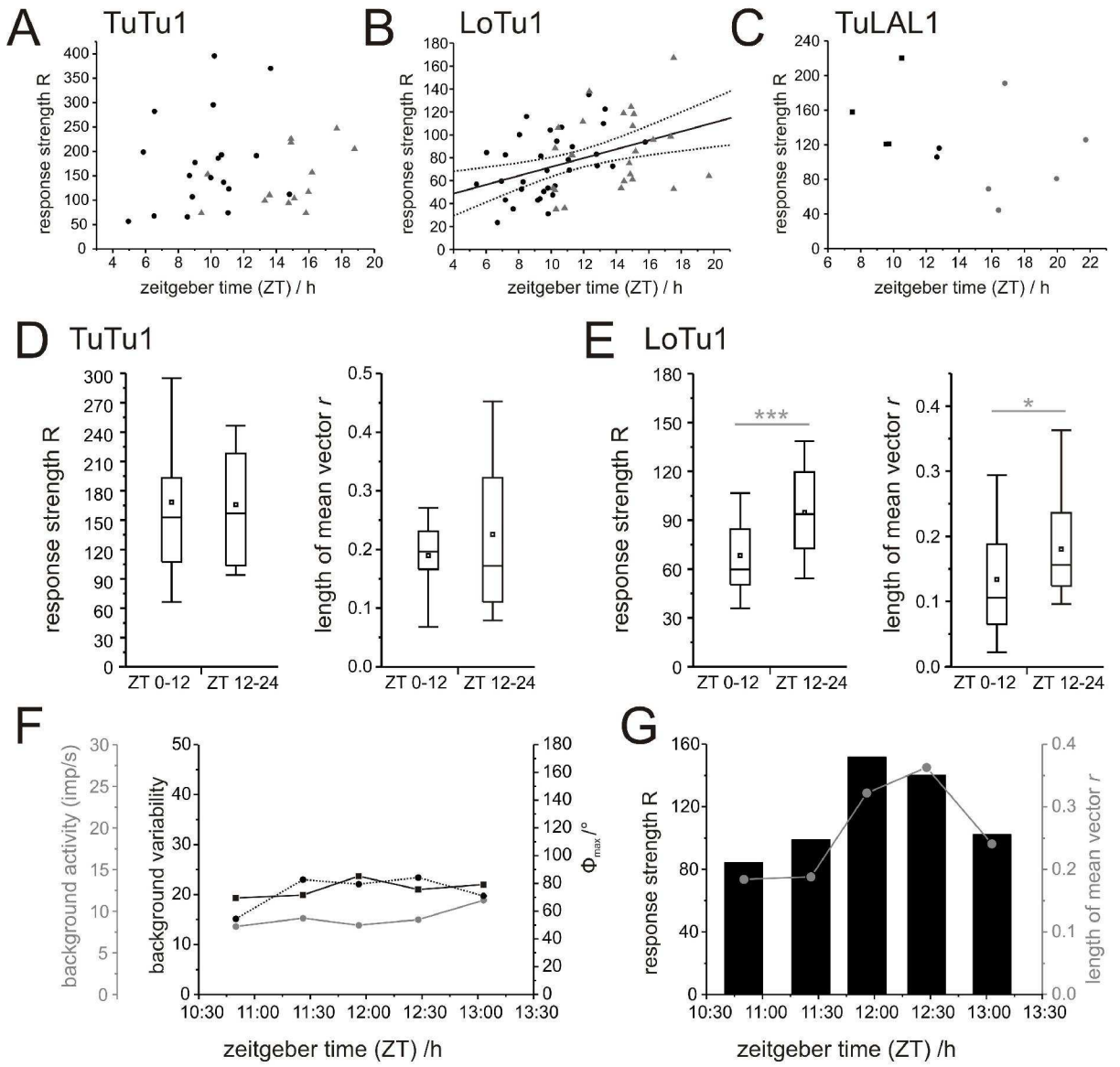

FIG. 9. Changes of the response strength R and the directedness *r* in the center of the receptive field of TuTu1 (*A*,*D*), LoTu1 (*B, E*) and TuLAL cells (C) during the time of day. In *D* and *E* the mean (squares) and median (horizontal lines) response strength R and the 25% and 75% quartiles (boxes) are shown. The whiskers indicate the 5-95% range of the data. *A:* The response strength R of TuTu1 neurons plotted against the time of the recording. Data from gregarious locusts are indicated as black circles, data from solitarious animals are shown as grey triangles. No correlation between response strength and recording time was observed (n = 32; R_{corr} = 0.09, t test against slope of 0, p = 0.63). *B:* Analysis of response strength R of LoTu1 during the time of day. Data from gregarious animals are indicated as black circles, data from solitarious animals are shown as grey triangles. In LoTu1 the modulation strength R correlated significantly with the time of day of the recording (n = 58; R_{corr} = 0.41, t test against slope of 0, p = 0.001). The linear regression is shown as solid line, 95% confidence bands are denoted as dotted lines. *C:* Response strength R of TuLAL neurons plotted against the time of day of the recording (n = 11; R_{corr} = -0.36, t test against slope of 0, p = 0.27). *D:* Comparison of the response strength (left panel) R between TuTu1 neurons analyzed during the day (*Zeitgeber* Time: 0-12h) and TuTu1 neurons that were recorded between ZT 12-24. The data are the same as the data shown in *A*. TuTu1 cells recorded during the day (n = 18) do not differ significantly from TuTu1 neurons recorded between ZT 12-24h (n = 14; Mann-Whitney U test, p= 0.68). Right plot: Analysis of the directedness of the same set of TuTu1 neurons as in *A*. The length of the mean vector *r* does not differ statistically between TuTu1 cells recorded during the day and TuTu1 neurons recorded at night (Mann-Whitney U test, p= 0.94). *E:* Left diagram: The response strength of LoTu1 is significantly stronger at night (n = 23) than during the day (n = 35; student t test, p = 0.0004). LoTu1 showed a higher directedness at night than during the day (right plot; Mann-Whitney U test, p = 0.042). The data are from the same set of LoTu1 neurons as in *B*. *G:* Recording from a single LoTu1 neuron over a period of about 2 hours, showing background activity (grey circles, grey solid line), background variability (black squares, solid black line), and *E*-vector tuning (black circles, black dotted line) at different *Zeitgeber* times. *H:* Diagram of the response strength R (black bars) and the length of mean vector *r* (grey circles, grey solid line) plotted against the time of day of the same LoTu1 neuron as in *G*.

brain hemisphere (Homberg et al. 2003). In contrast to LoTu1 and TuTu1, the preferred *E*-vector orientations of the TuLAL1 neurons varied considerably. This is in accordance with the existence of 40-50 TuLAL1 neurons as suggested from fiber counts (Homberg et al. 2003).

Receptive fields

The receptive fields of the intertubercle neurons are directed to the contralateral hemisphere with maximum response strength at an elevation of 60° along the left-right meridian. This fits very well to

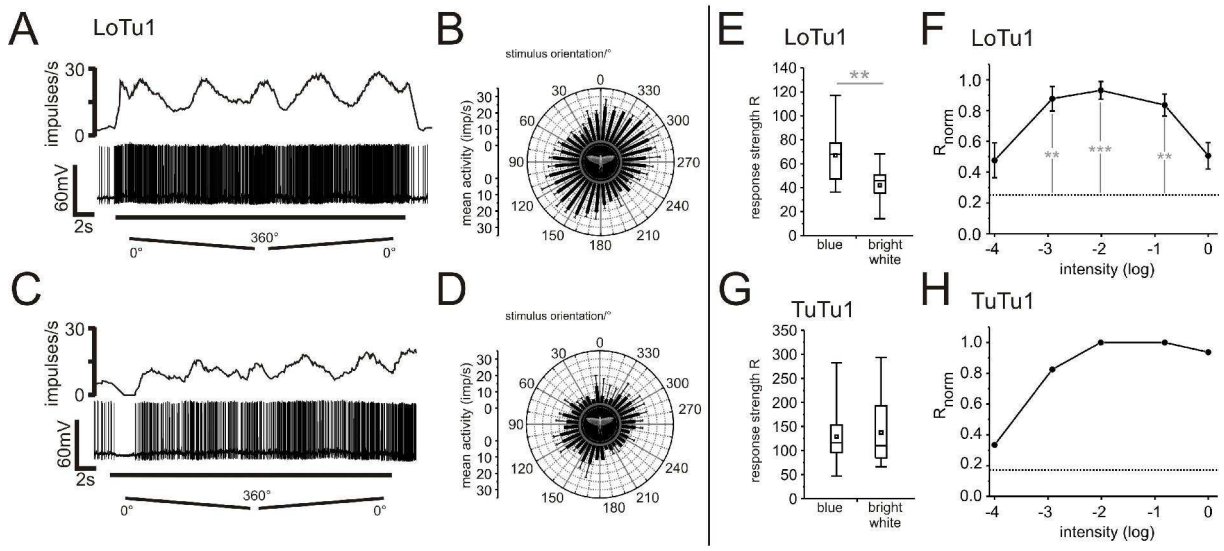

FIG. 10. Response strength of intertubercle neurons to zenithal stimulation with polarized blue light (30.82 µW/cm^2) and high intensity polarized white light (39.17 mW/cm^2). *A:* Spike train (upper trace) and mean firing activity (lower trace) of a LoTu1 neuron during stimulation with polarized blue light (moving average, bin size: 1s). The duration of the polarized light stimulus is denoted by a solid line. The start and the direction of the rotation of the polarization filter are indicated by the ramps. *B:* Circular plot of the mean spiking rate of the neuron to polarized light shown in *A* plotted against the *E*-vector orientation of the polarizer (bin size: 10°; n = 2; error bars = standard deviation, Φ_{max}= 138°, Rayleigh test, p = 1.08 × 10^{-5}). Grey circle indicates background activity of the neuron in darkness. *C:* The same neuron as in *A* stimulated with high intensity polarized white light. *D:* Circular diagram from the recording in *C* illustrates the mean firing rate as a function of *E*-vector orientation (bin size: 10°; n = 2; error bars = standard deviation, Φ_{max}= 121°, Rayleigh test, p = 0.008). *E, G:* Comparison of the absolute response strength R between LoTu1 *(E)* and TuTu1 neurons *(G)* to stimulation with zenithal polarized blue light and polarized bright white light. The median response strengths R are shown as horizontal lines, the mean values as square and the 25% and 75% quartiles boxes are indicated by boxes. The whiskers denote the 5-95% range of the data. *E:* LoTu1 neurons responded stronger to polarized blue light than to bright polarized white light (n = 19; paired student t test, p = 0.0007 *F:* Normalized I/R function of the LoTu1 neuron (n = 5) to stimulation with zenithal white light. Maximum light intensity: 39.17 mW/cm^2. Data points are connected by solid lines for better visibility. Dotted line indicates background variability. Error bars show the standard errors. For statistical analysis ANOVA combined with Games-Howell *post hoc* test was used (significance levels, *p < 0.05, **p < 0.01, ***p < 0.001).). *G:* Response strength R of TuTu1 neurons during zenithal stimulation with polarized blue light and bright white light (n = 7). No differences are observed in the modulation strength (paired student t test, p = 0.42). *H:* Normalized I/R function of one TuTu1 neuron stimulated with white polarized light from dorsal direction (light intensity at log 0: 39.17 mW/cm^2). Data points are connected by solid lines for visualization. Dotted line indicates the background variability of the neuron.

data from Pfeiffer et al. (2005), who showed that LoTu1 and TuTu1 receive polarization input from the ipsilateral eye (Pfeiffer et al. 2005) and to anatomical data showing contralaterally pointing visual axes of DRA ommatidia (Homberg and Paech 2002). The extent of the receptive fields of TuTu1 (110°-120°) and LoTu1 (130°-135°) along the left-right meridian was considerably wider than the receptive fields of DRA photoreceptor neurons (about 30°; Eggers and Gewecke 1993). This suggests that photoreceptor neurons with different spatial tuning are recruited by the intertubercle cells. In contrast to the intertubercle neurons, TuLAL1 neurons differed widely in receptive field properties including receptive field orientation and bilateral expansion. This is not surprising in view of the high number of TuLAL1 cells per brain hemisphere (Homberg et al. 2003). The receptive fields had centers in the contra- or ipsilateral hemisphere with strongest responses at elevations ranging from 30° contralaterally to 30° ipsilaterally.

One of the main functions of the intertubercle neurons is probably to provide contralateral visual input to postsynaptic TuLAL1 neurons. As shown here in one example, TuLAL1a neurons do receive binocular input, and their postsynaptic partners, type TL2 tangential neurons with projections to the lower division of the central body (Träger et al. 2008), are likewise binocular (Heinze et al. 2009). TuLAL1b neurons, in contrast, might receive ipsilateral visual input only, because their likely postsynaptic partners, TL3 tangential neurons of the lower division of the central body (Träger et al. 2008) are also dominated by ipsilateral visual input (Heinze et al. 2009).

In contrast to TuTu1 and TuLAL1b neurons, *E*-vector tuning in LoTu1 and TuLAL1a neurons changed systematically along the left-right meridian. In both types of neuron an increase in *E*-vector tuning from the ipsilateral to the contralateral hemisphere was observed. As already illustrated for neurons of the protocerebral bridge, this shift of Φ_{max} values within the receptive field suggests that neurons of the right AOTu respond more strongly when the sun is behind the animal and neurons of the left AOTu, when the locust faces the sun (Heinze et al. 2009). Together with input from the sky chromatic contrast, proposed by Pfeiffer and Homberg (2007) the *E*-vector tuning shift may further aid in distinguishing between the solar and antisolar hemisphere of the sky.

Responses of intertubercle neurons to different light intensities

Intensity/response (I/R) functions of the intertubercle cells were determined in the center of

their receptive fields. The response threshold at which the neurons showed no differences to firing activity at darkness was at a light intensity of about 18 $\times 10^8$ photons/cm^{2}s. This corresponds to the sensitivity of the intertubercle neurons analyzed during zenithal stimulation (Kinoshita et al. 2007). Clear differences were observed in I/R functions between LoTu1 and the remaining AOTu neurons. In TuTu1, TuLAL1a and TuLAL1b neurons the response strength remained relatively constant and showed a sharp drop within the final 2 log intensity steps. This is in accordance to data from cricket POL1 neurons, which were also intensity independent above a certain threshold level of polarized light intensity (Labhart and Petzold 1993; Labhart et al. 2001; Petzold 2001). These neurons should, therefore, not be susceptible to changes in clouding conditions and are thus, ideally suited to process polarized light signals for spatial orientation. In contrast, the response of LoTu1 was intensity dependent over at least four log units of light levels.

LoTu1 but not TuTu1 neurons were more sensitive at night than during the day as shown by higher response strength and increased directedness to polarized light. No difference, however, was observed in the absolute sensitivity of LoTu1 during the day and at night. As shown by Pfeiffer et al (2005), Kinoshita et al. (2007) and in this study, LoTu1 receives at least two visual inputs from dorsal direction: (1) a low threshold excitatory input that is polarization sensitive, and (2) a higher threshold inhibitory input that is insensitive to *E*-vector orientation. The lack of inhibition by unpolarized light at low light levels leads to stronger responses to polarized light at night than during the day and to a steeper I/R function of LoTu1 at night without affecting its absolute threshold for polarized light. When increasing the intensity of polarized light, however, the increasing contribution of the inhibitory unpolarized light input eventually dominates the response. It leads to a reduction and finally to complete elimination of the *E*-vector dependent response (Fig. 10*F*). Based on these characteristics, LoTu1 is probably adapted to signal polarized light at low light conditions during sunset or sunrise, while high light intensities at noon should inhibit LoTu1 and strongly reduce its polarization sensitivity. A model proposed by Pfeiffer et al. (2011) suggests that the temporal dynamics of neural responses might largely account for the reversal of responses of LoTu1 with increasing light intensities. According to that model, stimulus-dependent release of histamine by photoreceptors of the dorsal rim area combined with dynamic membrane properties of lamina neurons could explain the opposing effects of high and low intensity polarized light on LoTu1.

In contrast, the responses of TuTu1 to high and low intensity polarized light did not differ significantly. As shown in Kinoshita et al. (2007), an inhibition of TuTu1 by dorsal unpolarized light was observed in only one of a total of four recordings, and TuTu1 neurons did not show significant responses to UV or green unpolarized light presented from dorsal direction (Kinoshita et al. 2007). This correlates well with our data indicating intensity independent responses of TuTu1 to zenithal polarized light.

Comparison between gregarious and solitarious locusts

The transformation in locusts from the solitarious to the gregarious form is strongly dependent on population density and is mediated by the level of serotonin in the thoracic ganglia (Anstey et al. 2009). Field experiments suggest that solitarious locusts prefer to migrate as individuals during the night (Waloff 1963; Roffey 1963). While Roffey (1963) observed flight activity at night of locusts ranging from solitarious to transiens and gregarious, Waloff (1963) reported that flight of solitarious locust occurred exclusively at night. He observed spontaneous flight activity of solitarious locusts ranging from sunset to about 5 hours after disappearance of the sun. In both field studies, however, migrating solitarious locusts were also observed during the day, but their flight activity was interpreted as forced flights or as exceptions.

Substantial differences in the size and proportion of brain areas involved in visual processing were observed between gregarious and solitarious locusts (Ott and Rogers 2010). Thus, gregarious locusts have larger brains than solitarious locusts, a noticeable larger optic lobe and central complex and, in addition, a smaller optic lobe to midbrain ratio than solitarious locusts (Ott and Rogers 2010).

We did not find significant differences in the physiological responses of POL-neurons of the AOTu between both forms. Receptive field structures as well as absolute sensitivities were analyzed extensively in the intertubercle cells and in both, no correlation between physiological responses and locust phases were found. The *E*-vector tunings of the intertubercle cells were distributed more randomly in the solitarious phase, but did not differ significantly between both forms. Furthermore, no difference in I/R functions were found between the two phases. The data therefore suggest that the significance of polarized light signals as navigational cues does not differ between both forms. Although solitarious animals have larger eyes than gregarious locusts (Rogers et al. 2010), this difference is not reflected in the width and alignment of the receptive fields of AOTu intertubercle cells. The size and orientation of intertubercle receptive fields suggest that the size of the DRA as well as the number of DRA photoreceptors may not be different between both locust phases and thus, the increased eye size of solitarious locusts might be restricted to the main retina. It is, however, conceivable that different adaptations of AOTu neurons may be present in their responses to unpolarized chromatic stimuli, which were not tested here.

Possible functional role of AOTu neurons

LoTu1 and TuTu1 neurons receive polarized light signals mainly from the ipsilateral eye (Pfeiffer et al. 2005), thus an interconnection between the intertubercle cells of both hemispheres can be excluded. Both intertubercle neurons likely transmit signals to TuLAL1 neurons which provide input to the sky compass in the central complex. Physiologically TuTu1 neurons are similar to the TuLAL1 cells and could implement an early comparison of *E*-vector signals from both eyes in TuLAL1a neurons. Owing to the strong dependence of the firing activity of LoTu1 on changes of the light intensity and thus, on the solar elevation LoTu1 might act as a gain modulator that controls the response strength of TuLAL1 cells in a daytime dependent manner.

An additional factor contributing to neural activity of the intertubercle cells is the degree of polarization in the sky. Both intertubercle neurons are inhibited strongly when the degree of polarization is lower than $d = 0.3$ (Pfeiffer et al. 2011). Modeling of illumination of a horizontally oriented locust from the sun (see Appendix, Fig. A3*A,D*) and the degree of polarization in the center of the receptive field of the intertubercle neurons (see Appendix, Fig. A3*B,E*) show that both signals might contribute to an inhibition of neural activity at noon, when the degree of polarization is low and the light intensity is high. Owing to the higher absolute sensitivity of the LoTu1 neuron to polarized light than to unpolarized light, light intensity might be crucial in LoTu1 for the impact of the detected sky compass cue. As already discussed by Kinoshita et al. (2007), high light intensities and low degrees of polarization at noon will probably reduce the contribution of polarized light input and simultaneously increase the significance of unpolarized light input for detection of the azimuthal direction of the sun. Thus, LoTu1 could control the balance in TuLAL1 neurons between polarized light vs. unpolarized light input.

ACKNOWLEDGEMENTS

We thank Dr. Keram Pfeiffer for providing the Spike2-script for data analysis and Sebastian Richter and Manfred Peil for constructing the stimulation device and control equipment. We are grateful to Dr. Carsten Heuer for suggestions on the manuscript and to Martina Kern and Karl-Heinz Herklotz for maintaining the gregarious locust cultures. We thank Martin Kollmann for establishment of the solitarious culture and Evelyn Rieber and Tim-Henning Humberg for rearing the solitarious locusts.

GRANTS

This work was supported by grant HO 950/16-2 from the Deutsche Forschungsgemeinschaft. Parts of the effort were sponsored by the Air Force Office of Scientific Research, Air Force Material Command, USAF, under grant number FA8655-08-1-3021. The U.S. Government is authorized to reproduce and distribute reprints for Government purpose notwithstanding any copyright notation thereon. The views and conclusions contained herein are those of the authors and should not be interpreted as necessarily representing the official policies or endorsements, either expressed or implied, of the Air Force Office of Scientific Research or the U.S. Government.

AUTHOR CONTRIBUTIONS

The experiments were conceived and designed by Basil el Jundi and Uwe Homberg, Basil el Jundi performed the experiments and analyzed the data, and both autors wrote the manuscript.

DISCLOSURES

No conflicts of interest, financial or otherwise, are declared by the authors.

REFERENCES

Anstey ML, Rogers SM, Ott SR, Burrows M, Simpson SJ. Serotonin mediates behavioral gregarization underlying swarm formation in desert locusts. *Science* 323: 627–630, 2009.

Batschelet E. *Circular Statistics in Biology*. New York: Academic, 1981.

Chiappe ME, Seelig JD, Reiser MB, Jayaraman V. Walking modulates speed sensitivity in *Drosophila* motion vision. *Curr Biol* 20: 1470–1475, 2010.

Clements AN, May TE. Studies on locust neuromuscular physiology in relation to glutamic acid. *J Exp Biol* 60: 673–705, 1974.

Collett TS, Collett M. Path integration in insects. *Curr Opin Neurobiol* 10: 757–762, 2000.

Dacke M, Byrne MJ, Baird E, Scholtz CH, Warrant EJ. How dim is dim? Precision of the celestial compass in moonlight and sunlight. *Phil Trans R Soc B* 366: 697–702, 2011.

Dacke M, Byrne MJ, Scholtz CH, Warrant EJ. Lunar orientation in a beetle. *Proc R Soc Lond B* 271: 361–365, 2004.

Dacke M, Nilsson DE, Scholtz CH, Byrne M, Warrant EJ. Animal behaviour: insect orientation to polarized moonlight. *Nature* 424: 33, 2003.

Dirsh VM. Morphometrical studies on phases of the desert locust (*Schistocerca gregaria* Forskål). *Anti-Locust Bull* 16: 1–34, 1953.

Eggers A, Gewecke M. The dorsal rim area of the compound eye and polarization vision in the desert locust (*Schistocerca gregaria*). In: *Sensory Systems of Arthropods,* edited by Wiese K, Gribakin FG, Popov AV, and Renninger G. Basel: Birkhäuser, 1993, p. 101–109.

el Jundi B, Pfeiffer K, Homberg U. A distinct layer of the medulla integrates sky compass signals in the locust brain. *Submitted*.

Frost BJ, Mouritsen H. The neural mechanisms of long distance animal navigation. *Curr Opin Neurobiol* 16: 481–488, 2006.

Giurfa M, Capaldi E.A. Vectors, routes and maps: new discoveries about navigation in insects. *Trends Neurosci* 51: 237–242, 1999.

Heinze S, Homberg U. Maplike representation of celestial *E*-vector orientations in the brain of an insect. *Science* 315: 995–997, 2007.

Heinze S, Gotthardt S, Homberg U. Transformation of polarized light information in the central complex of the locust. *J Neurosci* 29: 11783–11793, 2009.

Homberg U. Flight-correlated activity changes in neurons of the lateral accessory lobes in the brain of the locust *Schistocerca gregaria. J Comp Physiol A* 175: 597–610, 1994.

Homberg U. In search of the sky compass in the insect brain. *Naturwissenschaften* 91: 199–208, 2004.

Homberg U, Paech A. Ultrastructure and orientation of ommatidia in the dorsal rim area of the locust compound eye. *Arthropod Struct Dev* 30: 271–280, 2002.

Homberg U, Heinze S, Pfeiffer K, Kinoshita M, el Jundi B. Central neural coding of sky polarization in insects. *Phil*

Trans R Soc B 366: 680–687, 2011.

Homberg U, Hofer S, Pfeiffer K, Gebhardt S. Organization and neural connections of the anterior optic tubercle in the brain of the locust, *Schistocerca gregaria*. *J Comp Neurol* 462: 415–430, 2003a.

Kinoshita M, Pfeiffer K, Homberg U. Spectral properties of identified polarized-light sensitive interneurons in the brain of the desert locust *Schistocerca gregaria*. *J Exp Biol* 210: 1350–1361, 2007.

Labhart T, Meyer EP. Detectors for polarized skylight in insects: a survey of ommatidial specializations in the dorsal rim area of the compound eye. *Microsc Res Tech* 47: 368–379, 1999.

Labhart T, Petzold J. Processing of polarized light information in the visual system of crickets. In: *Sensory Systems of Arthropods,* edited by Wiese K, Gribakin FG, Popov AV, and Renninger G. Basel: Birkhäuser, 1993, p. 158–169.

Labhart T. Polarization-opponent interneurons in the insect visual system. *Nature* 331: 435–437, 1988.

Labhart T. How polarization-sensitive interneurones of crickets perform at low degrees of polarization. *J Exp Biol* 199: 1467-1475, 1996.

Labhart T, Petzold J, Helbling H. Spatial integration in polarization-sensitive interneurones of crickets: a survey of evidence, mechanisms and benefits. *J Exp Biol* 204: 2423–2430, 2001.

Maimon G, Straw AD, Dickinson MH. Active flight increases the gain of visual motion processing in *Drosophila*. *Nat Neurosci* 13: 393–399, 2010.

Mappes M, Homberg U. Behavioral analysis of polarization vision in tethered flying locusts. *J Comp Physiol A* 190: 61–68, 2004.

Müller M, Homberg U, Kühn A. Neuroarchitecture of the lower division of the central body in the brain of the locust *(Schistocerca gregaria). Cell Tissue Res* 288: 159–176, 1997.

Naka KI, Rushton WAH. S-Potentials from colour units in the retina of fish (Cyprinidae). *J Physiol* 185: 536–555, 1966.

Ott SR, Rogers SM. Gregarious desert locusts have substantially larger brains with altered proportions compared with the solitarious phase. *Proc R Soc Lond B* 277: 3087–3096, 2010.

Petzold J. *Polarisationsempfindliche Neuronen im Sehsystem der Feldgrille Gryllus campestris: Elektrophysiologie, Anatomie und Modellrechnungen* (PhD thesis). Zürich: University of Zurich, 2001.

Pfeiffer K, Homberg U. Coding of azimuthal directions via time-compensated combination of celestial compass cues. *Curr Biol* 17: 960–965, 2007.

Pfeiffer K, Kinoshita M, Homberg U. Polarization-sensitive and light-sensitive neurons in two parallel pathways passing through the anterior optic tubercle in the locust brain. *J Neurophysiol* 94: 3903–3915, 2005.

Pfeiffer K, Negrello M, Homberg U. Conditional perception under stimulus ambiguity: Polarization-and azimuth-sensitive neurons in the locust brain are inhibited by low degrees of polarization. *J Neurophysiol* 105: 28–35, 2011.

Roessingh P, Simpson SJ, James S. Analysis of phase-related changes in behaviour of desert locust nymphs. *Proc R Soc Lond B* 252: 43–49, 1993.

Roffey J. Observations on night flight in the desert locust (*Schistocerca gregaria* Forskål). *Anti-Locust Bull* 39: 1–32, 1963.

Rogers SM, Harston GWJ, Kilburn-Toppin F, Matheson T, Burrows M, Gabbiani F, Krapp HG. Spatiotemporal receptive field properties of a looming-sensitive neuron in solitarious and gregarious phases of the desert locust. *J Neurophysiol* 103: 779–792, 2010.

Rosner R, Egelhaaf M, Warzecha AK 2010. Behavioural state affects motion-sensitve neurones in the fly visual system. *J Exp Biol* 213: 331–338, 2010.

Simpson S, McCaffery A, Hägele BF. A behavioural analysis of phase change in the desert locust. *Biol Rev* 74: 461–480, 1999.

Stower WJ, Davies DE, Jones IB. Morphometric studies of the desert locust *Schistocerca gregaria* (Forsk.). *J Anim Ecol* 29: 309–339, 1960.

Träger U, Wagner R, Bausenwein B, Homberg U. A novel type of microglomerular synaptic complex in the polarization vision pathway of the locust brain. *J Comp Neurol* 506: 288–300, 2008.

Uvarov B. *Grasshoppers and locusts. A handbook of general acridology*. Cambridge: Cambridge UP, 1966.

Vitzthum H, Müller M, Homberg U. Neurons of the central complex of the locust *Schistocerca gregaria* are sensitive to polarized light. *J Neurosci* 22: 1114–1125, 2002.

Waloff Z. Field studies on solitary and transiens desert locusts in the Red Sea area. *Anti-Locust Bull* 40: 1–91, 1963.

Wehner R, Labhart T. Polarization vision. In: *Invertebrate Vision,* edited by Warrant E and Nilsson DE. Cambridge: Cambridge UP, 2006, p. 291–348.

Wehner R. Astronavigation in insects. *Annu Rev Entomol* 29: 277–298, 1984.

Evidence for the Possible Existence of a Second Polarization-Vision Pathway in the Locust Brain

Journal of Insect Physiology 56 (2010) 971–979

Contents lists available at ScienceDirect

Journal of Insect Physiology

journal homepage: www.elsevier.com/locate/jinsphys

Evidence for the possible existence of a second polarization-vision pathway in the locust brain☆

Basil el Jundi, Uwe Homberg *

Fachbereich Biologie, Tierphysiologie, Philipps-Universität Marburg, D-35032 Marburg, Germany

ARTICLE INFO

Article history:
Received 25 February 2010
Received in revised form 11 May 2010
Accepted 11 May 2010

Keywords:
Polarization vision
Sky-compass orientation
Insect brain
Visual system
Desert locust

ABSTRACT

For spatial orientation and navigation, many insects derive compass information from the polarization pattern of the blue sky. The desert locust *Schistocerca gregaria* detects polarized light with a specialized dorsal rim area of its compound eye. In the locust brain, polarized-light signals are passed through the anterior optic tract and tubercle to the central complex which most likely serves as an internal sky compass. Here, we suggest that neurons of a second visual pathway, via the accessory medulla and posterior optic tubercle, also provide polarization information to the central complex. Intracellular recordings show that two types of neuron in this posterior pathway are sensitive to polarized light. One cell type connects the dorsal rim area of the medulla with the medulla and accessory medulla, and a second type connects the bilaterally paired posterior optic tubercles. Given the evidence for a role of the accessory medulla as the master clock controlling circadian changes in behavioral activity in flies and cockroaches, our data open the possibility that time-compensated polarized-light signals may reach the central complex via this pathway for time-compensated sky-compass navigation.

1. Introduction

During spatial orientation, insects, like vertebrates, combine a variety of sensory cues to assess navigational directions (Wehner, 1984; Frost and Mouritsen, 2006). Celestial cues are of particular importance for long-range migrations. In addition to the position of the sun in the sky, insects can also exploit the sky polarization pattern for navigational purposes (Wehner and Labhart, 2006). Owing to scattering of sunlight in the atmosphere, light from the blue sky is partly polarized, and electric field vectors (*E*-vectors) are oriented along concentric circles around the sun. Many insects, including locusts, detect the *E*-vector orientation of polarized light from dorsal directions with a specialized region of their compound eye, the dorsal rim area (Labhart and Meyer, 1999; Mappes and Homberg, 2004). Photoreceptors of the dorsal rim area of the eye are adapted for high polarization sensitivity and transfer their signals to dorsal rim areas of the lamina and medulla of the optic lobe (Labhart et al., 1992; Blum and Labhart, 2000; Homberg and Paech, 2002). Polarization-sensitive interneurons in the brain show sinusoidal modulations of spiking activity during dorsal stimulation with a rotating polarizer (Labhart, 1996; Labhart and Meyer, 2002; Homberg, 2004). Most neurons show polarization opponency, i.e. they are maximally excited by a particular *E*-vector orientation (Φ_{max}) and are maximally inhibited by an *E*-vector orientation (Φ_{min}) orthogonal to Φ_{max} (Labhart, 1988; Labhart and Meyer, 2002; Homberg, 2004).

The polarization-vision system has been studied particularly well in the brain of the desert locust, *Schistocerca gregaria* (Homberg, 2004). Interneurons with dendritic inputs in the dorsal rim of the medulla project via the anterior optic tract to the lower unit of the anterior optic tubercle in the brain (Homberg et al., 2003a; Pfeiffer et al., 2005). Postsynaptic neurons of the lower unit of the anterior optic tubercle receive additional information about the chromatic contrast of the sky and compensate diurnal changes in sky polarization associated with changes in solar elevation (Pfeiffer and Homberg, 2007). Anterior-optic-tubercle neurons send axonal processes to two distinct areas of the lateral accessory lobe, the median olive and the lateral triangle. Here, they form synaptic contacts in large microglomerular complexes with tangential neurons of the lower division of the central body, a subdivision of the central complex (Träger et al., 2008). In the central complex, a network of at least 13 morphological types of neuron is sensitive to polarized light (Vitzthum et al., 2002; Heinze et al., 2009). In the array of columns of the protocerebral bridge of the central complex, Φ_{max}-orientations of polarization-sensitive neurons are represented in a topographic compass-like manner (Heinze and Homberg, 2007, 2009), suggesting that the central

☆ This paper is a special issue edited by guest editors Amir Ayali and Yoram Yerushalmi focussing on Locust research in the age of model organisms, dedicated to Professor Meir Paul Pener.

* Corresponding author. Tel.: +49 6421 2823402; fax: +49 6421 2828941.
E-mail address: homberg@staff.uni-marburg.de (U. Homberg).

0022-1910/$ – see front matter © 2010 Elsevier Ltd. All rights reserved.
doi:10.1016/j.jinsphys.2010.05.011

complex acts as an internal celestial compass. Output neurons from the central-complex network send axonal processes to the lateral accessory lobes (Heinze et al., 2009; el Jundi et al., 2010) and most likely provide connections to descending pathways.

A major task for every celestial compass is the compensation of time. Constant migratory directions are only feasible when animals permanently adjust their flight direction in relation to the diurnally changing solar azimuth. In monarch butterflies circadian clocks in the antennae have been proposed to play a role in time compensation for navigation (Merlin et al., 2009) but their connection to an internal compass still has to be established. In cockroaches and flies and probably other species as well, master circadian clocks are associated with the accessory medulla in the optic lobe (Helfrich-Förster et al., 1998; Homberg et al., 2003b; Vafopoulou et al., 2010). Interestingly, polarization-sensitive neurons with sidebranches in the accessory medulla have been found in the brain of crickets (Labhart and Petzold, 1993), cockroaches (Loesel and Homberg, 2001), and desert locusts (Homberg and Würden, 1997). In locusts, specific interneurons connect the accessory medulla to the posterior optic tubercle in the central brain (Homberg et al., 1991; Homberg and Würden, 1997). The posterior optic tubercle is closely associated with the central complex, and tangential neurons of the protocerebral bridge with projections in the posterior optic tubercle participate in the compass-like representation of Φ_{max}-orientations in the bridge (Heinze and Homberg, 2007, 2009; Heinze et al., 2009).

Here we present two novel types of polarization-sensitive neuron in the brain of the desert locust. Our data are consistent with the hypothesis that polarization information is transmitted from the dorsal rim area of the medulla through the accessory medulla and posterior optic tubercle to the protocerebral bridge. Functionally, this second polarization-vision pathway through the posterior brain might provide the central complex with time-compensated celestial polarization information that is essential for sky-compass navigation.

2. Materials and methods

2.1. Preparation

Desert locusts (*S. gregaria*) were reared under crowded conditions at 28 °C on a 12:12 light/dark cycle. Only adult animals 1–3 weeks after imaginal moult were used for experiments. Locusts were immobilized by cooling for at least 30 min. Their legs and wings were removed, and the stumps were sealed with glue. After immobilizing the mouthparts with wax, animals were fixed anterior uppermost to a metal holder (Pfeiffer et al., 2005). A ridge of wax was mounted frontally around the head capsule, which encircled the head frontally and ranged from the mouthparts to the anterior edge of the compound eyes. The head capsule was opened anteriorly and fat surrounding the brain was removed. For stabilization, the esophagus was cut and the gut was removed from the opened abdomen. Hemolymph leakage was prevented by sealing the abdomen with a tightly knotted thread. To support the brain from posterior, a wire platform was inserted between the esophageal connectives and was fixed at the ridge of wax. Electrode penetration was facilitated by removing the neural sheath at the region of interest using forceps. During animal preparation and recording of neural activity the brain was immersed in locust saline (Clements and May, 1974).

2.2. Electrophysiology and stimulation

Neurons of the accessory medulla and the posterior optic tubercle were recorded intracellularly using sharp electrodes (resistance: 60–200 MΩ). Electrodes were drawn from borosilicate capillaries (inner diameter: 0.75 mm; outer diameter: 1.5 mm; Hilgenberg, Malsfeld, Germany) with a Flaming/Brown horizontal puller (P-97, Sutter, Novata, CA). Tips of the electrodes were filled with 4% Neurobiotin (Vector Laboratories, Burlingame, UK) in 1 M KCl and their shanks, with 1 M KCl. A silver wire inserted into the hemolymph/saline solution served as the reference electrode. Intracellular signals were amplified (10×) with a custom-built amplifier, monitored with an audiomonitor and a digital oscilloscope (Hameg HM 205-3, Frankfurt/Main, Germany). Signals were sampled with a CED 1401 plus (Cambridge Electronic Design, UK) at a sampling rate of 5 kHz and were stored on a personal computer using Spike2 software (version 6.02; Cambridge Electronic Design, UK). After recording, Neurobiotin was injected iontophoretically into the neurons with constant depolarized current (2–3 nA, 1–5 min).

Animals were stimulated with polarized blue light (Eggers and Gewecke, 1993; Kinoshita et al., 2007). Polarized blue light (photon flux 8.1×10^{12} photons/cm^2 s) was obtained by a xenon lamp (XBO 150W, LOT-Oriel Group; Darmstadt, Germany), passed a monochromatic filter (450 nm), a light guide (Schölly Fiberoptic, Denzingen, Germany) and a linear polarizer (HN38S, Polaroid, Cambridge, MA). The end of the light guide and polarizer were connected to a perimeter apparatus that allowed stimulating the animal with polarized light at different elevations of the visual field. Stimulation of the animal from the zenith is defined as 90° elevation, stimulation from lateral directions as 0° ipsilaterally or contralaterally. The terms ipsilateral and contralateral stimulation are defined with respect to the position of the soma of the recorded neuron in the brain. The angular extent of the stimulus at the locust eye was ~4.7°. For testing polarization sensitivity, the polarizer was rotated through 360° in clockwise (0–360°) and counterclockwise (360–0°) directions with a speed of 30°/s. An *E*-vector orientation of 0° was defined as being parallel to the longitudinal axis of the animal.

2.3. Histology

After Neurobiotin injection brains were dissected out of the head capsule and were fixed over night in 4% paraformaldehyde at 4 °C. Subsequently brains were rinsed four times 15 min with 0.1 M phosphate buffered saline (PBS, pH 7.4). Afterwards the brains were incubated at 1:1000 with streptavidin conjugated to Cy3 (Cy3-streptavidin; Dianova, Hamburg, Germany) in 0.1 M phosphate buffered saline containing 0.3% Triton X-100 (PBT) for at least 3 days. The brains were then rinsed two times in 0.1 M PBT and afterwards in 0.1 M PBS and were dehydrated in an ascending ethanol series (25–100%, 15 min each). After treatment in an ethanol/methyl salicylate (1:1, 15 min) solution, brains were cleared in methyl salicylate for 35 min and were, finally, mounted in Permount (Fisher Scientific, Pittsburgh, PA, USA) between two glass coverslips. To prevent compression of the brains, ten reinforcement rings (Zweckform, Oberlaindern, Germany) were used as spacers.

For detailed analysis of neuronal morphologies, selected brains were rehydrated and sectioned as described by Heinze and Homberg (2008). After removing the embedding medium by incubation in xylene (2–4 h), brains were rehydated in a descending ethanol series (100–20%, 15 min each) and were embedded in gelatine/albumin over night at 4 °C. They were sectioned in frontal plane at a thickness of 130–140 μm with a vibrating-blade microtome (Leica VT1200 S, Leica Microsystems, Wetzlar, Germany). The sections were rinsed in 0.1 M PBS (4 × 15 min). After preincubation in 5% normal goat serum (NGS; Jackson ImmunoResearch, Westgrove, PA, USA) in 0.1 M PBT at 4 °C over night, the sections were incubated for at least 6 days with a monoclonal mouse antibody against synapsin I

(SYNORF1, Klagges et al., 1996; kindly provided by Dr. E. Buchner, Würzburg; 1:50) for labeling of neuropil structures and with Cy3-streptavidin (1:1000) in 0.1 M PBT containing 1% NGS. After rinsing in 0.1 M PBT for 2 h, the sections were incubated with the secondary antibody goat anti mouse conjugated to Cy5 (GAM; Jackson ImmunoResearch; Westgrove, PA, USA; 1:300) and with Cy3-streptavidin (1:1000) in 1% NGS and 0.1 M PBT for 4 days at 4 °C. After washing, sections were dehydrated in an ascending ethanol series (30–100%, 15 min each) and were cleared with 1:1 ethanol/methyl salicylate (15 min) followed by methyl salicylate (at least 45 min). Sections were finally embedded in Permount between two coverslips.

The preparation of the projection neuron connecting the accessory medulla with the posterior optic tubercle was generated by employing the indirect peroxidase-antiperoxidase technique. The histological procedure is described in detail by Homberg and Würden (1997).

2.4. Image acquisition, processing and 3D reconstruction

Brain sections were scanned at 1024 × 1024 pixel resolution using a confocal laser scanning microscope (CLSM, Leica TCS SP5) equipped with a 20× (HCX PL APO lambda blue 20×/0.70 Imm UV, working distance: 260 μm, Leica) and a 40× (HCX PL APO lambda blue 40×/1.25 Oil UV, working distance: 100 μm; Leica) oil objective. Cy3-fluorescence was detected with a DPSS (561 nm) laser and the Cy5 signal, by using a HeNe (633 nm) laser. The peroxidase stained preparation was scanned with a second HeNe (594 nm) laser in the bright field mode. The stained neuron absorbed the light and was, therefore, darkly stained against a bright background. The resulting image stacks of this preparation were converted with Adobe Photoshop 8 software (Adobe Systems, San Jose, CA, USA). All neurons were scanned in several image stacks (voxel size: 0.1–0.5 μm × 0.1–0.5 μm × 0.5 μm).

Processing of all image stacks and reconstructions of the neurons were performed on a personal computer using Amira 4.1.2 software (Visage Imaging, Fürth, Germany). The 3D reconstructions of the neurons were performed with the *SkeletonTree* tool (Schmitt et al., 2004; Evers et al., 2005). The image stacks of each neuron were oriented to the correct position with respect to each other. Reconstructions of the neurons were then generated by opening image stacks consecutively and reconstructing the particular part of the neuron. For neuropil reconstruction, image stacks were downsampled to a voxel size of 1 μm × 1 μm × 1 μm and corresponding image stacks were merged together. Processing of image stacks for neuropil reconstruction and labeling of brain areas were described by Kurylas et al. (2008) and el Jundi et al. (2009). Maximum intensity projections and volume rendering visualization of the neurons were displayed in Amira 4.1.2.

2.5. Data analysis and visualization

Spike trains were evaluated by an analyze script for Spike2 (kindly provided by Dr. K. Pfeiffer). The occurrence of action potentials was determined through threshold-based event detection. The events of action potentials were displayed as mean frequency using a gliding average algorithm (bin size: 1 s). Mean background activities of the neurons were obtained by counting of spikes divided by the respective time in a part of the spike train without any stimulation. To analyze the response of the neurons to polarized light, events during the 360° *E*-vector rotations were assigned to the corresponding *E*-vectors, and lists of these angles were exported out of Spike2. *E*-vector dependent activity differences during stimulation with the rotating polarizer were analyzed statistically using Oriana 2.02 software (Kovach Computing Services, Anglesey, UK). A neuron was defined as polarization sensitive if the distribution of angles during *E*-vector rotation was significantly different from randomness (Rayleigh test for axial data; $\alpha = 0.05$). Mean preferred orientations of the neurons (Φ_{max}) were determined from equal numbers of clockwise and counterclockwise rotations of the polarizer. To measure the response strength at different elevations within the receptive field we used the response amplitude value *R* (Labhart, 1996). The spike train during stimulation with the rotating polarizer was divided into 18 consecutive bins of 20°. In each bin the difference between the actual mean spike frequency and the mean frequency during the total stimulation period was calculated. The summed differences in all 18 bins were defined as the value *R*. Response amplitudes were measured at each position and were normalized to the maximal value in each neuron. The width of the receptive field was defined as the half-maximal response amplitude in relation to the variability in background spiking activity. Circular activity plots of the polarization-sensitive neurons, receptive field plots, and a plot showing elevation-dependent differences in Φ_{max} were created in Origin 6.0 (Microcal, Northhampton, CA).

3. Results

3.1. Novel types of polarization-sensitive neurons in the locust brain

Neurons of the accessory medulla and the posterior optic tubercle were analyzed through intracellular recordings combined with tracer injection. We show that two novel types of neuron, one type with ramifications in the accessory medulla and the second type, connecting both posterior optic tubercles, are sensitive to the *E*-vector orientation of polarized light. The branching patterns of both cell types were analyzed through 3D reconstructions. Another cell type, connecting the accessory medulla and posterior optic tubercle, could not be studied physiologically but was, likewise, reconstructed in three-dimension. Together with previous data, these neurons might be part of a posterior polarization-vision pathway from the dorsal rim area of the medulla via the posterior optic tubercle to the central complex.

3.2. Polarization-sensitive neuron of the medulla

An intrinsic cell type of the medulla with wide ramifications in the medulla, processes in the dorsal rim area of the medulla and in the accessory medulla was studied in intracellular recordings from two animals (Fig. 1). Both recordings were from the medulla of the left brain hemisphere. In both cases, background activity without stimulation ranged from 17.5 to 18.7 impulses per second. During stimulation with a rotating polarizer from dorsal direction both neurons showed strong *E*-vector-dependent modulation of spiking activity. Maximum spiking activity of 31.8–32.3 impulses per second (Fig. 1A) occurred at an *E*-vector orientation (Φ_{max}) of 82° in one recording (not shown) and 103° in the second recording (Fig. 1B). Both neurons showed weak polarization opponency with maximal inhibition at an *E*-vector (Φ_{min}) perpendicular to Φ_{max}.

The morphologies of both neurons and of a third Neurobiotin-injected preparation without physiological data were indistinguishable from each other. The soma was located near the anterior face of the optic lobe and medially from the medulla (Fig. 1F). The primary neurite entered the medulla anterior-medially and gave rise to arborizations extending throughout the medulla in a narrow sheet within distal layer 4 (as defined by Wendt and Homberg, 1992). At the anterior edge of the medulla, the primary neurite bifurcated into two main branches. The dorsally projecting fiber gave rise to an extensive meshwork of processes in dorsal, equatorial and ventral aspects of the medulla. Several small branches extended into the dorsal rim area of the medulla (Fig. 1C and E). The second, ventrally projecting fiber more selectively

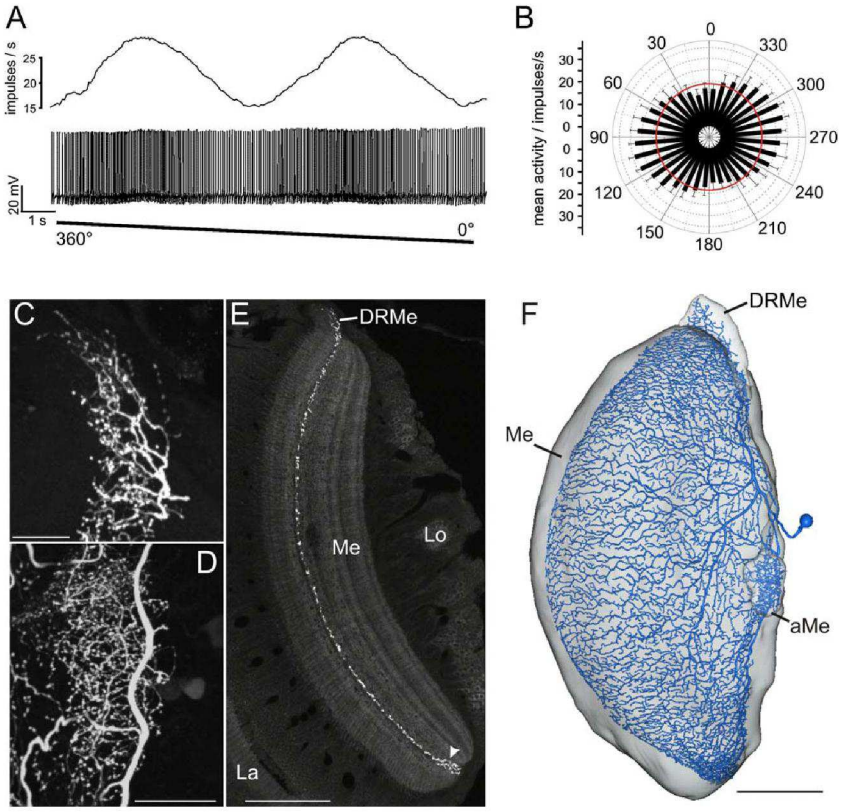

Fig. 1. Intrinsic medulla neuron. (A) Spiking activity of the neuron during stimulation with dorsally presented polarized light rotating through 360° (counterclockwise). Lower trace: spike train; upper trace: mean spiking frequency (moving average of spike rate in 1 s time windows). (B) Circular plot of mean spiking frequencies of the neuron plotted against *E*-vector orientation during dorsal stimulation with a rotating polarizer (n = 8, error bars = SD, bin size: 10°, Φ_{max} = 103.27°; Rayleigh test, $p < 10^{-12}$; R = 78). (C) Maximum intensity projection of a confocal image stack (anterior view) showing the arborizations of the neuron in the dorsal rim area of the medulla. (D) Maximum intensity projection of ramifications in the accessory medulla, anterior view. (E) Frontal slice through the optic lobe at a depth of about 325 μm. The neuron invades a narrow sheet within layer 4 of the medulla (Me) and has processes in the dorsal rim area of the medulla (DRMe). The sheet of ramifications widens at the ventral tip of the medulla (arrowhead). (F) Three-dimensional reconstruction of the intrinsic medulla neuron (blue) within the medulla (grey, transparent). aMe, accessory medulla; La, lamina; Lo, lobula. Scale bars: (C) 30 μm; (D) 50 μm; (E and F) 200 μm.

supplied anterior-ventral and ventralmost aspects of the medulla. It projected along the posterior face of the accessory medulla and gave rise to several small sidebranches that invaded the accessory medulla. Small beaded processes were largely concentrated in the core of the accessory medulla (Fig. 1D). The main fiber continued ventrally and sidebranches covered anterior-ventral aspects of the medulla. At the ventral edge of the medulla, the narrow sheet of ramifications widened and was innervated particularly densely (Fig. 1E).

All regions of arborization showed similar small beaded fiber specializations, which, however, were more numerous in the accessory medulla and in ventral aspects of the medulla ramifications (Fig. 1D). Because our recordings from the ventral fiber near the accessory medulla showed an even baseline without postsynaptic graded potentials, we assume that these arborizations are presynaptic. Accordingly, ramifications in the dorsal rim area of the medulla and in medulla regions supplied by the dorsally projecting main fiber might be input regions of this neuron.

3.3. Projection neurons from the accessory medulla to the posterior optic tubercle

Homberg and Würden (1997) described neurons connecting the accessory medulla to the posterior optic tubercle. A representative of this cell type is shown in three-dimension in Fig. 2. Because of their fine processes these neurons were only colabeled in double or multiple fills and no physiological data are available. The neurons had arborizations in the accessory medulla and axonal terminals in the ipsilateral posterior optic tubercle (Fig. 2A). Their somata were localized anteriorly in the optic lobe and medially from the accessory medulla (Homberg and Würden, 1997). Arborizations in the accessory medulla were confined to a core region and, in some cases, to an even smaller subregion (Fig. 2B). The main neurite left the accessory medulla medially and ran toward the posterior central brain. It gave rise to short sidebranches in the postero-lateral protocerebrum and major terminal ramifications confined to the posterior optic tubercle. Arborizations in the posterior optic tubercle were varicose (Fig. 2C), suggesting that these neurons receive their input in the accessory medulla and transmit signals to the posterior optic tubercle.

3.4. Intertubercle neurons of the posterior optic tubercles

In addition to tangential neurons of the protocerebral bridge, termed TB neurons that connect the posterior optic tubercle with the protocerebral bridge of the central complex (Heinze and Homberg, 2007, 2009; Heinze et al., 2009) we identified another type of polarization-sensitive neuron in the posterior optic

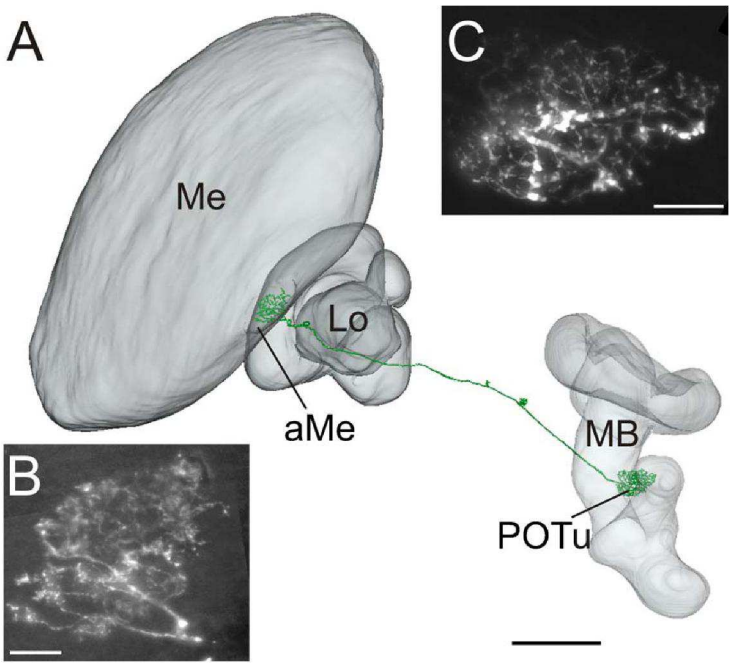

Fig. 2. Anatomy of an accessory medulla (aMe) neuron with projections to the posterior optic tubercle (POTu). (A) Three-dimensional reconstruction (anterior view) of the neuron (green) and of neuropils (grey, transparent) from the locust standard brain (Kurylas et al., 2008). A two-dimensional reconstruction of this neuron has been published by Homberg and Würden (1997). (B) Maximum intensity projection of an image stack reveals smooth input arborizations of the neuron in the aMe. (C) Arborizations in the POTu are varicose (maximum intensity projection). Lo, lobula; MB, mushroom body; Me, medulla. Scale bar: (A) 200 μm; (B) 20 μm; (C) 30 μm.

tubercle (Fig. 3). These neurons, termed intertubercle neurons, connected both posterior optic tubercles and were studied in three intracellular recordings. The neurons had their somata in the posterior protocerebrum lateral to the posterior optic tubercle (Fig. 3C). From the main fiber passing along the posterior ventral surface of the posterior optic tubercle several sidebranches projected with fine processes into the posterior optic tubercle (Fig. 3C, D, and F). The primary neurite crossed the brain hemisphere in a posterior commissure and gave rise to dense varicose terminals in the contralateral posterior optic tubercle (Fig. 3E and G).

The background activity of the intertubercle neurons ranged from 2.67 to 15.92 impulses/s. During stimulation with the rotating polarizer from dorsal direction, spiking activity was modulated sinusoidally (Fig. 3A). All neurons showed polarization opponency with maximum spiking activity ranging from about 18 to 37.3 impulses per second (Fig. 3A). Preferred *E*-vector orientations (Φ_{max}) were 145° (not shown) and 166° (Fig. 3B) for two neurons with somata in the left brain hemisphere and 104° for the third neuron with soma in the right brain hemisphere (not shown).

In all three neurons, the size of the receptive field to polarized light was studied by presenting the rotating polarizer (clockwise and counterclockwise rotation) at different elevations along the right–left meridian. Response amplitudes were calculated at each position and were normalized to the maximal value in each neuron (Fig. 3H). The averaged receptive field of all three intertubercle neurons of the posterior optic tubercle was zenith-centered, as in TB1 tangential and CPU1 and CP2 types of columnar neurons of the central complex (Heinze et al., 2009) (Fig. 3I). To define the width of the receptive field we calculated the half-maximal response amplitude in relation to the variability in background spiking activity. As a result, the width of the receptive fields of the neurons was about 90°. Potential differences of Φ_{max} along the right–left meridian were analyzed by calculating for each position of the receptive field the difference between Φ_{max} and Φ_{max} in the zenith (Fig. 3J). In one neuron, Φ_{max} decreased when moving the polarizer form the ipsilateral hemisphere to the contralateral side, whereas in the two other cells, Φ_{max} changed in the opposite way. To study whether these differences have a morphological correlation, the arborizations of the three neurons in the posterior optic tubercle were investigated in detailed. In all three neurons, ramifications were confined either to the ventral or to the dorsal hemisphere of the posterior optic tubercle. One of the three neurons arborized in the ipsilateral tubercle dorsally and innervated the contralateral tubercle ventrally (Fig. 3C–E). In this neuron, Φ_{max} decreased when moving the polarizer from the ipsilateral to the contralateral hemisphere. The other two neurons ramified in the ipsilateral tubercle ventrally and in the contralateral tubercle dorsally (Fig. 3F and G). In these neurons Φ_{max} increased when moving the polarizer from ipsilateral positions to positions in the contralateral hemisphere.

4. Discussion

4.1. Two polarization-vision pathways in the locust brain?

Tracer injections, dye fills and intracellular recordings revealed an anterior polarization-vision pathway in the locust brain (Homberg, 2004). It extends from the dorsal rim area of the compound eye via the dorsal rim area of the medulla, a ventral layer of the anterior lobe of the lobula, the lower unit of the anterior optic tubercle, and the median olive and lateral triangle to the central complex (Fig. 4, red pathway). Within the central

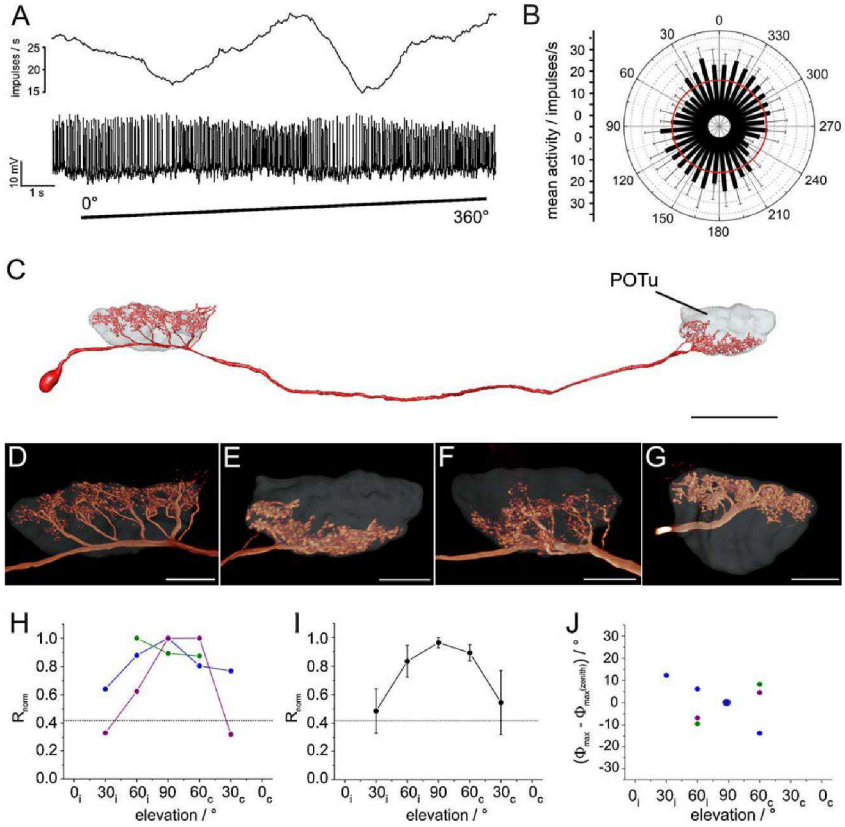

Fig. 3. Intertubercle neurons of the posterior optic tubercle (POTu). (A) Responses of the intertubercle neuron shown in (C) to a dorsally presented 360°-rotating polarizer (clockwise rotation); lower trace: spike train; upper trace: mean spiking frequency (moving average of spike rate in 1 s time window). (B) Circular diagram of mean frequencies of action potentials of the neuron in (A) and (C) plotted against *E*-vector orientation ($n = 8$, error bars = SD, bin size: 10°; $\Phi_{max} = 166°$; Rayleigh test, $p < 10^{-12}$). (C) Three-dimensional reconstruction of the neuron (red) with arborizations in the ipsi- and contralateral POTu (grey, transparent). (D) Three-dimensional volume rendering visualization of the input region of the neuron in (C) reveals smooth arborizations in a dorsal layer of the POTu (grey, transparent). (E) Ramifications in the contralateral POTu (grey, transparent) are varicose and confined to a ventral region of the POTu. (F and G) Another intertubercle neuron shows smooth branches concentrated in a ventral area of the ipsilateral POTu (F, grey, transparent) and axonal varicose projections confined to the dorsal region of the contralateral POTu (grey, transparent). (H) Normalized response amplitudes *R* from three intertubercle neurons of the POTu plotted against the elevation of polarized-light stimuli. Absolute values ranged from $R = 40$ to $R = 93$. Ipsilateral (i) and contralateral (c) stimulations are defined with respect to the position of the soma of the recorded neuron. Data points are connected by lines for better visibility. *R* values and mean background variability (dotted line) of all recorded neurons are normalized to the maximum *R* value in the receptive field of each neuron. (I) Average receptive fields of the three intertubercle neurons. Dotted line represents background variability. Values are means (±SE) based on the values shown in (H). (J) Φ_{max} distribution of the three neurons in the receptive field. Differences between Φ_{max} at each elevation and Φ_{max} in the zenith are plotted against the elevation. Colors of data points correspond to the colors in H. The data point at 90° elevation is identical for the three neurons. Scale bars: (C) 100 μm; (D–G) 30 μm.

complex, a network of more than a dozen types of neuron is involved in the processing of polarized-light signals (Heinze and Homberg, 2007, 2009). Finally, columnar output neurons from the central complex are likely to combine sky-compass information with additional, possibly landmark-related input, and provide connections to descending pathways leading to thoracic motor centers (Heinze et al., 2009; el Jundi et al., 2010).

Recordings from two novel types of neuron, presented here, suggest the possible existence of a second, posterior polarization-vision pathway from the dorsal rim area of the medulla via the accessory medulla and posterior optic tubercle to the central complex (Fig. 4, blue pathway). The prominent tangential projections of the intrinsic medulla neuron throughout all medulla columns strongly suggest that, in addition to polarized-light signals, visual input of unknown specificity from large parts of the compound eye is processed by this cell type as well. Neurons specifically connecting the accessory medulla to the posterior optic tubercle have been discovered by Homberg and Würden (1997) but so far, no physiological data exist for these cells. The posterior optic tubercles, finally, are connected bilaterally through polarization-sensitive intertubercle neurons shown here and with the protocerebral bridge of the central complex through TB tangential neurons characterized by Heinze and Homberg (2007, 2009).

4.2. Time compensation

For constant migratory directions using a sky compass, changes in solar azimuth during the day have to be compensated (Homberg, 2004). Behavioral data from honeybees, ants and monarch butterflies, indeed, showed that their internal sun compass is time-compensated (Lindauer, 1960; Wehner, 1992; Mouritsen and Frost, 2002), but corresponding evidence is still lacking for locusts. How time compensation is achieved at the neuronal level is unknown. Recent studies in the monarch butterfly suggest that an internal clock in the antennae plays a role in time compensation for compass navigation (Merlin et al., 2009). We propose in locusts

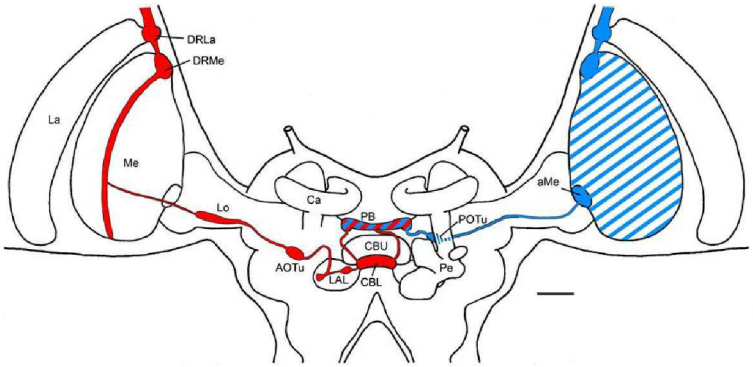

Fig. 4. Frontal schematic diagram of a locust brain showing the anterior polarization-vision pathway (red) and the proposed posterior polarization-vision pathway (blue) to the central complex. aMe, accessory medulla; AOTu, anterior optic tubercle; Ca, calyx; CBL, lower division of the central body; CBU, upper division of the central body; DRLa, dorsal rim area of the lamina; DRMe, dorsal rim area of the medulla; La, lamina; LAL, lateral accessory lobe; Lo, lobula; Me, medulla; PB, protocerebral bridge; Pe, pedunculus; POTu, posterior optic tubercle. Scale bar: 200 μm.Modified from Homberg et al. (2003a).

that the accessory medulla is the site of the internal circadian clock responsible for time compensation in sky-compass navigation. Extensive studies especially in the fruit fly *Drosophila melanogaster* and the cockroach *Leucophaea maderae* showed that neurons closely associated with the accessory medulla are circadian pacemakers controlling circadian changes in locomotion and other behaviors (Helfrich-Förster et al., 1998; Homberg et al., 2003b; Helfrich-Förster, 2004). Although direct evidence for the locust is lacking, striking similarities in the functional and neurochemical organization of the accessory medullae in cockroaches and locusts (see below) favor similar functional roles. If so, the proposed posterior polarization vision pathway to the central complex is a strong candidate to supply the central complex with information about time of day. The anterior polarization pathway, in contrast, more likely plays a key role in signaling head orientation in relation to solar azimuth.

4.3. The accessory medulla and polarization sensitivity

The accessory medulla in cockroaches and flies houses a network of neurons that constitute a master clock controlling circadian changes in locomotor activity (Helfrich-Förster et al., 1998; Homberg et al., 2003b; Helfrich-Förster, 2004). It is a small neuropil at the anterior-median edge of the medulla and has been studied in locusts, crickets, cockroaches, flies, bugs, and several other insect taxa (Homberg et al., 1991; Sehadová et al., 2003; Helfrich-Förster, 2005; Vafopoulou et al., 2010). In hemimetabolous insects the accessory medulla has been characterized in most detail in the brain of the cockroach *L. maderae* (Reischig and Stengl, 1996, 2003a,b). It is subdivided into dense central nodular neuropil and surrounding more loosely organized shell neuropil (Reischig and Stengl, 2003b). Both regions are innervated by neurons containing a large variety of neuropeptides (Petri et al., 1995, 2002; Hofer and Homberg, 2006a,b; Söhler et al., 2007). Neurons immunostained with antisera against pigment-dispersing factor connect the accessory medulla with the lamina, the medulla, and many areas in the central brain including the posterior optic tubercle (Homberg et al., 1991; Reischig and Stengl, 2002). A highly similar pattern of pigment-dispersing factor immunostaining in the desert locust led to the early hypothesis that the accessory medulla serves as a circadian neuropil controlling circadian changes in behavioral activity (Homberg et al., 1991). In addition, intracellular recordings from neurons of the accessory medulla in the cockroach and locust revealed similar response characteristics to light flashes (Homberg and Würden, 1997; Loesel and Homberg, 2001).

Polarization-sensitive neurons with ramifications in the accessory medulla were first discovered in the brain of the field cricket, *Gryllus campestris* (Labhart and Petzold, 1993). These neurons, termed POL1, connect the medullae and accessory medullae of both brain hemispheres. In the ipsilateral hemisphere, medulla arborizations of POL1 are concentrated in dorsal parts of the medulla and were suggested to be the site of polarization input. Similar neurons responding to polarized light, but with more sparse ramifications in the accessory medulla and lack of ramifications in dorsal rim areas of the medulla were found in the locust (Homberg and Würden, 1997) and the Madeira cockroach (Loesel and Homberg, 2001). In the cockroach, the neurons had additional arborizations in the central brain. A second type of polarization-sensitive intrinsic medulla neuron with ramifications in the accessory medulla was reported in the cricket (Petzold, 2001) and is presented here for the locust (Fig. 1). In this case, the neuron of the locust but not that of the cricket has ramifications in the dorsal rim area of the medulla. The varicose, presumably output ramifications of the locust neuron in the accessory medulla might suggest that polarized-light information serves as a zeitgeber for the internal clock. Loesel and Homberg (2001) argued that the degree of polarization could have a zeitgeber function for the accessory medulla, because in the zenith the degree of polarization is directly related to solar elevation. However, the degree of polarization also depends strongly on clouding conditions (Pomozi et al., 2001). Accordingly, a zeitgeber function of polarized light has so far not been shown in any animal.

The intrinsic medulla neuron shown here provides a direct connection between the dorsal rim area of the medulla and the accessory medulla. In addition, the neuron also arborizes extensively in the medulla. Therefore, it might also receive unpolarized-light input of unknown specificity from the remaining compound eye. Thus, unpolarized and polarized information could be directly integrated and transferred through this cell type to the accessory medulla. In addition to its ramifications in the accessory medulla and dorsal rim area of the medulla, this neuron also arborizes densely in an undefined region of the ventral medulla. Because the neurite that supplies the accessory medulla continues to the ventral medulla, it is likely to be a specific output region as well.

4.4. The posterior optic tubercle

The posterior optic tubercle has been recognized as a distinct brain area in locusts, crickets and cockroaches (Williams, 1972; Homberg et al., 1991). In desert locusts the posterior optic tubercle is innerved by neurons immunostained for Dip-allatostatin (Vitzthum et al., 1996), Mas-allatotropin (Homberg et al., 2004), dopamine (Wendt and Homberg, 1992), serotonin (Homberg, 1991), pigment-dispersing hormone (Homberg et al., 1991), crustacean cardioactive peptide (CCAP), and FMRFamide-related peptides (Würden and Homberg, 1995). Histochemical staining for NADPH diaphorase suggesting nitrergic neurons also revealed dense staining in the posterior optic tubercle (Kurylas et al., 2005). As a consequence of its small size and its posterior location in the brain, recordings from neurons of the posterior optic tubercles are difficult to obtain. In addition to the intertubercle neurons in this work, only two types of tangential neuron of the protocerebral bridge with ramifications in the posterior optic tubercle, termed TB1 and TB2 have been studied physiologically (Heinze and Homberg, 2007, 2009; Heinze et al., 2009). Like the central body, the protocerebral bridge is organized into an array of 16 columns and TB neurons contribute prominently to the compass-like representation of Φ_{max}-orientations in these columns. The polarity of TB neurons is, based on anatomical investigations, highly complex: each neuron has varicose arborizations in one column of the right and one column of the left hemisphere of the bridge and both arborization trees are exactly 8 columns apart. In between, the neurons have smooth and, thus, presumably dendritic ramifications in three columns of each hemisphere. Finally, each neuron has an ipsilateral projection in the posterior optic tubercle. Based on varicose appearance, Heinze and Homberg (2009) assumed that the ramifications of TB neurons in the posterior optic tubercle are output regions. TB1 neurons receive polarization input from both compound eyes and have large zenith-centered receptive fields of about 150° in bilateral width (Heinze et al., 2009). In contrast to uniform Φ_{max}-orientations throughout the receptive field, found in neurons of the lower division of the central body, the orientation of Φ_{max} within the receptive field of TB neurons and columnar neurons of the bridge increased from ipsilateral to contralateral. As a consequence, at solar elevations above the horizon, columnar neurons in the left hemisphere would be excited more strongly when the sun is in front of the animal and neurons in the right hemisphere of the bridge, when the sun is behind the animal (Heinze et al., 2009). This non-uniformity of Φ_{max}, thus, contributes to transform an orientation-dependent (180° periodicity) signaling of solar azimuth into a true head direction dependent signaling with 360° periodicity.

Similar to TB neurons, the intertubercle neurons of the posterior optic tubercle have zenith-centered receptive fields, however with substantially smaller width of around 90°. Like TB neurons, Φ_{max}-orientations change within the receptive field from right to left. Whereas two neurons showed an increase in Φ_{max} from the ipsilateral to the contralateral hemisphere, as found in TB and all other protocerebral bridge neurons, one neuron showed a decrease in Φ_{max}. Even more remarkable, this difference in Φ_{max}-shifts correlated with differences arborization pattern in the posterior optic tubercle.

Based on the available evidence and small number of recordings, a conclusive picture of signal transfer between the posterior optic tubercle and the protocerebral bridge cannot be given at present. The assumption, that the posterior optic tubercle arborizations of TB neurons are purely presynaptic (Heinze and Homberg, 2009), may have been premature. Immuno- and histochemical stainings suggest that TB neurons contain serotonin (Homberg, 1991), Dip-allatostatin (Vitzthum et al., 1996), Mas-allatotropin (Homberg et al., 2004) and the gaseous transmitter NO (Kurylas et al., 2005). Interestingly, serotonin immunostaining of these neurons was strong in the protocerebral bridge, but very weak in the posterior optic tubercle (Homberg, 1991) whereas NADPHd staining revealed intense staining in the posterior optic tubercle and only faint staining in the processes in the bridge (Kurylas et al., 2005). As discussed by Homberg and Hildebrand (1989) gradients in the intensity of transmitter immunoreactivity are not uncommon in insect brain neurons and might hint at the signaling polarity of these cells. Taken together, these immunocytochemical data suggest bilateral signaling between the posterior optic tubercles and the protocerebral bridge, perhaps via two hitherto unrecognized subpopulations of TB neurons. The functional role of this information flow and the role of the intertubercle neurons may be a key aspect to understand the processing of polarized light leading to the compass-like representation in the protocerebral bridge. The intertubercle neurons potentially play a crucial role in integrating the information from both eyes and/or in establishing the compass-like representation of *E*-vectors in the bridge. Detailed anatomical and physiological investigations of the posterior optic tubercles and the arborization pattern of TB neurons within these neuropils should help to test these hypotheses.

Acknowledgements

We are grateful to Dr. Keram Pfeiffer for providing Spike2 scripts and for fruitful discussions and to Dr. Erich Buchner for providing the anti-synapsin antibody. We thank Dr. Franz Grolig for assistance in confocal microscopy and Drs. Stanley Heinze and Keram Pfeiffer for introduction into intracellular recordings. We are grateful to Miklós Bech and Ulrike Träger for helpful suggestions on the manuscript and to Martina Kern and Karl Heinz Herklotz for maintaining the locust cultures. This work was supported by DFG grant HO 950/16-2.

References

Blum, M., Labhart, T., 2000. Photoreceptor visual fields, ommatidial array, and receptor axon projections in the polarisation-sensitive dorsal rim area of the cricket compound eye. Journal of Comparative Physiology A 186, 119–128.
Clements, A.N, May, T.E., 1974. Studies on locust neuromuscular physiology in relation to glutamic acid. Journal of Experimental Biology 60, 673–705.
Eggers, A., Gewecke, M., 1993. The dorsal rim area of the compound eye and polarization vision in the desert locust (*Schistocerca gregaria*). In: Wiese, K., Gribakin, F.G., Popov, A.V., Renninger, G. (Eds.), Sensory Systems of Arthropods. Birkhäuser Verlag, Basel, pp. 101–109.
el Jundi, B., Huetteroth, W., Kurylas, A.E., Schachtner, J., 2009. Anisometric brain dimorphism revisited: implementation of a volumetric 3D standard brain in *Manduca sexta*. Journal of Comparative Neurology 517, 210–225.
el Jundi, B., Heinze, S., Lenschow, C., Kurylas, A., Rohlfing, T., Homberg, U., 2010. The locust standard brain: a 3D standard of the central complex as a platform for neural network analysis. Frontiers in Systems Neuroscience 3, 21.
Evers, J.F., Schmitt, S., Sibila, M., Duch, C., 2005. Progress in functional neuroanatomy: precise automatic geometric reconstruction of neuronal morphology from confocal image stacks. Journal of Neurophysiology 93, 2331–2342.
Frost, B.J., Mouritsen, H., 2006. The neural mechanisms of long distance animal navigation. Current Opinion in Neurobiology 16, 481–488.
Heinze, S., Homberg, U., 2007. Maplike representation of celestial *E*-vector orientations in the brain of an insect. Science 315, 995–997.
Heinze, S., Homberg, U., 2008. Neuroarchitecture of the central complex of the desert locust: intrinsic and columnar neurons. Journal of Comparative Neurology 511, 454–478.
Heinze, S., Homberg, U., 2009. Linking the input to the output: new sets of neurons complement the polarization vision network in the locust central complex. Journal of Neuroscience 29, 4911–4921.
Heinze, S., Gotthardt, S., Homberg, U., 2009. Transformation of polarized light information in the central complex of the locust. Journal of Neuroscience 29, 11783–11793.
Helfrich-Förster, C., 2004. The circadian clock in the brain: a structural and functional comparison between mammals and insects. Journal of Comparative Physiology A 190, 601–613.
Helfrich-Förster, C., 2005. Organization of endogenous clocks in insects. Biochemical Society Transactions 33, 957–961.

Helfrich-Förster, C., Stengl, M., Homberg, U., 1998. Organization of the circadian system in insects. Chronobiology International 15, 567–594.

Hofer, S., Homberg, U., 2006a. Evidence for a role of orcokinin-related peptides in the circadian clock controlling locomotor activity of the cockroach *Leucophaea maderae*. Journal of Experimental Biology 209, 2794–2803.

Hofer, S., Homberg, U., 2006b. Orcokinin immunoreactivity in the accessory medulla of the cockroach *Leucophaea maderae*. Cell and Tissue Research 325, 589–600.

Homberg, U., 1991. Neuroarchitecture of the central complex in the brain of the locust *Schistocerca gregaria* and *S. americana* as revealed by serotonin immunocytochemistry. Journal of Comparative Neurology 303, 245–254.

Homberg, U., 2004. In search of the sky compass in the insect brain. Naturwissenschaften 91, 199–208.

Homberg, U., Hildebrand, J.G., 1989. Serotonin-immunoreactive neurons in the median protocerebrum and suboesophageal ganglion of the sphinx moth *Manduca sexta*. Cell and Tissue Research 258, 1–24.

Homberg, U., Würden, S., 1997. Movement-sensitive, polarization-sensitive, and light-sensitive neurons of the medulla and accessory medulla of the locust, *Schistocerca gregaria*. Journal of Comparative Neurology 386, 329–346.

Homberg, U, Paech, A., 2002. Ultrastructure and orientation of ommatidia in the dorsal rim area of the locust compound eye. Arthropod Structure & Development 30, 271–280.

Homberg, U., Würden, S., Dircksen, H., Rao, K.R., 1991. Comparative anatomy of pigment-dispersing hormone-immunoreactive neurons in the brain of orthopteroid insects. Cell and Tissue Research 266, 343–357.

Homberg, U., Hofer, S., Pfeiffer, K., Gebhardt, S., 2003a. Organization and neural connections of the anterior optic tubercle in the brain of the locust, *Schistocerca gregaria*. Journal of Comparative Neurology 462, 415–430.

Homberg, U., Reischig, T., Stengl, M., 2003b. Neural organization of the circadian system of the cockroach *Leucophaea maderae*. Chronobiology International 20, 577–591.

Homberg, U., Brandl, C., Clynen, E., Schoofs, L., Veenstra, J.A., 2004. Mas-allatotropin/Lom-AG-myotropin I immunostaining in the brain of the locust, *Schistocerca gregaria*. Cell and Tissue Research 318, 439–457.

Kinoshita, M., Pfeiffer, K., Homberg, U., 2007. Spectral properties of identified polarized-light sensitive interneurons in the brain of the desert locust *Schistocerca gregaria*. Journal of Experimental Biology 210, 1350–1361.

Klagges, B.R.E., Heimbeck, G., Godenschwege, T.A., Hofbauer, A., Pflugfelder, G.O., Reifegerste, R., Reisch, D., Schaupp, M., Buchner, S., Buchner, E., 1996. Invertebrate synapsins: a single gene codes for several isoforms in *Drosophila*. Journal of Neuroscience 16, 3154–3165.

Kurylas, A.E., Ott, S.R., Schachtner, J., Elphick, M.R., Williams, L., Homberg, U., 2005. Localization of nitric oxide synthase in the central complex and surrounding midbrain neuropils of the locust *Schistocerca gregaria*. Journal of Comparative Neurology 484, 206–223.

Kurylas, A.E., Rohlfing, T., Krofczik, S., Jenett, A., Homberg, U., 2008. Standardized atlas of the brain of the desert locust, *Schistocerca gregaria*. Cell and Tissue Research 333, 125–145.

Labhart, T., 1988. Polarization-opponent interneurons in the insect visual system. Nature 331, 435–437.

Labhart, T., 1996. How polarization-sensitive interneurones of crickets perform at low degrees of polarization. Journal of Experimental Biology 199, 1467–1475.

Labhart, T., Petzold, J., 1993. Processing of polarized light information in the visual system of crickets. In: Wiese, K., Gribakin, F.G., Popov, A.V., Renninger, G. (Eds.), Sensory Systems of Arthropods. Birkhäuser Verlag, Basel, pp. 158–169.

Labhart, T., Meyer, E.P., 1999. Detectors for polarized skylight in insects: a survey of ommatidial specializations in the dorsal rim area of the compound eye. Microscopy Research and Technique 47, 368–379.

Labhart, T., Meyer, E.P., 2002. Neural mechanisms in insect navigation: polarization compass and odometer. Current Opinion in Neurobiology 12, 707–714.

Labhart, T., Meyer, E.P., Schenker, L., 1992. Specialized ommatidia for polarization vision in the compound eye of cockchafers, *Melolontha melolontha* (Coleoptera, Scarabaeidae). Cell and Tissue Research 268, 419–429.

Lindauer, M, 1960. Time-compensated sun orientation in bees. Cold Spring Harbor Symposia on Quantitative Biology 25, 371–377.

Loesel, R., Homberg, U., 2001. Anatomy and physiology of neurons with processes in the accessory medulla of the cockroach *Leucophaea maderae*. Journal of Comparative Neurology 439, 193–207.

Mappes, M., Homberg, U., 2004. Behavioral analysis of polarization vision in tethered flying locusts. Journal of Comparative Physiology A 190, 61–68.

Merlin, C., Gegear, R.J., Reppert, S.M., 2009. Antennal circadian clocks coordinate sun compass orientation in migratory monarch butterflies. Science 325, 1700–1704.

Mouritsen, H., Frost, B.J., 2002. Virtual migration in tethered flying monarch butterflies reveals their orientation mechanisms. Proceedings of the National Academy of Sciences of the United States of America 99, 10162–10166.

Petri, B., Stengl, M., Würden, S., Homberg, U., 1995. Immunocytochemical characterization of the accessory medulla in the cockroach *Leucophaea maderae*. Cell and Tissue Research 282, 3–19.

Petri, B., Homberg, U., Loesel, R., Stengl, M., 2002. Evidence for a role of GABA and Mas-allatotropin in photic entrainment of the circadian clock of the cockroach *Leucophaea maderae*. Journal of Experimental Biology 205, 1459–1469.

Petzold, J., 2001. Polarisationsempfindliche Neuronen im Sehsystem der Feldgrille *Gryllus campestris*: Elektrophysiologie, Anatomie und Modellrechnungen. PhD Thesis. University of Zürich.

Pfeiffer, K., Kinoshita, M., Homberg, U., 2005. Polarization-sensitive and light-sensitive neurons in two parallel pathways passing through the anterior optic tubercle in the locust brain. Journal of Neurophysiology 94, 3903–3915.

Pfeiffer, K., Homberg, U., 2007. Coding of azimuthal directions via time-compensated combination of celestial compass cues. Current Biology 17, 960–965.

Pomozi, I., Horvath, G., Wehner, R., 2001. How the clear-sky angle of polarization pattern continues underneath clouds: full-sky measurements and implications for animal orientation. Journal of Experimental Biology 204, 2933–2942.

Reischig, T., Stengl, M., 1996. Morphology and pigment-dispersing hormone immunocytochemistry of the accessory medulla, the presumptive circadian pacemaker of the cockroach *Leucophaea maderae*: a light-and electron-microscopic study. Cell and Tissue Research 285, 305–319.

Reischig, T., Stengl, M., 2002. Optic lobe commissures in a three-dimensional brain model of the cockroach *Leucophaea maderae*: a search for the circadian coupling pathways. Journal of Comparative Neurology 443, 388–400.

Reischig, T., Stengl, M., 2003a. Ectopic transplantation of the accessory medulla restores circadian locomotor rhythms in arrhythmic cockroaches (*Leucophaea maderae*). Journal of Experimental Biology 206, 1877–1886.

Reischig, T., Stengl, M., 2003b. Ultrastructure of pigment-dispersing hormone-immunoreactive neurons in a three-dimensional model of the accessory medulla of the cockroach *Leucophaea maderae*. Cell and Tissue Research 314, 421–435.

Schmitt, S., Evers, J.F., Duch, C., Scholz, M., Obermayer, K., 2004. New methods for the computer-assisted 3-D reconstruction of neurons from confocal image stacks. NeuroImage 23, 1283–1298.

Sehadová, H., Sauman, I., Sehnal, F., 2003. Immunocytochemical distribution of pigment-dispersing hormone in the cephalic ganglia of polyneopteran insects. Cell and Tissue Research 312, 113–125.

Söhler, S., Neupert, S., Predel, R., Nichols, R., Stengl, M., 2007. Localization of leucomyosuppressin in the brain and circadian clock of the cockroach *Leucophaea maderae*. Cell and Tissue Research 328, 443–452.

Träger, U., Wagner, R., Bausenwein, B., Homberg, U., 2008. A novel type of microglomerular synaptic complex in the polarization vision pathway of the locust brain. Journal of Comparative Neurology 506, 288–300.

Vafopoulou, X., Terry, K.L., Steel, C.G.H., 2010. The circadian timing system in the brain of the fifth larval instar of *Rhodnius prolixus* (Hemiptera). Journal of Comparative Neurology 518, 1264–1282.

Vitzthum, H., Homberg, U., Agricola, H., 1996. Distribution of Dip-allatostatin I-like immunoreactivity in the brain of the locust *Schistocerca gregaria* with detailed analysis of immunostaining in the central complex. Journal of Comparative Neurology 369, 419–437.

Vitzthum, H., Müller, M., Homberg, U., 2002. Neurons of the central complex of the locust *Schistocerca gregaria* are sensitive to polarized light. Journal of Neuroscience 22, 1114–1125.

Wehner, R., 1984. Astronavigation in insects. Annual Review of Entomology 29, 277–298.

Wehner, R., 1992. Arthropods. In: Papi, F. (Ed.), Animal Homing. Chapman and Hall, London, pp. 45–144.

Wehner, R., Labhart, T., 2006. Polarization vision. In: Warrant, E.J., Nilsson, D.-E. (Eds.), Invertebrate Vision. Cambridge University Press, Cambridge, pp. 291–348.

Wendt, B., Homberg, U., 1992. Immunocytochemistry of dopamine in the brain of the locust *Schistocerca gregaria*. Journal of Comparative Neurology 321, 387–403.

Williams, J.L.D., 1972. Some observations on the neuronal organisation of the supraoesophageal ganglion in *Schistocera gregaria* Forskål with particular reference to the central complex. PhD Thesis. University of Wales, Cardiff.

Würden, S., Homberg, U., 1995. Immunocytochemical mapping of serotonin and neuropeptides in the accessory medulla of the locust, *Schistocerca gregaria*. Journal of Comparative Neurology 362, 305–319.

The Locust Standard Brain: A 3D Standard of the Central Complex as a Platform for Neural Network Analysis

frontiers in
SYSTEMS NEUROSCIENCE

ORIGINAL RESEARCH ARTICLE
published: 03 February 2010
doi: 10.3389/neuro.06.021.2009

The locust standard brain: a 3D standard of the central complex as a platform for neural network analysis

Basil el Jundi[1], Stanley Heinze[1†], Constanze Lenschow[1†], Angela Kurylas[1], Torsten Rohlfing[2] and Uwe Homberg[1]*

[1] Fachbereich Biologie, Tierphysiologie, Philipps-Universität Marburg, Marburg, Germany
[2] Neuroscience Program, SRI International, Menlo Park, CA, USA

Edited by:
Randolf Menzel, Freie Universitat Berlin, Germany

Reviewed by:
Jürgen Rybak, Norwegian University of Science and Technology, Norway
Hanna Mustaparta, Norwegian University of Science and Technology, Norway

***Correspondence:**
Uwe Homberg, Fachbereich Biologie, Tierphysiologie, Philipps-Universität Marburg, D-35032 Marburg, Germany. e-mail: homberg@staff.uni-marburg.de

***†Present address:**
Stanley Heinze, Department of Neurobiology, University of Massachusetts Medical School, Worcester, Massachusetts 01605, USA; Constanze Lenschow, Fachbereich Biologie, Freie Universität Berlin, Germany.

Many insects use the pattern of polarized light in the sky for spatial orientation and navigation. We have investigated the polarization vision system in the desert locust. To create a common platform for anatomical studies on polarization vision pathways, Kurylas et al. (2008) have generated a three-dimensional (3D) standard brain from confocal microscopy image stacks of 10 male brains, using two different standardization methods, the Iterative Shape Averaging (ISA) procedure and the Virtual Insect Brain (VIB) protocol. Comparison of both standardization methods showed that the VIB standard is ideal for comparative volume analysis of neuropils, whereas the ISA standard is the method of choice to analyze the morphology and connectivity of neurons. The central complex is a key processing stage for polarization information in the locust brain. To investigate neuronal connections between diverse central-complex neurons, we generated a higher-resolution standard atlas of the central complex and surrounding areas, using the ISA method based on brain sections from 20 individual central complexes. To explore the usefulness of this atlas, two central-complex neurons, a polarization-sensitive columnar neuron (type CPU1a) and a tangential neuron that is activated during flight, the giant fan-shaped (GFS) neuron, were reconstructed 3D from brain sections. To examine whether the GFS neuron is a candidate to contribute to synaptic input to the CPU1a neuron, we registered both neurons into the standardized central complex. Visualization of both neurons revealed a potential connection of the CPU1a and GFS neurons in layer II of the upper division of the central body.

Keywords: iterative shape averaging, virtual insect brain, single-cell registration, central complex, desert locust, digital neuroanatomy, standard brain, 3D

INTRODUCTION

Many insects are able to perceive the pattern of polarized light in the blue sky (Horváth and Varjú, 2004). Studies on bees and ants have shown that these insects use the celestial polarization pattern for spatial orientation and navigation (Wehner, 1992). These and other insect species detect the plane of skylight polarization (*E*-vector) with a specialized dorsal rim area (DRA) of their compound eye (Labhart and Meyer, 1999; Mappes and Homberg, 2004). Photoreceptors in the DRA are highly sensitive to polarized light and send axonal projections to distinct dorsal regions of the lamina and medulla (Blum and Labhart, 2000; Homberg and Paech, 2002). Polarization-sensitive (POL) interneurons have been studied in the brain of the field cricket (Labhart, 1988; Labhart et al., 2001; Sakura et al., 2008) and in the desert locust *Schistocerca gregaria* (Vitzthum et al., 2002; Pfeiffer et al., 2005; Kinoshita et al., 2007; Pfeiffer and Homberg, 2007; Heinze and Homberg, 2009; Heinze et al., 2009).

In locusts, POL-neurons innervate specific, mostly small and distinct neuropils in the brain that are specialized for integration and processing of polarized-light information. These neuropils are connected by distinct fiber bundles and can be regarded as elements of a polarization vision pathway in the locust brain (Homberg, 2004). Neurons of a small ventral layer of the anterior lobe of the lobula (ALo) receive polarization information from the dorsal rim area of the medulla (DRMe) and send these signals to the anterior optic tubercle (AOTu) in the central brain. Only neurons of the lower unit of the AOTu are sensitive to polarized light (Pfeiffer et al., 2005). These neurons integrate signals from the sky polarization and chromatic contrast and compensate their *E*-vector tuning for diurnal changes in solar elevation (Pfeiffer and Homberg, 2007). Polarization information is transmitted from the AOTu to two distinct regions of the lateral accessory lobe, the median olive (MO) and the lateral triangle (LT) (Homberg et al., 2003). From these areas, neurons transfer polarization information to a final processing stage of the polarization vision pathway, the central complex.

Abbreviations: 3D, Three-dimensional; aCa, Accessory calyx; AL, Antennal lobe; aL, Anterior lip; ALo, Anterior lobe of the lobula; aMe, Accessory medulla; AOTu, Anterior optic tubercle; CBU, Upper division of the central body; CBL, Lower division of the central body; CPU, Columnar neuron of the CBU and PB; CL, Columnar neuron of the CBL; CLSM, Confocal laser scanning microscope; CC, Central complex; DLo, Dorsal lobe of the lobula; DRA, Dorsal rim area; DRMe, Dorsal rim area of the medulla; DS, Dorsal shell; GAM, Goat anti-mouse; GAR, Goat anti-rabbit; GFS, Giant fan-shaped (neuron); ILo, Inner lobe of the lobula; ISA, Iterative shape averaging (method); LAL, Lateral accessory lobe; lAOTu, Lower unit of the anterior optic tubercle; LH, Lateral horn; LT, Lateral triangle; MB, Mushroom body; Me, Medulla; MN, Midbrain neuropil; MO, Median olive; NGS, Normal goat serum; No, Nodulus; NoL, Lower unit of the nodulus; NoU, Upper unit of the nodulus; OLo, Outer lobe of the lobula; PB, Protocerebral bridge; PBS, Phosphate-buffered saline; PBT, PBS containing 0.3% Triton X-100; pCa, Primary calyx; Pe, Peduncu-lus; POL, Polarization-sensitive; TB, Tangential neuron of the PB; TL, Tangential neuron of the CBL; uAOTu, Upper unit of the anterior optic tubercle; VIB, Virtual insect brain (method); VS, Ventral shell

The central complex comprises a group of neuropils spanning the midline of the brain and consists of the protocerebral bridge (PB), the upper (CBU) and lower (CBL) divisions of the central body, and a pair of postero-ventral neuropils, termed noduli (No).

Studies in *Drosophila* suggest a role of the central complex in walking and leg coordination (Strauss and Heisenberg, 1993; Strauss, 2002; Poeck et al., 2008), flight control (Ilius et al., 1994), spatial orientation (Strauss, 2002; Neuser et al., 2008), and memory for visual object parameters (Liu et al., 2006; Wang et al., 2008). Together with evidence from locusts for a prominent role in sky compass orientation (Vitzthum et al., 2002; Heinze and Homberg, 2007), the central complex can be regarded as an integration center for multisensory information that is relevant to spatial memory and spatial orientation in diverse behaviours. One of the key features of the central complex is a highly modular neuroarchitecture. The CBU and CBL are organized into sets of clearly defined horizontal layers (Homberg, 1991; Müller et al., 1997) and the CBU, CBL and PB, in addition, into arrays of 16 regular vertical modules, called columns (Williams, 1975). Three major classes of cell types have been distinguished in the central complexes of locusts and other insects: (i) tangential neurons arborize in various areas outside the central complex and provide signaling input to distinct layers (Strausfeld, 1976; Hanesch et al., 1989); (ii) pontine neurons interconnect defined columns of the CBU in a regular way (Hanesch et al., 1989; Siegl et al., 2009), and (iii) columnar neurons provide signaling output from columnar domains to follower neurons in the lateral accessory lobes (LALs) (Hanesch et al., 1989; Heinze and Homberg, 2008). A subset of at least 13 different types of columnar and tangential neurons in the locust central complex are sensitive to polarized light (Vitzthum et al., 2002; Heinze and Homberg, 2009; Heinze et al., 2009), and many of these contribute to a topographic representation of *E*-vectors underlying the columnar neuroarchitecture of the PB (Heinze and Homberg, 2007).

For a deeper understanding of information processing in the neuronal network of the central complex, detailed knowledge about the synaptic connections between the different cell types is essential. An important step towards this goal is the generation of a high-quality three-dimensional (3D) anatomical atlas of the brain in which individual variations in shape, position and size of brain structures have been eliminated. This standard atlas can then serve as a platform to pool and simultaneaously visualize neurons from different preparations. Improvements in 3D imaging, processing, and computational capacity have permitted the creation of 3D standard brain atlases of the fruit fly, *Drosophila melanogaster* (Rein et al., 2002), the honey bee, *Apis mellifera* (Brandt et al., 2005), the desert locust, *Schistocerca gregaria* (Kurylas et al., 2008), and the moths, *Manduca sexta* (el Jundi et al., 2009) and *Heliothis virescens* (Kvello et al., 2009). For generation of these atlases, two different standardization methods have been established. The Virtual Insect Brain (VIB) protocol (Jenett et al., 2006) was used for the *Drosophila* and *Manduca* standard brains, whereas the Iterative Shape Averaging (ISA) method (Rohlfing et al., 2001) was used for the *Apis* and *Heliothis* standard brains. The VIB standard brains of *Drosophila* and *Manduca* were used primarily to compare volumes of brain areas between sexes. In contrast, the ISA brain of the honey bee was created to register single neurons from individual brains into a common standard. To reveal the limitations and advantages of the ISA and VIB procedures, both techniques were applied in comparison for the generation of a standard brain of the desert locust (Kurylas et al., 2008).

In this study we review the ISA and VIB standard brains of the desert locust and compare their advantages and limitations. As our goal is the analysis of neural connections in the central-complex network, we determined the ISA standardization method as the more appropriate one. To facilitate accurate representation of central-complex neurons, it is essential to have available an atlas of higher spatial resolution than is typically available for the whole brain. We, therefore, created a new, high-resolution ISA standard atlas of the central complex and immediately adjacent neuropils associated with the central complex. We show herein that this new 3D standard central complex is a highly suitable platform to investigate potential connections between central-complex neurons.

In the current work, we focus our attention to the columnar cell type CPU1a (Vitzthum et al., 2002). Previous analyses suggested that CPU1a neurons receive input from single columns of the PB and from a pair of columns of the CBU (Heinze and Homberg, 2008). In addition to polarized-light input, which is most likely provided in the PB arborizations (Heinze et al., 2009), the CPU1a neuron receives input in the CBU columns which is probably polarization-independent. A candidate neuron to provide synaptic input in the CBU is the tangential giant fan-shaped (GFS) neuron (Williams, 1972; Homberg, 1994), which arborizes in the CBU. To investigate possible connections between both neurons, we reconstructed a GFS and a CPU1a neuron in 3D and registered both into the standard central complex. The visualization of both neurons in the standard central complex reveals potential connections between these neurons in layer II of the CBU.

MATERIALS AND METHODS

ANIMALS

Desert locusts (*Schistocerca gregaria)* were reared under crowded conditions at 28°C on a 12:12 light/dark cycle. Only adult gregarious male locusts (1–3 weeks after imaginal moult) were used for reconstructions of the central complexes.

STANDARDIZED CENTRAL COMPLEX

Immunocytochemistry

Brains were dissected out of the head capsule and were fixed over night in 4% formaldehyde/0.1 M phosphate-buffered saline (4% FA/PBS, pH 7.4) at 4°C. They were then embedded in gelatine/albumin and sectioned from anterior to posterior with a vibrating-blade microtome (Leica VT1200 S, Leica Microsystems, Wetzlar, Germany) into 250-μm thick frontal sections. Brain sections were rinsed in 0.1 M PBS containing 0.3% Triton X-100 (PBT) for 1 h at room temperature and were preincubated (4°C, over night) in 5% normal goat serum (NGS; Jackson ImmunoResearch, Westgrove, PA, USA) in 0.1 M PBT containing 0.02% sodium azide. For visualization of distinct brain areas, all specimens were incubated with a monoclonal mouse antibody against the presynaptic vesicle protein synapsin I (SYNORF1, Klagges et al., 1996, kindly provided by Dr. E. Buchner, Würzburg) for 4–6 days at 4°C. Anti-synapsin was diluted 1:50 in 0.1 M PBT containing 1% NGS and 0.02% sodium azide. To distinguish the layers of the central body, a rabbit antibody against

serotonin was added to the primary antibody solution (1:20,000; Diasorin, Dietzenbach, Germany). After extensive rinsing, sections were incubated with goat anti-mouse (GAM) antibody conjugated to Cy5 and goat anti-rabbit (GAR) antibody conjugated to Cy2 (both 1:300; Jackson ImmunoResearch, Westgrove, PA, USA) in 0.1 M PBT, 1% NGS and 0.02% sodium azide for up to 3 days at 4°C. After rinsing, preparations were dehydrated in an ascending ethanol series (30–100%, 15 min each) and were cleared with a solution of 1:1 ethanol/methyl salicylate (15 min) followed by methyl salicylate (at least 40 min). Brain sections were embedded between two coverslips in Permount (Fisher Scientific, Pittsburgh, PA, USA). Compression of the preparations was prevented by spacers (Zweckform, Oberlaindern, Germany).

CLSM image acquisition

The brain sections were scanned using a confocal laser scanning microscope (CLSM, Leica TCS SP2) with a 20× oil objective (HC PL APO 20×/0.70 lmm Corr CS, Leica, Bensheim, Germany). The fluorescent signal of Cy5 was detected with a HeNe laser (633 nm). In addition, the sections were also scanned with an Ar laser (488 nm) to detect the serotonin staining signal (Cy2). The sections were scanned with 1024 × 1024 pixels per stack in xy direction (pixel size in xy direction: 1 × 1 μm) and 1 μm step size in z direction. Sections were scanned from anterior and posterior.

Image processing and reconstruction

The image stacks of the central complex and surrounding neuropils obtained from the brain sections were processed using Amira 4.1.2 software (Visage Imaging, Fürth, Germany). Because the central complex and surrounding neuropils extended across several brain sections we first aligned the corresponding image data. Pairs of image stacks from adjacent brain sections were opened in Amira and the matching optical slices in both stacks of data were selected. These optical slices were exactly overlapped with the *TransformEditor* by translation in *x*, *y* and *z* direction and by rotation of the image stacks. The image stacks were then connected using the module *Merge*. The resulting image data showed a detailed representation of staining for synapsin and serotonin of the central complex and surrounding brain areas.

For 3D reconstructions, *Labelfield* files were created with the same dimensions (voxel size and resolution) as the corresponding merged image stacks. Using the *Segmentation Editor*, reconstructions of selected neuropils were performed. All neuropils were labeled based on the anti-synapsin image stacks except for layers II and III of the CBU. These layers could not be distinguished in the synapsin channel and were, therefore, reconstructed using the corresponding anti-serotonin image stacks. Regions of interest were labeled in 3D in several optical slices and contiguous 3D structures were reconstructed using the tool *Wrap*.

Standardization of the central complex

We used 20 sectioned brains from male locusts to generate a 3D standardized central complex using the ISA method. For an exact registration of the neuropils of interest it was essential to mask the areas surrounding the central complex and LALs in the image stacks with the module *Arithmetic*. In some of the image stacks we corrected the tonal value using Adobe Photoshop 8 (Adobe Systems, San Jose, CA, USA) Furthermore, due to computer memory limitations, it was necessary to downsample the image stacks and the labelfield files with the module *Resample* to a voxel size of 2 × 2 × 2 μm.

For registration of the central complexes the central-complex image stacks and corresponding labelfields were exported to 3D image files in Analyze format. The overall registration procedure was controlled by a shell script, which used command-line driven registration tools developed by one of the authors (TR) and available in source code as part of the Computational Morphometry Toolkit (http://nitrc.org/projects/cmtk/). To reduce the time for image registration and transformation of the 20 central complexes, standardization of the central complex was calculated on a Linux-based cluster provided by Philipps-University of Marburg.

Analogous to the whole-brain procedure, CLSM images of the central complexes were first globally registered to a chosen reference specimen using an affine registration. Then, the iterative averaging and non-rigid transformation procedure was repeated four times. After completion of the averaging process, corresponding standardized 3D reconstructions of the labeled central-complex structures were created by applying the final transformation parameter to the label image stacks that corresponded to the standardized CLSM images. For an accurate standardization of the image stacks, the registration parameters were optimized and refined after repeated visual inspection of the results.

CENTRAL-COMPLEX NEURONS

Staining and immunocytochemistry

Central-complex neurons were injected iontophoretically with 4% Neurobiotin (Vector, Burlingame, CA) through glass microelectrodes with a resistance of 50–180 MΩ. The Neurobiotin was injected with a continuous depolarizing current of 1–3 nA for 1–5 min. The brains were dissected out of the head capsule and were fixed over night in 4% paraformaldehyde at 4°C. Both preparations were processed further as described by Heinze and Homberg (2008). Briefly, after fixation and rinsing, the brains were incubated at 1:1000 with Cy3-streptavidin (Dianova, Hamburg, Germany) in 0.1 M PBT for 3 days. After rinsing in buffer, they were dehydrated in an ascending ethanol series (25%–100%, 15 min each), transferred to ethanol/methyl salicylate (1:1, 15 min), and cleared in methyl salicylate for 35 min. Brains were mounted in Permount between two glass cover slides.

After scanning with the CLSM (10× oil objective) the embedded brains were incubated in xylene (2–4 h) to remove the embedding medium. Brains were rehydated in a descending ethanol series (100%–20%, 15 min. each) and were embedded in gelatine/albumin over night at 4°C. They were sectioned with the vibrating-blade microtome in 130–140-μm thick frontal sections. The sections were rinsed in 0.1 M PBS (4 × 15 min) and, after preincubation in 5% NGS in 0.1 M PBT at 4°C over night, were incubated for 6 days in anti-synapsin (1:50) and Cy3-streptavidin (1:1000) in 0.1 M PBT containing 1% NGS. After washing in 0.1 M PBT for 2 h, the sections were treated with Cy5-GAM (1:300), Cy3-streptavidin (1:1000) and 1% NGS in 0.1 M PBT for up to 3 days at 4°C. After rinsing, the preparations were dehydrated in an ascending ethanol series (30%–100%, 15 min. each) and were cleared with 1:1

ethanol/methyl salicylate (15 min.) followed by methyl salicylate (at least 40 min.). Sections were finally embedded in Permount between two coverslips.

Reconstruction and registration

The dye-injected neurons and the corresponding anti-synapsin stainings were scanned with the CLSM using a 20× or 40× objective (HCX PL APO 40×/1.25–0.75 Oil CS) at a resolution of 1024 × 1024 pixels (voxel size in xy direction: 0.22–0.35 × 0.22–0.35 μm) and a distance of 0.5 μm between optical slices. For neuron reconstructions in 3D we used the *SkeletonTree* tool in Amira 4.1.2 (Schmitt et al., 2004; Evers et al., 2005). Because of the limited computational capacity it was not possible to merge the scanned image stacks of the neurons with the anti-synapsin staining at high resolution. Therefore, we oriented all individual image stacks to the correct position with respect to each other using the *TransformEditor* and saved their positions with the module *ApplyTransform*. Reconstructions of the neurons were performed by opening image stacks consecutively and reconstructing the particular part of the neurons. For reconstruction of the corresponding neuropils the anti-synapsin-labeled image stacks were also transformed to their exact position, downsampled to a voxel size of 1 × 1 × 1 μm, and then merged into a single image stack. The nomenclature for central-complex neuropils and layers follows Heinze and Homberg (2008), the nomenclature for the lateral accessory lobe structures is based on Homberg (1994).

The reconstructed neurons were registered into the standardized central complex and into the standard locust brain of Kurylas et al. (2008). For registration of the neurons we registered distinct neuropils of the individual central complex into the standardized central complex and the standard brain using Amira 4.1.2. Neuropils of the individual central complex were first registered into the standard central complex and the standard brain using an affine transformation, computed by the *AffineRegistration* module. Afterwards, an elastic registration of the neuropils was performed using the module *ElasticRegistration*. The transformation parameters of the registrations were then applied to the neurons using the modules *ApplyTransform* and *ApplyDeformation*. Because of limited computational capacity it was not possible to register all neuropils in one process into the standard central complex. Therefore, we registered only two neuropils into the standard central complex in each case and then applied the registration parameters for the registration of the corresponding part of the neuron. Finally, all registered neuron parts were connected.

Visualization

To visualize our data we used several tools in Amira. The 3D surface views of the reconstructed neuropils were generated with the module *SurfaceGen* and were visualized with the tool *SurfaceView*. Direct volume rendering displays of the CLSM analogous image data of the standard central complex were created with the tool *Voltex*. To hide irrelevant structures surrounding the standardized neuropils and to distinguish the neuropils we masked the image data with the module *Arithmetic*. To this end, we used the standardized neuropil labelfield as a mask and removed surrounding synapsin-immunostained regions. Reconstructed neurons of the central complex were visualized with the *SkeletonView*. Volume data of the neuropils were calculated with the module *TissueStatistics*. Neuropil sizes were measured by the *Measuring* tool. Statistical analysis of these data was performed in SPSS 11.5 (Chicago, IL, USA) for Windows.

RESULTS

STANDARD ATLAS OF THE LOCUST BRAIN

As a basis for further analysis of the neuroarchitecture of the locust brain and, in particular, for better understanding of neural networks associated with polarization vision and sky compass orientation Kurylas et al. (2008) have previously established a standard atlas of the locust brain, based on data from ten male locust brains. Like other standard insect brains (Rein et al., 2002; Brandt et al., 2005) the reconstructions of the brains used for the registration process were based on staining against a synaptic neuropil marker. We briefly review the major findings of that study to illustrate the necessity for higher resolution standard atlases of particular brain areas of interest. In total, 33 distinct neuropils were reconstructed and registered for the standard locust brain (**Figure 1**). Seven neuropils were registered in the optic lobe: the medulla proper (Me) was distinguished from two associated neuropils, the DRMe, which receives polarized-light information from the DRA of the compound eye (Homberg, 2004), and the accessory medulla (aMe). Four subunits were distinguished in the lobula complex: the anterior (ALo), the dorsal (DLo), the inner (ILo) and the outer lobe of the lobula (OLo). In the median protocerebrum, the lateral horn (LH), the AOTu, the mushroom body, and the central complex were reconstructed. The AOTu is subdivided into an upper unit (uAOTu), which receives visual input from the optic lobe, and a lower unit (lAOTu), which is innervated by POL neurons (Pfeiffer et al., 2005). The mushroom bodies (MB) were divided into the combined pedunculus (Pe)-lobes, the accessory calyx (aCa), and the primary calyx (pCa). In the central complex (CC) in the center of the brain, the PB, the upper division of the central body (CBU), the lower division of the central body (CBL), and the paired noduli (No) were distinctly registered. Below the MB the deutocerebral antennal lobes (AL) were the most ventral neuropils reconstructed in the brain. Although several brain regions, such as the tritocerebrum, the LALs, or the antennal mechanosensory and motor center, were reconstructed in some individual brains, they were not included in the standard brains due to difficulties in reproducibly identifying their boundaries to adjacent brain structures. These neuropils and brain regions were assigned to a common, artificial "midbrain neuropil" structure for standardization (Kurylas et al., 2008).

For creation of a visual 3D standard brain, two methods have been established: The Virtual Insect Brain protocol (VIB; Jenett et al., 2006) and the Iterative Shape Averaging method (ISA, Rohlfing et al., 2001). Both methods were applied to create a standardized brain of the locust (**Figures 1A,B**). For an evaluation of both standardization procedures the relative distances to the center of the brain and the relative volumes of the standardized brains were compared to the mean distances and volumes of the ten individual brains (Kurylas et al., 2008). In the VIB standard brain, neuropil volumes showed lower deviation from the mean volumes compared with the ISA standard brain. In contrast, the ISA standard brain showed higher invariance in relative distances, displayed brain structures more distinctly and showed higher sym-

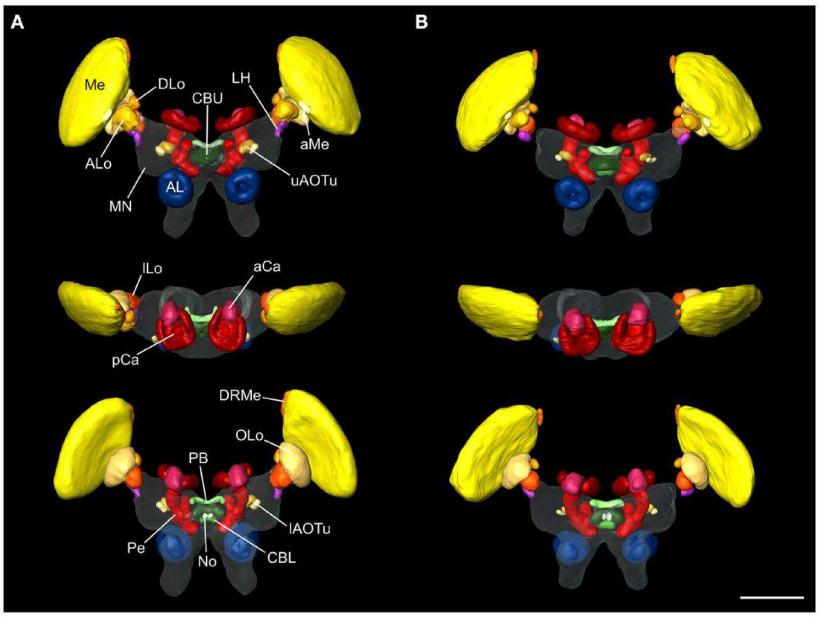

FIGURE 1 | Visual comparison of the 10-animal ISA and VIB whole standard brains of the desert locust *Schistocerca gregaria*. Surface reconstruction of 33 distinct neuropils plus a "midbrain neuropil" (MN, transparent) **(A)** ISA standard brain in anterior (top), dorsal (middle), and posterior (bottom) view (aCa, accessory calyx; AL, antennal lobe; ALo, anterior lobe of the lobula; aMe, accessory medulla; CBL, lower division of the central body; CBU, upper division of the central body; DLo, dorsal lobe of the lobula; DRMe, dorsal rim area of the medulla; lLo, inner lobe of the lobula; lAOTu, lower unit of the anterior optic tubercle; LH, lateral horn; Me, medulla; No, noduli; OLo, outer lobe of the lobula; PB, protocerebral bridge; pCa, primary calyx; Pe, pedunculus; uAOTu, upper unit of the anterior optic tubercle). **(B)** VIB standard brain viewed from anterior (top), dorsal (middle), and posterior (bottom) sides. Visualization of the "midbrain neuropil" is based on average image data (modified from Kurylas et al., 2008, **Figures 5A–C**, right panel). The color coding of the neuropils is consistent with Brandt et al. (2005). Scale bar: 600 μm.

metry in brain structures than the VIB standard. Therefore, the VIB standard brain is ideal for comparative volume analysis at the level of neuropils, whereas the standardized ISA brain is more useful as a platform to register and combine the morphologies of individual neurons (Kurylas et al., 2008). The small relative size of some neuropils of interest, like the noduli, layers of the central complex, or the subunits of the AOTu posed a severe limitation to both atlases. These neuropils were represented by only small numbers of voxels. To analyze and to fit neuron branches faithfully into subunits of the central complex, we therefore decided to create an ISA standard of the locust central complex and associated brain areas at a higher image resolution.

THE STANDARD CENTRAL COMPLEX

For detailed reconstruction and identification of central-complex subunits, scanning of whole brains was not feasible due to limitations in focal depth of the 10× microscope objective. Therefore, a new set of 20 brains was dissected and sectioned in 250 μm-thick sections, followed by scanning and reconstruction of the regions of interest. In total, we reconstructed and standardized 22 neuropils and layers in the central complex. Analogous to whole-mount brains, reconstructions were based on anti-synapsin immunostaining, except for reconstruction of the layers of the CBU. The CBU consists of three layers (layers I–III) from anterior to posterior (Homberg, 1991). Based on anti-synapsin staining, the boundary between layers I and II was well defined (**Figure 2A**), but layers II and III could not be distinguished. The boundary between layers II and III was instead determined by serotonin immunostaining (Homberg, 1991; Heinze and Homberg, 2008; Siegl et al., 2009; **Figure 2B**). Although layers I and II can be further subdivided into the dorsal sublayers Ia and IIa and the ventral sublayers Ib and IIb (Homberg, 1991), their precise boundaries are fuzzy (Heinze and Homberg, 2008), and these sublayers were, therefore, not included in the standardized central complex. The CBL was reconstructed as a single neuropil. It is located anterior of the posterior groove and consists of six layers (Müller et al., 1997). These layers were not well defined in synapsin- or serotonin immunostaining and were hence not reconstructed individually. Postero-dorsal to the CB we reconstructed the protocerebral bridge (PB, **Figure 2B**). Although the CBU, CBL, and the PB are divided into 16 columns (Williams, 1975; Heinze and Homberg, 2007), it was not possible to reveal these substructures based on synapsin- or serotonin immunostaining. The paired noduli are located posterior to the CB (**Figure 2D**) and consist of upper (NoU) and lower units (NoL). The upper unit shows three sublayers termed nodular layer I (NoUI), II (NoUII) and III (NoUIII) from dorsal to ventral. All subunits and layers of the noduli were reconstructed individually based on distinct anti-synapsin staining. Anterior to the ventral groove and dorsal to the CBU we reconstructed the anterior lip (aL), a neuropil that is directly connected to the central complex (**Figure 2A**). Two other

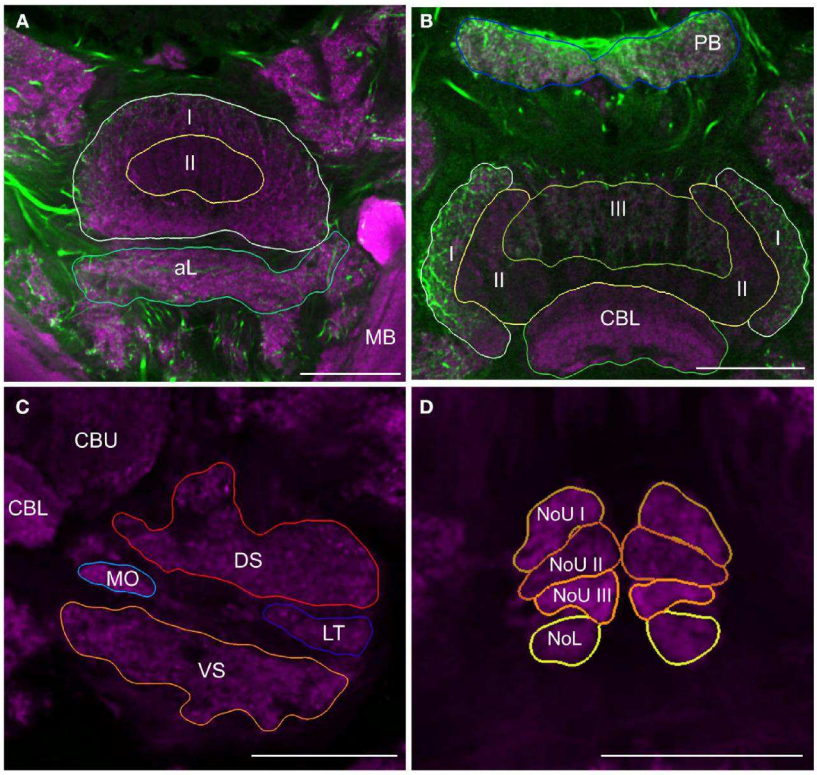

FIGURE 2 | Images from frontal sections through the central complex and lateral accessory lobe at different levels based on immunostaining for synapsin *(magenta)* and serotonin *(green)*. (A) Optical slice through layer I (I) and II (II) of the upper division of the central body and the anterior lip (aL) at the level of the mushroom bodies (MB). **(B)** Axial slice through the protocerebral bridge (PB), layer I (I), II (II) and III (III) of the upper division of the central body and the lower division of the central body (CBL). **(C)** Frontal section through the lateral accessory lobe, ventrolateral of the upper (CBU) and the lower (CBL) division of the central body. The lateral accessory lobe is subdivided into the dorsal shell (DS), the ventral shell (VS), the median olive (MO), and the lateral triangle (LT). **(D)** Confocal image through the upper and the lower units of the noduli (NoL). The upper units of the noduli are subdivided into layers I–III (NoU I, II, III). Scale bars: 100 μm.

structures that are closely associated with the central complex are the paired lateral accessory lobes (LALs; **Figure 2C**). The LALs are located posterior of the medial lobes of the MB and ventrolateral of the central complex. They consist of four well-defined subunits (Homberg, 1994). Most prominent are a large dorsal shell extending anteriorly around the medial lobe of the mushroom body and a large ventral shell (VS). Both major subunits are separated by fibers in the isthmus tracts, which give rise to two further subunits, the LT and the MO.

For standardization, we reconstructed 20 individual adult male central complexes. Based on the results from Kurylas et al. (2008) and our aim to create a visual standardized model of these 22 neuropils for neural network analysis, we created the standard central complex using the ISA method (Rohlfing et al., 2001). For standardization, one of the 20 brains had to be used as an initial affine registration template. Because the template brain determines the absolute scale of the ultimate standard atlas, we chose the brain with the smallest differences in neuropil distances from the mean distances of all brains to the brain center. Optical slices of this template brain are shown in **Figure 2**. The ISA method created a fuzzy initial standardized atlas of the central complex based on affine registrations, followed by four iterations of averaging and non-rigid transformations. During registration in the iterative procedure the image stacks of the standard central complex converged into increasingly accurate alignment, and neuropil structures became increasingly sharp and well defined. The final outputs of the ISA procedure were an averaged intensity image (CLSM) stack and an "averaged" label image stack of the reconstructions of the neuropils. The average intensity image of the ISA standard central complex is shown in **Figures 3A,B** as a direct volume rendering visualization. A 3D surface visualization of the reconstructed structures in the standard brain is shown in **Figures 3C–G** from different perspectives. The mean shape property of standardized structures generated by the ISA method has been demonstrated previously through a comparison of the degree of deformation between two individual brains and between the standard brain and an individual brain (Brandt et al., 2005; Kurylas et al., 2008). The ISA standard central complex, therefore, represents a "typical" central complex in terms of shape and appearance and provides a reliable, high-resolution reference coordinate space for registration and analysis of central-complex neurons of the desert locust.

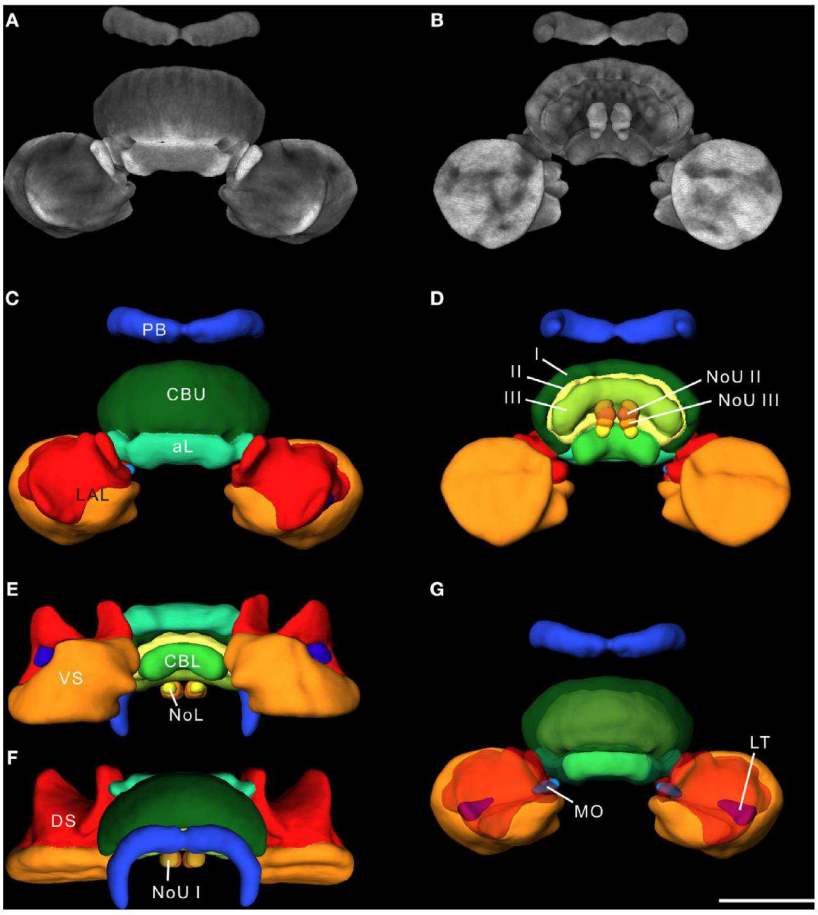

FIGURE 3 | The 20-animal standard central complex calculated using the ISA method. (A,B) 3D reconstruction of the standardized image stack by direct volume rendering. For visualization, synapsin labeling in brain areas surrounding the image data was deleted. **(A)** 3D visualization of the standardized CLSM image stack from anterior. **(B)** Posterior view of the standard central complex image data. **(C–G)** Surface reconstruction of all 22 segmented neuropils from different perspectives. **(C)** Anterior view **(D)** posterior view **(E)** ventral view **(F)** dorsal view **(G)** anterior view with transparent layer I of the upper division of the central body and dorsal shells. I, II, III, layers I–III of the upper division of the central body; aL, anterior lip; CBL, lower division of the central body; CBU, upper division of the central body; DS, dorsal shell; LAL, lateral accessory lobe; LT, lateral triangle; MO, median olive; NoL, lower unit of the nodulus; NoU I, II, III, layers I–III of the upper units of the noduli; PB, protocerebral bridge; VS, ventral shell. Scale bar: 200 μm.

Comparison of volumes and sizes of central-complex subdivisions between the standard brain and the standardized central complex revealed significantly smaller mean neuropil volumes of the PB and CBL (student *t*-test; two tailed; **Figure 4A**) in the sections than in the whole-mount brains. The CBU ($p = 0.062$) and the No ($p = 0.551$) were not significantly smaller. These differences in mean volumes probably resulted from larger tissue shrinkage of the brain sections and perhaps from differences in image resolution between the whole-mounts and the brain sections. Although the mean sizes of the PB and CBL were significantly different, the corresponding sizes in the ISA whole brain atlas do not reflect this (**Figure 4A**). Similarly, the sizes of the neuropils between the standard central complex and the central-complex neuropils in the whole-brain ISA standard do not exhibit the same differences (**Figure 4B**).

CPU1A NEURON

The POL columnar CPU1 and CPU2 neurons are among the largest columnar cell types of the central complex. To further analyze the neural connections of these neurons, we reconstructed a subtype of CPU1 neurons termed CPU1a in 3D, based on high-resolution image stacks obtained with a 20× and a 40× oil objective (**Figure 5**). The somata of all CPU1 neurons are located in the pars intercerebralis; the neurons have arborizations in the PB, the central body, and in one or both LALs (Heinze and Homberg, 2008). CPU1a neurons have arborizations in a single ipsilateral column of the PB and in two adjacent contralateral columns of the CBU. Axonal ramifications are concentrated in the contralateral LAL (**Figure 5A**). The reconstructed neuron has its cell body in the anterior pars intercerebralis and, judged from the location of its arborization domain in the PB, densely arborizes in the

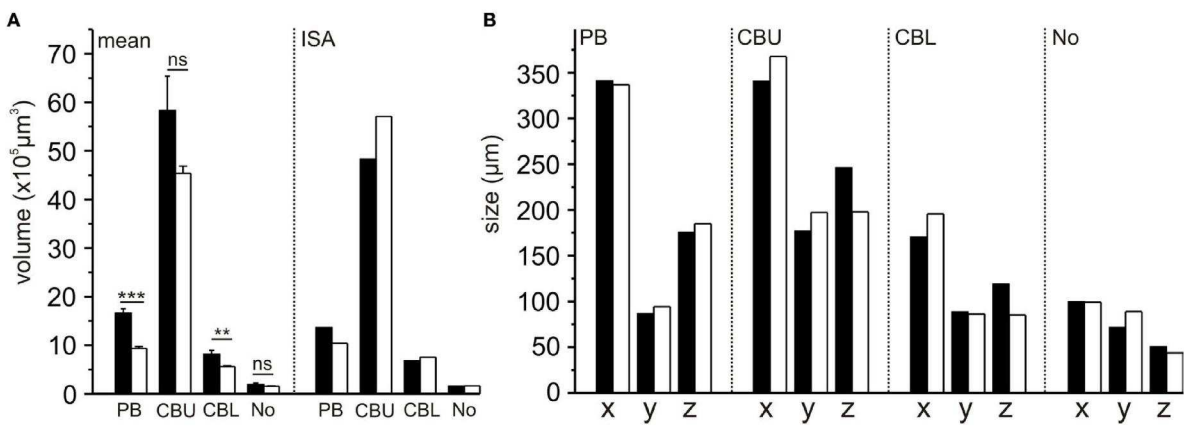

FIGURE 4 | Comparison of volumes and sizes of central-complex subdivisions between the 10-animal standard whole brain (*black bars*; from Kurylas et al., 2008) and the 20-animal standard central complex (*white bars*, this work). (A) Comparison of the means and ISA neuropil volumes (bars: standard error; ***$p < 0.001$; **$p < 0.01$; ns, not significant). **(B)** Comparison of neuropil sizes in the ISA standard brain and in the ISA standard central complex. CBL, lower division of the central body; CBU, upper division of the central body; No, noduli; PB, protocerebral bridge; *x, y, z* neuropil sizes in *x, y*, and *z* directions.

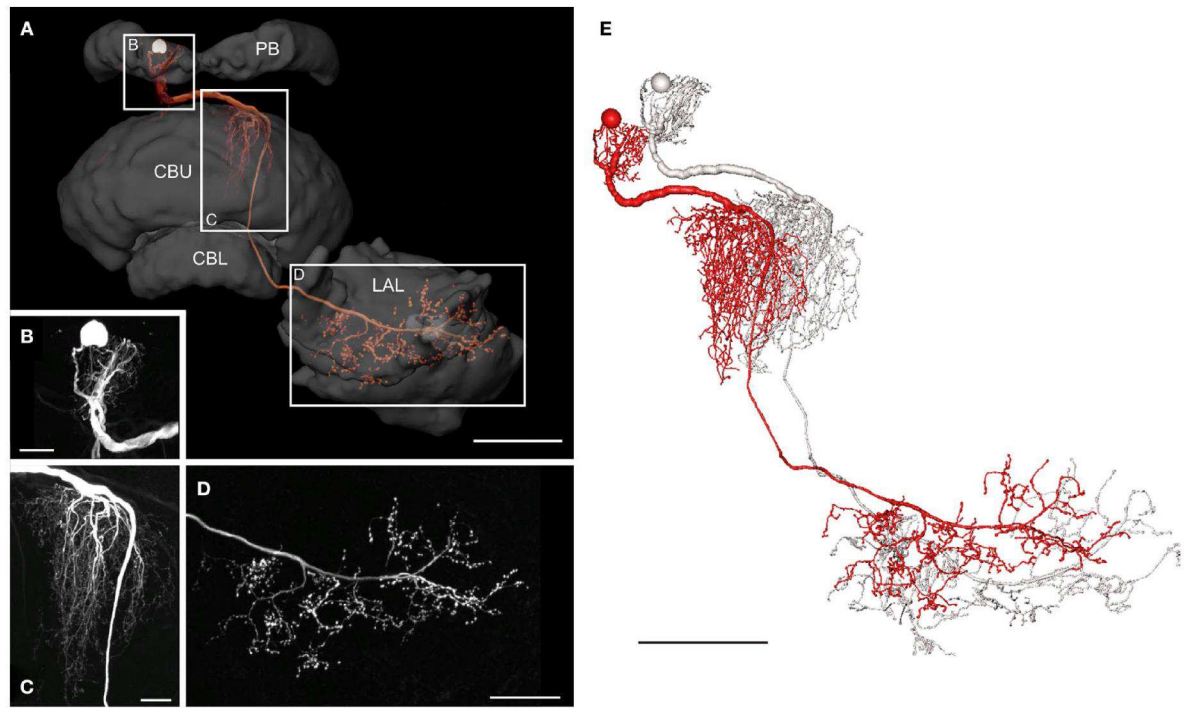

FIGURE 5 | Morphology of a CPU1a neuron. (A) Anterior view of a 3D volume rendering visualization of the CPU1a neuron and reconstruction of several neuropils of the central complex and lateral accessory lobe. CBL, lower division of the central body; CBU, upper division of the central body; LAL, lateral accessory lobe; PB, protocerebral bridge. Boxes show areas enlarged in **B–D**. **(B)** Location of cell body and arborizations in column R7 of the PB; maximum intensity projection of a confocal image stack. **(C)** Maximum intensity projections of ramifications of the CPU1 cell in two columns of the CBU, viewed from anteriorly. **(D)** Maximum intensity projection of optical slices of the arborizations in the ventral shell of the left LAL shown in anterior view. **(E)** 3D reconstruction of the CPU1a neuron before (*red*) and after affine and elastic registration (*grey*). Scale bars: **(A,E)** 100 µm; **(B,C)** 20 µm; **(D)** 50 µm.

second innermost column (column R7) of the right PB hemisphere (Williams, 1975; Heinze and Homberg, 2008; **Figure 5B**). The primary neurite leaves the PB on the anterior side and runs ventrally to the CB. The neurite crosses the hemisphere via the z-bundle between the PB and the CB and enters the CBU at its dorsal contralateral side. There, the CPU1a cell gives rise to a large tree of smooth dendritic arborizations, extending through two adjacent columns of the CBU (**Figure 5C**). The main neurite projects ventrally along the anterior face of the CBU, continues between layer I of the CBU and the anterior lip, and enters the ventral groove. Anterior to the CBL, the axonal fiber joins the isthmus tract and invades the contralateral LAL. Varicose and beaded ramifications are confined to the VS of the LAL (**Figure 5D**). The 3D reconstructions of the neuron before (*red*) and after transformation (*grey*) for registration into the standard central complex are shown in **Figure 5E**.

The distribution of smooth and beaded terminal fiber specializations suggests that the CPU1a neuron receives synaptic input from column R7 of the PB and from two columns of the CBU and sends this information to the VS of the LAL. In the PB the CPU1a neuron most likely receives polarization information (Heinze and Homberg, 2007). In addition to polarization vision input, CPU1a neurons likely receive input from unknown sources in the CBU. To determine candidate neurons to provide this input, we reconstructed the GFS neuron, a tangential neuron with ramifications in the CBU.

GIANT FAN-SHAPED NEURON

The GFS neuron (Williams, 1972; Homberg, 1994) is a tangential neuron of the central body. Tangential neurons connect various brain regions to the PB or to particular layers of the CB. The soma of the GFS neuron lies posterior to the LAL in the ventro-median protocerebrum (**Figure 6A**). The main neurite runs dorsally through the ventro-median protocerebrum and enters the ipsilateral LAL through the posterior surface of the VS. In the LAL the GFS neuron has smooth ramifications, especially in the dorsal shell and less prominently in the VS (**Figure 6C**), but not in the LT and MO. Additional dendritic processes extend around the medial lobe of the mushroom body toward anterior regions of the brain and arborize with fine terminals in the ipsilateral anteromedian protocerebrum (**Figures 6D and 7A**). Finally, a few dendritic processes extend to lateral aspects of the anterior lip (**Figure 7A**). The main neurite runs through the LAL dorsally from the isthmus tract toward the CB. Laterally from the CBL, it bends posteriorly and enters the posterior groove. Here the main neurite gives rise to eight major side branches. They enter eight

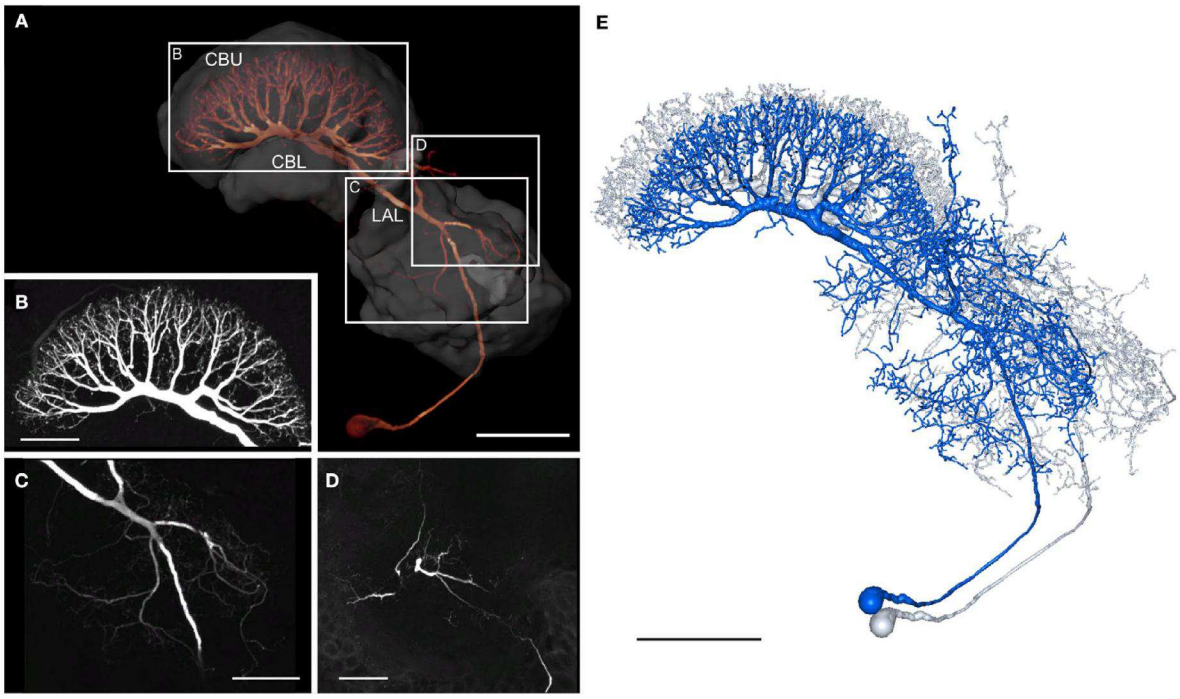

FIGURE 6 | Morphology of the giant fan-shaped (GFS) neuron. **(A)** Anterior view of the GFS neuron by direct volume rendering. Reconstructions of central-complex neuropils and the lateral accessory lobe are shown transparently. CBL, lower division of the central body; CBU, upper division of the central body; LAL, lateral accessory lobe. Boxes show areas enlarged in **B–D**. **(B)** Maximum intensity projection of the arborization tree in the CBU, anterior view. **(C)** Maximum intensity projection of a confocal image stack from anterior showing ramification in the left LAL. **(D)** Maximum intensity projections of optical slices showing arborizations in the anterior median protocerebrum, anterior view. **(E)** 3D reconstruction of the GFS neuron before (*blue*) and after registration (*grey*). Scale bars: **(A,E)** 100 μm; **(B–D)** 50 μm.

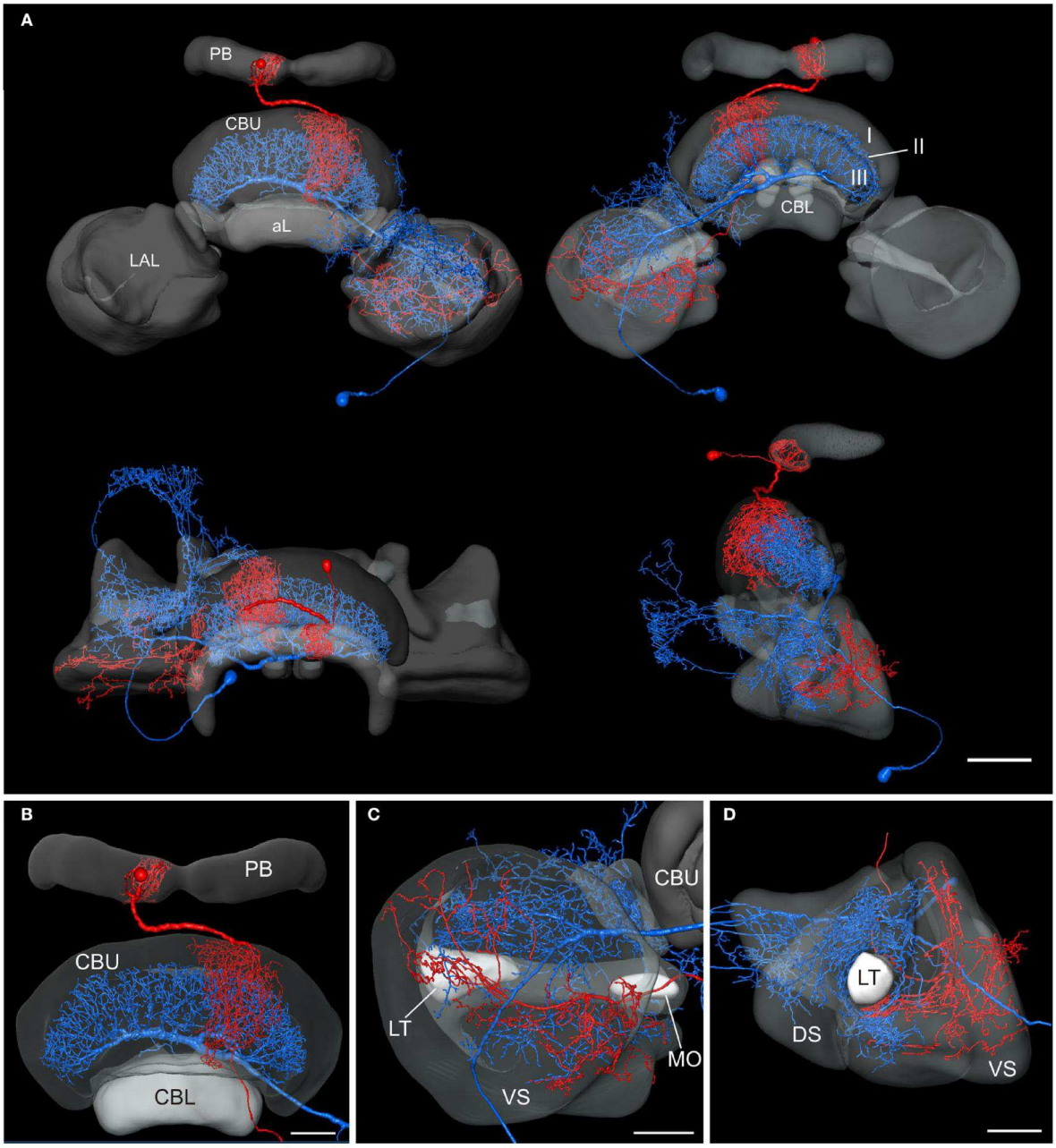

FIGURE 7 | Registration of the CPU1a (*red*) and GFS (*blue*) neurons into the 3D standard central complex. (A) Anterior view (top left), posterior view (top right), dorsal view (bottom left) and lateral view (bottom right). **(B)** Anterior view showing arborizations in the upper division of the central body (*CBU*) and in the protocerebral bridge (*PB*). **(C)** Posterior view of the standardized right lateral accessory lobe with processes of the CPU1a and GFS neurons. **(D)** Ventrolateral view of the lateral accessory lobe. I, II, III, layers I–III of the upper division of the central body; aL, anterior lip; CBL, lower division of the central body; DS, dorsal shell; LAL, lateral accessory lobe; LT, lateral triangle; MO, median olive; VS, ventral shell. Scale bars: **(A)** 100 μm; **(B–D)** 50 μm.

pairs of columns of the CBU and ramify into highly varicose fiber processes, concentrated in layer II (**Figure 6B**). The 3D reconstructions of the GFS neuron before (*blue*) and after registration (*grey*) are shown in **Figure 6E**.

NEURONS IN THE STANDARD CENTRAL COMPLEX

To analyze whether the tangential GFS neuron is a candidate to provide synaptic input to the columnar CPU1a cell, we registered both cells into the standardized central complex (**Figure 7**). For an

exact fit of the two neurons into the virtual central-complex atlas, corresponding brain areas of the individual brains were reconstructed (**Figures 5A and 6A**) and were registered into the standard central complex. For registration of the neuropils we used an affine registration followed by a non-rigid elastic registration. The transformation and deformation parameters were then applied to the reconstructed neurons to visualize both neurons in the standard central complex (**Figure 7A**). The ramifications in column R7 of the PB of the registered CPU1a neuron indicate high accuracy of the registration process (**Figure 8C**, arrow). The CPU1a neuron shows arborizations only in the VS of the LAL of the standard central complex, as is observed in the original brain. The GFS cell, in contrast, innervates the ventral and dorsal shells of the LAL, however, with the majority of ramifications in the dorsal shell (**Figure 7C**), again as observed in the original brain. As in the individual brains, both registered neurons do not enter the LT and the MO (**Figures 7C,D**). To investigate whether the output region of the GFS neuron and the input region of the CPU1a cell co-localize, we analyzed the CBU ramifications in detail. The CPU1a cell shows ramifications in layer I of the CBU (**Figure 7B**) and fewer arborizations in layers II and III of the CBU (**Figure 8D**). Neurites of the GFS neuron, in contrast, do not enter layer I, but show highest concentration of arborizations in layer II of the CBU (**Figure 8D**). Although the CPU1a cell shows fewer arborizations in layer II, processes of both neurons clearly overlap in layer II of the CBU (**Figures 7A and 8D**). This co-localization of input processes of the CPU1a cell and output areas of the GFS neuron shows that the GFS neuron is a candidate to contribute to synaptic input to CPU1a neurons in layer II of the CBU.

DISCUSSION

COMPARISON OF VIB AND ISA STANDARDS

Kurylas et al. (2008) have generated two whole standard brains of the desert locust, one following the VIB protocol (Jenett et al., 2006) and the second using the ISA method (Rohlfing et al., 2001). Both standardization methods were performed with the

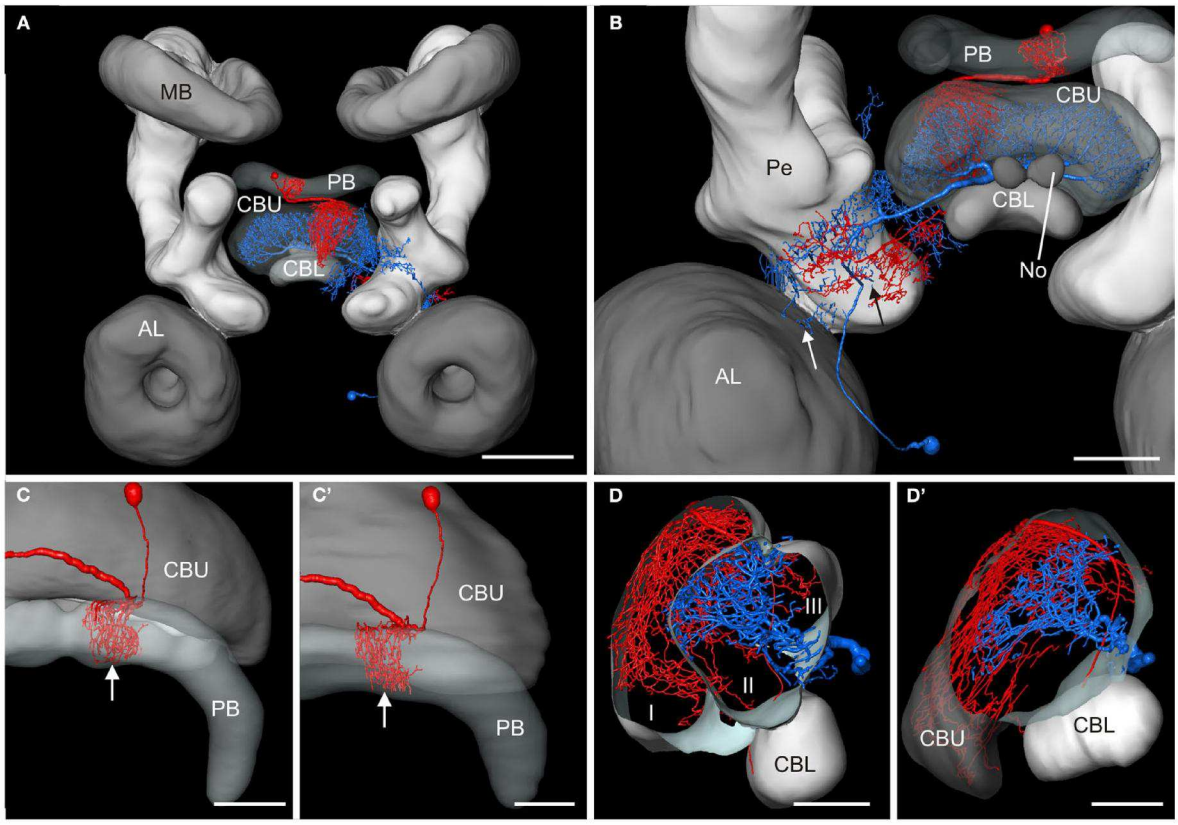

FIGURE 8 | Registration of the CPU1a *(red)* and GFS *(blue)* neurons into the ISA standard brain and into the standard central complex. (A) Anterior view of the central brain of the standard brain showing the central complex, the mushroom bodies (MB) and the antennal lobes (AL). **(B)** Postero-lateral view of the central standard brain. Arrows indicate displacement of arborizations of the GFS neuron into the pedunculus (Pe) and antennal lobe. **(C,C')** Dorsal view showing cell body and ramifications of the CPU1a neuron in column R7 (white arrows) of the protocerebral bridge (PB) registered into the standard central complex **(C)** and into the central complex neuropils of the standard brain **(C')**. **(D,D')** Oblique sagittal sections through the central body of the standardized central complex (section thickness: 42 μm, **D**) and the standard brain (section thickness: 54 μm, **D'**) illustrating common projections of both neurons in layer II of the upper division of the central body. I, II, III, layers I–III of the upper division of the central body; CBL, CBU lower, resp. upper division of the central body; No, nodulus. Scale bars: **(A)** 200 μm; **(B)** 100 μm; **(C–D')** 50 μm.

same set of ten brain preparations. For future applications it was particularly interesting to analyze advantages and limitations of both methods. Standard brains also exist for the fruit fly (Rein et al., 2002), the moths *Manduca sexta* (el Jundi et al., 2009) and *Heliothis virescens* (Kvello et al., 2009), and the honeybee (Brandt et al., 2005). Whereas the *Drosophila* and *Manduca* standards were generated using the VIB method, the honeybee and *Heliothis* standard brains are based on the ISA method. The standard brains of *D. melanogaster* and of *M. sexta* were primarily developed to compare volumes of brain neuropils. Accordingly, standard volumes were calculated and compared between the sexes (Rein et al., 2002; el Jundi et al., 2009). An additional motivation for the *Drosophila* standard brain was the prospect to quantitatively compare volumes of brain areas between wildtype and genetically manipulated flies. The honeybee and *Heliothis* standard brains were instead created to register neurons from different preparations into a common anatomical framework (Brandt et al., 2005; Kvello et al., 2009).

A comparison of the two locust standard brains showed that the VIB method creates an ideal standard brain for inter- and intraspecific volume comparisons, because it keeps neuropil volumes unchanged. This is not surprising, because the calculation of the standard or mean volumes does not depend on the process of registration. Instead, the VIB protocol calculates mean volumes of all segmented neuropils based on the labelfields before the brains are registered. The most meaningful result of the VIB protocol is the image stack of all registered segmented neuropils, as shown in Jenett et al. (2006, **Figure 4**), Kurylas et al. (2008, **Figures 5D–F**) and el Jundi et al. (2009, **Figures 4D,F**). The 3D surface view of the standard brain is a threshold representation of this registered image stack.

The ISA method, in contrast, generated the more exact visual standard atlas regarding positions and shapes of the neuropils and bilateral symmetry of the brain (Kurylas et al., 2008). The ISA script registers the brains based on intensity image stacks (here, CLSM). After registration, deformation parameters are applied to the corresponding label fields to create a 3D model of standard brain structures. In contrast to the VIB method, which is easy to use through a step-by-step script in Amira, the ISA standard brain has to be calculated outside Amira, currently via a shell script. Both methods require choosing an individual brain as a template for the registration procedure. Whereas in the visual standard brain of the VIB method the positions of the neuropils are highly dependent on this template brain, the spatial relationships of neuropil positions in the ISA standard are largely independent from this template but their orientations may be affected (el Jundi et al., 2009). During the initial, affine registration stage of the ISA method, the brains are also scaled depending on the template brain (Rohlfing et al., 2004; el Jundi et al., 2009) to minimize anatomical differences (Kuß et al., 2007; Kurylas et al., 2008). To minimize these possible sources of bias, Kurylas et al. (2008) calculated for all brains the relative distances of neuropils to the brain center and chose the brain with the lowest deviations from the mean distances as the template brain.

THE STANDARD CENTRAL COMPLEX

In this work, we have generated a standardized central complex of the desert locust brain based on 20 individual central complexes. The central complex is involved in the control of locomotion and flight and plays an important role in spatial orientation in response to polarized light. In locusts it is the final processing stage in the polarization vision pathway (Heinze and Homberg, 2007) and is probably the main integration site of polarization information from both eyes (Heinze et al., 2009). The central complex is innervated by a large variety of neuronal cell types (Heinze and Homberg, 2008, 2009), whose roles in information processing and integration are largely unknown. To generate an anatomical platform for analysis of central-complex neurons from different brains, we used the ISA method based on Kurylas et al. (2008) and, for the first time, implemented this technique for the registration of only one brain area. This required masking of the regions surrounding the central complex in the CLSM image stacks. To hide the surrounding brain regions of the stacks we used the corresponding label fields with the module *Arithmetic*, after we enlarged the label fields by about 15 voxels in all directions and removed irrelevant regions.

A limitation of the locust standard brain of Kurylas et al. (2008) is the relative low resolution of images (5.9 × 5.9 × 3 μm). Thereby, it was unfeasible to increase the number of reconstructed neuropils in the central brain. As a result, the subdivisions of the LALs, the anterior lip, and the layers of the CBU and noduli were not included into the standard whole brain. However, most of these structures are crucially involved in polarized-light signaling and are, thus, innerved by POL neurons (LAL: Vitzthum et al., 2002; Pfeiffer et al., 2005; CBU: Heinze and Homberg, 2007, 2009; No: Heinze and Homberg, 2009). Especially the LALs are an important processing stage for polarized-light signals. They receive polarized-light input from the AOTu (Homberg, 2004) and send this information to the central complex (Vitzthum et al., 2002). In addition, they receive polarized-light information from the central complex and transfer it to descending pathways (Homberg, 1994; Heinze and Homberg, 2009).

The absence of these neuropils in the standard whole brain resulted in substantial imprecision during transformation of the two neurons (**Figure 8**). As a result of the absence of the LAL in the standard whole brain, ramifications of the GFS neuron in the DS and VS were displaced into the Pe and the antennal lobe (**Figure 8B**, arrows). In contrast, the arborizations of the CPU1a- and GFS neurons in the central-complex neuropils of the standard whole brain show that it is an adequate atlas for neurons that ramify in reconstructed brain areas (**Figures 8C',D'**). Nevertheless, the additional information provided by the additionally reconstructed neuropils and layers is indispensable for precise fitting of neurons into these compartments.

For future studies it will be important to incorporate the ISA standard central complex into the ISA whole-brain standard. To do this, we have to face the potential problem that the registration of the central complex atlas is based on brain sections, whereas the construction of the whole-brain standard was performed through a whole-mount protocol (Kurylas et al., 2008). Compared to whole-mount preparations, which show already noticeable tissue shrinkage (Bucher et al., 2000; Ott, 2008), morphological distortions may be even larger in brain sections. Comparisons of mean volumes showed that the CBL and PB are significantly smaller in the standard central complex than in the standard brain, whereas the slightly smaller sizes of the CBU and

No are not significant. Interestingly, these differences between mean volumes are not reflected when comparing the volumes of the ISA standards (**Figure 4A**). Both, the ISA volumes and the overall dimensions of the central-complex neuropils are similar in the standard brain and the standard central complex (**Figures 4A,B**). Taken together, the similar ISA volumes and sizes are a promising basis for our next goal to register the standardized central complex into the standard brain.

A similar potential problem arises when transforming neurons into the standard central complex. For detailed neuronal reconstructions, an adequate resolution of the CLSM image stacks is necessary. Owing to the limited working distance of the 20× and 40× objectives, the individual neurons of the central complexes were imaged from 130–140-μm brain sections. These sections may differ in shrinkage artifacts from the 250-μm brain sections used for the standardized central complex. For registration of the neurons into the standard central complex it was, therefore, necessary to transform, scale, and deform the cells in a fitting process. To do this, defined neuropils of the individual central complexes were registered into the standardized central complex, and the same transformation parameters of the registrations were then applied to the neurons.

THE POLARIZATION VISION NETWORK IN THE CENTRAL COMPLEX

The central complex comprises a group of highly modular midline neuropils in the insect brain. The topographic representation of zenithal *E*-vector tunings in the columns of the PB of the locust strongly suggests that coding of solar azimuth is a major aspect of the functional role of the central complex (Heinze and Homberg, 2009; Heinze et al., 2009). Based on anatomical and physiological data, a flow of information processing in the polarization vision network of the central complex has been suggested (Heinze and Homberg, 2008, 2009; Heinze et al., 2009). Tangential neurons TL2 and TL3 represent the input neurons of the polarization vision network in the central complex. They receive their inputs in the LT and MO of the LAL and send axonal projections to the CBL (Vitzthum et al., 2002). Columnar CL1 neurons connect the CBL to the PB and, together with tangential TB neurons of the PB, are most likely involved in generating the compass-like representation of *E*-vectors in the PB (Heinze and Homberg, 2007). Processed polarization information is, finally, transferred via CPU1 and CPU2 cells to the LALs and is then transmitted indirectly to descending neurons.

CPU1 AND GFS NEURONS

In addition to polarized light, a brain area involved in spatial orientation and memory has to integrate a variety of other inputs, including landmark information, motivational input, and feedback from ongoing motor activity (Heinze et al., 2009). This may lead to suppression of output if motivation for spatially-oriented behavior is low or to a context-dependent ratio of activation of motor centers in the right and left hemispheres of the nervous system for a spatial motor task. Because of their morphology, polarity, and hierarchy in the polarization vision system, the CPU1- and the conditionally POL CPU2 cells (Heinze and Homberg, 2009) are ideal candidates to receive modulatory input, in addition to solar azimuth coding. CPU1/2 cells most likely receive their polarized-light input in the PB (Heinze and Homberg, 2009; Heinze et al., 2009), but have a second, even larger dendritic input region in the CBU. Two principal subclasses of CPU neurons have axonal projections to one (CPU1) or to both (CPU2) LALs (Heinze and Homberg, 2008). Three subtypes of CPU1 cells are distinguished based on ramifications in the ipsilateral (CPU1a,c) or contralateral (CPU1b) hemisphere of the PB (Heinze and Homberg, 2008). Whereas in all CPU1 neurons the ramifications in the PB are limited to single columns, the arborizations in the CBU either extend over several columns (CPU1b), are confined to two to three columns (CPU1a), or occur in a single column (CPU1c). Thus, the ratio between the polarization and non-polarization inputs may be defined through anatomical broadening in the CBU. In contrast, ramifications of all CPU1 and CPU2 cells invade layers I–III of the CBU but decline in density from layer I to III.

Co-registration suggests that the GFS neuron is a promising candidate to provide input to CPU1a neurons and perhaps to all types of CPU1/2 neurons. Spiking activity in CPU1a cells is modulated by the *E*-vector of polarized light (Vitzthum et al., 2002). CPU1 cells receive polarized-light input from both eyes and have zenith-centered receptive fields extending over 120° (Heinze et al., 2009). The GFS neuron, by contrast, is not sensitive to polarized light (Heinze, 2009), but is weakly inhibited by frontally presented unpolarized light (Homberg, 1994). The GFS neuron responds more strongly to movement stimulation in the ipsilateral field of view, is phasically excited by frontal wind stimulation, and shows strong activity bursts associated with tethered flight (Homberg, 1994; Müller, 1997; Heinze, 2009). Interestingly, CPU1a cells also respond to frontal light with an inhibition of spiking (Vitzthum et al., 2002). Taken together, these data support the hypothesis that the GFS neuron transfers non-polarized visual input and perhaps flight-associated excitation to the CPU1/2 cells.

In addition to the GFS neuron, a variety of other tangential neurons of the CBU, such as TU1 and TU2 cells (Homberg et al., 1999), are possible candidates to provide synaptic input to CPU cells. Registering further neurons into the standard central complex will allow us to explore the neuronal connectivities in the central-complex network with increasing depth and complexity, and to formulate hypotheses on neural pathways and novel physiological properties of particular cell types that can then be tested in subsequent recordings. Our current achievements of a common platform for the whole brain and, with higher resolution, for the central complex provide an ideal basis for this enterprise.

ACKNOWLEDGMENTS

We are grateful to Dr. Thomas Gebhardt for providing the Linux cluster and help in Linux, and to Erich Buchner for providing the anti-synapsin antibody. We thank Ulrike Träger for helpful suggestions on the manuscript and Karl Heinz Herklotz for maintaining the locust cultures. This work was supported by DFG grants HO 950/14 and HO 950/16 to Uwe Homberg. Torsten Rohlfing was supported by NIAAA under grant AA013521-INIA and NIBIB under Grant EB008381. Registration tools and scripts for Iterative Shape Averaging are available in source code as part of the Computational Morphometry Toolkit from http://www.nitrc.org/projects/cmtk/.

REFERENCES

Blum, M., and Labhart, T. (2000). Photoreceptor visual fields, ommatidial array, and receptor axon projections in the polarisation-sensitive dorsal rim area of the cricket compound eye. *J. Comp. Physiol. A* 186, 119–128.

Brandt, R., Rohlfing, T., Rybak, J., Krofczik, S., Maye, A., Westerhoff, M., Hege, H. C., and Menzel, R. (2005). Three-dimensional average-shape atlas of the honeybee brain and its applications. *J. Comp. Neurol.* 492, 1–19.

Bucher, D., Scholz, M., Stetter, M., Obermayer, K., and Pflüger, H. J. (2000). Correction methods for three-dimensional reconstructions from confocal images: I. Tissue shrinking and axial scaling. *J. Neurosci. Methods* 100, 135–143.

el Jundi, B., Huetteroth, W., Kurylas, A. E., and Schachtner, J. (2009). Anisometric brain dimorphism revisited: implementation of a volumetric 3D standard brain in *Manduca sexta*. *J. Comp. Neurol.* 517, 210–225.

Evers, J. F., Schmitt, S., Sibila, M., and Duch, C. (2005). Progress in functional neuroanatomy: precise automatic geometric reconstruction of neuronal morphology from confocal image stacks. *J. Neurophysiol.* 93, 2331–2342.

Hanesch, U., Fischbach, K. F., and Heisenberg, M. (1989). Neuronal architecture of the central complex in *Drosophila melanogaster*. *Cell Tissue Res.* 257, 343–366.

Heinze, S. (2009). Characterization of Polarization Sensitive Neurons of the Central Complex in the Brain of the Desert Locust (*Schistocerca gregaria*). PhD Thesis, Philipps University Marburg, Marburg.

Heinze, S., Gotthardt, S., and Homberg, U. (2009). Transformation of polarized light information in the central complex of the locust. *J. Neurosci.* 29, 11783–11793.

Heinze, S., and Homberg, U. (2007). Maplike representation of celestial *E*-vector orientations in the brain of an insect. *Science* 315, 995–997.

Heinze, S., and Homberg, U. (2008). Neuroarchitecture of the central complex of the desert locust: intrinsic and columnar neurons. *J. Comp. Neurol.* 511, 454–478.

Heinze, S., and Homberg, U. (2009). Linking the input to the output: new sets of neurons complement the polarization vision network in the locust central complex. *J. Neurosci.* 29, 4911–4921.

Homberg, U. (1991). Neuroarchitecture of the central complex in the brain of the locust *Schistocerca gregaria* and *S. americana* as revealed by serotonin immunocytochemistry. *J. Comp. Neurol.* 303, 245–254.

Homberg, U. (1994). Flight-correlated activity changes in neurons of the lateral accessory lobes in the brain of the locust *Schistocerca gregaria*. *J. Comp. Physiol. A* 175, 597–610.

Homberg, U. (2004). In search of the sky compass in the insect brain. *Naturwissenschaften* 91, 199–208.

Homberg, U., Hofer, S., Pfeiffer, K., and Gebhardt, S. (2003). Organization and neural connections of the anterior optic tubercle in the brain of the locust, *Schistocerca gregaria*. *J. Comp. Neurol.* 462, 415–430.

Homberg, U., and Paech, A. (2002). Ultrastructure and orientation of ommatidia in the dorsal rim area of the locust compound eye. *Arthropod Struct. Dev.* 30, 271–280.

Homberg, U., Vitzthum, H., Müller, M., and Binkle, U. (1999). Immunocytochemistry of GABA in the central complex of the locust *Schistocerca gregaria*: identification of immunoreactive neurons and colocalization with neuropeptides. *J. Comp. Neurol.* 409, 495–507.

Horváth, G., and Varjú, D. (2004). Polarization Patterns in Nature and Polarized Light in Animal Vision. Berlin, Heidelberg, New York, Springer Verlag.

Ilius, M., Wolf, R., and Heisenberg, M. (1994). The central complex of *Drosophila melanogaster* is involved in flight control: studies on mutants and mosaics of the gene ellipsoid body open. *J. Neurogenet.* 9, 189–206.

Jenett, A., Schindelin, J. E., and Heisenberg, M. (2006). The virtual insect brain protocol: creating and comparing standardized neuroanatomy. *BMC Bioinformatics* 7, 544.

Kinoshita, M., Pfeiffer, K., and Homberg, U. (2007). Spectral properties of identified polarized-light sensitive interneurons in the brain of the desert locust *Schistocerca gregaria*. *J. Exp. Biol.* 210, 1350–1361.

Klagges, B. R. E., Heimbeck, G., Godenschwege, T. A., Hofbauer, A., Pflugfelder, G. O., Reifegerste, R., Reisch, D., Schaupp, M., Buchner, S., and Buchner, E. (1996). Invertebrate synapsins: a single gene codes for several isoforms in *Drosophila*. *J. Neurosci.* 16, 3154–3165.

Kurylas, A. E., Rohlfing, T., Krofczik, S., Jenett, A., and Homberg, U. (2008). Standardized atlas of the brain of the desert locust, *Schistocerca gregaria*. *Cell Tissue Res.* 333, 125–145.

Kuß, A., Hege, H. C., Krofczik, S., and Borner, J. (2007). Pipeline for the creation of surface-based averaged brain atlases. In Proceedings of Winter School of Computer Graphics 2007, 1, 17–24.

Kvello, P., Løfaldli, B. B., Rybak, J., Menzel, R., and Mustaparta, H. (2009). Digital, three-dimensional average shaped atlas of the *Heliothis virescens* brain with integrated gustatory and olfactory neurons. *Front. Syst. Neurosci.* 3:14. doi: 10.3389/neuro.06.014.2009.

Labhart, T. (1988). Polarization-opponent interneurons in the insect visual system. *Nature* 331, 435–437.

Labhart, T., and Meyer, E. P. (1999). Detectors for polarized skylight in insects: a survey of ommatidial specializations in the dorsal rim area of the compound eye. *Microsc. Res. Tech.* 47, 368–379.

Labhart, T., Petzold, J., and Helbling, H. (2001). Spatial integration in polarization-sensitive interneurones of crickets: a survey of evidence, mechanisms and benefits. *J. Exp. Biol.* 204, 2423–2430.

Liu, G., Seiler, H., Wen, A., Zars, T., Ito, K., Wolf, R., Heisenberg, M., and Liu, L. (2006). Distinct memory traces for two visual features in the *Drosophila* brain. *Nature* 439, 551–556.

Mappes, M., and Homberg, U. (2004). Behavioral analysis of polarization vision in tethered flying locusts. *J. Comp. Physiol. A* 190, 61–68.

Müller, M. (1997). Anatomische und funktionelle Charakterisierung der unteren Einheit des Zentralkörpers im Gehirn der Heuschrecke Schistocerca gregaria. Doctoral Thesis, Universität Regensburg, Germany.

Müller, M., Homberg, U., and Kühn, A. (1997). Neuroarchitecture of the lower division of the central body in the brain of the locust (*Schistocerca gregaria*). *Cell Tissue Res.* 288, 159–176.

Neuser, K., Triphan, T., Mronz, M., Poeck, B., and Strauss, R. (2008). Analysis of a spatial orientation memory in *Drosophila*. *Nature* 453, 1244–1247.

Ott, S. R. (2008). Confocal microscopy in large insect brains: Zinc–formaldehyde fixation improves synapsin immunostaining and preservation of morphology in whole-mounts. *J. Neurosci. Methods* 172, 220–230.

Pfeiffer, K., and Homberg, U. (2007). Coding of azimuthal directions via time-compensated combination of celestial compass cues. *Curr. Biol.* 17, 960–965.

Pfeiffer, K., Kinoshita, M., and Homberg, U. (2005). Polarization-sensitive and light-sensitive neurons in two parallel pathways passing through the anterior optic tubercle in the locust brain. *J. Neurophysiol.* 94, 3903–3915.

Poeck, B., Triphan, T., Neuser, K., and Strauss, R. (2008). Locomotor control by the central complex in *Drosophila* – An analysis of the *tay bridge* mutant. *Dev. Neurobiol.* 68, 1046–1058.

Rein, K., Zöckler, M., Mader, M. T., Grübel, C., and Heisenberg, M. (2002). The *Drosophila* standard brain. *Curr. Biol.* 12, 227–231.

Rohlfing, T., Brandt, R., Maurer, C. R. Jr, and Menzel, R. (2001). Bee brains, B-splines and computational democracy: Generating an average shape atlas. Proceedings of the IEEE Workshop on Mathematical Methods in Biomedical Image Analysis, MMBIA, Kauai, Hawaii. 187–194.

Rohlfing, T., Brandt, R., Menzel, R., and Maurer, C. R. (2004). Evaluation of atlas selection strategies for atlas-based image segmentation with application to confocal microscopy images of bee brains. *Neuroimage* 21, 1428–1442.

Sakura, M., Lambrinos, D., and Labhart, T. (2008). Polarized skylight navigation in insects: model and electrophysiology of e-vector coding by neurons in the central complex. *J. Neurophysiol.* 99, 667–682.

Schmitt, S., Evers, J. F., Duch, C., Scholz, M., and Obermayer, K. (2004). New methods for the computer-assisted 3-D reconstruction of neurons from confocal image stacks. *Neuroimage* 23, 1283–1298.

Siegl, T., Schachtner, J., Holstein, G. R., and Homberg, U. (2009). NO/cGMP signalling: L-citrulline and cGMP immunostaining in the central complex of the desert locust *Schistocerca gregaria*. *Cell Tissue Res.* 337, 327–340.

Strausfeld, N. J. (1976). Atlas of an Insect Brain. Heidelberg, Springer.

Strauss, R. (2002). The central complex and the genetic dissection of locomotor behaviour. *Curr. Opin. Neurobiol.* 12, 633–638.

Strauss, R., and Heisenberg, M. (1993). A higher control center of locomotor behavior in the *Drosophila* brain. *J. Neurosci.* 13, 1852–1861.

Vitzthum, H., Müller, M., and Homberg, U. (2002). Neurons of the central complex of the locust *Schistocerca gregaria* are sensitive to polarized light. *J. Neurosci.* 22, 1114–1125.

Wang, Z., Pan, Y., Li, W., Jiang, H., Chatzimanolis, L., Chang, J., Gong, Z., and Liu, L. (2008). Visual pattern memory requires foraging function in the central complex of *Drosophila*. *Learn. Mem.* 15, 133–142.

Wehner, R. (1992). Arthropods. In Animal Homing, F. Papi, ed. (London, Chapman and Hall), pp. 45–144.

Williams, J. L. D. (1972). Some Observations on the Neuronal Organisation of the Supra-Oesophageal Ganglion in *Schistocerca gregaria* Forskål with Particular Reference to the Central Complex. PhD Thesis, University of Wales, Cardiff

Williams, J. L. D. (1975). Anatomical studies of the insect central nervous system: a ground-plan of the midbrain and an introduction to the central complex in the locust, *Schistocerca gregaria* (Orthoptera). *J. Zool.* 176, 67–86.

Conflict of Interest Statement: The authors declare that the research was conducted in the absence of any commercial or financial relationships that could be construed as a potential conflict of interest.

Received: 04 September 2009; paper pending published: 29 October 2009; accepted: 19 December 2009; published online: 03 February 2010.

*Citation: el Jundi B, Heinze S, Lenschow C, Kurylas A, Rohlfing T, and Homberg U (2010) The locust standard brain: a 3D standard of the central complex as a platform for neural network analysis. Front. Syst. Neurosci. **3**:21. doi: 10.3389/neuro.06.021.2009*

Appendix

Calculation of sky compass signals with MatLab

Within the context of possible functional roles of interneurons of the anterior optic tubercle during my PhD thesis I modeled compass signals of the sky. For this, a script was written in the software program MatLab (MathWorks) that allows the calculation of the changes of the solar elevation at a particular year/day and geographical location. Furthermore, changes of sky compass signals, like the light illumination of the sun, the changes of the *E*-vector orientation and degree of polarization in a distinct observed point in the sky can also be evaluated by the script. As basis for the model calculations the following publications were used:

- Brines ML, Gould JL (1982) Skylight polarization patterns and animal orientation. *J Exp Biol* 96: 69-91.
- Elvegård E, Sjöstedt G (1940) The calculation of illumination from sun and sky. *Illum Engin* 35: 333-342.
- Pfeiffer K, Homberg U (2007) Coding of azimuthal directions via time-compensated combination of celestial compass cues. *Curr Biol* 17: 960-965.
- Pfeiffer K, Negrello M, Homberg U (2011) Conditional perception under stimulus ambiguity: polarization- and azimuth-sensitive neurons in the locust brain are inhibited by low degrees of polarization. J *Neurophysiol* 105: 28-35.
- Strutt JW (1871) On the light from the sky, its polarization and color. *Phil Mag* 41: 274-279.
- Suhai B, Horváth G (2004) How well does the Rayleigh model describe the E-vector distribution of skylight in clear and cloudy conditions? A full-sky polarimetric study. *J Opt Soc Am A Opt Image Sci Vis* 21: 1669-1676.

For a simple application of the script for each user, an intuitive graphical user interface (GUI) was created. Here, a small introduction of the script is given, as well as the used equations are given.

Equations for calculations of sky compass signals

Equations for the calculation of the changes of the solar elevation

As a basis for all further calculations, at first the changes of the solar elevation at an arbitrary year/day and geographical position on earth were modeled. For the determination of the changes of solar elevation, the equation of time (*EOT)*, the declination δ and the hour angle (*HA*) are important physical values. Therefore, first the equation of time (*EOT*) was

determined. *EOT* is the difference between the apparent solar time and the mean solar time and can be calculated with the following equation:

- (1) $$EOT = 229.2 \cdot \left(\begin{pmatrix} 0.000075 + (0.001868 \cdot \cos(B)) - (0.032077 \cdot \sin(B)) - \\ (0.014615 \cdot \cos(2B)) - 0.04089 \cdot \sin(2B) \end{pmatrix} \right)$$

  with

  (2) $$B = (n-1) \cdot \left(\frac{360}{365} \right)$$

- The solar declination δ is defined through the next equation:

  (3) $$\delta = 23.45 \cdot \sin\left(\frac{360 \cdot (284 + n)}{365} \right)$$ (n = number of days)

- The hour angle (*HA,* angular distance between sun and local meridian) can be determined as follows:

  (4) $$HA = -1 \cdot (180 - LAT \cdot 15)$$

  LAT is the local apparent time and can be evaluated with equation 5:

  (5) $$LAT = 24 \cdot (LT + (4 \cdot (\lambda - 15) + EOT) / 24 / 60)$$

  In this equation, *LT* is the local time and λ is the geographical longitude.

Based on all this equations, the changes of the solar elevation (α_S) can be modeled:

(6) $$\alpha_S = \arcsin(\sin(\delta) \cdot \sin(\varphi) + \cos(HA) \cdot \cos(\delta) \cdot \cos(\varphi))$$

φ is the latitude of the geographical coordinates.

Equations for the calculation of the illumination from the sun at different solar elevations

The sun illumination is dependent from the air mass *(AM)*.

(7) $$AM = \frac{1}{\cos(90 - \alpha_S)}$$

The sun illumination *S* was modeled for a horizontally oriented surface:

(8) $$S = 1.232 \cdot 10^4 \cdot \sin(\alpha_S) \cdot 10^{-0.1 \cdot AM}$$

Equation for the determination of the degree of polarization as a function of the solar elevation

The changes of the degree of polarization d in the zenith can be calculated as follows:

$$(9) \qquad d = 0.75 \cdot \left(\frac{1 - \cos^2 \sigma}{1 + \cos^2 \sigma} \right)$$

σ is the angular distance between the sun and the zenith

Equations for modeling of sky compass signals in distinct observed points

The coordinates of the solar position are given by the vector $\vec{s}$:

$$(10) \qquad \vec{s} = \begin{pmatrix} \sin(90° - \alpha_S) \cdot \cos(\varphi_S) \\ \sin(90° - \alpha_S) \cdot \sin(\varphi_S) \\ \cos(90° - \alpha_S) \end{pmatrix}$$

where φ_S is the azimuthal direction of the sun.

In the same manner, the coordinates (azimuth and elevation) of an observed point $(\vec{o})$ can be defined:

$$(11) \qquad \vec{o} = \begin{pmatrix} \sin(90° - \alpha_O) \cdot \cos(\varphi_O) \\ \sin(90° - \alpha_O) \cdot \sin(\varphi_O) \\ \cos(90° - \alpha_O) \end{pmatrix}$$

The E-vector $\vec{e}$ was evaluated as the product of the vectors $\vec{s}$ and $\vec{o}$.

$$(12) \qquad \vec{e} = \vec{s} \cdot \vec{o}$$

The E-vector orientation ϕ in a distinct observed point can now be calculated with the following equation:

$$(13) \qquad \phi = \arctan\left(\frac{e_2}{e_1} \right)$$

e_1 and e_2 are components of the E-vector $\vec{e}$.

For the degree of polarization, first the angular distance θ between the observed point and the sun was calculated:

$$(14)\ \theta = \operatorname{arcos}\left(\frac{\vec{s}\cdot\vec{o}}{|\vec{s}|\cdot|\vec{o}|}\right)$$

By replacing σ with θ in equation 9, the changes of the degree of polarization in a particular observed point were defined.

Application of the sky compass calculator script (ssc)

The application of the script is simplified by a GUI.
Unzip files and copy both files (ssc01_BeJ.m, ssc01_BeJ.fig) in one folder. Open the M-file (ssc01_BeJ.m) and run the script. Now automatically the GUI will open (Figure A1). In the first lines, now the geographical position (longitude, latitude) as well as the date (day, month, and year) has to be entered. Exemplary, we used as input values now the coordinates of the Tropic of Cancer (23.4° N, 5.2°E) to calculate the changes of the solar elevation in the natural habitat of the locusts in northern Africa. As date we used the day August 1, 2011. Now the changes of the solar elevation at this particular day can be evaluated in the line 'Calculate solar elevation during the day' by pressing the button 'DO IT' in the same line. A new window will then open in which the solar elevation at a distinct day and geographical location is plotted against the time of day (Figure A2).

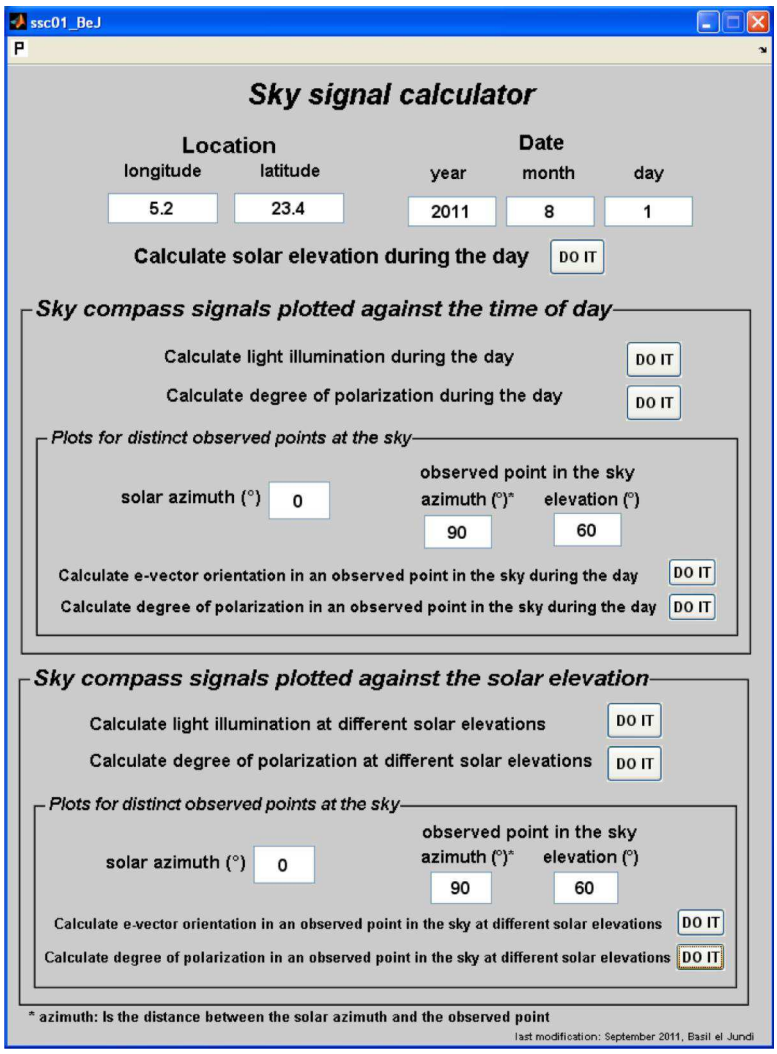

Figure A1: Graphical user interface of the MatLab script for calculation of compass signals of the sky. The program allows the calculation of the changes of the solar elevation at a particular day/year and geographical location as well as the modeling of the corresponding changes of the light illumination and the degree of polarization. Furthermore, the *E*-vector orientation and the degree of polarization can be calculated at any given observed point at the sky.

Simultaneously the script saves automatically three data files in the same folder as the script exists (solar-elevation). The first data file is a bitmap-file of the plot, according to the generated figure. The second data file is again the figure, however, as eps-file (eps-files are ideal for further processing of the plots in graphic software programs). The third created data file is a text-file (txt) in which a list of times of day and the corresponding elevations of the sun are saved. Note: If you will create a new figure of the changes of the solar elevation during the day with other

parameters, the saved data files will be overwritten with new values and figures of the new generated plot.

The further user interface is in general divided into two subparts. In the upper subpart, sky compass signals can be calculated as a function of the time of day. In the lower part of the interface, celestial compass cues can be plotted against the solar elevation. Both subparts calculate sky compass clues dependent on the entered input parameters in the first line. The structure of both subparts is similar. At first, the changes of the light illumination for a horizontal surface during the day (or at different elevations of the sun) can be plotted when pressing the corresponding 'DO IT' button at the line 'Calculate light illumination during the day' (or 'Calculate light illumination at different solar elevations'). Again, a new figure will be created and, the program autosaves the three data files for the corresponding created plot.

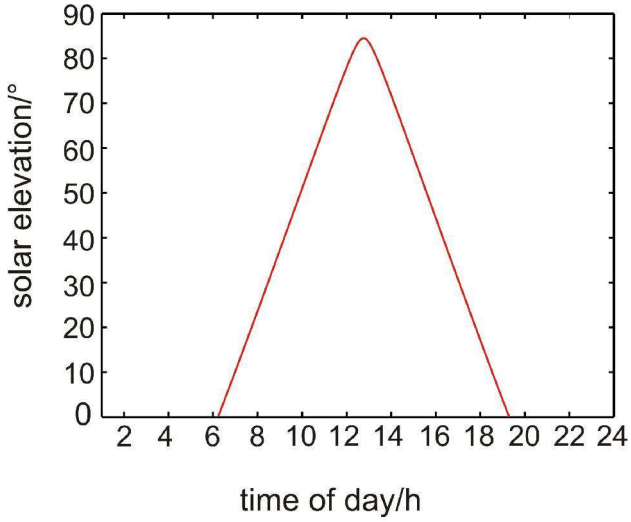

Figure A2: Output file of the sky compass script. Calculation of the course of the sun during August 1, 2011 in Tropic of Cancer (23.4°N, 5.4°E).

Next, the changes of the degree of polarization during the day (or at different solar elevations) in the zenith can be calculated when pressing the button 'Calculate degree of polarization during the day' (or 'Calculate degree of polarization at different solar elevations').

In the small inserted boxes ('Plots for distinct observed points at the sky'), the changes of the *E*-vector orientation as well as of the degree of polarization in an observed point at the sky can be measured. To do this, the azimuthal position of the sun has to be defined in the input box 'solar

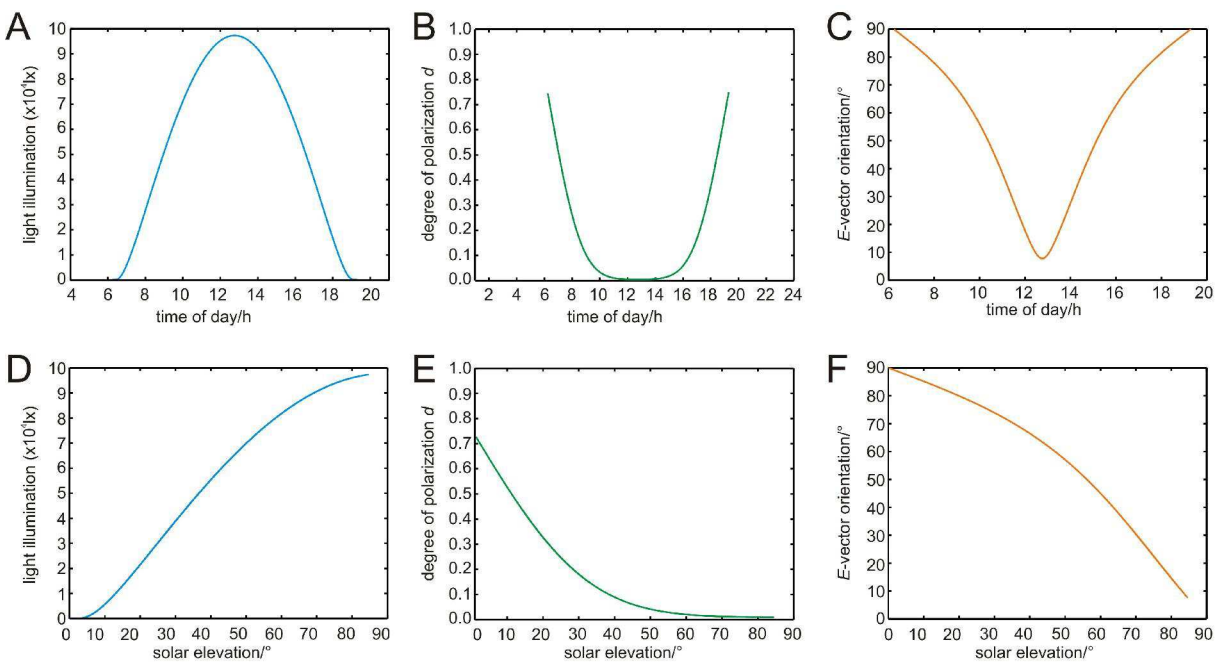

Figure A3: Output data files of the sky compass calculation script. All calculations are dependent on the course of the sun as shown in Figure A2. B, C, E F were calculated for an observed point at 90° azimuthal angular distance to the solar azimuth, and 60° elevation (A) light illumination of the sun on a horizontal surface plotted against the time of day. (B) Degree of polarization in an observed point plotted against the time of day. (C) Observed *E*-vector at different times of day. (D) Light illumination as a function of the solar elevation. (E) The degree of polarization as a function of the elevation of the sun. (F) The changes of the *E*-vector orientation at different solar elevations.

azimuth'. In our example in Figure 1 we defined the solar position as 0°, which means that the sun is during the whole day in front of the locust. Now the azimuth and the elevation of the observed point have to be determined ('observed point in the sky'). Note: The azimuth of the observed point is defined as the angular distance to the solar azimuth. According to the center of the receptive fields of the intertubercle neurons of the AOTu, in our example we used an observed point at an elevation of 60° and in an azimuthal distance of 90° from the sun. Now we can model how sky compass signals changes during the day, when the sun is in front of the locust. When pressing now the DO IT button, in each case, the changes of the observed *E*-vector orientation or of the degree of polarization can be calculated as a function of the time of day. Again, the created plot is autosaved as bitmap-file and as eps-file and as a table of the corresponding values. In the lower subpart, the changes of *E*-vector and the alteration of the degree of polarization can be calculated as a function of the solar elevation.

Basil el Jundi - Curriculum Vitae

Address

Basil el Jundi
Reitgasse 12
35037 Marburg

Telephone: 0049/ 6421/ 1601987 (private)
0049/ 6421/ 28-23380 (office)
Fax: 0049/ 6421/ 28-28941

Email: eljundib@biologie.uni-marburg.de

Personal Details

Date of birth: April 7th 1983
Place of birth: Stuttgart, Germany
Nationality: German
Marital status: unmarried

Academic Education

06/2010 – 07/2010 Participation in the summer course 'Neural Systems and Behavior' at the Marine Biological Laboratory in Woods Hole, MA, USA.

Since 05/2008 PhD thesis in the laboratory group of Prof. Dr. Homberg at the University of Marburg / department neurobiology / ethology (working title: Characterization of polarization-sensitive interneurons in the brain of the desert locust *Schistocerca gregaria)*.

04/2008 Diploma thesis (with honours) in the research group of Prof. Dr. Schachtner department neurobiology / ethology at the University of Marburg (title: Creating of a 3D standard brain of the sphinx moth *Manduca sexta* – sexual dimorphism and development). Final examinations in the subjects: animal physiology, developmental biology and cell biology (mark: 1.1, 'very good').

09/2005 Prediploma at the University of Marburg, (mark: 2.5, 'good').

11/2003 – 04/2008	Studies of Biology at the University of Marburg.
08/1993 – 06/2002	Gramma school in Stuttgart (Eberhard- Ludwigs- Gymnasium). Final examination 2002: Abitur (mark: 2.1, 'good').

Awards & Grants

2008	Faculty award of the biological faculty of the University of Marburg for the best diploma thesis of the year.
2010	Marine Biological Laboratory Scholarship funded by Neural Systems & Behavior Course Endowed Scholarship Fund, $3,250.
2010	Travel allowances, Boehringer Ingelheim Fonds, Germany, €3,500.
2010	Talk prize of the Arthropod Neuroscience Network Meeting.

Organized Workshops

10/2011	1-week Amira Workshop at the Philipps-University of Marburg: 3D reconstruction, visualization and animation of brain areas and neurons of the insect brain.

Vocational Experience

Tutor in undergraduate courses

2006	Zoology anatomy
2006 – 2010	Student assistant in lab, animal physiology (chronobiological analysis)
2007	Teaching assistant in lab, neurophysiology (3D reconstructions of insect brains)
2007	Behavioral and genetic experiments for medical science students
2007 – 2008	Confocal microscopy courses

2008	Multimedia in biology
2008 - 2011	Teaching assistant in lab (intracellular recordings from neurons of the locust brain)

Specific qualifications

- Experience with electrophysiological recordings in insects (intracellular recordings; in particular recordings from polarization sensitive neurons in the desert locust brain).
- Experience with iontophoretic dye injections in single neurons and histochemical tissue processing.
- Detailed anatomical knowledge of the insect brain.
- Experience with immunocytochemistry (vibratome sections and wholemount preparations) and scanning with a confocal laser scanning microscope (CLSM).
- Pharmacological studies and injections in the antennae of *Manduca sexta* during the metamorphic development.
- Experience in 3D-reconstructions of neuropils and single neurons with the software Amira
- Creating of standard brains and brain regions with the virtual insect brain protocol (VIB) and the iterative shape averaging (ISA) method.
- Animation of brain development with the software MAXON Cinema 4D.
- Working with the system software's Windows and Linux; working on a linux cluster.
- Experience with following software products: Spike2, MatLab, Amira, Cinema 4D, Adobe Photoshop, Corel-Draw, Oriana, Origin, SPSS, MS-Office.
- Basic knowledge of molecular biology and *Drosophila* genetics.

Publications

el Jundi B, Pfeiffer K, Homberg U. A distinct layer of the medulla integrates sky compass signals in the brain of an insect, *in revision*.

Wei H, **el Jundi B**, Homberg U, Stengl M (2010). Implementation of pigment-dispersing factor-immunoreactive neurons in a standardized atlas of the brain of the cockroach *Leucophaea maderae. J Comp Neurol,* 518:4113–4133.

el Jundi B, Homberg U (2010) Evidence for the possible existence of a second polarization vision pathway in the locust brain. *J Insect Physiol*, 56(8): 971-979.

Huetteroth W, **el Jundi B**, el Jundi S, Schachtner J (2010). 3D-reconstructions and virtual 4D-visualization to study metamorphic brain development in the sphinx moth *Manduca sexta. Front Syst Neurosci*, 4:7.

Dreyer D, Vitt H, Dippel S, Goetz B, **el Jundi B**, Kollmann M, Huetteroth W, Schachtner J (2010). 3D standard brain of the red flour beetle *Tribolium castaneum:* A tool to study metamorphic development and adult plasticity. *Front Syst Neurosci*, 4:3.

el Jundi B, Heinze S, Lenschow C, Kurylas A, Rohlfing T, Homberg U (2010). The locust standard brain: a 3D standard of the central complex as a platform for neural network analysis. *Front Syst Neurosci*, 3:21.

el Jundi B, Huetteroth W, Kurylas AE, Schachtner J (2009). Anisometric brain dimorphism revisited: implementation of a volumetric 3D standard brain in *Manduca sexta*. *J Comp Neurol* 517(2), 210-225.

Reviews

Homberg U, Heinze S, Pfeiffer K, Kinoshita M, **el Jundi B** (2011). Central neural coding of sky polarization in insects. *Phil Trans R Soc B*, 366(1565): 680-687.

Other Publications

el Jundi B (2008) Erstellung eines 3D Standardgehirnes des Tabakschwärmes *Manduca sexta* – Ontogenie und Geschlechtsdimorphismus [Creation of a 3D standard brain of the sphinx moth *Manduca sexta* – sexual dimorphism and development]. Diploma thesis, University of Marburg, Germany.

Conference Contributions

el Jundi B, Homberg U (2011) A distinct layer of the medulla integrates polarized light information in the locust brain. 9th NWG meeting, Göttingen, Germany, T14-2A.

el Jundi B, Homberg U (2010) A distinct layer of the medulla integrates polarization information in the locust brain. Arthropod Neuroscience Network meeting, Hamburg, Germany.

Rosner R, **el Jundi B**, Heinze S, Müller M, Homberg U (2010) Integration of polarized and unpolarized light information in the central complex of the desert locust. 9th International Congress of Neuroethology, Salamanca, Spain, P 152, p440.

Kinoshita M, **el Jundi B**, Arikawa K, Homberg U (2009) Visual inputs to the mushroom bodies in the swallowtail butterfly. 40th meeting of the Society for Neuroscience, Chicago, IL, USA, No. 287.2-SU.

Wei H, **el Jundi B**, Homberg U, Stengl M (2009) Implementation of pigment-dispersing factor-immunoreactive circadian pacemaker neurons into a three-dimensional standardized atlas of the brain of the cockroach *Leucophaea maderae.* 102th DZG meeting, Regensburg, Germany P NB.23.

Backasch B, **el Jundi B**, Homberg U (2009) Behavioral and physiological analysis of polarotaxis and phototaxis in gregarious and solitarious desert locusts. 102th DZG meeting, Regensburg, Germany P NB.2.

el Jundi B, Heinze S, Pfeiffer K and Homberg U (2009) Transformation of receptive field structure and ocular dominance between different stages of the polarization vision pathway in the brain of the locust. 8th NWG meeting, Göttingen, Germany, T14-5A.

el Jundi B, Huetteroth W, Schachtner J (2008) 3D standard brain of the sphinx moth *Manduca sexta*: Sexdimorphism and development. 101th DZG meeting, Jena, Germany, NB.4, p76 [conference talk].

Rulla S, Huetteroth W, **el Jundi B**, Schachtner J (2008) Developmental influence of procaine and lanthan chloride on the antennal lobe of the sphinx moth *Manduca sexta.* 101th DZG meeting, Jena, Germany, P NB.17, p178.

el Jundi B, Huetteroth W, Schachtner J (2007) 3D reconstruction of *Manduca sexta* adult brain and of brains during metamorphic development. 7th NWG meeting, Göttingen, Germany, TS8-7B.

Schachtner J, Huetteroth W, Dreyer D, Dippel S, **el Jundi B** (2006) 3D-reconstructions of the *Tribolium* brain: a tool to study developmental and adult plasticity. 36th meeting of the Society for Neuroscience, Atlanta, GA, USA, No. 35.1/W24.

Dreyer D, Dippel S, **el Jundi B**, Huetteroth W, Schachtner J (2006) 3D reconstruction of the *Tribolium* brain: a tool to study developmental and adult plasticity. 99th DZG meeting Münster, Germany, PM_NB_1.19, p44.

Danksagung

Zunächst möchte ich mich herzlichst bei Prof. Dr. Uwe Homberg für die Bereitstellung des spannenden Themas, sowie für die hervorragende Zusammenarbeit bedanken. Außerdem bedanke ich mich für sein unermüdliches Korrigieren von Manuskripten, sowie für ein sehr kollegiales Verhältnis. Er hat mich zu jeder Zeit hervorragend unterstützt und mir bestmöglich geholfen, wenn ich um Rat gefragt habe. Vor allem aber hat er mir ein freies Arbeiten ermöglicht, was ihn mir eine große Begeisterung für die Wissenschaft geweckt hat.

Bei Prof. Dr. Joachim Schachtner möchte ich mich nicht nur wegen der Zweitkorrektur bedanken. Vor allem möchte ich mich bei ihm für einen guten Einstieg in die Wissenschaft, für die Motivation auch in schlechten Zeiten und für sehr schöne zwei Jahre in seiner Arbeitsgruppe während meiner Studienzeit bedanken. Außerdem bedanke ich mich für zahlreiche Diskussionen und richtungweisende Gespräche.

Bei Prof. Dr. Hassel und Prof. Dr. Renkawitz-Pohl möchte ich mich herzlich bedanken, da sie sich mit einer Selbstverständlichkeit als Mitglieder der Prüfungskommission zur Verfügung gestellt haben.

Zudem möchte ich mich bei allen Mitgliedern und Ehemaligen der Neurobiologie (AG Ho/Scha/We/Ste) bedanken, die stets für eine entspannte und lustige, sowie inspirierende Atmosphäre gesorgt haben.

In allerhöchstem Masse möchte ich mich allerdings bei folgenden Personen bedanken:

Meinem Elektrophysiologie-Mentoren Dr. Stanley Heinze und meinem Elektrophysiologie-Mentoren aus Kanada, Dr. Keram Pfeiffer, möchte ich danken, die mich beide hervorragend in die Elektrophysiologie eingelernt haben und immer ein offenes Ohr für meine Fragen hatten. Dr. Keram Pfeiffer möchte ich vor allem für die Bereitstellung seines Auswertskriptes danken. Ohne ihn wäre meine Arbeit in dieser Form nicht durchführbar gewesen. Beide haben mein wissenschaftliches Denken maßgeblich geprägt.

Im gleichen Atemzug sollte auch Dr. Wolf Hütteroth genannt werden. Bei ihm und bei Dr. Angela Kurylas bedanke ich mich für eine detaillierte Einführung in die Immunzytochemie, sowie für die Einweisung in die 3D-Software Amira.

Für das Korrekturlesen vieler Manuskripte und der Doktorarbeit und für tolle Jahre bzw. ein tolles Jahr möchte ich mich bei Miklós Bech und Carsten Heuer bedanken.

Weiterhin danke ich den technischen Assistentinnen Martina Kern und Jutta Seyfarth, die für einen reibungslosen Ablauf im Labor und in der Arbeitsgruppe gesorgt haben.

Für viele inspirierende Gespräche, in denen es nicht nur um die Arbeit ging, möchte ich mich außerdem bei Bianca Backasch, Marlene Binzer, Tobias Bockhorst, Stefan Dippel, Dr. Christian Flecke, Nico Funk, Dr. Martina (Mappes) Heitmann, Tim Humberg, Martin Kollmann, Dr. Dennis Pauls, Wencke Reiher, Dr. Ronny Rosner, Fabian Schmeling, Dr. Mareike Selcho, Sigrid Stöhr, Dr. Ulrike Träger, Dr. Sandra Utz, Prof. Dr. Christian Wegener und Achim Werckenthin bedanken.

Bei meinen Freunden, die mich über die Unizeit und teilweise weit darüber hinaus stets unterstützt haben möchte ich mich ebenfalls außerordentlich bedanken: Sebastian Braun, Sebastian Dintner, David Dreyer, Christian Grabner, Christopher Grosche, Michael (Smi) Hamann, Sebastian Höger, Octavian Knoll, Christian Neumann-Semerow, Rebecca Ölkrug, Christopher Schirwitz.

Zuletzt gehört der allergrößte Dank meinen Eltern, und meinen Geschwistern. Die grenzenlose Unterstützung auf all meinen Wegen haben mir immer die Energie und Kraft gegeben die notwendig war, um alles bestmöglich zu erreichen.

Erklärung

Hiermit versichere ich, dass ich meine Dissertation

"Processing of sky compass signals at different stages of the polarization-vision pathway in the brain of the desert locust *(Schistocerca gregaria)*"

(Prozessierung von Himmelskompasssignalen auf verschiedenen Ebenen der Polarisationssehbahn im Gehirn der Wüstenheuschrecke (*Schistocerca gregaria*))

selbstständig, ohne unerlaubte Hilfe angefertigt und mich keiner anderen als der von mir ausdrücklich bezeichneten Quellen und Hilfen bedient habe.

Die Dissertation wurde in der jetzigen oder in einer ähnlichen Form noch bei keiner anderen Hochschule eingereicht und hat noch keinen sonstigen Prüfungszwecken gedient.

Marburg, den

_____

(Basil el Jundi)